Polyethylene Product Property Control

Modelling, Estimation and Control of Product Properties in a Gas Phase Polyethylene Reactor

By

Kim Beirnes McAuley, B.A.Sc.

A Thesis

Submitted to the School of Graduate Studies

in Partial Fulfilment of the Requirements

for the Degree of

Doctor of Philosophy

McMaster University

(c) Copyright by Kim Beirnes McAuley, August 1991

DOCTOR OF PHILOSOPHY (1991) McMASTER UNIVERSITY

(Chemical Engineering) Hamilton,Ontario

TITLE:

Modelling, Estimation and Control of Product Properties

in a Gas Phase Polyethylene Reactor

AUTHOR: Kim Beirnes McAuley, B.A.Sc. (University of Waterloo)

SUPERVISOR: Professor John F. MacGregor

NUMBER OF PAGES: xiv, 328

ABSTRACT

The focus of this thesis is the modelling and control of product properties in gas phase polyethylene reactors. The main product properties of concern are melt index (*MI*) and density (ρ), which are related to the molecular weight and composition of the ethylene/α-olefin copolymer. A kinetic model is developed which accounts for the effects of gas composition, reactor temperature, and active site distribution of the Ziegler-Natta catalyst on the *MI* and ρ of the polymer product. The model predicts the behaviour of *MI* and ρ in an industrial reactor, as well as broadened molecular weight distribution and bimodal composition distributions, which are typical for commercial linear polyethylenes.

Because measurements of *MI* and ρ are not available on-line, a methodology is developed to infer product properties from available measurements. Simple, theoretically-based models are derived which relate *MI* and ρ to reactor operating conditions. Parameters in the models are adjusted using off-line measurements, providing an effective means for inferring both *MI* and ρ.

In a series of three product grade changeovers, dynamic optimization is used to determine optimal profiles for: hydrogen and butene feed rates, the reactor temperature setpoint, the gas bleed flow, the catalyst feed rate, and the bed level setpoint. It is shown that large transitions in *MI* are hampered by slow hydrogen dynamics, and that the time required for such a transition can be reduced by manipulation of the temperature setpoint and the bleed stream flow. Reduction of the bed level and catalyst feed rates during

transitions can significantly decrease the quantity of off-specification polymer produced. In the absence of feedback control, disturbances and model mismatch can result in product property trajectories which differ significantly from the nominal optimal trajectory.

A novel nonlinear model-based strategy is developed for on-line product property control. This feedforward/feedback control scheme is capable of both regulating product quality about a given target and of implementing optimal transition policies with feedback. The simplified mass balance model used in the controller design contains four adjustable parameters which are updated using an extended Kalman filter (*EKF*). The controller and *EKF* provide excellent regulatory and grade transition control for the range of poleythylene products simulated. The nonlinear controller is superior to an analogous linear time-invariant internal model control (*IMC*) design. The control system developed in the thesis is both simple and effective, and it has great potential for improving product quality in the polymer industry.

ACKNOWLEDGEMENTS

I have learned many things from my supervisor, Dr. John F. MacGregor. He has been a fine role model, and I thank him for his encouragement and guidance.

I would also like to thank the members of my supervisory committee, Drs. A.E. Hamielec, T.E. Marlin, and S.K Rajput for their valuable input, and NSERC for financial support.

On many occasions, I have gone to Dr. Andy Hrymak for advice, both technical and professional. I know that I will miss him after I leave McMaster.

Sara Gallo-O'Toole deserves special thanks. She is a valued friend who always found a way to squeeze me into Dr. MacGregor's hectic schedule.

I have spent many happy days in the Chemical Engineering Penthouse. My fellow graduate students, especially Paul Gossen, Derrick Kozub, Alan Hugo, Jim Kresta, and Fraser Forbes, have provided both intellectual stimulation and emotional support.

I especially appreciate my husband Paul for his help, love, and stabilizing influence. He was always there for me, whether I was irritable and frustrated, or excited and jubilant about my research.

Table of Contents

Table of Figures

Chapter 1

Chapter 2

Chapter 3

Chapter 4

Chapter 5

Chapter 6

Table of Tables

Chapter 2

Chapter 4

Chapter 5

Chapter 6

THESIS INTRODUCTION

1 THESIS INTRODUCTION

During the past decade, the desire for consistency in the properties of both high performance and commodity polymers has led to increased interest in on-line product quality control schemes for polymerization reactors. Unfortunately, for several reasons, successful design of polymer quality control schemes is difficult. First, product quality is a complex issue in polymer systems; the interrelationships between structural properties, such as the molecular weight distribution, and end-use properties are not well-understood. Second, there is a lack of on-line measurement technology for many of the important quality variables, so means for inferring estimates of product quality from available on-line measurements must be developed. Finally, traditional linear empirical models and controller design techniques are often inadequate for polymer systems. Fundamental reactor models describing complex reaction kinetics and accounting for multiple phases must be developed to predict the nonlinear behaviour of polymerization reactors. Design of nonlinear multivariable controllers based on this modelling information is not trivial.

In this thesis, strategies for overcoming the difficulties associated with polymer quality control are illustrated using a gas phase polyethylene reactor example. A mechanistic model is developed in Chapters 2 and 3 to predict the effects of reactor operating conditions on important quality variables. These quality variables cannot be measured on-line, so in Chapter 4 a model-based inference scheme is developed to predict product quality from on-line temperature, flow and gas composition measurements. The model parameters required for the property prediction are updated using infrequent product quality

measurements determined in the quality control laboratory. The property predictions provided by the inference scheme are used as feedback to the on-line quality control scheme. Two aspects of quality control must be considered when evaluating a controller design: trajectory control during grade transitions and regulation of quality variables while producing a single polymer grade. Optimal grade transition trajectories are determined in Chapter 5 using dynamic optimization techniques. Controller design solutions which address both grade transitions and quality regulation are proposed in Chapter 6.

Although the reactor modelling, product quality inference, and control scheme design procedures presented in this thesis are discussed in the context of a gas phase ethylene copolymerization reactor system, the problems encountered and approaches used to solve them are applicable to many other polymerization systems. As such, a general introduction to the problems commonly faced by the developers of on-line control schemes for polymerization reactors is provided in the following section. After this general introduction, a gas phase polyethylene process is described and the specific problems associated modelling and control of this system are introduced.

1.1 PRODUCT QUALITY CONTROL ISSUES IN POLYMERIZATION REACTORS

In the past decade, several reviews dealing with the problems of controlling polymerization systems have appeared in the literature on polymer reaction engineering and process control (MacGregor et al., 1984; MacGregor, 1986; Ray, 1986; Elicabe and Meira, 1988). In these reviews, the common problems associated with the control of polymer reactors are highlighted and the solutions which have been applied are discussed. The major problems addressed in these reviews are: the definition and prediction of product quality variables, a lack of on-line measurements and the need to account for

nonlinear steady state and dynamic behaviour in control scheme design.

1.1.1 Defining and Predicting Product Quality Variables

Product quality in polymerization systems is a more complex issue than in conventional small molecule systems. Reactor upsets, such as those caused by reactive impurities, can alter copolymer composition, molecular weight distributions and particle shape and size. Variations in polymer architecture can have serious, but poorly understood effects on the end-use and polymer processing properties specified by the customer. While the effects that variations in impurity levels and in other reactor operating conditions have on molecular weight, branching, and composition have been modelled theoretically for certain polymerization systems (Schmidt and Ray, 1981; Penlidis et al., 1985; Ray, 1986; Hamielec et al., 1987; Rincon-Rubio et al., 1990), only empirical models exist to predict the effects that changes in the structural variables will have on end-use and processing properties. These properties include strength, hardness, brittleness, elasticity, melting temperature, glass transition temperature, melt viscosity, and optical properties of the polymer product.

In cases where mechanistic models do not exist, empirical statistical models can be determined from plant data in order to elucidate the relationships between plant operating conditions and quality variables. For example, Motkei and Arai (1986) have used multivariable statistical techniques to correlate steady state process operating conditions to polymer end-use properties. Although the models developed by such techniques cannot be used to reliably extrapolate beyond known reactor operating conditions, they can be used to develop an empirical understanding of the relationships between reactor operating variables and the properties of the polymer product of interest to the customer.

1.1.2 Lack of On-Line Measurements

In most industrial settings, polymer quality variables cannot be measured by on-line instrumentation. However, some promising new research is being conducted in the field of on-line instrumentation for polymer systems (Chien and Penlidis, 1990). In latex systems, on-line techniques have been developed for particle size determination (Nicoli et al. 1992) and novel statistical techniques such as partial least squares (PLS) are being used in conjunction with near infrared probes to infer polymer quality variables (Gossen, 1991). In fluidized bed polyethylene systems, on-line measurements of product quality have yet to be developed. Thus, it could be several years before reliable on-line measures of product quality are routinely available. As such, feed back to the control scheme being developed in this research will be provided by off-line laboratory measurements. Model based techniques such as Kalman filtering have been used in polymer reactors to infer quantities which are either not measured (Kozub and MacGregor, 1989; Schuler and Suzhen, 1985; Adebekun and Schork, 1989b) or which are measured infrequently (Jo and Bankhoff, 1976; Ardell and Gumowski, 1983; Ellis et al. 1988). Under certain conditions recursive prediction error techniques (Ljung, 1987) can also be used to update a model-based scheme using infrequent laboratory measurements. Both the Kalman filtering and recursive estimation approaches are described in this thesis.

1.1.3 Influence of Nonlinear Reactor Behaviour on Control Schemes

The treatment of process non-linearities and the level of complexity of models required for reactor control depend both on the objectives of the control scheme and on the degree of nonlinearity of the process. For simple quality regulation

at a single steady state, empirical linear models can be identified from input/output data (MacGregor and Tidwell, 1980). These models can be used to design linear control schemes for use in narrow operating regions (Kelly et al., 1987). Alternatively, nonlinear transformations of input/output data can be performed to give nearly linear relationships between the transformed variables. Linear control schemes developed using the transformed variables can result in satisfactory regulation over a wide operating region (Rushing, 1986). For some severely nonlinear reactors, even regulation about a single steady state can be difficult. Many continuous polymer reactors are so nonlinear that they exhibit exotic dynamics and multiple steady states (Jaisinghani and Ray, 1979; Schmidt et al., 1984; Choi and Ray, 1985; Hutchinson and Ray, 1987; Teymour and Ray, 1989; Adebekun et al., 1989). Depending on the reactor operating conditions, a small disturbance from an initial stable steady state could drive the reactor to operate at a different undesirable steady state or to exhibit periodic limit cycle behaviour. Thus, for certain operating regimes, linear feedback control may not be successful in regulating product quality. Either a nonlinear control scheme or even reactor system redesign (Pollock, 1983) may be required to ensure stable control at the desired operating point.

While most quality regulation problems in continuous polymerization reactors can be handled adequately by linear controllers, operating policies for batch and semi-batch reactors, and grade changeover policies in continuous reactors, usually require that the nonlinear character of the polymerization system be reflected in the on-line quality control scheme. One method of accounting for nonlinearities is to use model-based dynamic optimization techniques to determine optimal control polices. The temperature and feed rate trajectories specified by the solution to an off-line optimization problem are then implemented as open-loop quality control

policies. Some examples of this approach to quality control include the works of Wu et al. (1982), Tirrell and Gromley (1981) and Secchi et al. (1990) who determined optimal batch reactor operating policies for different polymerization systems, and the work of Johnson et al. (1982) who determined optimal operating policies for a styrene-MMA semi-batch copolymerization reactor. Optimal grade transition policies for specific polymer systems in continuous stirred tank reactors have been determined by Guyot et al. (1981) and Farber (1986). In addition, the production of polymer products with specified molecular weight distributions in continuous living polymerization systems using forced oscillations in the monomomer feed rates has been studied using dynamic optimization techniques (Meira, 1981; Meira and Johnson, 1981; Frontini et al., 1987). Computation of optimal operating policies is very useful in that the results provide the polymer reaction engineer with a knowledge of the best possible performance achievable in the reactor. However, due to disturbances which affect product quality and model deficiencies, open-loop implementation of these policies can result in actual product properties which are very different from the model predictions. To prevent this offset, on-line feedback control is required to compensate for the difference between measured quality variables and open-loop model predictions. Currently, on-line implementation of nonlinear dynamic optimization schemes requires prohibitive computing effort and implementation expertise for general use in the polymer industry. Nevertheless, on-line optimization of chemical processes is an important topic in the current control literature (Jang et al., 1987; Li and Biegler, 1988; Eaton and Rawlings, 1990; Chen and Hwang, 1990; Bequette, 1991).

One method which has been suggested for feedback control of nonlinear polymer reactors is the use of traditional adaptive control, based on linear process models (Kiparissides and Shaw, 1983; Takamatsu et al. (1986), Temeng and Schork, 1989). As the state of the reactor changes, model-based controller parameters are adjusted to account for process nonlinearities. Unfortunately, this simple adaptive approach to nonlinear control can lead to serious problems (MacGregor, 1986) because the model parameters must often adapt rapidly to account for reaction nonlinearities. Such rapid changes in model parameters can lead to periods of unrealistic model predictions and possibly to instability. Furthermore, adaptation mechanisms require sufficient input excitation to properly tune the parameters. When there is a lack of information in the input signal, some means must be provided for inhibiting the rate of parameter adaptation (Fortescue et al., (1981)). Otherwise, correlated parameter estimates can drift to undesirable values, leading to poor controller performance when disturbances enter the system. The potential for problems with parameter drifting increases with the number of parameters to be updated on-line. Therefore, for adaptive control scheme design, it is often better to use a mechanistically-based nonlinear model with only a few adjustable parameters (Slotine and Ydstie, 1989), rather than a linear model which contains little process information and requires that many parameters be updated on-line.

In recent years, the application of nonlinear model-based feedback controller designs for polymer reactors have begun to appear in the literature. Input/output linearizing controllers have been suggested for control of a continuous polypropylene reactor (Lie and Balchen, 1988), a semi-batch styrene butadiene rubber reactor (Kozub, 1989) and a continuous methyl methacrylate reactor (Adebekun and Schork, 1989a). In this approach, a nonlinear controller is designed so that the closed loop

behaviour of the system is specified by a linear differential equation. A comprehensive review of these nonlinear control design techniques is provided by McLellan et al. (1990). The benefit of this approach to polymer quality control is that system nonlinearities are handled directly by the on-line control system in a relatively simple fashion. The limitations of this approach are that it is not well-suited for systems with large amounts of dead-time, for problems with a different number of manipulated variables than outputs nor for control problems with constraints. Input/output linearizing controllers are discussed further in Chapter 6.

1.2 POLYETHYELENE PRODUCTION IN GAS PHASE REACTORS

Prior to the 1950's, polyethylene was produced exclusively by high-pressure free radical polymerization processes operating at temperatures and pressures above 200 $^{\circ}C$ and 1000 atm, respectively. Since that time, the development of Ziegler-Natta (*ZN*) catalysts has led to the design of low pressure ethylene polymerization processes which operate at much milder conditions near 100 $^{\circ}C$ and 2000 kPa. The polyethylenes produced by free radical mechanisms contain long chain branches, whereas those produced by low pressure processes are linear. As a result, free radical processes are still used to produce branched polyethylene polymers for certain applications. In order to produce linear low density polyethylenes, short chain branches several carbon atoms long can be inserted along the chain by copolymerizing with α-olefins such as butene and hexene.

Current commercial low pressure polyethylene processes can be classified according to the reaction medium as slurry, solution, or gas-phase. Descriptions of the major polyethylene production technologies are provided by Choi and Ray (1985), James

(1985) and by Tait (1989). Of the low pressure processes, Union Carbide's UNIPOL technology has become the most succesful, with more than 40 reactors operating in 15 countries (Tait, 1989). The popularity of this gas-phase technology over slurry and solution processes is attributable to several factors: elimination of the need to store and handle large quantities of solvents resulting in cost savings and safety and environmental improvements; the simplification of polymerization system resulting from the lack of a catalyst or solvent recovery stage after the reactor; and the wide range of products which can be produced in a single reactor (Tait, 1989).

1.2.1 Process Description

In this thesis, both the modelling and control of product quality in an industrial gas phase polyethylene reactor are studied. A schematic diagram of a typical reactor configuration is shown in Figure 1.1 (Burdett, 1988; Choi and Ray, 1985). The feed to the reactor comprises ethylene, comonomers , hydrogen and inerts. These gases provide the fluidization and heat transfer media and supply reactants for the growing polymer particles. A heterogeneous *ZN* catalyst and an aluminum alkyl cocatalyst are fed continuously to the reactor. The fluidized particles disengage from the reactant gas in the expanded top section of the reactor. The unreacted gases are combined with fresh feed streams and recycled to the base of the reactor. Since the reaction is highly exothermic, heat must be removed from the cycle gas before it is returned to the reactor. The conversion per pass through the bed is very low (2-5%) (Choi and Ray, 1985). Thus, the recycle stream is much larger that the fresh feed streams. Periodically the product discharge valve near the base of the reactor opens and fluidized product flows into a surge tank. The unreacted gas is recovered from the product which proceeds to the finishing area of the plant for additive incorporation

and pelletization. To prevent the accumulation of impurities and inerts in the system, either a portion of the recovered gas, or a small vent stream from the reactor is removed as a bleed stream.

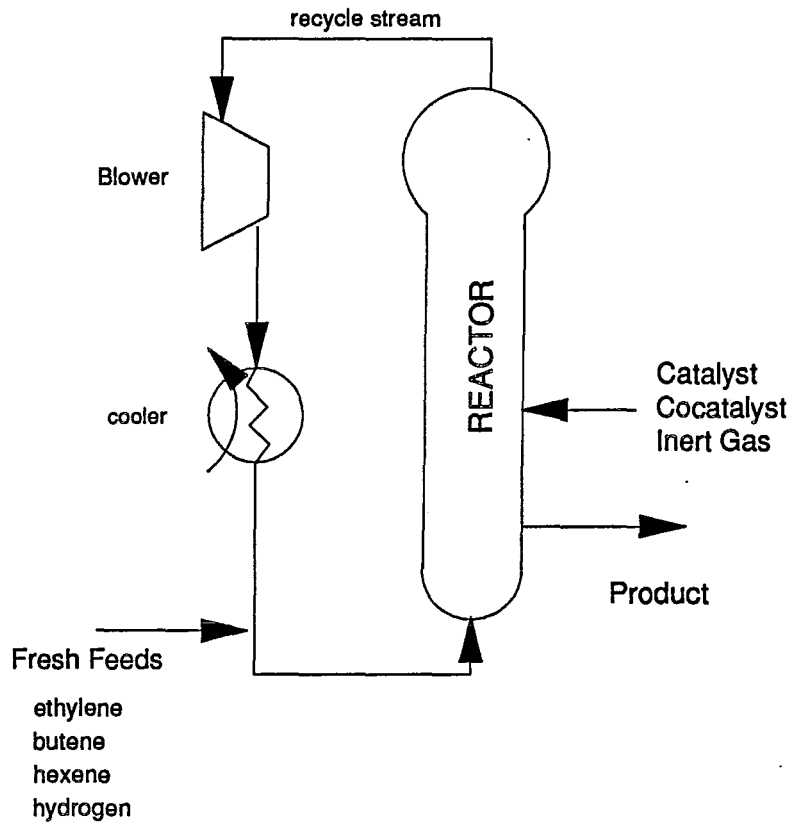

Figure 1.1 Industrial Gas Phase Polyethylene Reactor System Schematic

1.2.2 Product Quality Control Challenges

This reactor system exhibits many of the common problems faced in the design of automatic polymer quality control schemes discussed in section 1.1. The relationships between the joint polymer molecular weight and compositional distribution and the physical properties required by the customer are not well known.

In addition, actual molecular weight and composition measurements are not available at the plant, either on-line or in the quality control laboratory, because it is difficult to obtain fast, accurate and reproducible results required for plant operation. Instead, two more easily measured surrogate variables, melt index and density, are determined every few hours in the laboratory. These off-line measurement results will provide feedback to any automatic quality control scheme. Melt index (ASTM D 1238) and density (ASTM D 1505, 1928, 2838) have become the standard industry-wide measurements for specifying polyethylene grades. Melt index, indicative of the molecular weight of the polymer, is the flow rate of a molten polymer through a rheometer orifice, under a specific load condition. The density of the polymer depends on the fraction of amorphous and crystalline domains in the polymer, which in turn is affected by the amount of comonomer incorporated along the chains. The *ZN* catalyst used in the reactor under study produces a narrow molecular weight polymer with a polydispersity in the range from 3 to 3.5. In other gas phase reactors chromium catalysts are used to produce polymers with much broader molecular weight distributions (Karol, 1986). For the narrow MWD polethylenes, the breadth of the distribution is determined mainly by the structure of the catalyst and little can be done to control the polydispersity on-line. However, for the broad MWD polymers, additional gas phase components are added to the feed to influence the breadth of the MWD. In these situations, an extra surrogate variable, the melt flow ratio, which is the ratio of two melt index measurements taken under different load conditions, is used to characterize the breadth of the MWD. The control problem studied in this thesis will involve only narrow MWD polymers produced using *ZN* catalysts. As such, modelling and control of the melt flow ratio will not be pursued.

The response of melt index and density to reactor operating conditions is highly nonlinear. A theoretically based model is required to predict the complex interations among the reaction kinetics, the reactor mass and energy balances and the resulting effects on product properties. This model is developed in Chapters 2 and 3. The modelling results are then used to design and test control schemes in Chapters 4 to 6.

KINETIC MODEL FOR INDUSTRIAL GAS PHASE ETHYLENE COPOLYMERIZATION

2 KINETIC MODEL FOR INDUSTRIAL GAS PHASE ETHYLENE COPOLYMERIZATION

2.1 INTRODUCTION

Until recently, the cause of broad molecular weight distribution and compositional inhomogeneity observed in steady state olefin copolymerization with Ziegler-Natta (*ZN*) catalysts remained poorly understood. Some causes have however been proposed, including: the existence of more than one type of reactive site on the catalyst surface (Floyd et al., 1988) and the existence of concentration gradients within polymer particles caused by diffusional phenomena (Nagel et al., 1980). If a catalyst surface contains different types of active site structures, each with its own kinetic rate constants for propagation, copolymerization and transfer reactions, copolymers with broad molecular weight and compositional distributions can be produced. Alternatively, if diffusional barriers to mass transfer govern the reaction rate, catalyst sites at different radial positions in a growing polymer particle are subject to different reactant concentrations, which can account for a broad distribution of molecular weights and composition (Galvan, 1986).

Authors of recent literature reviews (Zucchini and Cecchin, 1983; deCarvalho et al., 1989; Boehm et al., 1986) have concluded that broad molecular weight distributions produced by heterogeneous *ZN* catalysts are most likely the result of multiple active sites, although in certain instances (eg. very broad particle size distributions or high

molecular weight comonomers) diffusional resistances could play some role. The most convincing evidence cited for the existence of more than one type of active site has been provided by Usami et al. (1986) who have studied linear low density polyethylene (*LLDPE*) copolymers of ethylene and butene. They collected *LLDPE* samples produced by processes with very different monomer mass transfer characteristics, namely, solution, slurry, gas phase and bulk polymerization. All of these samples had been polymerized using heterogeneous *ZN* catalysts. Cross fractionation according to short chain branching (*SCB*) frequency and molecular weight distribution was performed by temperature rise elution fractionation (*TREF*) and by size exclusion chromatography (*SEC*). Usami et al. (1986) found that all of the *LLDPE* samples had a characteristic bimodal *SCB* distribution which could not have been caused by diffusional effects. They attributed their experimental findings to the existence of at least two types of active catalyst sites. One site produces butene rich, low molecular weight material and the other produces a higher molecular weight polymer with lower butene incorporation and hence fewer short chain branches.

In this chapter, a dynamic multiple active site model to describe the copolymerization of ethylene and alpha-olefins in a gas phase fluidized bed reactor is presented. Other authors (Galvan , 1986; Choi and Ray, 1985; Hutchinson and Ray, 1987; Talbot, 1990) have presented models for gas phase ethylene polymerization in fluidized bed reactors in order to investigate temperature control problems and to predict system stability. To explain these phenomena, a comprehensive model detailing heat, mass and momentum transfer among the phases of the fluidized bed is required (Kunii and Levenspiel, 1968). The present model, however, has been developed to predict copolymer composition and molecular weight properties in a commercial gas phase reactor under good temperature regulation. Because of the uniform temperature

distribution in the bed, the large recycle stream, and kinetic rather than diffusion control of the reaction rate, this system can be modelled as a well-mixed gas in equilibrium with a solid phase. As such, the modelling effort has focussed on characterizing the copolymerization kinetics occurring at the multiple active sites of the catalyst. Two potential uses for such a model are the simulation and testing of on-line quality control schemes and the prediction of the effects of grade transition policies on molecular weight and compositional distributions.

2.2 REACTION MECHANISMS

The mechanisms described here are similar to those outlined by Kissin (1987) and deCarvalho et al. (1989). In general, each site type is associated with different rate constants for formation, initiation, propagation and transfer. These reaction mechanisms consider the effects of terminal monomers on reaction rates; penultimate effects are neglected. The model is developed to account for any number of active site types and for copolymerization of ethylene and several comonomers. Throughout this section, the index j will refer to the type of active site and i will refer to the monomer type.

2.2.1 Formation and Initiation of Active Sites

Potential active sites of type j undergo a formation reaction with the organometallic cocatalyst (Kissin, 1987). If the cocatalyst concentration is constant and in excess, this reaction can be described as:

$$N^*(j) \overset{kf(j)}{\rightarrow} N(0,j) \tag{1}$$

where $kf(j)$ is a pseudo rate constant for the formation reaction, $N^*(j)$ is a potential active site of type j and $N(0,j)$ is an active site of type j with no attached monomer.

The newly formed sites undergo initiation reactions with monomers:

$$N(0,j)+M_i \xrightarrow{ki_i(j)} N_i(1,j) \qquad i=1,2... \tag{2}$$

M_i denotes monomer of type i. If $i=1$, the monomer is ethylene; $i=2$ and $i=3$ correspond to alpha-olefin comonomers such as butene or hexene. $ki_i(j)$ is an initiation rate constant and $N_i(1,j)$ is a living polymer chain of length one.

2.2.2 Propagation

Living polymer chains grow by the following propagation reactions:

$$N_i(r,j)+M_k \xrightarrow{kp_{ik}(j)} N_k(r+1,j) \qquad i=1,2,\ldots \qquad k=1,2,\ldots \tag{3}$$

$N_i(r,j)$ is a living polymer chain of length r with terminal monomer i attached to the active center of type j. $kp_{ik}(j)$ is the propagation rate constant for the reaction of monomer M_k with an active center of type j, bonded to a terminal monomer M_i.

2.2.3 Chain Transfer Reactions

Most dead polymer chains are produced by chain transfer reactions. These reactions occur with monomers, hydrogen and organometallic cocatalyst. As well, spontaneous transfer reactions have been documented (Kissin, 1987).

2.2.3.1 Transfer to Monomer

The following chain transfer to monomer reactions can occur:

$$N_i(r,j)+M_k \xrightarrow{kfm_{ik}(j)} N_k(1,j)+Q(r,j) \qquad i=1,2,\ldots \qquad k=1,2,\ldots \tag{4}$$

$Q(r,j)$ is a dead polymer segment of length r which cannot undergo any further reactions. Note that transfer to monomer reactions produce living polymer chains of length one, $N_k(1,j)$ which can propagate to form new polymer chains.

2.2.3.2 Transfer to Hydrogen

Hydrogen is added to industrial reactors making linear polyethylene to control molecular weight development via chain transfer:

$$N_i(r,j)+H_2 \xrightarrow{kfh_i(j)} N_H(0,j)+Q(r,j) \qquad i=1,2,\ldots \tag{5}$$

Species $N_H(0,j)$ is an active site with no reacted monomer which can undergo reinitiation reactions:

$$N_H(0,j)+M_i \xrightarrow{kh_i(j)} N_i(1,j) \qquad i=1,2,\ldots \tag{6}$$

These sites are quickly reinitiated by reactions with the cocatalyst. If the cocatalyst, AlA is triethyl aluminum, the reinitiation reaction is (Kissin, 1987):

$$N_H(0,j)+AlA \xrightarrow{kh_r(j)} N_1(1,j) \tag{7}$$

The product $N_1(1,j)$ has the same reactive characteristics as the sites produced by initiation and transfer reactions with ethylene. This is not the case for a general cocatalyst.

2.2.3.3 Transfer to Cocatalyst

Growing polymer chains can undergo transfer reactions with the cocatalyst:

$$N_i(r,j)+AlA \xrightarrow{kfr_i(j)} N_1(1,j)+Q(r,j) \qquad i=1,2,\ldots \tag{8}$$

2.2.3.4 Spontaneous Transfer

Depending on the catalyst, spontaneous transfer reactions may be significant for some or all site types:

$$N_i(r,j) \xrightarrow{kfs_i(j)} N_H(0,j)+Q(r,j) \qquad i=1,2,\ldots \tag{9}$$

The sites produced by spontaneous transfer are thought to have a structure similar to those produced by transfer to hydrogen reactions (Kissin, 1987) .

2.2.3.5 Deactivation Reactions

Active sites may decay spontaneously to form dead sites and dead polymer chains:

$$N_i(r,j) \xrightarrow{kds(j)} N_d(j)+Q(r,j) \qquad i=1,2,\ldots \tag{10}$$

$$N(0,j) \xrightarrow{kds(j)} N_d(j) \tag{11}$$

$$N_H(0,j) \xrightarrow{kds(j)} N_d(j) \tag{12}$$

where $N_d(j)$ is a dead site of type j and $kds(j)$ is a decomposition rate constant.

In this formulation, it has been assumed that the rate of deactivation is not influenced by the terminal monomer nor chain length.

2.2.3.6 Reactions with Poisons

Even low levels of some reactive impurities, such as carbon monoxide, can cause a nearly instantaneous drop in propagation rates. The adsorption of such an impurity onto a catalyst site renders it inactive:

$$N_i(r,j)+I_m \xrightarrow{kdI(j)} N_{dIH}(0,j)+Q(r,j) \qquad i=1,2,\ldots \tag{13}$$

$$N_H(0,j)+I_m \overset{kdI(j)}{\rightarrow} N_{dIH}(0,j) \tag{14}$$

$$N(0,j)+I_m \underset{kdI(j)}{\rightarrow} N_{dI}(0,j) \tag{15}$$

I_m is the impurity, $kdI(j)$ is an impurity deactivation rate constant and $N_{dIH}(0,j)$ and $N_{dI}(0,j)$ are sites deactivated by adsorbed impurities. The reactions above may be reversible for some poisons, in which case, desorption of the impurity leaves sites which can undergo reinitiation reactions:

$$N_{dIH}(0,j) \overset{ka(j)}{\rightarrow} N_H(0,j)+I_m \tag{16}$$

$$N_{dI}(0,j) \overset{ka(j)}{\rightarrow} N(0,j)+I_m \tag{17}$$

$ka(j)$ is an impurity desorption rate constant.

2.3 MODEL DEVELOPMENT

When modelling a single pass fluidized bed reactor or a recycle reactor with high conversion per pass, one must account for gas phase concentration gradients between the bottom and top of the bed and for mass transfer between bubble and emulsion phases. However, the modelling of the input/output characteristics of a recycle dominated fluidized bed reactor for polymers can be greatly simplified by making suitable assumptions. Since the industrial fluidized bed reactor system under consideration has a sizable recycle stream and a low conversion per pass through the bed, the vertical concentration gradient through the bed is very small and can be neglected. Back-mixing of both the gas and solid phases in the fluidized bed does occurs. Even with poor mixing, the large recycle to fresh feed ratio makes the well mixed assumption valid for the gas

phase since recycle plug flow reactor dynamics approach those of continuous stirred tank reactor (CSTR) as the recycle to fresh feed ratio becomes very large (Levenspiel, 1972). In normal industrial reactor operation, the recycle to fresh feed ratio is approximately 40:1 (Choi and Ray, 1985). Thus modelling the fluidized bed reactor plus recycle system as a CSTR containing a well-mixed solid phase interacting with a well-mixed gas phase is justified. Talbot (1990) discusses the range of reactor operating conditions under which the well-mixed CSTR assumption is valid for fluidized bed polyethylene reactors.

Thermocouples at different vertical positions in the reactor indicate that vertical temperature gradients are small in the reaction zone. A rise of only a few $^{\circ}C$ between the bottom and top of the bed is typical at steady state. In this model it is assumed that the effects of any small radial or vertical temperature gradients within the reaction zone can be neglected.

2.3.1 Temperature Effects

It is important to include temperature effects in the kinetic model because the dynamic temperature changes have a marked effect on the properties of the polymer produced. The main effect of temperature on product quality is due to the different activation energies for propagation and chain transfer reactions. Increasing reactor temperature increases the ratio of chain transfer to propagation reactions and results in a lower molecular weight polymer. A secondary effect results from the influence of temperature on the solubility of monomers in the polymer particles where the polymerization reaction occurs.

The effect of temperature on propagation and chain transfer rate constants has been included in the model using Arrhenius expressions:

$$k(T) = A \exp\left(\frac{-E_a}{RT}\right) \tag{2.1}$$

where k is a temperature dependent rate constant, E_a is the activation energy, A is the pre-exponential factor, R is the ideal gas constant and T is the reactor temperature. If a value of k is known at some reference temperature T_{ref}, then:

$$k(T) = k(T_{ref}) \exp\left\{\frac{-E_a}{R}\left(\frac{1}{T} - \frac{1}{T_{ref}}\right)\right\} \tag{2.2}$$

This type of expression can be written for each of the rate constants in the model. If a set of rate constants is known for some reference temperature, then all that is required to incorporate temperature effects into the individual rate constants is a set of corresponding activation energies. Choi and Ray (1985) suggest a value of 9000 cal/mol for both ethylene and propylene propagation reactions using a heterogeneous *ZN* catalyst. Although each individual rate constant at each site type may have a different activation energy, for lack of better informaion, a single value of 9000 cal/mol has been adopted for all propagation reactions in the model. It has been observed in industrial reactors that copolymer composition and density are insensitive to changes in operating temperature if gas compositions remain constant. The assumption of similar activation energies for both ethylene and comonomer propagation reactions is consistent with this observation. The activation energy used in this thesis for all chain transfer reactions has been arbitrarily set at 14000 cal/mol. Since this value is higher than that for propagation reactions, the model predicts that temperature increases result in the formation of lower molecular weight polyethylene. This type of response is typical for *ZN* catalysts (Kissin, 1987).

Several different catalysts are used in commercial gas phase polyethylene reactors. Each has its own set of values for rate constants and activation energies. The purpose of including temperature effects in the model is to show the qualitative effects of changing temperature on reactor operation, rather than to achieve a quantitative match for a specific industrial catalyst. While the addition of Arrhenius expressions to the rate constants captures the major effect of temperature on reactor behaviour, changes in temperature also influence the partitioning of reactants between the gas and polymer phases. This effect is discussed in section 2.3.2.

2.3.2 Effect of Gas Sorption in the Polymer Particles

When new catalyst particles are injected into a gas phase reactor, the active sites are quickly covered by the growing polymer chains. Thus, reaction rates are controlled by the concentrations of reactants dissolved in the polymer surrounding the sites rather than by bulk concentrations in the gas phase. Since diffusional resistances can be neglected for gas phase olefin polymerizations (Floyd et al., 1986), the concentrations of species at the active sites are determined by the composition of the gas phase and on the equilibrium partitioning of components between the gas and polymer phases. In general, the solubility of gaseous substances in olefin polymers depends on the degree of crystallinity. Gases are sorbed only into the amorphous regions of the polymer. In a recent paper, Hutchinson and Ray (1990) suggest that, during the reaction, successive polymerization and crystallization occur. Since the polymer chains grow away from the catalyst surface, the polymer at the sites is in a nascent, amorphous state. Thus, the crystallinity or density of the polymer being produced is not expected to affect monomer concentrations at the catalyst sites.

2.3.2.1 Prediction of Gas Sorption in Amorphous Polymer

At low pressures, the sorption of gases in the amorphous regions of the polymer is governed by Henry's law:

$$[M_i]^* = k_{Hi}^* P_i \tag{2.3}$$

where $[M_i]^*$ is the concentration of component i in the polymer expressed in moles of i dissolved per gram of amorphous polymer. P_i is the partial pressure of i in atm and k_{Hi}^* is the Henry's law coefficient for component i in moles/(g amorphous polymer • atm).

At higher pressures, the sorbed vapour swells and plasticizes the polymer resulting in higher polymer chain mobility and enhanced penetrant solubility. Most modelling of gas-polymer solubility outside of the Henry's law region is based on the Flory-Huggins model:

$$\ln(a_i) = \ln(v_i) + v_p + \chi_{ip}(v_p)^2 \tag{2.4}$$

The activity coefficient a_i is usually expressed as:

$$a_i = \frac{P_i}{P_i^0} \tag{2.5}$$

where P_i is the partial pressure of the vapour above the polymer and P_i^0 is the vapour pressure of the pure liquid. v_i and v_p are the volume fractions of the penetrant and polymer, respectively. χ_{ip} is the Flory-Huggins interaction parameter. If χ_{ip} is small, then the solubility of the gas in the polymer is high. Conversely, a large value of χ_{ip} corresponds to low gas solubility in the polymer. Hutchinson and Ray (1990) show that, at low pressures, $v_p \approx 1$, so that equation 2.4 is equivalent to:

$$v_i = \frac{1}{P_i^0[\exp(1+\chi_{ip})]} P_i \tag{2.6}$$

which is a form of Henry's law. For the hydrocarbon vapours present in gas phase polyethylene reactors, Hutchinson and Ray (1990) suggest the following semi-empirical model form to describe deviations from Henry's law:

$$k^* = k_H^* \exp(\sigma[M]^*) \tag{2.7}$$

This model form can also be derived from the Flory-Huggins expression (Frensdorff, 1964). k^* is the solubility coefficient at the penetrant concentration and σ is a proportionality constant. As $[M]^*$ approaches zero, k^* approaches k_H^*, the Henry's law constant.

It has been shown that Henry's law coefficients change with temperature according to:

$$\log(k_H^*) = a + b\left(\frac{T_c}{T}\right)^2 \tag{2.8}$$

Equation 2.8 was proposed by Stern et al. (1969) who observed that Henry's law coefficients for the solubility of common gases in polyethylene increase with the critical temperature, T_c, and decrease with the actual temperature, T. Hutchinson and Ray (1990) fitted parameters a and b using experimental data from the literature for alkane and alkene solubility in polyethylene to obtain the following relationship:

$$\log(k_H^*) = -2.38 + 1.08\left(\frac{T_c}{T}\right)^2 \tag{2.9}$$

They obtained an excellent fit for k_H^* spanning several orders of magnitude.

Whether or not Henry's law is applicable depends to some extent on temperature as well as pressure. Stern et al. (1969) developed a single component correlation to predict when deviations from Henry's law become significant:

$$\log\left(\frac{P_{dev}}{P_c}\right) = 3.025 - 3.50\left(\frac{T_c}{T}\right) \tag{2.10}$$

P_c is the critical pressure of the gas and P_{dev} is the pressure at which a 5% deviation from Henry's law occurs. Under most operating conditions in gas phase polyethylene reactors, the partial pressures of the individual components are less than the corresponding values of P_{dev}. However, for some grades which are produced with higher comonomer concentrations, significant deviations from Henry's law are predicted.

When Henry's law is valid, the concentrations of individual species sorbed in the polymer are independent. However, when a heavier vapour component is sorbed beyond the Henry's law region, this penetrant plasticizes the polymer, resulting in enhanced solubility of both itself and other vapour phase components. The assumption that the sorption of the individual components is independent no longer applies. Robeson and Smith (1968) have illustrated this concept experimentally for a system of butane and ethane in polyethylene. They show that butane sorption beyond the Henry's law region enhances ethane solubility even though ethane by itself would obey Henry's law at the partial pressures considered. At constant temperature, their experiments show that:

$$\frac{k^*_{but}}{k^*_{eth}} \approx constant \tag{2.11}$$

regardless of the individual partial pressures, indicating that the percentage enhancements in butane and ethane sorption are very similar. There is little theory currently available to predict multi-component solubility of gases in polyethylene beyond the Henry's law region. Equations 2.7 and 2.10 have been developed for single penetrant systems. However, if one assumes that the relative change in the solubility coefficients is the same for all components, then the principal of corresponding states can be applied to predict multi-component sorption in polyethylene. A pseudo-critical temperature and pressure can be calculated for the gas mixture using procedures outlined by Reid et al. (1977). These pseudo-critical properties can then be used in equation 2.10 to calculate P_{dev} for the gas mixture. If P_{dev} is greater than the total system pressure, the predicted deviation from Henry's law is less than 5% and the assumption of independent sorption can be applied. Otherwise, a value of k_H^* for the mixture can be obtained from equation 2.9. Since P_{dev} results in a 5% deviation from Henry's law, at the deviation pressure:

$$[M]^*_{dev} = 1.05\, k_H^*\, P_{dev} = k_H^* \exp(\sigma[M]^*_{dev}) P_{dev} \tag{2.12}$$

Equation 2.12 can be solved to obtain both $[M]^*_{dev}$, the total monomer sorbed in the polymer at the deviation pressure, and σ the proportionality constant for the gas mixture. Assuming that all components experience the same percentage deviation in solubility, this value of σ can be used in:

$$[M]^*_T = k_H^* \exp(\sigma[M]^*_T)\, P_T \tag{2.13}$$

to calculate $[M]^*_T$ which is a pseudo total penetrant concentration in the polymer at the total pressure P_T. The ratio of the true quantitiy of gas sorbed to that predicted

by Henry's law is then given by $\exp(\sigma[M]_T^*)$. This correction factor should be applied to each of the Henry's law predictions for the individual monomer concentrations.

2.3.2.2 Expressing Reaction Rates in Terms of Gas Phase Concentrations

It is very convenient to express the kinetic model of the reactor in terms of gas phase monomer concentrations and corresponding pseudo-rate constants which incorporate partition coefficients. The effects of both temperature and deviations from Henry's law can be incorporated into the model by calculating a correction factor, ξ, for each partition coefficient. If $K_p(M_i, 360)$ is the Henry's law partition coefficient for monomer M_i at 360 K, then at 360 K and low pressures:

$$[M_i]_{pol} = K_p(M_i, 360)\,[M_i]_{gas} \tag{2.14}$$

At all other temperatures and when Henry's law does not apply, the relationship becomes:

$$[M_i]_{pol} = \xi\, K_p(M_i, 360)\,[M_i]_{gas} \tag{2.15}$$

The correction factor ξ can be determined from:

$$\xi = 12.023^{\left(\frac{T_c}{T}\right)^2 - \left(\frac{T_c}{360}\right)^2} \exp(\sigma[M]_T^*) \tag{2.16}$$

The first term in equation 2.16 accounts for the effect of temperature on the Henry's law constant (Hutchinson and Ray, 1990). The exponential term accounts for deviations from Henry's law.

For each component one can write:

$$[M_i]_{pol} = K_p[M_i]_{gas} \tag{2.17}$$

gas where $[M_i]_{pol}$ and $[M_i]_{gas}$ are the concentrations of component i at the catalyst sites within the polymer particles and in the gas phase, respectively. K_p is a partition coefficient which accounts for temperature effects and deviations from Henry's law as in equation 2.15. If the rate, R, of a certain reaction, occurring at a site of type j is given by:

$$R = k[M_i]_{pol} Y(0,j) \tag{2.18}$$

where k is a rate constant and $Y(0,j)$ is the number of moles of active sites of type j in the reactor, then one can also write:

$$R = k^g [M_i]_{gas} Y(0,j) \tag{2.19}$$

where

$$k^g = (kK_p) \tag{2.20}$$

is a pseudo rate constant. In the following model equations, all rate constants are of the same type as k^g and all concentrations are those in the gas phase. This convention is used because gas phase concentrations are measured on-line in the industrial reactor, whereas concentrations in the amorphous polymer are not well known.

2.3.3 Mass Balance Equations for Active Sites

Dynamic mass balances of the form:

$$Accumulation = Inflow + Generation - Consumption - Outflow \tag{2.21}$$

can be developed for each reacting species. The balance on the number of moles of potential active sites $N^*(j)$ in the reactor is given by:

$$\frac{dN^*(j)}{dt} = F^*_{in}(j) - kf(j)N^*(j) - N^*(j)\frac{R_v}{V_p} \tag{2.22}$$

where $F_{in}^{*}(j)$ is the molar flow rate of potential active sites into the reactor which is proportional to the mass feed rate of the catalyst, R_v is the volumetric flow rate of polymer from the reactor and V_p is the volume of the polymer phase in the reactor. Similarly, for the number of moles of initiation sites $N(0,j)$ and $N_H(0,j)$:

$$\frac{dN(0,j)}{dt} = kf(j)N^{*}(j) + ka(j)N_{dl}(0,j) - N(0,j)\left\{ki_T(j)[M_T] + kds(j) + kdI(j)[I_m] + \frac{R_v}{V_p}\right\} \tag{2.23}$$

$$\frac{dN_H(0,j)}{dt} = Y(0,j)\{kfh_T(j)[H_2] + kfs_T(j)\} + ka(j)N_{dlH}(0,j) \tag{2.24}$$

$$-N_H(0,j)\left\{kh_T(j)[M_T] + kds(j) + kh_r(j)[AlA] + kdI(j)[I_m] + \frac{R_v}{V_p}\right\}$$

where $[M_T]$ is the total molar monomer concentration given by:

$$[M_T] = [M_1] + [M_2] + \ldots \tag{2.25}$$

$[M_1]$, $[M_2]$, $[M_3]$ and $[H_2]$ are the concentrations of ethylene, butene, hexene and hydrogen, respectively. $Y(0,j)$ is the zeroth moment of the living polymer chain length distribution:

$$Y(0,j) = \sum_{r=1}^{\infty}\{N_1(r,j) + N_2(r,j) + \ldots \quad\} \tag{2.26}$$

$ki_T(j)$, $kfh_T(j)$, $kfs_T(j)$ and $kh_T(j)$ are pseudo-kinetic rate constants.

The following mass balance can be written for initiated polymer chains of length one with ethylene as the terminal monomer :

$$\frac{dN_1(1,j)}{dt} = ki_1(j)N(0,j)[M_1] + N_H(0,j)\{kh_1(j)[M_1] + kh_r(j)[AlA]\} \tag{2.27}$$

$$+Y(0,j)\{kfm_{T1}(j)[M_1] + kfr_T(j)[AlA]\}$$

$$-N_1(1,j)\{kp_{1T}(j)[M_T] + kfm_{1T}(j)[M_T] + kfh_1(j)[H_2]$$

$$+kfr_1(j)[AlA] + kfs_1(j) + kds(j) + kdI(j)[I_m] + \frac{R_v}{V_p}\}$$

Similarly, for any other terminal monomer, M_i:

$$\frac{dN_i(1,j)}{dt} = ki_i(j)N(0,j)[M_i] + N_H(0,j)kh_i(j)[M_i] \tag{2.28}$$

$$+Y(0,j)kfm_{Ti}(j)[M_i]$$

$$-N_i(1,j)\{kp_{iT}(j)[M_T] + kfm_{iT}(j)[M_T] + kfh_i(j)[H_2]$$

$$+kfr_i(j)[AlA] + kfs_i(j) + kds(j) + kdI(j)[I_m] + \frac{R_v}{V_p}\} \qquad i = 2,3,\ldots$$

The numbers of moles of impurity deactivated sites conform to the following mass balances:

$$\frac{dN_{dIH}(0,j)}{dt} = kdI(j)[I_m]\{Y(0,j) + N_H(0,j)\} - N_{dIH}(0,j)\left\{ka(j) + \frac{R_v}{V_p}\right\} \tag{2.29}$$

$$\frac{dN_{dI}(0,j)}{dt} = kdI(j)[I_m]N(0,j) - N_{dI}(0,j)\left\{ka(j) + \frac{R_v}{V_p}\right\} \tag{2.30}$$

Balances on living polymer of chain length r with terminal monomers M_i ($i = 1,2,\ldots$) were generated and added together to give the following mass balance on $Y(0,j)$, the zeroth moment of the living polymer chain length distribution:

$$\frac{dY(0,j)}{dt} = [M_T]\{ki_T(j)N(0,j) + kh_T(j)N_H(0,j)\} + kh_r(j)N_H(0,j)[AlA] \tag{2.31}$$

$$-Y(0,j)\left\{kfh_T(j)[H_2] + kfs_T(j) + kds(j) + kdI(j)[I_m] + \frac{R_v}{V_p}\right\}$$

As well, mass balances on the first and second moments of the living polymer distribution were determined:

$$\frac{dY(1,j)}{dt} = [M_T]\{ki_T(j)N(0,j) + kh_T(j)N_H(0,j)\} + kh_r(j)N_H(0,j)[AlA] \tag{2.32}$$

$$+[M_T]kp_{TT}(j)Y(0,j) + \{Y(0,j) - Y(1,j)\}\{kfm_{TT}(j)[M_T] + kfr_T(j)[AlA]\}$$

$$-Y(1,j)\left\{kfh_T(j)[H_2] + kfs_T(j) + kds(j) + kdI(j)[I_m] + \frac{R_v}{V_p}\right\}$$

$$\frac{dY(2,j)}{dt} = [M_T]\{ki_T(j)N(0,j) + kh_T(j)N_H(0,j)\} + kh_r(j)N_H(0,j)[AlA] \tag{2.33}$$

$$+[M_T]kp_{TT}(j)\{2Y(1,j) - Y(0,j)\}$$

$$+\{Y(0,j) - Y(2,j)\}\{kfm_{TT}(j)[M_T] + kfr_T(j)[AlA]\}$$

$$-Y(2,j)\left\{kfh_T(j)[H_2] + kfs_T(j) + kds(j) + kdI(j)[I_m] + \frac{R_v}{V_p}\right\}$$

where $Y(n,j)$, the $n-th$ moment of the living polymer chain length distribution, is given by:

$$Y(n,j) = \sum_{r=1}^{\infty} r^n\{N_1(r,j) + N_2(r,j) + \ldots\} \qquad n = 0,1,2... \tag{2.34}$$

The molecular weight of the polymer produced in the reactor is determined by the method of moments. As such, the following balances are required for the $n-th$ moments of the chain length distributions for dead polymer chains:

$$\frac{dX(n,j)}{dt} = \{Y(n,j) - N_T(1,j)\}\{kfm_{TT}(j)[M_T] + kfr_T(j)[AlA] + kfh_T(j)[H_2] \tag{2.35}$$

$$+kfs_T(j) + kds(j) + kdI(j)[I_m]\} - X(n,j)\frac{R_v}{V_p} \qquad n = 0,1,2$$

The moments of the dead polymer distribution are defined by:

$$X(n,j) = \sum_{r=2}^{\infty} r^n Q(r,j) \tag{2.36}$$

The summation above starts at $r = 2$ because dead chains of length one are not considered polymer. The mass balances for the moments of the dead polymer chain length distribution were obtained by writing a mass balance on dead polymer segments of length r and substituting the result into the definition for the moments given above.

2.3.4 Pseudo-Kinetic Rate Constants

The use of pseudo-kinetic rate constants for general copolymerization kinetics is outlined by Hamielec et al. (1987). The model mass balance equations contain the following pseudo-kinetic rate constants which depend upon the composition of the reaction medium and upon the distribution of terminal monomers at each site type. The pseudo-kinetic rate constants shown here are for a three monomer system. The definitions can be expanded to include more monomer types if required.

Pseudo-rate constant $kh_T(j)$ is defined as:

$$kh_T(j) = f_1\, kh_1(j) + f_2\, kh_2(j) + f_3\, kh_3(j) \tag{2.37}$$

An analogous relationship can be written for $ki_T(j)$. f_i is the mole fraction of the total monomer which is of type i:

$$f_i = \frac{[M_i]}{[M_1]+[M_2]+[M_3]} \tag{2.38}$$

There are three types of pseudo-kinetic propagation constants used in the model:

$$kp_{iT}(j) = f_1\, kp_{i1}(j) + f_2\, kp_{i2}(j) + f_3\, kp_{i3}(j) \tag{2.39}$$

$$kp_{Ti}(j) = \phi_1(j)\, kp_{1i}(j) + \phi_2(j)\, kp_{2i}(j) + \phi_3(j)\, kp_{3i}(j) \tag{2.40}$$

$$kp_{TT}(j) = f_1\, kp_{T1}(j) + f_2\, kp_{T2}(j) + f_3\, kp_{T3}(j) \tag{2.41}$$

$\phi_i(j)$ is the fraction of active sites of type j having terminal monomer M_i. For a three monomer system:

$$\phi_1(j) = \frac{f_1^2\, kp_{21}(j)kp_{31}(j) + f_1f_2\, kp_{21}(j)kp_{32}(j) + f_1f_3\, kp_{23}(j)kp_{31}(j)}{\Psi(j)} \tag{2.42}$$

$$\phi_2(j) = \frac{f_1f_2\, kp_{12}(j)kp_{31}(j) + f_2^2\, kp_{12}(j)kp_{32}(j) + f_2f_3\, kp_{13}(j)kp_{32}(j)}{\Psi(j)} \tag{2.43}$$

$$\phi_3(j) = 1 - \phi_1(j) - \phi_2(j) \tag{2.44}$$

where the denominator $\Psi(j)$ is given by:

$$\begin{aligned}\Psi(j) = {} & f_1^2\, kp_{21}(j)kp_{31}(j) + f_1f_2\, kp_{21}(j)kp_{32}(j) + f_1f_3\, kp_{23}(j)kp_{31}(j) \\ & + f_1f_2\, kp_{12}(j)kp_{31}(j) + f_2^2\, kp_{12}(j)kp_{32}(j) + f_2f_3\, kp_{13}(j)kp_{32}(j) \\ & + f_2f_3\, kp_{12}(j)kp_{23}(j) + f_1f_3\, kp_{13}(j)kp_{21}(j) + f_3^2\, kp_{13}(j)kp_{23}(j)\end{aligned} \tag{2.45}$$

The equations for $\phi_i(j)$ were obtained by making the second long chain approximation for growing polymer chains.

The transfer to monomer pseudo rate constants $kfm_{iT}(j)$, $kfm_{Ti}(j)$ and $kfm_{TT}(j)$ are defined analogously to the propagation pseudo rate constants. The three other transfer pseudo rate constants for transfer to hydrogen, to cocatalyst and for spontaneous transfer are:

$$kfh_T(j) = \phi_1(j)kfh_1(j) + \phi_2(j)kfh_2(j) + \phi_3(j)kfh_3(j) \tag{2.46}$$

$$kfr_T(j) = \phi_1(j)kfr_1(j) + \phi_2(j)kfr_2(j) + \phi_3(j)kfr_3(j) \tag{2.47}$$

$$kfs_T(j) = \phi_1(j)kfs_1(j) + \phi_2(j)kfs_2(j) + \phi_3(j)kfs_3(j) \tag{2.48}$$

2.3.5 Mass Balances for Reacted Monomers in the Copolymer

In order to predict the composition of the copolymer in the reactor at any time, mass balances have been performed on the number of moles of each type of monomer incorporated or bound in the polymer particles:

$$\frac{dB_i}{dt} = R_i - B_i\frac{R_v}{V_p} \qquad i = 1,2,\ldots \tag{2.49}$$

B_i is the number of moles of monomer i which are bound in the polymer in the reactor and R_i is the instantaneous consumption rate of monomer i to form polymer. Assuming that the only significant consumption of monomers is by propagation leads to the following expression for consumption rate:

$$R_i = \sum_{j=1}^{NS}[M_i]Y(0,j)kp_{Ti}(j) \qquad i = 1,2,\ldots \tag{2.50}$$

where NS is the number of types of active sites. The volumetric outflow rate of polymer, R_v, which appears in the model equations, can be determined from the consumption rates of the monomers and from the rate of change of the weight of polymer in the reactor:

$$R_v = \frac{mw_1 R_1 + mw_2 R_2 + \ldots}{\rho} - \frac{dB_w/dt}{\rho} \qquad (2.51)$$

mw_i is the molecular weight of monomer i in g/mol, ρ is the density of the polymer in g/L and B_w is the mass of resin in the reactor.

2.3.6 Model Simplification

The set of model equations has been solved numerically by LSODE, a differential equation solving package (Hindmarsh, 1980). This set of equations is stiff because the dynamics associated with changes in intermediate species $N^*(j)$, $N_H(0,j)$, $N(0,j)$ and $N_i(1,j)$ are very fast compared to the dynamics associated with the other states in the model. In order to reduce the computational effort for model solution, the stationary state hypothesis was made for these species. The corresponding differential equations were, thus, converted to algebraic equations by setting the left hand side derivative terms to zero. Simulations were performed, using realistic rate constants, to compare the predictions of the full set of stiff equations with those of the non-stiff system of algebraic and differential equations solved in the simplified model. No significant differences between the two solutions were observed, indicating that the pseudo steady state hypothesis was valid.

2.3.7 Copolymer Composition and Molecular Weight Properties

The mole fraction of each reacted comonomer bound in the polymer, F_i, can be calculated from:

$$F_i = \frac{B_i}{B_1 + B_2 + \ldots} \qquad i = 1,2,\ldots \qquad (2.52)$$

The cumulative number and weight average molecular weights, $\overline{M}_n$ and $\overline{M}_w$, can be determined using the method of moments:

$$\overline{M}_n = \frac{\overline{m} \sum_{j=1}^{NS} \{X(1,j) + Y(1,j)\}}{\sum_{j=1}^{NS} \{X(0,j) + Y(0,j)\}} \tag{2.53}$$

$$\overline{M}_w = \frac{\overline{m} \sum_{j=1}^{NS} \{X(2,j) + Y(2,j)\}}{\sum_{j=1}^{NS} \{X(1,j) + Y(1,j)\}} \tag{2.54}$$

where $\overline{m}$ is the mean monomer molecular weight defined by:

$$\overline{m} = mw_1 F_1 + mw_2 F_2 + \ldots \tag{2.55}$$

The polydispersity, Z, is defined by the ratio of weight average to number average molecular weights:

$$Z = \frac{\overline{M}_w}{\overline{M}_n} \tag{2.56}$$

Note that although this model predicts that each active site type produces polymer with a polydispersity of 2, the cumulative polymer produced at all sites can have a much broader molecular weight distribution (Floyd et al., 1988).

In addition to cumulative average molecular weights and copolymer compositions, the entire instantaneous molecular weight and compositional distributions can be generated for polymer produced at each site type using the Stockmayer (1945) bivariate distribution for two monomer systems. In Ziegler-Natta systems, the only important reactions which produce dead polymer chains are transfer

reactions. Thus, the Stockmayer (1945) equation for the weight fraction of dead polymer produced at a site of type j which has chain length between r and $r+dr$ and composition between y and $y+dy$ can be expressed as:

$$W(r,y,j)dr\,dy = \tau(j)^2 r \exp(-\tau(j)r)dr \quad \frac{1}{\sqrt{2\pi\sigma(j)^2}}\exp\left(\frac{-y^2}{2\sigma(j)^2}\right)dy \tag{2.57}$$

$\tau(j)$ is the ratio of the total rate of chain transfer to the total rate of propagation at the sites of type j:

$$\tau(j) = \frac{kfm_{TT}(j)[M_T] + kfh_T(j)[H_2] + kfr_T(j)[AlA] + kfs_T(j)}{kp_{TT}(j)[M_T]} \tag{2.58}$$

$\sigma(j)^2$ is the variance of the compositional distribution at the sites of type j given by:

$$\sigma(j)^2 = \overline{F_1}(j)(1-\overline{F_1})\kappa/r \tag{2.59}$$

$$\kappa = \{1 + 4\overline{F_1}(j)(1-\overline{F_1}(j))(r_1 r_2 - 1)\}^{0.5} \tag{2.60}$$

y is the deviation of the composition from $\overline{F_1}(j)$, the mean mole fraction of ethylene in the dead polymer chains produced instantaneously at sites of type j:

$$\overline{F_1}(j) = \frac{R_1(j)}{R_1(j)+R_2(j)} \tag{2.61}$$

where $R_i(j)$ is the instantaneous rate of consumption of monomer i at sites of type j:

$$R_i(j) = kp_{Ti}[M_i]Y(0,j) \tag{2.62}$$

The individual site specific distributions can then be combined to give the overall instantaneous composition and chain length distribution:

$$W(r,y)drdy = \frac{\sum_{j=1}^{NS} M_x(j)W(r,y,j)drdy}{\sum_{j=1}^{NS}\int_y\int_r M_x(j)W(r,y,j)drdy} \tag{2.63}$$

$M_x(j)$ is the instantaneous mass rate of production of polymer at sites of type j:

$$M_x(j) = mw_1R_1(j) + mw_2R_2(j) + \ldots \tag{2.64}$$

The overall compositional distribution is obtained by integrating the expression for $W(r,y)drdy$ over all chain lengths. Similarly, $W(r,y)drdy$ can be integrated over all compositions to obtain the molecular weight distribution.

In the original development of the Stockmayer (1945) equation, it was assumed that the molecular weights of the two monomers were equal. For cases when the monomers have molecular weights which differ by an order of magnitude, a correction factor developed by Tacx et al. (1988) can be used to account for the effect of the monomer molecular weight difference. For the ethylene/butene copolymers considered in this study, the frequency distributions predicted by the corrected and uncorrected Stockmayer distribution differed by less than 2 per cent, even at the site characterized by high butene incorporation. Thus, the simpler uncorrected Stockmayer distribution was used for instantaneous molecular weight and compositional distributions.

2.3.8 Melt Index and Density Predictions

The model solution predicts reaction rate, weight and number average molecular weights and comonomer composition from reactor operating conditions. In the industrial reactor, the reaction rate is estimated on-line using an energy balance. Fundamental molecular weight and compositional properties, however, are neither measured on-line nor in the quality control laboratory. Instead, melt index (MI) and

density, which are related to molecular weight and composition, are determined. In order to compare model predictions with operating results, it is necessary to relate *MI* and density to fundamental properties predicted by the model.

Sinclair (1983) has compiled a collection of data from commercial and patent literature. A graph of melt index vs weight average molecular weight, $\overline{M}_w$, has been plotted from data in this report and is shown in Figure 2.1. From the data, it appears that *MI* and $\overline{M}_w$ can be related by a power law. Linear regression was performed on the data in Figure 2.1 to yield the following correlation:

$$\ln(\overline{M}_w) = 11.622 - 0.288 \ln(MI) \tag{2.65}$$

or

$$\overline{M}_w = 111525 \quad MI^{-0.288} \tag{2.66}$$

This equation has been used to convert laboratory *MI* results to approximate weight average molecular weights for comparison with model predictions. Since melt index is inversely proportional to the apparent viscosity of the molten polymer under low shear, η, the preceding equation can be written as:

$$\overline{M}_w \propto \eta^{0.288} \tag{2.67}$$

or

$$\eta \propto \overline{M}_w^{3.47} \tag{2.68}$$

This relationship corresponds to the general observation (Vinogradov and Malkin, 1980; Bremner et al., 1990) for linear polymers that:

$$\eta = b M_w^{3.5} \qquad M_w \geq M_c \tag{2.69}$$

where M_w is the molecular weight of the monodisperse polymer fraction and M_c is the critical molecular weight above which this expression is valid. The critical molecular weight for polyethylene is approximately 4000. The preceding power law

equation is valid for polydisperse polymers where M_w is the weight average molecular weight, provided that the fraction of the polymer with molecular weight less than M_c is insignificant.

The relationship between density and polymer structure is complex. Density is influenced by both the number and length of the short chain branches (Sinclair, 1980) and to a small extent by the polymer molecular weight. An empirical correlation has been developed to relate the density of linear polyethylene to comonomer incorporation in the polymer:

$$\rho = 0.966 - A C_x^{\ B} \tag{2.70}$$

C_x is the mole percent of the comonomer in the polymer and A and B are comonomer dependent parameters. The model structure was chosen so that the density of the polymer approaches the density of ethylene homopolymer, 0.966 g/ml, as the comonomer content approaches zero. For butene grades, A and B have been fitted at 0.02386 and 0.514. A plot of the correlation and the commercial and patent data from Sinclair (1980) which was used for parameter estimation is given in Figure 2.2. This relationship was used to convert laboratory density measurements to comonomer incorporation data so that reactor operating data and model predictions could be compared quantitatively.

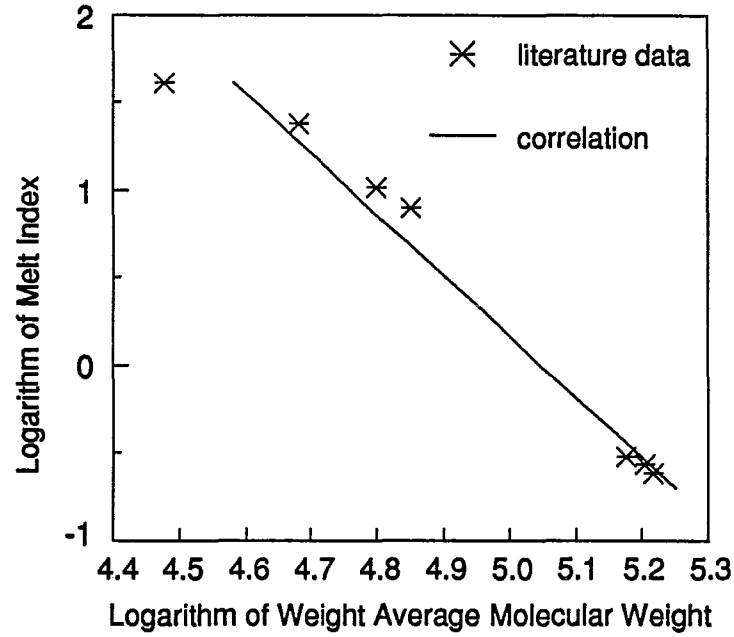

Figure 2.1 Correlation between molecular weight and melt index.

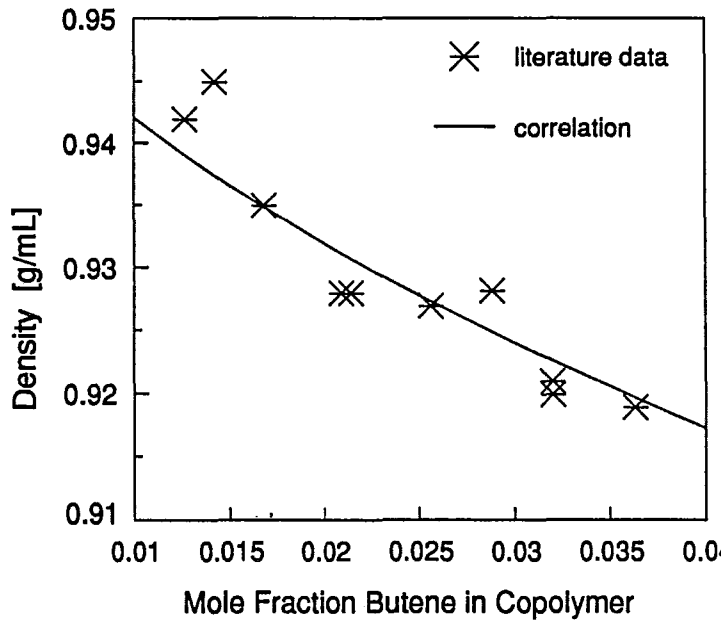

Figure 2.2 Correlation between composition and density.

2.4 MODEL VALIDATION

Two interesting historical data sets from a commercial gas phase reactor were chosen for model validation. During the corresponding operating periods, the reactor temperature remained constant and 1-butene was used as the comonomer. Input data to the computer model included the measured reactant gas concentrations, reactor pressure, catalyst and cocatalyst feed rates and the mass of polymer in the fluidized bed.

2.4.1 Choosing Rate Constants

Experimental determination of rate constants for multiple site systems is not a trivial task. deCarvalho et al. (1989) discuss one methodology which involves cross-fractionation of polymer samples by *TREF* and *SEC*, followed by ^{13}C *NMR* analysis of the cross-fractions (Wild et al., 1982; Usami et al., 1986). In this manner the polymer sample can be divided into fractions produced at individual site types. Important rate parameters can then be determined from the *NMR* results and reactor operating conditions. To obtain reasonable parameter estimates using this technique would require an experimental design wherein the reactor operated under many sets of conditions. Once the experimental measurements were obtained, a multivariate error in variables model *EVM* technique (Patino Leal and Reilly, 1981) would be required to account for the effects of the many sources of error on rate parameter estimates. This type of systematic study has not yet been performed for the proprietary catalyst system under study.

Since rate constants have not been determined for the industrial catalyst system used, initial order of magnitude estimates for rate constants were obtained from Kissin (1987) for similar catalyst systems. Propagation and transfer rate constants at individual sites were then manipulated to produce results corresponding

to those determined experimentally by Usami et al. (1986). Two active site types were employed in the simulations. Rate constants were chosen such that site one produces higher molecular weight polymer, low in butene, and site 2 produces butene rich, lower molecular weight polymer. Propagation rate constants were chosen so that the reactivity ratio product, r_1r_2, for site 1 was unity and r_1r_2 for site 2 was 0.55 as determined for a similar industrial catalyst by Usami et al. (1987). Transfer rate constants were manipulated in order to achieve weight average molecular weights corresponding to the melt index laboratory data and to achieve a polydispersity between consistent with the commercial gas phase process.

2.4.2 Comparison of Model Predictions with Plant Data

Predictions were generated using the rate constants given in Table 2.1 and two industrial data sets as model input. While the constants from Table 2.1 give reasonable predictions of plant phenomena, they are not a unique set. Other combinations of constants can be developed to give identical predictions. From the simulations, it was determined that model predictions of production rate and copolymer composition were most sensitive to changes in the rate constants for propagation and copolymerization at the individual active site types. When CO was present in the reactor, impurity deactivation and desorption rate constants also became important. Molecular weight properties were influenced by the site-specific propagation, transfer to hydrogen and transfer to comonomer rate constants. Order of magnitude changes in the formation, initiation, transfer to cocatalyst, spontaneous transfer and spontaneous catalyst deactivation reaction rate constants had very little influence on model predictions. A single set of rate constants were used to develop copolymer composition, molecular weight and reaction rate predictions for both data

sets. When a catalyst grade change was made, the numbers of active sites of each type per gram of catalyst were altered to reflect the hypothesis that each catalyst grade has a different distribution of the same two site types. The individual site 1 and site 2 rate constants, however, were not altered.

Table 2.1

Rate Parameters Used for Model Predictions

		Site Type 1	Site Type 2	Units
Formation	$kf(j)$	1	1	s^{-1}
Initiation	$ki_1(j)$	1	1	L/(mol s)
	$ki_2(j)$	0.14	0.14	L/(mol s)
	$kh_1(j)$	1	1	L/(mol s)
	$kh_2(j)$	0.1	0.1	L/(mol s)
	$kh_r(j)$	20	20	L/(mol s)
Propagation	$kp_{11}(j)$	85	85	L/(mol s)
	$kp_{12}(j)$	2	15	L/(mol s)
	$kp_{21}(j)$	64	64	L/(mol s)
	$kp_{22}(j)$	1.5	6.2	L/(mol s)
Transfer	$kf_{11}(j)$	0.0021	0.0021	L/(mol s)
	$kf_{12}(j)$	0.006	0.11	L/(mol s)
	$kf_{21}(j)$	0.0021	0.0021	L/(mol s)
	$kf_{22}(j)$	0.006	0.11	L/(mol s)
	$kfh_1(j)$	0.088	0.37	L/(mol s)
	$kfh_2(j)$	0.088	0.37	L/(mol s)
	$kfr_1(j)$	0.024	0.12	L/(mol s)
	$kfr_2(j)$	0.048	0.24	L/(mol s)
	$kfs_1(j)$	0.0001	0.0001	s^{-1}
	$kfs_2(j)$	0.0001	0.0001	s^{-1}
Deactivation	$kds(j)$	0.0001	0.0001	s^{-1}
	$kdl(j)$	2000	2000	L/(mol s)
Impurity Desorption	$ka(j)$	0.0003	0.0003	s^{-1}

2.4.2.1 Data Set 1

In this period, the molecular weight remained relatively constant while a transition to a lower density resin with a higher comonomer incorporation was performed. An interesting feature of this data set is that *CO* was injected into the reactor and then the catalyst feed rate was interrupted. This data set represents 65 time periods of continuous reactor operation. A single grade of catalyst was used throughout the operating period. Shown in Figure 2.3 is a comparison of the simulated rate of reaction and the overall rate of reaction as measured by an on-line heat balance. There is good qualitative agreement between the simulated and measured rates over the entire duration of the simulation. The marked drops in the reaction rate at time periods 13 and 25 were caused by the presence of *CO* in the reactor, followed by a catalyst feed disruption. Figure 2.4 is a plot of the *CO* concentration which was measured by an on-line gas chromatograph. Several simulations were run using different values of deactivation and reactivation rate constants $k_{dI}(j)$ and $k_a(j)$. Because of the nature of the catalyst feed rate, shown in Figure 2.5, one cannot determine both the rates of desorption and subsequent reactivation of dead sites from this data set. Various combinations of k_{dI} and k_a gave similar reaction rate predictions. The results shown in Figure 2.3 were obtained using $k_{dI} = 2000$ L/(mol·s) and $k_a(j) = 0.0003$ L/(mol·s) for both site types. For the first 25 time periods, the predicted reaction rate is very similar to the rate estimated by the heat balance. After 28 time periods, however, there is a quantitative mismatch between predicted and measured reaction rates. This discrepancy could not be alleviated by further tuning of the rate constants. Between time periods 28 and 32 the measured rate is lower than the predicted rate. Thereafter, the measured rate remains higher than the prediction. The

sustained mismatch in level after 32 time periods may be due to several unmodelled phenomena. As shown in Figure 2.6 the level of butene in the reactor was significantly higher after 32 timer periods than during the first 25 time periods. In McAuley et al. (1990) it was suggested that the production rate mismatch might be due to plasiticization effects which were not accounted for initially in the model. Since that publication, however, it has been determined using equation 2.10 that the deviation from Henry's law resulting from the higher butene concentration after 32 time periods was well below 5% and that even a 5% deviation could not account for the level of production rate mismatch observed in Figure 2.3. More likely causes for the rate mismatch include batch to batch catalyst variability or a possible recalibration of the catalyst metering system. The presence of reactive feed impurities other than *CO* may also have contributed to the rate mismatch.

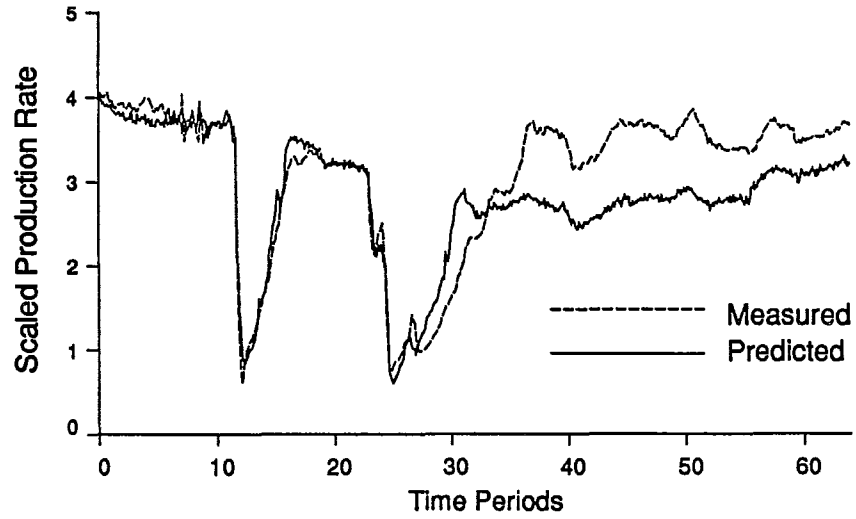

Figure 2.3 Comparison of predicted and measured production rates
Data Set 1

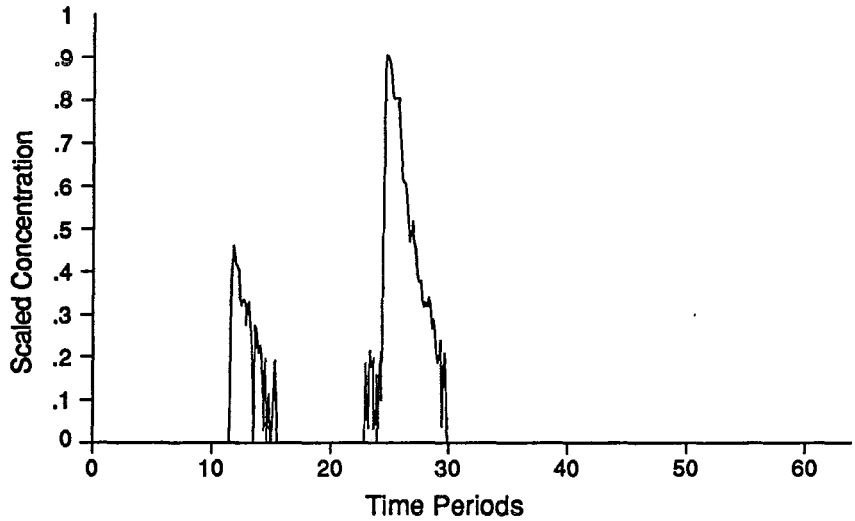

Figure 2.4 Carbon monoxide concentration in gas phase
Data Set 1

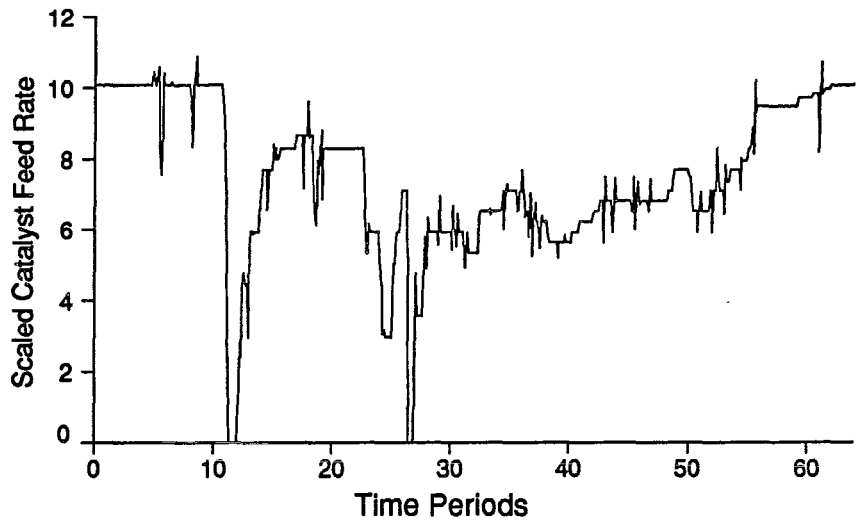

Figure 2.5 Catalyst feed rate to reactor
Data Set 1

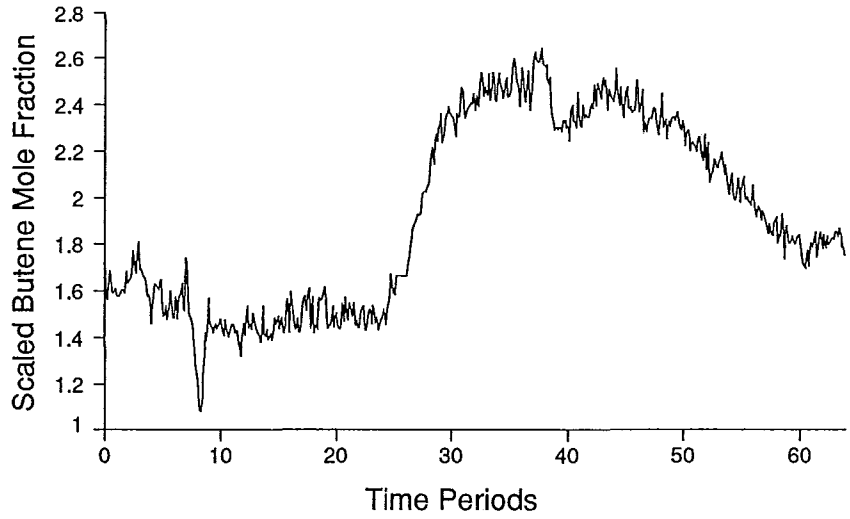

Figure 2.6 Scaled gas-phase butene concentration:
Data Set 1

A plot of the predicted active site distribution throughout the run is given in Figure 2.7. Since one grade of catalyst was used throughout the run and a negligible decay rate was assumed for both types sites, the ratio between the two site types remained constant throughout the simulation. Note that the introduction of CO into the cycle gas resulted in a marked decrease in the number of active sites of each type. As shown in Figure 2.8, the molecular weight remained relatively constant throughout the run, except for a drop to 0.95 scaled molecular weight units between time periods 30 and 35. The model predicts the qualitative trend in the molecular weight, but there is a slight mismatch in level between time periods 35 and 60. As illustrated in Figure 2.9, the comonomer incorporation predicted by the model corresponds nearly perfectly to the laboratory density measurements during the entire operating period.

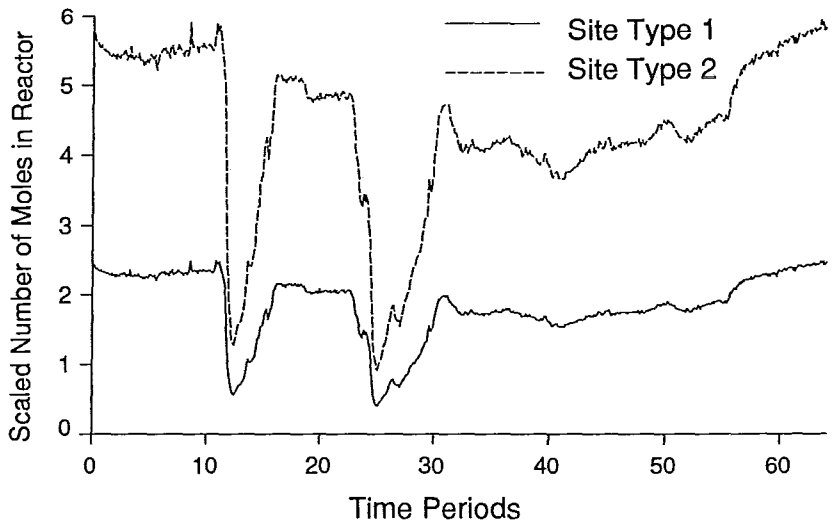

Figure 2.7 Number of moles of growing polymer chains at each site type
Data Set 1

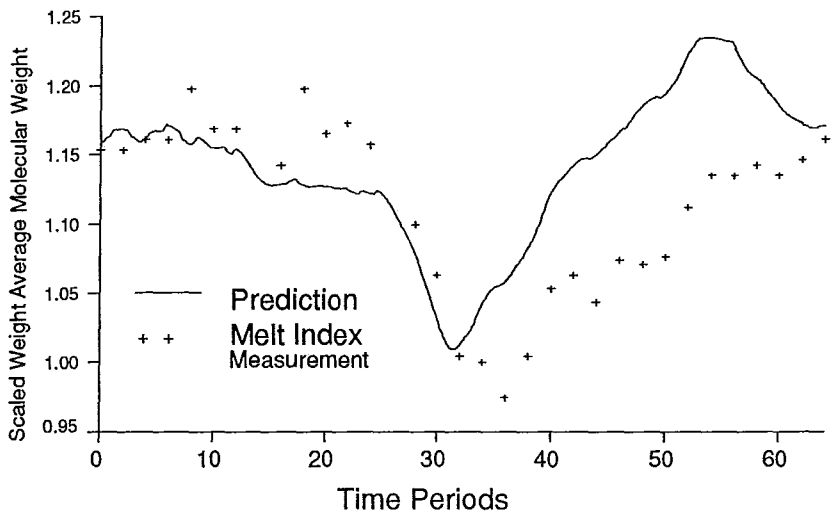

Figure 2.8 Predicted molecular weight vs. estimates from
melt index laboratory data
Data Set 1

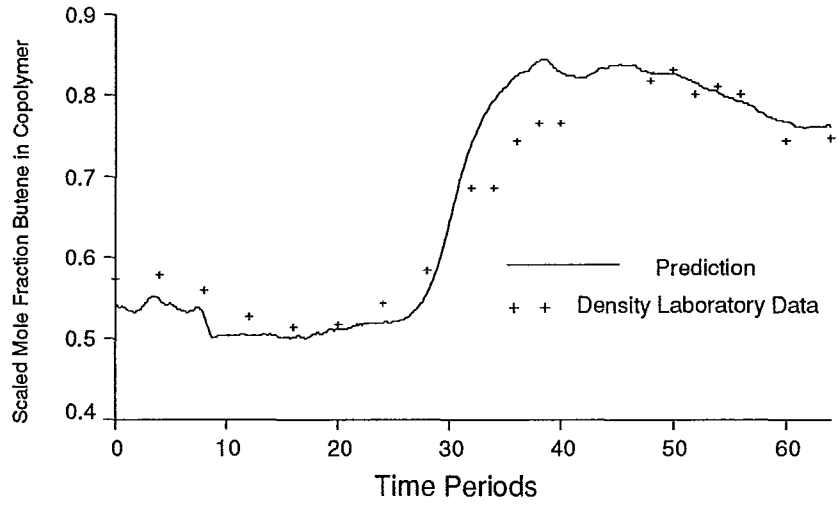

Figure 2.9 Predicted copolymer composition vs. estimates from density laboratory data
Data Set 1

2.4.2.2 Data Set 2

The second data set, which contains several molecular weight transitions, a transition in comonomer incorporation or density, and a catalyst grade change, corresponds to 120 time periods of continuous reactor operation. During this operating period, CO impurity levels were low, as indicated by Figure 2.10. Illustrated in Figure 2.11 is a comparison of predicted and measured reaction rates. Both the detail and the overall level of the production rate is well predicted by the model except between time periods 80 and 85 when a change in the catalyst grade occurs. A plot of the number of moles of active sites of each type is given in Figure 2.12. The catalyst grade change at 85 time periods markedly changed the active site distribution. From the simulation results shown, it appears that the catalyst used to produce low molecular weight, high melt index material contained

relatively more of active site 1 than did the catalysts used to produce high molecular weight, low melt index grades. Figure 2.13 is a comparison of weight average molecular weight predicted by the simulation and that determined from the laboratory melt index measurements. The comonomer incorporation predictions and estimates from laboratory density measurements are compared in Figure 2.14. The model was able to predict both molecular weight and copolymer composition very accurately throughout the entire operating period.

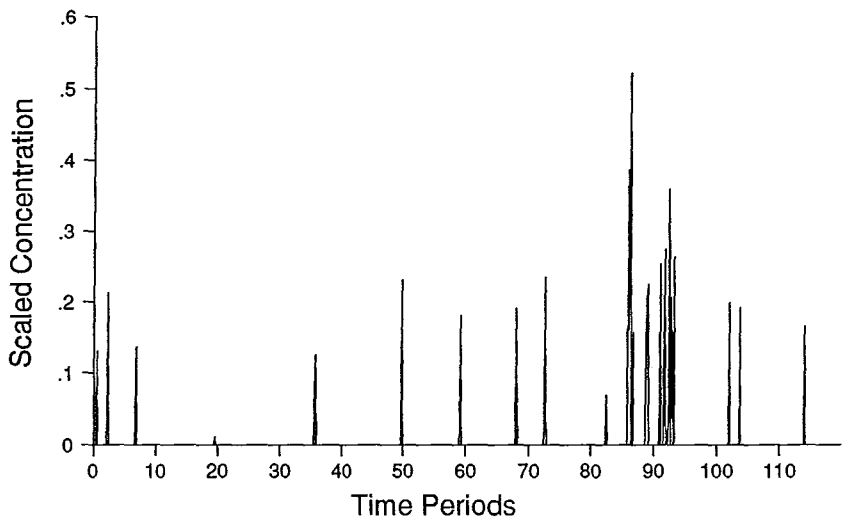

Figure 2.10 Carbon monoxide concentration in gas phase
Data Set 2

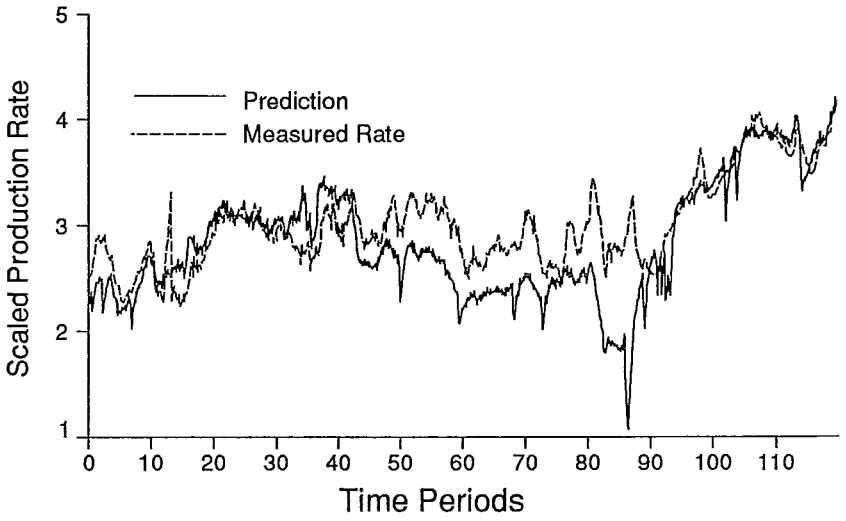

Figure 2.11 Comparison of predicted and measured production rates
Data Set 2

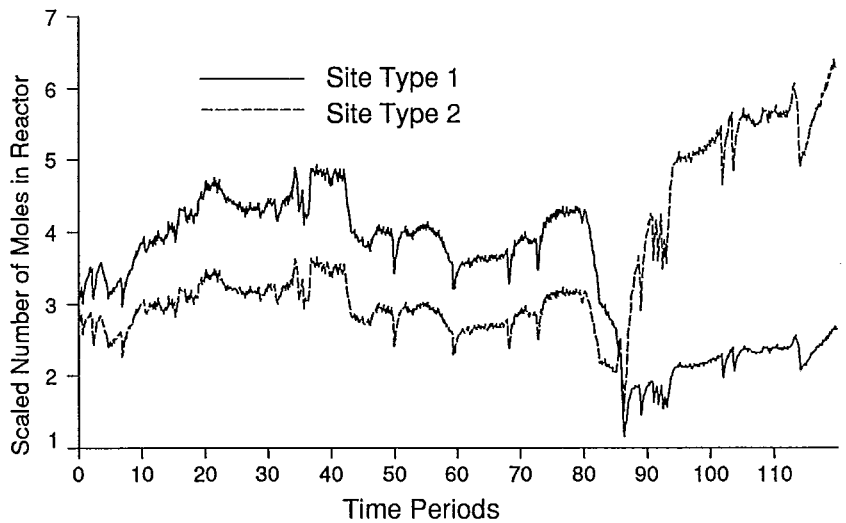

Figure 2.12 Number of moles of growing polymer chains at each site type
Data Set 2

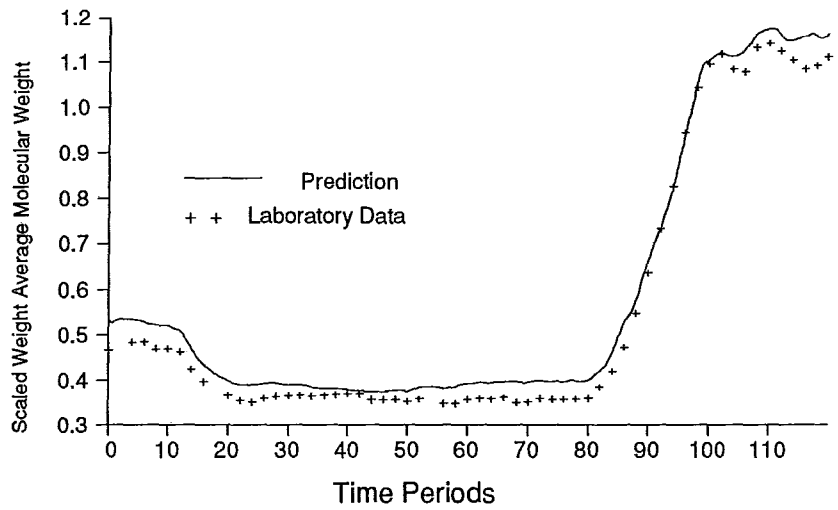

Figure 2.13 Predicted molecular weight vs. estimates from melt index laboratory data
Data Set 2

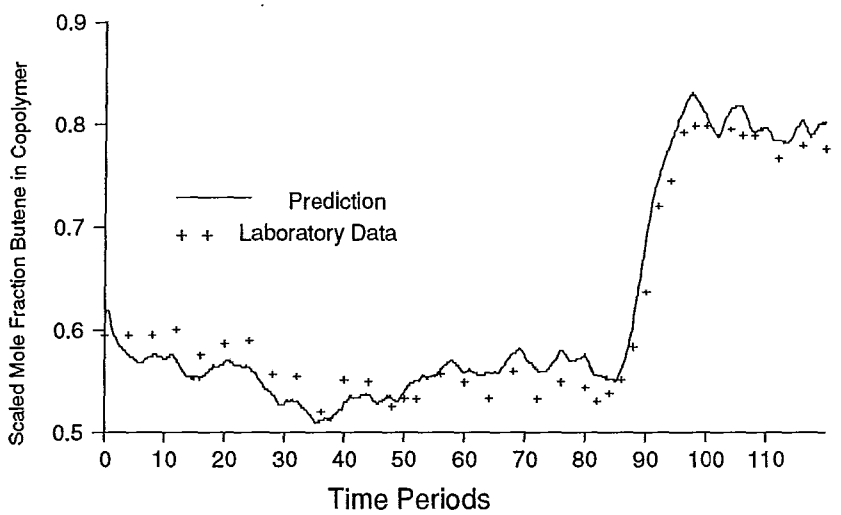

Figure 2.14 Predicted copolymer composition vs. estimates from density laboratory data
Data Set 2

2.4.3 Molecular Weight and Copolymer Composition Distributions

From a comparison of the model predictions and the industrial production rate, *MI* and density data, it is apparent that the bulk properties of the polymer produced in the industrial reactor can largely be explained by the model. As well, the model can predict bimodal instantaneous molecular weight and compositional distributions which were observed by Usami et al. (1986) and Wild et al. (1982). Shown in Figures 2.15 and 2.16 are plots of instantaneous molecular weight and compositional distributions predicted from the model results for data set 2 at time period 10. This time was chosen because the reactor was operating at essentially steady state and, as such, the instantaneous properties correspond closely to bulk polymer properties in the reactor. Note that the polydispersity of the molecular weight distribution of the whole polymer is near 3.1 which is larger than 2.0, the polydispersity of the polymer produced at each individual site type. The sites which produced the higher molecular weight polymer are responsible for the low butene peak in the compositional distribution. These results are very similar to Wild's experimental findings for a commercial polyethylene sample which are shown in Figure 2.17.

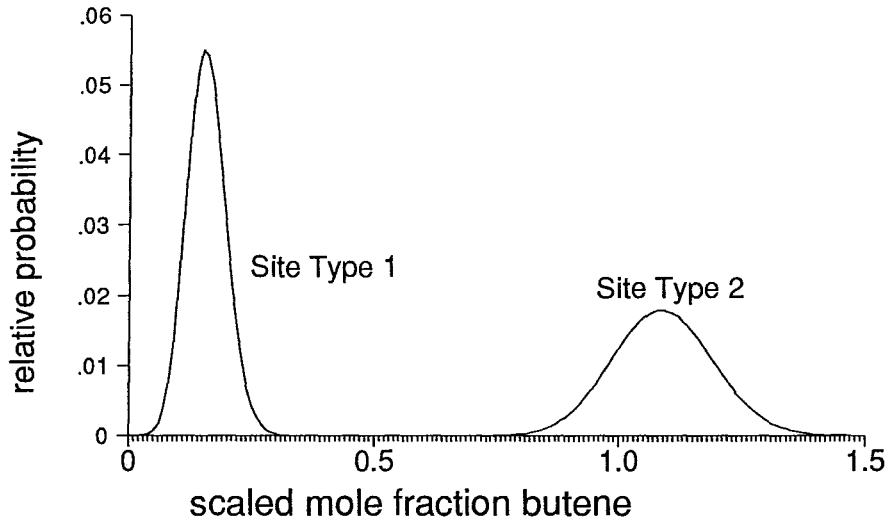

Figure 2.15 Instantaneous comonomer incorporation probability distribution function: Data Set 2. Time = 10 periods

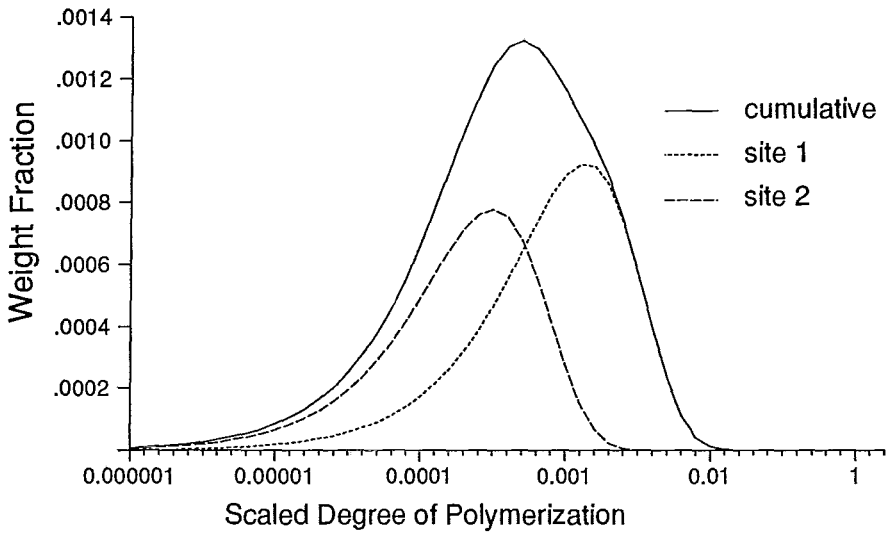

Figure 2.16 Instantaneous molecular weight distribution: Data Set 2. Time = 10 periods

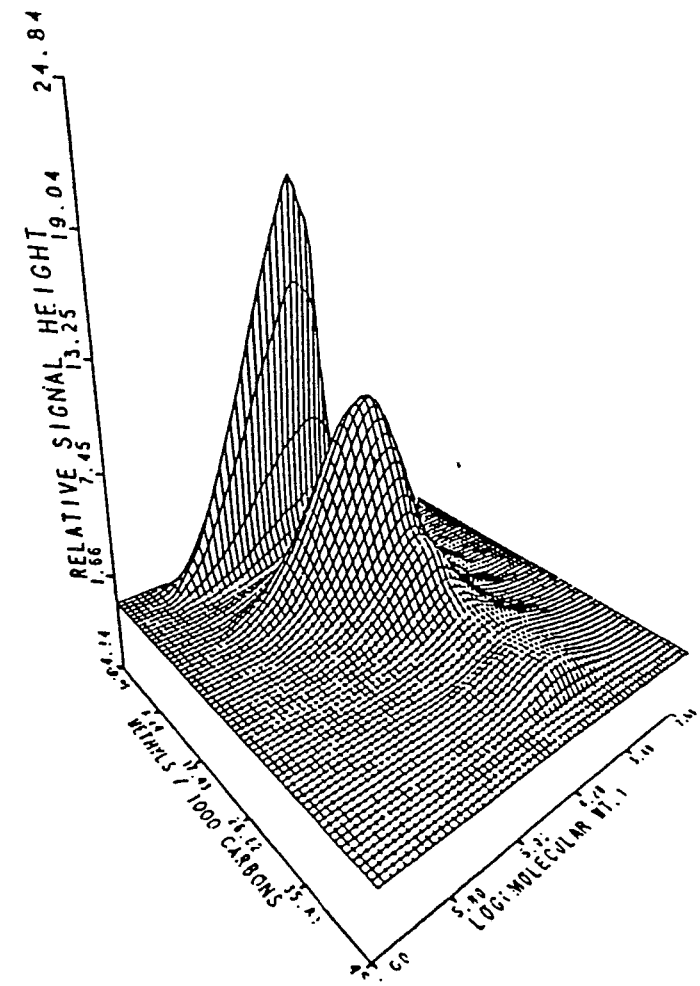

Figure 2.17 Experimental Joint Frequency Distribution of Molecular Weight and short Chain Branching in a Commercial linear low-density Polyethylene Sample.

Reproduced from Wild et al. (1982) with permission

2.5 CONCLUSIONS

A dynamic kinetic model for the production of linear polyethylenes in a gas phase reactor has been presented. This model considers the existence of multiple types of active sites on the heterogeneous Ziegler-Natta catalyst. It has been shown that a two-site model can predict the changes in production rate, weight average molecular weight and copolymer composition which occur in response to gas phase composition and catalyst grade changes in an industrial reactor. As well, this model predicts a broadened molecular weight distribution and a bimodal copolymer compositional distribution which are typical of commercial linear polyethylenes.

2.6 NOTATION

A	Arrhenius pre-exponential factor
AlA	Aluminum alkyl cocatalyst
B_i	Moles of reacted monomer of type i bound in the polymer in the reactor
E_a	Activation energy
F_i	Mole fraction of the total polymer in the reactor which is composed of reacted monomer i
$\overline{F_1}(j)$	Mean mole fraction ethylene in the polymer produced at sites of type j
f_i	fraction of total monomer in the reactant gas which is monomer M_i
$F^*_{in}(j)$	Molar flow rate of potential active sites of type j into the reactor
H_2	Hydrogen
I_m	Impurity such as carbon monoxide
i	Monomer type
j	Active site type
k^*	Solubility coefficient
$ka(j)$	Impurity desorption rate constant for a site of type j
k^*_{but}, k^*_{eth}	Solubility coefficients for butane and ethane in polyethylene
$kdI(j)$	Deactivation by impurities rate constant for a site of type j
$kds(j)$	Spontaneous deactivation rate constant for a site of type j
$kf(j)$	Formation rate constant for a site of type j

$kfh_i(j)$	Transfer rate constant for a site of type j with terminal monomer M_i reacting with hydrogen
$kfm_{ik}(j)$	Transfer rate constant for a site of type j with terminal monomer M_i reacting with monomer M_k
$kfr_i(j)$	Transfer rate constant for a site of type j with terminal monomer M_i reacting with AlA
$kfs_i(j)$	Spontaneous transfer rate constant for a site of type j with terminal monomer M_i
k^g	pseudo kinetic rate constant based on gas phase concentrations
$kh_i(j)$	Rate constant for reinitiation of a site of type j by monomer M_i
$kh_r(j)$	Rate constant for reinitiation of a site of type j by cocatalyst
k^*_{Hi}	Henry's law constant for component i
$ki_i(j)$	Rate constant for initiation of a site of type j by monomer M_i
K_p	Partition coefficient between the gas and polymer phases
$kp_{ik}(j)$	Propagation rate constant for a site of type j with terminal monomer M_i reacting with monomer M_k
$[M^*]_{dev}$	Monomer concentration in the polymer at which the deviation from Henry's law is 5%
$[M_i]_{gas}, [M_i]_{pol}$	Concentration of monomer i in the gas and amorphous polymer phases respectively
$[M^*]_T$	Total monomer concentration in the amorphous polymer
$\overline{m}$	Mean monomer molecular weight
M_1	Ethylene
M_2, M_3	Butene, hexene

M_c	Critical molecular weight for application of power law relationship between viscosity and molecular weight
MI	Melt Index
M_i	Monomer of type i
$\overline{M}_n$	Number average molecular weight of polymer
$\overline{M}_w$	Weight average molecular weight of polymer
mw_i	Molecular weight of monomer M_i
$M_x(j)$	The instantaneous mass rate of polymer production at sites of type j.
$N^*(j)$	Potential active site of type j
$N(0,j)$	Uninitiated site of type j produced by formation reaction
$N_d(j)$	Spontaneously deactivated site of type j
$Nd_I(0,j), Nd_{IH}(0,j)$	Impurity killed sites of type j
$N_H(0,j)$	Uninitiated site of type j produced by transfer to hydrogen reaction
$N_i(r,j)$	Living polymer molecule of length r, growing at an active site of type j, with terminal monomer M_i
NS	Number of active site types
P_c	Critical pressure
P_i	Partial pressure of component i
P_i^0	Vapour pressure of pure component i
P_{dev}	Pressure at which the predicted deviation from Henry's law is 5%
P_T	Total pressure of all gas phase components

$Q(r,j)$	Dead polymer molecule of length r produced at a site of type j
R	Ideal gas constant
r	Number of units in polymer chain
$r_1 r_2$	propagation reactivity ratio product
R_i	Instantaneous consumption rate of monomer i
$R_i(j)$	Rate at which monomer i is consumed by propagation reactions at sites of type j
R_v	Volumetric polymer phase outflow rate from the reactor
T	Subscript referring to total of all monomer types
T	Absolute temperature
t	Time
T_c	Critical temperature
T_{ref}	Reference temperature
V_p	Volume of polymer phase in the reactor
$W(r,y,j)dr\,dy$	Weight fraction of instantaneous copolymer produced at a site of type j with chain length between r and $r+dr$ and composition between y and $y+dy$.
$W(r,y)dr\,dy$	Weight fraction of instantaneous copolymer produced at all sites with chain length between r and $r+dr$ and composition between y and $y+dy$.
$Y(n,j)$	$n-th$ moment of chain length distribution for living polymer produced at a site of type j
$X(n,j)$	$n-th$ moment of chain length distribution for dead polymer produced at a site of type j
Z	Polydispersity of molecular weight distribution

α_i	Activity coefficient for component *i*
ν_i, ν_p	Volume fractions of small molecule *i* and polymer, respectively, in the amorphous polymer phase
ξ	Correction factor for gas/polymer partition coefficient
$\phi_i(j)$	Fraction of active sites of type *j* which have terminal monomer M_i
η	Viscosity of polymer melt at low shear
X_{ip}	Flory-Huggins interaction parameter
κ	Parameter in the Stockmayer bivariate distribution
ρ	Polymer density
σ	Factor which accounts for deviations from Henry's law
$\sigma(j)^2$	Standard deviation of the copolymer compositional distribution at site type *j*
$\tau(j)$	Ratio of the total rate of transfer to the total rate of propagation at sites of type *j*

REACTOR MODEL

3 REACTOR MODEL

Given the concentrations of reactants in the gas phase and the reactor temperature, the kinetic model described in Chapter 2 is very powerful for predicting production rate and polymer quality variables. Nevertheless, if the model is to be used for control scheme design, development and testing, several model extensions are required. Dynamic mass balances on the reactants are required in order to predict gas compositions in the reactor. The variables which can be manipulated by process operators or by on-line product quality control schemes, are the feed rates, rather than the concentrations, of the individual reactants. It is essential for the model to predict the effects of feed flow changes on reactor operation so that control schemes can be tested. This capability can be provided through the addition of dynamic mass balances. Dynamic energy balances on both the reactor and the cycle gas cooler are required to predict the operating temperature of the reactor and the rate of heat removal from the cycle gas. In addition, equations for low level controllers which regulate the reactor temperature, the quantity of polymer in the bed and the ethylene inventory in the reactor are required so that interactions between product quality control schemes and other controllers can be investigated.

3.1 DYNAMIC MASS BALANCES

Mass balances on components in the gas phase have been added to the model in order to predict the reactant concentrations required for reaction rate expressions. For

the purpose of these mass balances, the entire reactor volume (excluding the space occupied by the polymer) and the recycle stream volume are treated as a single well-stirred tank. Components enter the reactor system via the fresh feed streams. They leave the gas phase in several ways: by reaction to form polymer; by dissolving in the polymer bed; as interstitial gas which flows out in the product stream along with the polymer particles; and by outflow in a bleed stream. The bleed stream is removed from the reactor system through this vent in order to control the accumulation of inerts and impurties in the system.

3.1.1 Mass Balance on Inerts

An inert component, such as nitrogen, is injected into the reactor along with the catalyst. (Choi and Ray, 1985). Since nitrogen does not participate in reactions and is only sparingly soluble in polyethylene, the mass balance is very simple:

$$V_g \frac{d[in]_g}{dt} = \Gamma_{in} - b_{in} \tag{3.1}$$

Only gas inflow to the reactor and gas outflow in the vent stream and with the polymer must be considered. V_g is the total volume of the gas phase and $[in]_g$ is the molar concentration of inerts in the gas phase. Γ_{in} is the inflow rate of inert components to the reactor and b_{in} is the outflow rate of inerts in the vent stream. Most of the interstitial gases which exit the reactor with the polymer product are recovered and returned to the reactor. Thus, this portion is not included separately in the bleed rate calculation. The bleed rate of inerts from the reactor depends on the total bleed stream flow rate, b_T which is controlled by the vent position:

$$b_T = \nu_p \, c_v \sqrt{P - P_v} \tag{3.2}$$

ν_p is the position of the vent (fraction open), c_v is a constant coefficient, P is the reactor pressure and P_v is the pressure downstream from the vent. If the total molar gas phase concentration of species in the reactor, $[C_T]_g$ is:

$$[C_T]_g = [M_1]_g + [M_2]_g + [M_3]_g + [AlA]_g + [I_m]_g + [H_2]_g + [in]_g \tag{3.3}$$

then the bleed flow rate of inerts is:

$$b_{in} = \frac{[in]_g}{[C_T]_g} b_T \tag{3.4}$$

3.1.2 Mass Balance on Hydrogen

To account for the rate of hydrogen consumption by chain transfer, the hydrogen mass balance has an extra term when compared with the balance on inerts. Since hydrogen is only sparingly soluble in polyethylene, removal from the gas phase by sorption in the polymer need not be considered:

$$V_g \frac{d[H_2]_g}{dt} = \Gamma_H - R_H - b_H \tag{3.5}$$

Γ_H and b_H are fresh feed and bleed rates analogous to Γ_{in} and b_{in}. R_H is the rate of hydrogen consumption by reaction:

$$R_H = [H_2] \sum_{j=1}^{2} kfh_T(j) \, Y(0,j) \tag{3.6}$$

The rate constant in equation 3.6 is a pseudo kinetic rate constant corrected for partitioning effects using the correction factor in equation 2.16. This type of correction is incorporated into all other rate constants in the model.

3.1.3 Balances on Monomers

Ethylene, butene and higher alpha olefin (*HAO*) comonomers are all soluble in polyethylene at significant levels. Thus, the quantity of monomers which leave the gas phase by dissolving in the polymer bed must be considered in the mass balances. Since gases dissolve only in the amorphous sections of the polymer, it is important to know the fraction of the polymer which is non-crystalline. Crystallinity is related to polymer density, ρ, by the following correlation:

$$\alpha_v = \frac{\rho_c - \rho}{\rho_c - \rho_a} \tag{3.7}$$

α_v is the amorphous volume fraction, $\rho_c = 0.990 g/mL$ is the density of crystalline polyethylene and $\rho_a = 0.859 g/mL$ is the amorphous density. At equilibrium the total quantity of ethylene in the gas phase and dissolved in the polymer is given by $[M_1]_g V_g + \alpha_v [M_1]_p V_p$ which is equal to $[M_1]_g \left(V_g + \alpha_v k_1^* V_p P / [C_T]_g\right)$ where k_1^* is the gas sorption coefficient for ethylene, P is the total system pressure, and $[C_T]_g$ is the total concentration of all components in the gas phase. A mass balance on the total ethylene in the system is given by:

$$\left(V_g + \frac{\alpha_v k_1^* V_p P}{[C_T]_g}\right) \frac{d[M_1]_g}{dt} = \Gamma_{M1} - b_{M1} - R_{M1} - S_{M1} \tag{3.8}$$

assuming that the bracketed terms on the left hand side of equation 3.8 do not change appreciably compared with the rate of change of $[M_1]_g$. Γ_{M1} and b_{M1} are fresh feed and bleed flow rates of ethylene. R_{M1} is the rate of consumption of ethylene by reaction. Since monomer consumption by propagation reactions is much greater than consumption by either transfer or initiation reactions, R_{M1} can be approximated by:

$$R_{MI} = [M_1]_g \sum_{j=1}^{2} kp_{TI}(j)Y(0,j) \tag{3.9}$$

S_{MI} is the rate at which ethylene leaves the reactor dissolved in the polymer product:

$$S_{MI} = \alpha_v k_1^* [M_1]_g R_v \tag{3.10}$$

R_v is the volumetric outflow rate of polymer particles from the reactor. In equation 3.8, it was assumed that the time rate of change of $V_g + \alpha_v k_1^*$ is small. Equations analogous to 3.8 to 3.10 have been incorporated into the model for butene and higher alpha olefin, *HAO*, comonomer.

3.1.4 Cocatalyst Mass Balance

The mass balance for the cocatalyst shown below is similar in structure to equation 3.8:

$$(V_g + \alpha_v k_R^*) \frac{d[AlA]_g}{dt} = \Gamma_R - b_R - R_R - S_R \tag{3.11}$$

The rate of cocatalyst consumption is given by:

$$R_R = [AlA]_g \sum_{j=1}^{2} \{kfr_T(j)Y(0,j) + kh_r(j)N_H(0,j) \tag{3.12}$$

3.1.5 Impurity Mass Balance

Impurities such as carbon monoxide which poison catalyst sites are generally not very soluble in polyethylene. Thus the mass balance on impurities is simply:

$$V_g \frac{d[I_m]_g}{dt} = \Gamma_I - R_I - b_I \tag{3.13}$$

where the net rate of impurity consumption by reaction is:

$$R_I = [I_m]_g \sum_{j=1}^{2} \{kdI(j)(Y(0,j)+N(0,j)+N_H(0,j)) - ka(j)(Nd_I(0,j)+Nd_{IH}(0,j))\} \quad (3.14)$$

Equation 3.14 above contains terms which account for both impurity consumption at the active sites and the possible desorption of impurities from the sites.

3.2 DYNAMIC ENERGY BALANCES

Dynamic energy balances on the reactor and recycle gas cooler are required to predict the reactor operating temperature.

3.2.1 Reactor Energy Balance

Due to the turbulent mixing in the fluidized bed reactor, gas temperatures are nearly uniform throughout the bed. Cooled gases which enter the bottom of the reactor quickly mix with the hot gases in the bed. As a result, industrial reactors commonly experience a temperature rise of only a few $°C$ from the bottom of the bed to the top. With proper catalyst design and dispersal throughout the bed, heat transfer from the growing particles to the gas phase is fast; particle temperatures are not significantly higher than the gas temperature. Detailed fluidynamic models describing the temperature deviations in the gas phase and differences between polymer particle and gas phase temperatures under different operating conditions have been developed by Choi and Ray (1985) and Talbot (1990). The main purpose of the present work, however, is to predict temperature effects on polymer quality and production rate for operating conditions which are industrially applicable. For this type of model, the uniform temperature assumption is valid.

The rate of accumulation of thermal energy in the reactor is given by:

$$(M_w C_{pw} + V_p \rho C_{p\,pol}) \frac{dT}{dt} = H_f + H_{gi} - H_{go} - H_r - R_v \rho C_{p\,pol} \quad (3.15)$$

where M_w is the mass of the reactor wall and C_{pw} is the corresponding heat capacity of the wall material. $C_{p\,pol}$ is the heat capacity of polymer in the bed. It is assumed that neither of these heat capacities changes significantly over the temperature range of interest in the model. The heat capacity of the gas contained in the reactor is very small compared with that of the polymer bed or the reactor wall. Thus, it has been neglected in the accumulation term of equation 3.15. The enthalpy inflows to the reactor associated with the recycle gas and the fresh feed are specified by H_{gi} and H_f, respectively. The enthalpy outflow streams are H_{go}, which is enthalpy of the recycle gas outflow, and $R_v \rho C_{p\,pol}$ which accounts for the polymer product stream. $-H_r$ accounts for the heat liberated by the polymerization reaction. Since the enthalpy of the vent stream and the heat loss through the reactor wall are very small when compared with the terms on the right hand side of equation 3.15, they have been neglected. H_f, H_{gi} and H_{go} can be calculated by integrating temperature dependent heat capacity relationships (Reid et al, 1971) for the individual components in the streams. A specific heat of reaction of -894 cal/g for the production of copolymer at 360 K is used in the calculation of H_r. The heat capacity of polyethylene used in the model is 0.850 cal/g K.

3.2.2 Recycle Gas Cooler Energy Balance

In gas phase polyethylene reactors an external cooler on the recycle gas line is used to regulate the reactor temperature. The cooler might operate as follows: The hot gases flowing through the exchanger are cooled by a constant flow of water on the shell side. The amount of heat removed from the gas is regulated by manipulating the set point of the cooling water inlet temperature. This temperature is influenced by the relative flows of a warm and cold stream which are mixed before entering the

cooler. This type of arrangement (Liptak, 1972), can respond quickly and effectively to systems which experience rapid load changes. Manipulation of the inlet temperature setpoint results in faster exchanger dynamics than if the coolant flow rate were manipulated. A fast response is essential in order to react to changes in the polymer production rate. Mixing of two streams also prevents cooling water system disturbances from affecting the operation of the gas cooler

A complete description of this cooling system would require a distributed parameter model to account for temperature changes along the length of the exchanger. In the interest of simplicity, a simpler ordinary differential model of the system is used. The recycle gas cooler is modelled as a steady state, counter-current heat exchanger with added first order dynamics. In addition, first order dynamics are applied to the cooling water inflow temperature to account for the lag between the specification and realization of the desired inlet temperature. This approach to cooler modelling is used to achieve model simplicity while maintaining a mechanistic explanation of the effects of temperatures and compositions on steady state heat transfer rates. The overall heat transfer coefficient has been assumed constant and a mean heat capacity of the gas stream has been used to determine the steady state heat transfer rate.

The heat transfer between the two small elements of fluid, with temperatures T_w and T_g shown in Figure 3.1 is given by dQ:

$$dQ = U\,dA\,(T_g - T_w) \tag{3.16}$$

where dA is the area available for heat transfer between the two infinitessimally small elements, and U is the overall heat transfer coefficient. The following steady state energy balances can be written for each element of the fluid:

$$0 = F_g C_{pg} T_g(x + dx) - F_g C_{pg} T_g(x) - dQ \tag{3.17}$$

$$0 = F_w C_{pw} T_w(x + dx) - F_w C_{pw} T_w(x) + dQ \tag{3.18}$$

$F_g C_{pg}$ and $F_w C_{pw}$ are the products of the flow rates and specific heat capacities for the cycle gas and cooling water streams, respectively. Equations 3.16 to 3.18 can be combined to give:

$$\frac{d(T_g - T_w)}{dA} = U(T_g - T_w)\left(\frac{1}{F_g C_{pg}} + \frac{1}{F_w C_{pw}}\right) \tag{3.19}$$

which can be integrated over the length of the exchanger:

$$\ln\left(\frac{T_{gi} - T_{wo}}{T_{go} - T_{wi}}\right) = AU\left(\frac{1}{F_g C_{pg}} + \frac{1}{F_w C_{pw}}\right) \tag{3.20}$$

T_{gi} and T_{go} are the inlet and outlet gas temperatures. Similarly, T_{wi} and T_{wo} refer to the inlet and outlet water temperatures. An overall energy balance on the exchanger gives:

$$F_g C_{pg}(T_{gi} - T_{go}) = AU\left(\frac{1}{F_g C_{pg}} + \frac{1}{F_w C_{pw}}\right) \tag{3.21}$$

Combining equations 3.20 and 3.21 gives the following expression for $T_{go\,ss}$, the steady state recycle gas temperature at the exchanger exit:

$$T_{go\,ss} = \frac{T_{wi}(1 - \exp(Y)) - T_{gi}\left(1 - \frac{F_g C_{pg}}{F_w C_{pw}}\right)}{\frac{F_g C_{pg}}{F_w C_{pw}} - \exp(Y)} \tag{3.22}$$

$$Y = AU\left(\frac{1}{F_g C_{pg}} + \frac{1}{F_w C_{pw}}\right) \tag{3.23}$$

The total steady state heat removal rate is given by:

$$Q_{ss} = F_g C_{pg}(T_{gi} - T_{go\,ss}) \tag{3.24}$$

If first order heat exchanger dynamics are assumed, the dynamic heat removal rate, Q_d, is given by:

$$\frac{dQ_d}{dt} = \frac{Q_{ss} - Q_d}{\tau_e} \tag{3.25}$$

where τ_e is the first order time constant of the exchanger. Similarly, the cooling water inflow temperature can be determined from:

$$\frac{dT_{wi}}{dt} = \frac{T_{wi\,sp} - T_{wi}}{\tau_{cw}} \tag{3.26}$$

where $T_{wi\,sp}$ is the specified cooling water temperature setpoint and τ_{cw} is the corresponding first order time constant for the response. Thus, the enthalpy associated with the recycle gas leaving the cooler and entering the reactor is:

$$H_{gi} = H_{go} - Q_d \tag{3.27}$$

Note that no deadtime has been considered in either the reactor or cooler models because the actual deadtimes are very small when compared with the characteristic time constants of the system.

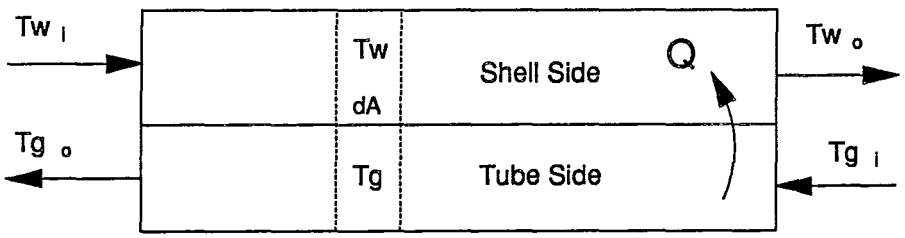

Figure 3.1 Schematic diagram of recycle gas cooler.

3.3 LOW-LEVEL CONTROLLERS

Equations for the controllers which regulate the quantity of polymer in the bed, the ethylene inventory in the gas phase and the reactor temperature are required to ensure

that the model behaves like an industrial reactor. The product quality control schemes designed in Chapter 6 will be added on top of these basic mass and energy balance controllers.

3.3.1 Bed Level Control

In gas phase polyethylene reactors, polymer is withdrawn from the reactor by opening a valve on the product discharge line. When the quantity of polymer in the reactor increases beyond the setpoint, the bed level controller opens the discharge valve and polymer flows into a surge tank, causing a small drop in the bed level. Since these small, frequent changes in bed level have little effect on the polymerization rate, the reactor has been modelled as a continuous outflow system. Since changes in the bed level cannot be accomplished instantaneously, it has been assumed that the closed loop response to bed level setpoint changes is first-order with a time constant τ_{bw} of 1 time period. This type of dynamic response is reasonable for most bed level setpoint changes. This assumption leads to the following differential equation:

$$\frac{db_w}{dt} = \frac{b_{wsp} - b_w}{\tau_{bw}} \tag{3.28}$$

where b_w is the mass of polymer in the fluidized bed and b_{wsp} is the corresponding setpoint. It is important to include an expression, such as equation 3.28 in the model, because changes in the bed level setpoint have important consequences in terms of the quantity of catalyst in the reactor and the production rate.

3.3.2 Ethylene Inventory Control

The concentration of ethylene in the reactor influences the polymerization rate, and the molecular weight and composition of the copolymer as well as the size and shape of the polymer particles. Thus, regulation of the quantity of ethylene in the reactor is essential. The ethylene partial pressure in the reactor can be measured continuously on-line using an infrared analyzer. A simple *PI* pressure controller which manipulates the ethylene feed rate has been included in the model to maintain the ethylene inventory in the reactor despite disturbances caused by changes in the polymerization and gas venting rates. The tuning constants for this PI controller are $K = 286.85$ kg/(time period/scaled pressure unit), and $T_I = 0.4247$ time periods.

3.3.3 Temperature Control and Reactor Stability

Good temperature control is essential for gas phase polyethylene reactors. The reactor temperature influences the polymer production rate and the molecular weight of the polymer produced. It is important that the reactor temperature is maintained well below the melting temperature of the polyethylene particles. Otherwise, particle agglomeration occurs leading to the formation of large chunks of molten polymer which can block product discharge lines. In the model, temperature control is accomplished by manipulating the inlet coolant temperature setpoint as discussed in section 3.2.2.

To assist in the analysis of reactor stability without temperature control, a Van Heerden (1953) diagram, shown in Figure 3.2, has been constructed around a typical reactor operating point. This diagram reveals that the rate of heat removal from the gas in the exchanger and the net rate of heat addition to the gas in the reactor both increase with increasing reactor temperature. The slope of the heat removal

line, however, is much steeper than that of the heat addition line. A small temperature perturbation above the steady state results in a greater increase in heat removal from the system than in heat addition by reaction. As a result, the temperature tends to move back towards the steady state operating point. While this is a necessary condition for the existence of a stable steady state, it is not sufficient to guarantee local stability.

The reactor model consists of the set of ordinary non-linear differential equations given in Chapter 2 and 3. These equations could be linearized about the steady state shown in Figure 3.2 using a truncated Taylor Series expansion to give the following model form:

$$\underline{\dot{x}} = \underline{\underline{A}}\,\underline{x} \tag{3.29}$$

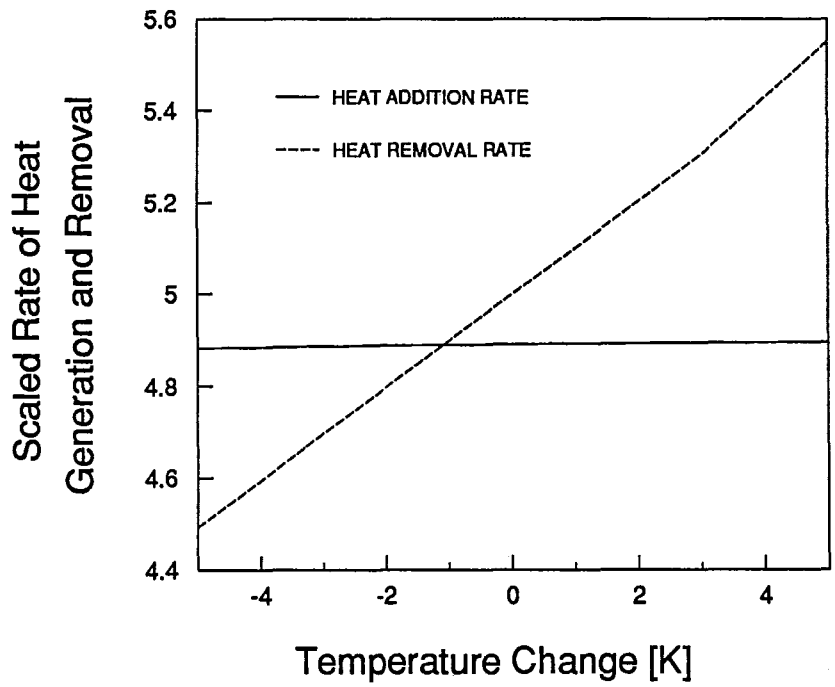

Figure 3.2 Steady state heat addition and removal rates near the operating point

where $\underline{x}$ is a vector of the model states and, $\dot{\underline{x}}$ contains the corresponding first derivatives of theses states with respect to time. $\underline{\underline{A}}$ is a Jacobian Matrix. The Liapunov condition for local stability requires that all eigenvalues of $\underline{\underline{A}}$ lie in the left-half of the complex plane. This condition is equivalent to the following two requirements (Uppal et al., 1974):

$$det\underline{\underline{A}} > 0 \tag{3.30}$$

$$tr\underline{\underline{A}} > 0 \tag{3.31}$$

The first requirement is often called the slope condition because it corresponds to Van Heerden's (1953) observation that a steady state is unstable if the slope of the heat addition curve is larger than that of the heat removal curve. As shown in Figure 3.2, the slope requirement corresponding to equation 3.30 is satisfied. Equation 3.31 is often called the dynamic condition. If this constraint is violated, then $\underline{\underline{A}}$ has right-half-plane eigenvalues with imaginary parts. Small perturbations from such a steady state will lead to growing oscillations. Examination of $\underline{\underline{A}}$ reveals that Equation 3.31 is violated for the reactor model when it is linearized about industrially applicable steady states. As expected, small perturbations from the stationary point do indeed lead to growing oscillations as shown in Figure 3.3. This simulation begins with the reactor at steady state at time period 10. After a short period of time, however, small numerical deviations from the exact steady state lead to oscillations in the reactor temperature. These oscillations initially grow and then appear to approach a stable oscillatory pattern or limit cycle. Growing temperature oscillations have also been predicted by Choi and Ray (1985) using their gas phase ethylene homopolymerization model.

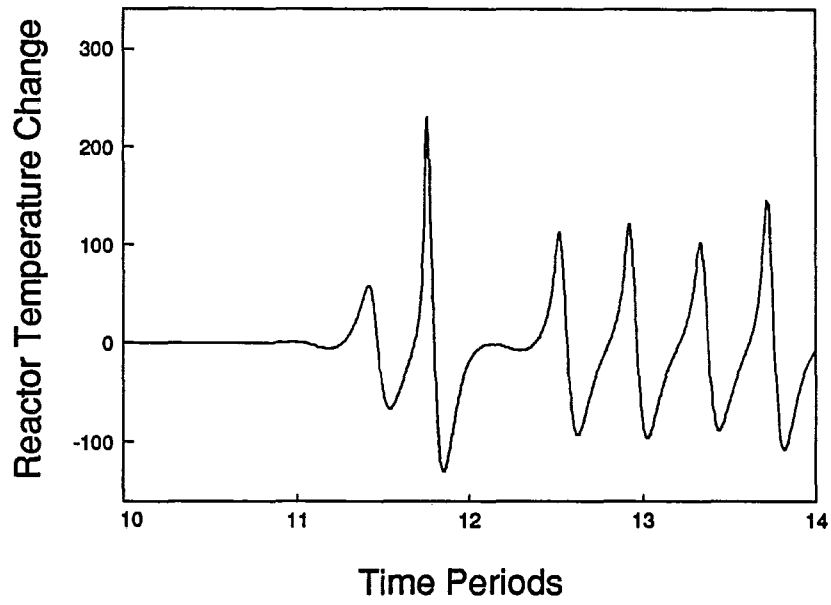

Figure 3.3 Open loop temperature response to a small perturbation from steady state (fast exchanger dynamics)

The size of the initial oscillations, and the period and amplitude of the limit cycle approached depend on reactor and cooler design and operating variables. The simulation shown in Figure 3.3 assumed relatively fast heat exchanger dynamics ($\tau_{cw} = 8.33E-3$ time periods, $\tau_{ex} = 0.1$ time periods). The response shown in Figure 3.4 is more extreme; here the corresponding first order time constants were 0.0167 and 0.15 time periods, leading to a faster departure from the stationary point and to a larger amplitude for the resulting limit cycle. A phase plot corresponding to Figure 3.4 is shown in Figure 3.5, wherein the reactor temperature is plotted against the instantaneous polymerization rate. Initially, the increasing temperature leads to an increase in the production rate until the gas concentration in the reactor becomes very low. The lack of available reactants then leads to a drop in both the production rate and temperature. Increasing gas concentrations finally result in an increase in

production rate and thus, the reactor temperature. This cycle is then repeated. The first few orbits of the limit cycle in Figure 3.5 have been labelled from 1 to 4. Further discussions of reactor stability and limit cycles are beyond the scope of this thesis. Comprehensive reviews of these topics have been provided by Razon and Schmitz (1987), Morbidelli et al. (1987) and Ray (1977).

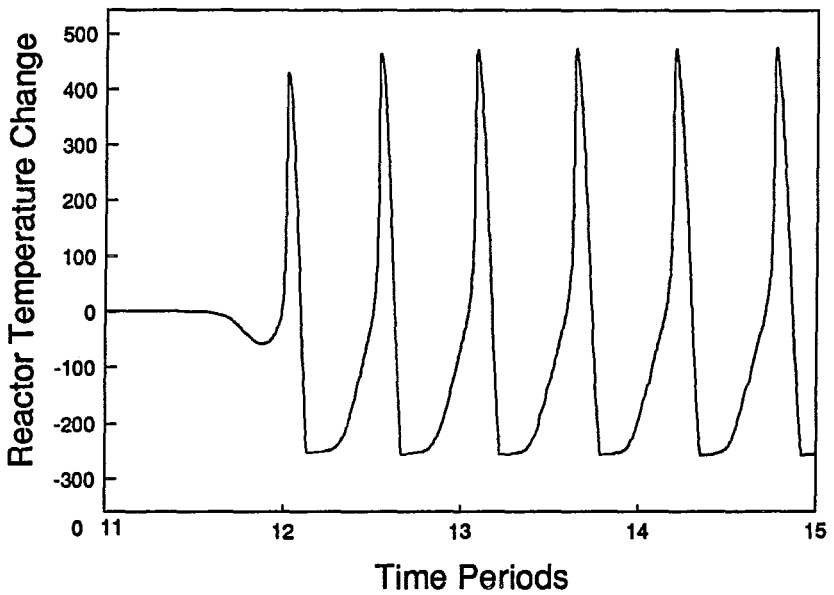

Figure 3.4 Open loop temperature response to a small perturbation from steady state (Slow exchanger dynamics)

The temperature at which particle sticking and agglomeration occurs depends to some extent on the grade of polymer being produced. All grades, however, experience sticking at 35 temperature units above the initial steady stae. As a result, the reactor model is no longer valid above this temperature and the limit cycle predicted in Figures 3.4 and 3.5 could not be realized experimentally. By the time the reactor temperature reached 40 units, a large chunk of molten polymer would have formed in the reactor, requiring a costly reactor shut-down. It is the instability

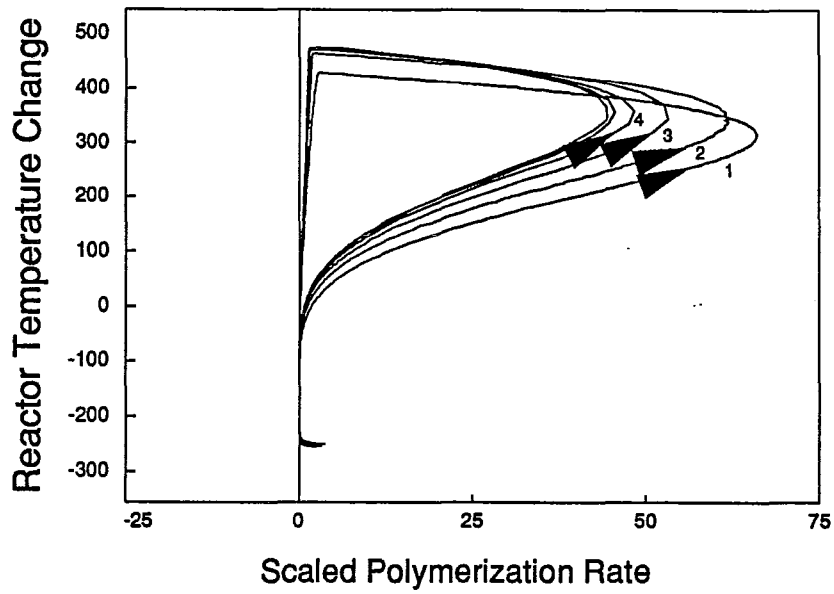

Figure 3.5 Phase plot (Slow exchanger dynamics)

of the steady state operating point, rather than the existence of stable limit cycles which is the important result of this reactor stability analysis. A stabilizing temperature controller must be used at to prevent temperature runaway.

Fortunately, the system can be stabilized using a proportional temperature controller which manipulates the cooling water inlet temperature setpoint, as long as the controller has a suitably large gain. Better performance is achieved, however, if a PID controller is used. Shown in Figure 3.6 is the closed loop step response of the system to a setpoint change of 4 temperature units.

The cooling water and heat exchanger time constants in this simulation were 8.33E-3 and 0.1 time periods, respectively, as in Figure 3.3. The tuning constants for the PID temperature controller were $K = 3.0$, $T_I = 0.133$ time periods, and $T_D = 0.4167$ time periods. This feedback temperature controller leads to stable reactor dynamics over the entire range of reactor behaviour simulated in this study.

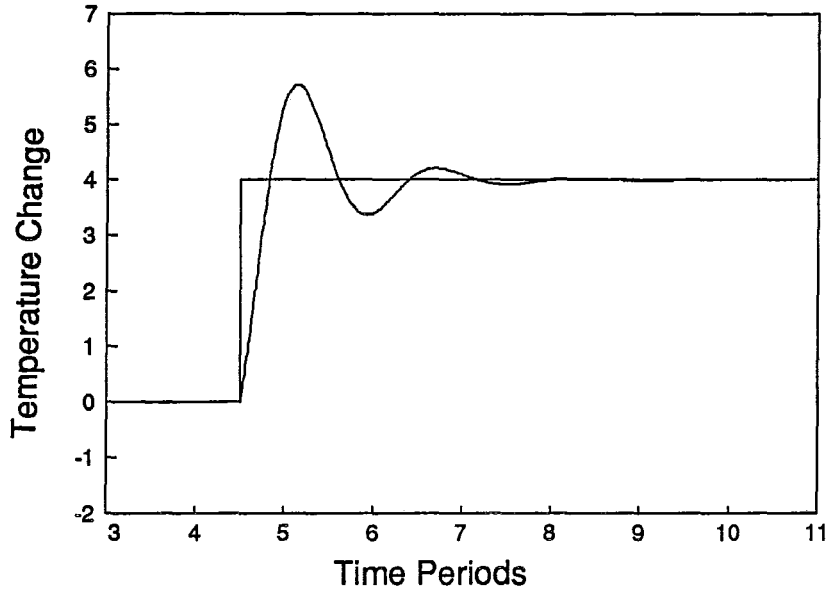

Figure 3.6 Closed loop temperature response to a step test

3.4 CONCLUSIONS

The mass and energy balance equations in this chapter allow the user to simulate the effects of changes in reactant feed rates and heat exchanger operation on the product properties. This capability is essential for simulating product property control schemes. Although the steady state operating point is open-loop unstable, in can be easily stabilized using a *PID* temperature controller.

3.5 NOTATION

$\underline{\underline{A}}$	Jacobian matrix
A	Arrhenius pre-exponential factor
A	Area available for heat transfer
a_i	Activity of component i
AlA	Aluminum alkyl cocatalyst
b_i	Rate of outflow of component i in the vent stream
b_{wsp}	Bed weight setpoint
b_w	Mass of polymer in the fluidized bed
$C_{p\,pol}$	Specific heat capacity of the polymer
C_{pg}	Specific heat capacity of the gas phase in the heat exchanger
c_v	Vent flow coefficient
$[C_T]_g$	Total gas phase concentration of all species in the reactor
$det\underline{\underline{A}}$	Determinant of matrix $\underline{\underline{A}}$
E_a	Activation energy
F_g	Molar flow rate of the gas phase through the heat exchanger
$F_w C_{pw}$	Product of cooling water flow rate and heat capacity in the heat exchanger
H_2	Hydrogen
H_f	Enthalpy of fresh feed stream
H_{gi}	Enthalpy of total gas inflow stream

H_{go}	Enthalpy of total gas outflow stream
$-H_r$	Heat liberated by the polymerization reaction
I_m	Impurity such as carbon monoxide
i	Monomer type
$[in]_g$	Concentration of inert components in the gas phase
j	Active site type
K	Proportional controller gain
$ka(j)$	Impurity desorption rate constant for a site of type j
$kdI(j)$	Deactivation by impurities rate constant for a site of type j
$kfh_T(j)$	Transfer pseudo-rate constant for a site of type j reacting with hydrogen
$kfr_T(j)$	Transfer pseudo-rate constant for a site of type j reacting with $AlEt_3$
$kh_r(j)$	Rate constant for reinitiation of a site of type j by cocatalyst
$kp_{Ti}(j)$	Propagation pseudo-rate constant for a site of type j reacting with monomer M_i
M_1	Ethylene
M_2, M_3	Butene, Higher alpha-olefin
M_i	Monomer of type i
$M_w C_{pw}$	Product of the mass and specific heat capacity of the reactor wall
$N(0,j)$	Uninitiated site of type j produced by formation reaction
$Nd_I(0,j), Nd_{IH}(0,j)$	Impurity killed sites of type j
$N_H(0,j)$	Uninitiated site of type j produced by transfer to hydrogen reaction

P_v	Pressure downstream of the vent
Q	Rate of heat transfer in the cycle gas cooler
Q_d	Dynamic rate of heat removal from the cycle gas
Q_{ss}	Rate of heat removal from the cycle gas at steady state
R	Ideal gas constant
R_i	Instantaneous consumption rate of monomer i
R_v	Volumetric polymer phase outflow rate from the reactor
S_i	Rate at which component i leaves the reactor dissolved in the polymer
T	Reactor temperature
t	Time
T_D	Derivative time
T_I	Integral time
T_g	Temperature of gas phase in the heat exchanger
T_{gi}	Gas temperature at the inlet to the heat exchanger
T_{go}	Gas temperature at the outlet of the heat exchanger
$T_{go\,ss}$	Gas temperature at the outlet of the heat exchanger at steady state
$tr\underline{\underline{A}}$	Trace of matrix $\underline{\underline{A}}$
T_{ref}	Reference temperature
T_w	Cooling water temperature in the heat exchanger
T_{wi}	Cooling water temperature at the exchanger inlet
T_{wo}	Cooling water temperature at the exchanger outlet

U	Overall heat transfer coefficient
V_g	Volume of gas phase in the reactor
V_p	Volume of polymer phase in the reactor
$\underline{x}$	Vector of model states
Y	Heat exchanger operating parameter
$Y(0,j)$	$zero_{th}$ moment of chain length distribution for living polymer produced at a site of type j
Γ_i	Molar feed rate of component i in the fresh feed stream
ν_p	Vent position
ρ	Polymer density
ρ_a	Density of amorphous polymer
ρ_c	Density of crystalline polymer
τ_{bw}	First-order time constant for closed loop bed level respons
τ_{cw}	First-order time constant for cooling water temperature response
τ_e	First-order time constant for heat exchanger dynamics

ON-LINE INFERENCE OF POLYMER PROPERTIES

4 ON-LINE INFERENCE OF POLYMER PROPERTIES

In this chapter, a model-based scheme to infer polymer quality variables in a fluidized bed polyethylene reactor is developed. First, simple theoretically-based models relating reactor operating conditions to molecular weight and copolymer composition are derived. Next, the development of a recursive technique for updating model parameters using off-line melt index (*MI*) and ρ measurements is described. Results are presented which show that both *MI* and ρ can be successfully predicted using this technique.

The purpose of this inference scheme is to provide on-line estimates of both *MI* and density (ρ) for use in on-line polymer quality monitoring and control. Since measurements of *MI* and ρ are performed only every few hours in the quality control laboratory, on-line model predictions of product quality are essential for automatic quality control scheme development. Although the inference technique presented is discussed in the context of predicting product quality in gas-phase polyethylene reactors, the approach is applicable to other chain growth polymerization systems with well-defined reactor mixing behavior.

4.1 MODELS FOR MELT INDEX AND DENSITY

Any scheme to predict melt index and density between measurements requires a model describing how these variables are affected by reactor operating conditions. If

the reactor is operated near one set of operating conditions to produce a limited number of polymer products, then an empirical linear plant model will often suffice. However, one of the advantages of gas phase processes over traditional liquid phase systems is the wider range of products that can be produced (Burdett, 1988). The models developed for this application must be valid over the range of products made in the reactor. Thus, linear empirical models are not suitable.

A kinetic model describing molecular weight and copolymer composition development and their relationships to melt index and density is presented in Chapter 2. While this model can predict *MI*, ρ, and production rate in an industrial reactor, the structure of this model is prohibitively complex for use in an on-line quality inference scheme. The approach taken in this chapter is to simplify the theoretical model so that it becomes appropriate for on-line use. Although several different comonomers are used to produce linear polyethylene in gas phase systems, it is uncommon to operate with ethylene and more than two comonomers in the reactor simultaneously. Hence, the simple models for *MI* and ρ are developed for ethylene, butene and one higher alpha-olefin (*HAO*) comonomer. Extensions to more comonomers are straightforward.

Unmeasured impurities and unmodelled disturbances can result in sustained offset between model predictions and measured quality variables. If such drifts in product quality are not accounted for in the control scheme, then large quantities of off-grade polymer can be produced. One way to alleviate this problem is to force the model to track the process by updating parameters and predictions recursively on-line. If the common sources of the expected mismatch are known, then this information can be used to choose which parameters remain constant and which are likely to change due to the disturbances. Theoretically-based models have an advantage over empirical models in

that the designer may have some prior knowledge about which parameters require on-line updating. Usually only a few meaningful parameters need to be updated, thereby making the on-line schemes easier to maintain and monitor.

4.1.1 Instantaneous vs. Cumulative Properties

Compared with the time scale of the gas phase and solid phase reactor dynamics, polymerization reactions involving Ziegler-Natta catalysts occur very quickly. Under the assumption of uniform gas composition and temperature, all of the polymer made, at a specific type of catalyst site, during a short time interval is similar in structure because it is produced under the same reaction conditions. The composition and molecular weight distributions of the polymer produced during this short time period are referred to as instantaneous properties, whereas the molecular weight and composition distributions of the total polymer in the fluidized bed are cumulative properties. At steady state the instantaneous and cumulative properties are identical. However, under unsteady conditions, instantaneous and cumulative properties can be significantly different. Cumulative polymer properties can be obtained by integrating the contributions of instantaneous polymer produced in the past, as is done in this application. First, models are developed for instantaneous melt index and density, and then a dynamic mass balance on the fluidized bed is then used to obtain the cumulative properties.

4.1.2 Instantaneous Melt Index Model Development

Above a certain critical molecular weight, the viscosity, η, of a linear polymer melt at low shear rates is related to the weight average molecular weight, $\overline{M}_w$, by:

$$\eta \propto \overline{M}_w{}^a \tag{4.1}$$

where the exponent a is approximately 3.5 (Vinodograv and Malkin, 1980). Since melt index is inversely proportional to the low shear viscosity, MI and $\overline{M}_w$ are related by:

$$MI \propto \overline{M}_w{}^{-3.5} \tag{4.2}$$

This power law relationship has been confirmed experimentally for linear polyethylenes by Bremner et al. (1990).

Gas-phase *ZN* olefin copolymerizations are generally controlled by reaction kinetics rather than by monomer diffusion limitations (Floyd et al., 1986). The broad molecular weight and compositional distributions which have been observed for these systems (Usami et al., 1986) result from multiple types of active sites on the catalyst. The polymer produced at each individual site type contributes to the overall product properties. In this system, growing polymer chains are terminated exclusively by chain transfer and site deactivation reactions. The instantaneous molecular weight distribution for polymer made at each site type is the Flory-Schultz most probable distribution and the corresponding polydispersity is 2 (Rudin, 1989). Thus, for an active site of type j, the instantaneous $\overline{M}_w$ and number average molecular weight, $\overline{M}_n$, are related by:

$$\overline{M}_w(j) = 2\,\overline{M}_n(j) \tag{4.3}$$

Hence, the instantaneous MI of the polymer produced at a site of type j is related to $r_n(j)$, the instantaneous number average degree of polymerization by:

$$MI(j) \propto \left[\frac{1}{r_n(j)}\right]^{3.5} \tag{4.4}$$

$r_n(j)$ is equal to the ratio of the rate of propagation of living polymer chains, $R_p(j)$, to the rate of production of dead chains, $R_{tr}(j)$:

$$r_n(j) = \frac{R_p(j)}{R_{tr}(j)} \tag{4.5}$$

$R_p(j)$ is the sum of the consumption rates for individual monomers:

$$R_p(j) = R_{p1}(j) + R_{p2}(j) + R_{p3}(j) \tag{4.6}$$

$$R_{p1}(j) = [M_1]\{kp_{11}(j)\phi_1(j) + kp_{21}(j)\phi_2(j) + kp_{31}(j)\phi_3(j)\}C^*(j) \tag{4.7}$$

$$R_{p2}(j) = [M_2]\{kp_{12}(j)\phi_1(j) + kp_{22}(j)\phi_2(j) + kp_{32}(j)\phi_3(j)\}C^*(j) \tag{4.8}$$

$$R_{p3}(j) = [M_3]\{kp_{13}(j)\phi_1(j) + kp_{23}(j)\phi_2(j) + kp_{33}(j)\phi_3(j)\}C^*(j) \tag{4.9}$$

The individual propagation rates depend on $[M_1]$, $[M_2]$ and $[M_3]$, which are the concentrations ethylene, butene and *HAO* in the gas phase, and on $C^*(j)$, the number of moles of active sites of type j in the reactor. The $kp_{im}(j)$ terms are propagation rate constants for the addition of monomer m to a growing chain with terminal monomer i. $\phi_i(j)$ is the fraction of propagating sites of type j which have terminal monomer i. Expressions for $\phi_1(j), \phi_2(j)$and $\phi_3(j)$ can be found in Chapter 2.

For industrial polyethylenes, the incorporation of comonomer into the polymer chains is generally less than 5 mole per cent (Sinclair, 1983). Thus, at any one time the fraction of growing chains with a terminal butene or *HAO* group is expected to be small. Propagation rate constants for the addition of a given monomer to the chain are of the same order of magnitude, regardless of the terminal monomer on the growing chain. As a result, the first term in the parentheses in equation 4.7 is much larger than the remaining two terms. Similarly, the first terms in equations 4.8 and 4.9 are much larger than the terms which follow them. Substitution into

equation 4.6 with the added assumption that $\phi_1(j)$ is near unity gives:

$$R_p(j) = \{[M_1]kp_{11}(j) + [M_2]kp_{12}(j) + [M_3]kp_{13}\}C^*(j) \tag{4.10}$$

Neglecting spontaneous transfer and deactivation reactions, the rate of production of dead chains consists of transfer to monomer, transfer to hydrogen, transfer to cocatalyst and impurity deactivation terms:

$$R_{tr}(j) = R_{f1}(j) + R_{f2}(j) + R_{f3} + R_{fH}(j) + R_{fR}(j) + R_{dI}(j) \tag{4.11}$$

The rates of chain transfer to ethylene, butene, *HAO*, hydrogen and cocatalyst are shown below:

$$R_{f1}(j) = [M_1]\{kf_{11}(j)\phi_1(j) + kf_{21}(j)\phi_2(j) + kf_{31}(j)\phi_3(j)\}C^*(j) \tag{4.12}$$

$$R_{f2}(j) = [M_2]\{kf_{12}(j)\phi_1(j) + kf_{22}(j)\phi_2(j) + kf_{32}(j)\phi_3(j)\}C^*(j) \tag{4.13}$$

$$R_{f3}(j) = [M_3]\{kf_{13}(j)\phi_1(j) + kf_{23}(j)\phi_2(j) + kf_{33}(j)\phi_3(j)\}C^*(j) \tag{4.14}$$

$$R_{fH}(j) = [H_2]\{kf_{1H}(j)\phi_1(j) + kf_{2H}(j)\phi_2(j) + kf_{3H}(j)\phi_3(j)\}C^*(j) \tag{4.15}$$

$$R_{fR}(j) = [R]\{kf_{1R}(j)\phi_1(j) + kf_{2R}(j)\phi_2(j) + kf_{3R}(j)\phi_3(j)\}C^*(j) \tag{4.16}$$

$[H_2]$ and $[R]$ are the concentrations of hydrogen and cocatalyst, respectively. The *kf*'s are transfer rate constants defined in Chapter 2. The rate of active site deactivation by impurities, $R_{dI}(j)$, is:

$$R_{dI}(j) = [I]kdI(j)C^*(j) \tag{4.17}$$

$[I]$ is the concentration of impurities in the reactor and $k_{dI}(j)$ is a deactivation rate constant. Equations 4.12 to 4.16 can be simplified in a similar manner to equations 4.7 to 4.9. Equations 4.10 to 4.17 can then be combined to give the following expression:

$$\frac{R_{tr}(j)}{R_p(j)} = \frac{[M_1]kf_{11}(j) + [M_2]kf_{12}(j) + [M_3]kf_{13}(j) + [H_2]kf_{1H}(j) + [R]kf_{1R}(j) + [I]kdI(j)}{[M_1]kp_{11}(j) + [M_2]kp_{12}(j) + [M_3]kp_{13}(j)} \tag{4.18}$$

This equation can be further simplified by neglecting $[M_2]kp_{12}(j)$ and $[M_3]kp_{13}(j)$ in the denominator. This can be done without incurring much additional error because the incorporation of butene and *HAO* into the polymer chains is small compared with ethylene incorporation. Combination of equations 4.5 and 4.18 yields:

$$\frac{1}{r_n(j)}=\frac{kf_{11}(j)}{kp_{11}(j)}+\frac{kf_{12}(j)[M_2]}{kp_{11}(j)[M_1]}+\frac{kf_{13}(j)[M_3]}{kp_{11}(j)[M_1]}+\frac{kf_{1H}(j)[H]}{kp_{11}(j)[M_1]}+\frac{kf_{1R}(j)[R]}{kp_{11}(j)[M_1]}+\frac{kdI(j)[I]}{kp_{11}(j)[M_1]} \tag{4.19}$$

resulting in the following relationship between melt index and the reaction kinetics:

(4.20)

$$MI(j)\propto\left\{\frac{kf_{11}}{kp_{11}}+\frac{kf_{12}[M_2]}{kp_{11}[M_1]}+\frac{kf_{13}[M_3]}{kp_{11}[M_1]}+\frac{kfh_1[H_2]}{kp_{11}[M_1]}+\frac{kfr_1[R]}{kp_{11}[M_1]}+\frac{kdI[I]}{kp_{11}[M_1]}\right\}^{3.5}$$

The j's on the right hand side of equation 4.20 have been eliminated in the interest of brevity. The effect of temperature on melt index can be incorporated into the model by assuming that all chain transfer and deactivation reactions have a similar activation energy, Ea_{tr}. For a general chain transfer rate constant, $kf(T)$, Arrhenius behavior implies that:

$$kf(T)=kf(T_0)\exp\left(-\frac{Ea_{tr}}{R}\left\{\frac{1}{T}-\frac{1}{T_0}\right\}\right) \tag{4.21}$$

where T_0 is a reference temperature. Thus, the ratio of a chain transfer rate constant to kp_{11} is:

$$\frac{kf(T)}{kp_{11}(T)}=\frac{kf(T_0)}{kp_{11}(T_0)}\exp\left(\frac{-Ea_{tr}+Ea_p}{R}\left\{\frac{1}{T}-\frac{1}{T_0}\right\}\right) \tag{4.22}$$

where Ea_p is the activation energy for propagation. Equation 4.20 becomes:

$$MI(j)=\exp\left\{k_7\left(\frac{1}{T}-\frac{1}{T_0}\right)\right\}\left\{k_6+k_1\frac{[M_2]}{[M_1]}+k_2\frac{[M_3]}{[M_1]}+k_3\frac{[H_2]}{[M_1]}+k_4\frac{[R]}{[M_1]}+k_5\frac{[I]}{[M_1]}\right\}^{3.5} \tag{4.23}$$

The overall instantaneous melt index of the polymer could be calculated from the individual, site-specific, instantaneous melt indices, $MI(1)$ and $MI(2)$, if the parameters in equation 4.23 were known for each site type. The overall instantaneous weight average molecular weight of the combined polymer produced at two different active site types is:

$$\overline{M}_w = w_1 \overline{M} w(1) + w_2 \overline{M}_w(2) \tag{4.24}$$

where w_1 and w_2 are the weight fractions of the polymer produced at sites 1 and 2, and $\overline{M}_w(1)$ and $\overline{M}_w(2)$ are the corresponding weight average molecular weights. From equation 4.2:

$$MI^{-0.286} = w_1 MI(1)^{-0.286} + w_2 MI(2)^{-0.286} \tag{4.25}$$

Since it is very difficult to determine the parameters k_1 to k_7 for each separate active site type, it is proposed that the same structure as equation 4.23 be used to predict the overall instantaneous melt index. The parameters values k_1 to k_7 will be influenced by the combined effects of the individual sites. When catalyst grade changes are made, altering the ratio of the two types of sites, the values of the parameters will change. Taking natural logarithms of both sides of equation 4.23 and eliminating the j gives the final model form:

$$\ln(MI) = k_7\left(\frac{1}{T} - \frac{1}{T_0}\right) + 3.5\ln\left(k_6 + k_1\frac{[M_2]}{[M_1]} + k_2\frac{[M_3]}{[M_1]} + k_3\frac{[H_2]}{[M_1]} + k_4\frac{[R]}{[M_1]} + k_5\frac{[I]}{[M_1]}\right) \tag{4.26}$$

Although many assumptions and simplifications have been made in order to obtain this instantaneous MI model, the main mechanisms which affect molecular weight development are still reflected in the model structure.

4.1.3 Instantaneous Density Model Development

The density of a polymer sample depends on how closely the polymer chains can fit together. Incorporation of comonomers into polyethylene causes short chain branches (*SCB*'s) to protrude from the polymer backbone. These *SCB*'s inhibit crystalline structures and reduce the density of the polymer. Both the number of branches along the chain and the length of the side chains influence density. Polymer molecular weight or, alternatively, melt index also has a small influence on polyethylene density (Sinclair, 1983). A model of the form:

$$\rho = p_0 + p_1 \ln(MI) - \{a_2 mf_2 + a_3 mf_3\}^{p_4} \tag{4.27}$$

reflects these ideas. mf_2 and mf_3 are the mole fractions of butene and *HAO*, respectively, in the polymer chains. As mf_2 and mf_3 increase, the number of *SCB*'s increases causing the density to fall. Parameters a_2 and a_3 are different from one another because the side chains produced by the *HAO* are longer than those produced by butene. A smaller mole fraction of *HAO* than butene is required to produce the same drop in density. When ethylene homopolymer is produced, mf_2 and mf_3 are zero. Thus, p_0 represents the density of pure homopolymer with a melt index of unity.

At a site of type j, the instantaneous mole fraction of butene in the polymer chain is:

$$mf_2(j) = \frac{R_{p2}(j)}{R_p(j)} \tag{4.28}$$

When comonomer incorporation is small, this expression reduces to:

$$mf_2(j) = \frac{[M_2]kp_{12}(j)}{[M_1]kp_{11}(j)} \tag{4.29}$$

Similarly for the HAO:

$$mf_3(j) = \frac{[M_3]kp_{13}(j)}{[M_1]kp_{11}(j)} \tag{4.30}$$

The overall mole fraction of butene and HAO in the polymer depend on the relative numbers of the two active site types:

$$mf_2 = m_1 mf_2(1) + m_2 mf_2(2) \tag{4.31}$$

$$mf_3 = m_1 mf_3(1) + m_2 mf_3(2) \tag{4.32}$$

where m_1 and m_2 are the mole fractions of the total monomer being consumed instantaneously at site types 1 and 2, respectively. Thus, for a given catalyst:

$$mf_2 \propto \frac{[M_2]}{[M_1]} \tag{4.33}$$

$$mf_3 \propto \frac{[M_3]}{[M_1]} \tag{4.34}$$

The instantaneous density model becomes:

$$\rho = p_0 + p_1 \ln(MI) - \left\{ p_2 \frac{[M_2]}{[M_1]} + p_3 \frac{[M_3]}{[M_1]} \right\}^{p_4} \tag{4.35}$$

The structure of this model agrees with the observation that reactor temperature has a minimal effect on the density of polyethylene. Temperature effects enter the preceding model only through the melt index term.

4.1.4 Cumulative Melt Index and Density Models

When two polymer samples, labelled A and B, with different molecular weights are mixed together, $\overline{M}_w$ of the mixture is given by:

$$\overline{M}_w = w_A \overline{M}_{wA} + w_B \overline{M}_{wB} \tag{4.36}$$

where w_A and w_B are the weight fractions of polymers A and B in the mixture and $\overline{M}_{wA}$ and $\overline{M}_{wB}$ are the respective weight average molecular weights. If the same samples have densities ρ_A and ρ_B and no volume change occurs during the mixing process, then the overall density is given by:

$$\frac{1}{\rho} = \frac{w_A}{\rho_A} + \frac{w_B}{\rho_B} \tag{4.37}$$

In fluidized bed polyethylene reactors, the solid polymer particle phase is well-mixed by the turbulent action of the gas phase. New polymer is added continuously to the bed by the polymerization of monomers, and the accumulated polymer leaves the bed in frequent small batches via the product discharge system. Hence, the mixing and residence time behavior of the solid phase can be approximated by that of an ideal continuous stirred tank. Instantaneous polymer with weight average molecular weight $\overline{M}_{wi}$, melt index MI_i, and density ρ_i is fed continuously to the mixer at a mass flow rate P_R equal to the instantaneous polymer production rate. The well-mixed bed contains a mass of polymer, M_p, which has a cumulative weight average molecular weight $\overline{M}_{wc}$, cumulative melt index MI_c, and cumulative density ρ_c. If there is no net accumulation of polymer during a short period of time, Δt, then $P_R \Delta t$ kg of new instantaneous polymer enter the bed and the same quantity of cumulative polymer leaves the bed. After the time period, Δt, the mass fraction of new instantaneous polymer in the reactor will be $P_R \Delta t / M_p$ and the mass fraction of the old cumulative polymer will be $1 - P_R \Delta t / M_p$. Thus, the new weight average molecular weight and density are given by:

$$\overline{M}_{wc}(t + \Delta t) = \frac{P_R \Delta t}{M_p} \overline{M}_{wi}(t) + \left(1 - \frac{P_R \Delta t}{M_p}\right) \overline{M}_{wc}(t) \tag{4.38}$$

$$\frac{1}{\rho_c(t+\Delta t)} = \frac{P_R \Delta t}{M_p}\frac{1}{\rho_i(t)} + \left(1 - \frac{P_R \Delta t}{M_p}\right)\frac{1}{\rho_c(t)} \tag{4.39}$$

Therefore:

$$\frac{\overline{M}_{wc}(t+\Delta t) - \overline{M}_{wc}(t)}{\Delta t} = \frac{1}{\tau}\overline{M}_{wi}(t) - \frac{1}{\tau}\overline{M}_{wc}(t) \tag{4.40}$$

$$\frac{\frac{1}{\rho_c(t+\Delta t)} - \frac{1}{\rho_c(t)}}{\Delta t} = \frac{1}{\tau}\frac{1}{\rho_i(t)} - \frac{1}{\tau}\frac{1}{\rho_c(t)} \tag{4.41}$$

where $\tau = M_p/P_R$ is the solid phase residence time. Taking the limit as $\Delta t \rightarrow 0$ gives the following differential equations:

$$\frac{d\overline{M}_{wc}}{dt} = \frac{1}{\tau}\overline{M}_{wi} - \frac{1}{\tau}\overline{M}_{wc} \tag{4.42}$$

$$\frac{d\left(\frac{1}{\rho_c}\right)}{dt} = \frac{1}{\tau}\frac{1}{\rho_i} - \frac{1}{\tau}\frac{1}{\rho_c} \tag{4.43}$$

Equation 4.2 can be used to express equation 4.42 in terms of melt index:

$$\frac{d(MI_c^{-0.286})}{dt} = \frac{1}{\tau}MI_i^{-0.286} - \frac{1}{\tau}MI_c^{-0.286} \tag{4.44}$$

Given the initial cumulative *MI* and ρ of the polymer bed, equations 4.43 and 4.44 can be used to predict the effects of time varying instantaneous *MI* and ρ on the cumulative properties. It is these cumulative properties which are measured in the quality control laboratory. Gas compositions in the reactor are measured periodically using on-line gas chromatographs. Since the gas sampling interval, h, is very small with respect to the polymer phase residence time, τ, little error is incurred by assuming that the instantaneous properties remain constant over the gas sampling interval. Using this assumption, equation 4.44 is equivalent to the following difference

equation:

$$MI_c^{-0.286}(t) = \exp(-h/\tau)MI_c^{-0.286}(t-h) + \{1-\exp(-h/\tau)\}MI_i^{-0.286}(t-h) \tag{4.45}$$

Similarly for density, equation 4.43 becomes:

$$\frac{1}{\rho_c(t)} = \exp(-h/\tau)\frac{1}{\rho_c(t-h)} + \{1-\exp(-h/\tau)\}\frac{1}{\rho_i(t-h)} \tag{4.46}$$

These are the model forms used in the on-line inference scheme. All that is required to predict cumulative melt index and density estimates are initial estimates of MI_c and ρ_c, estimates of the parameters $\underline{k} = (k_1, k_2, \ldots k_7)^T$ and $\underline{p} = (p_0, p_1, \ldots p_4)^T$ in the instantaneous property equations 4.26 and 4.35, and a series of gas compositon, temperature, production rate and bed mass measurements.

4.2 RECURSIVE TECHNIQUES FOR UPDATING PARAMETERS AND PREDICTIONS IN NONLINEAR MODELS

Recursive techniques are ideal for updating model parameters in on-line applications. The traditional nonlinear least squares approach to parameter estimation is usually not used because it requires the storage of past input variables and observations in a table. As this data table continues to grow, successive calculations take longer to complete. In recursive schemes, the measured input and output data are processed sequentially and old measurements need not be stored. Each parameter updating step requires the same amount of computational effort. The approaches which can be used for recursive parameter estimation with nonlinear models include the extended Kalman filter and recursive prediction error methods (Ljung, 1987).

4.2.1 The Extended Kalman Filter

The extended Kalman Filter (*EKF*) provides a framework for both state estimation and parameter updating in nonlinear process models. One of the first reported applications of this technique to polymer reactors was by Jo and Bankhoff (1976) who used an *EKF* to both estimate process states and update several time varying parameters on-line. Recent applications of *EKF*'s to polymerization systems have been reported by Kozub and MacGregor (1989),by Gagnon (1990) and by Ellis et al. (1988) among others.

For the polyethylene reactor study in this paper, the *EKF* could be implemented as follows. Given an initial set of parameter estimates ($\underline{k}^o, \underline{p}^o$), and some initial estimate of the model states ($MI_c^{-0.286\,o}$, $1/\rho_c^o$), the nonlinear model equations 4.45 and 4.46 can be linearized about these initial conditions to give:

$$\underline{x}(t) = \underline{A}(t)\,\underline{x}(t-1) + \underline{G}(t)\,\underline{u}(t) + \underline{w}(t) \tag{4.47}$$

$$\underline{y}(t) = \underline{H}(t)\,\underline{x}(t) + \underline{v}(t) \tag{4.48}$$

where $t-1$ refers to the time at which the last polymer sample was taken and t is the time of the current sample. The state vector $\underline{x}$ is an augmented vector consisting of the model and parameter states, that is:

$$\underline{x}^T = (MI_c^{-0.286}, 1/\rho_c, \underline{k}^T, \underline{p}^T) \tag{4.49}$$

The $\underline{A}$ and $\underline{G}$ matrices in equation 4.47 are composed of several parts as shown below:

$$\underline{A} = \begin{pmatrix} \underline{A}' & | & \underline{0} \\ - & | & - \\ \underline{0} & | & \underline{I} \end{pmatrix} \tag{4.50}$$

$$\underline{G}(t)=\begin{pmatrix}\underline{G'}\\ \underline{0}\end{pmatrix} \tag{4.51}$$

The $\underline{A'}$ part in equation 4.49 is the linearized relationship describing how $MI_c^{-0.286}$ and $1/\rho_c$ at time $t-1$ contribute to the properties at time t. An expression for $MI_c^{-0.286}$ at time t can be obtained by successive application of equation 4.45 for each interval of length h contained in the product sampling interval from time $t-1$ to t. In a similar manner, $1/\rho_c$ can be determined by successive applications of equation 4.46. These equations can be linearized using Taylor series approximations to give $\underline{A'}$ and also $\underline{G'}$ in equations 4.50 and 4.51. $\underline{y}(t)$ in equation 4.48 is the vector of new measurements available at time t and $\underline{H}(t)=(1,0,\underline{0}),(0,1,\underline{0})$ or $(1,0,\underline{0})$ depending upon which measurements are available at the current sampling interval. $\underline{u}$ is the set of inputs to the model including temperature and gas composition ratios. $\underline{w}$ and $\underline{v}$ represent the modelling errors and the measurement errors, with covariance matrices $\underline{R}_w$ and $\underline{R}_v$, respectively. When new measurements become available, the state estimation and parameter updating are accomplished by solving the following filter equation:

$$\underline{\hat{x}}(t\mid t)=\underline{\hat{x}}(t\mid t-1)+\underline{K}(t)\{\underline{y}(t)-\underline{\hat{y}}(t\mid t-1)\} \tag{4.52}$$

where $\underline{\hat{y}}(t\mid t-1)$ is the predicted output vector at time t made by evaluating the nonlinear model equations 4.45 and 4.46 from time $t-1$ to t. The Kalman gain matrix, $\underline{K}(t)$, comes from solving the following set of recursive matrix Ricatti equations:

$$\underline{K}(t)=\underline{P}(t\mid t-1)\,\underline{H}^T(t)\,[\underline{H}(t)\,\underline{P}(t\mid t-1)\,\underline{H}^T(t)+\underline{R}_v]^{-1} \tag{4.53}$$

$$\underline{P}(t\mid t-1)=\underline{A}(t)\,\underline{P}(t-1\mid t-1)\,\underline{A}^T(t)+\underline{R}_w \tag{4.54}$$

$$\underline{P}(t\mid t)=\underline{P}(t\mid t-1)-\underline{K}(t)\,\underline{H}(t)\,\underline{P}(t\mid t-1) \tag{4.55}$$

$\underline{P}(t \mid t)$ is the covariance matrix for the state and parameter estimates at time t, given all of the information available at that time. After each update, the predictions of the model states ($MI_c^{-0.286}$, $1/\rho_c$) are again made by successive evaluations of equations 4.45 and 4.46 over the next product sampling interval. These equations are then relinearized about the predictions to the forms in equations 4.47 and 4.48. The entire sequence is repeated with each laboratory measurement. The *EKF* is tuned by changing the relative sizes of the elements in $\underline{R}_v$ and $\underline{R}_w$ as explained by MacGregor et al. (1986). *EKF*'s are very versatile in that they can be used to update one or more parameters appearing in several model equations simultaneously and they provide updated estimates of the model states and the parameters with each new product measurement. Nevertheless, care must be taken in the formulation of *EKF*'s. If too few parameter or disturbance states are included in $\underline{x}$, then biased estimates will be obtained due to unaccounted for non-stationary disturbances (MacGregor et al., 1986).

4.2.2 The Recursive Prediction Error Method

The recursive prediction error method (*RPEM*) is closely related to the parameter estimation part of the extended Kalman filter. Recursive prediction error schemes are generally simpler to design, tune and implement than *EKF*'s, but they are also less flexible. *RPEM*'s are usually formulated to update a vector of parameters, $\underline{\theta}$, in a single model equation of the form:

$$y = f(\underline{\theta}, \underline{u}(t-1), y(t-1)) \tag{4.56}$$

If this model is linear in the parameters, then the *RPEM* collapses to recursive least squares (*RLS*) estimation. *RLS* and other variants of the *RPEM* are commonly used in self-tuning regulator applications (Goodwin and Sin, 1984). Given the variance

of the measurement error, σ_e^2, an initial vector of parameter estimates, $\underline{\hat{\theta}}(0)$, and the covariance of these estimates, $Cov(\underline{\hat{\theta}}(0))$, recursive parameter identification is accomplished by solving the following Ricatti equations:

$$\underline{\hat{\theta}}(t) = \underline{\hat{\theta}}(t-1) + \underline{L}(t-1)\varepsilon(t) \tag{4.57}$$

$$\varepsilon(t) = y_{meas}(t) - y(\underline{\hat{\theta}}(t-1)) \tag{4.58}$$

$$\underline{L}(t-1) = \frac{\underline{\underline{Q}}(t-1)\underline{Z}(t)}{\lambda + \underline{Z}^T(t)\underline{\underline{Q}}(t-1)\underline{Z}(t)} \qquad 0 \le \lambda \le 1 \tag{4.59}$$

$$\underline{\underline{Q}}(t) = \frac{1}{\lambda}\underline{\underline{Q}}(t-1) - \frac{\underline{\underline{Q}}(t-1)\underline{Z}(t)\underline{Z}^T(t)\underline{\underline{Q}}(t-1)}{\lambda + \underline{Z}^T(t)\underline{\underline{Q}}(t-1)\underline{Z}(t)} \tag{4.60}$$

$$\underline{Z}(t) = -\frac{\partial \varepsilon}{\partial \underline{\theta}} = \frac{\partial y}{\partial \underline{\theta}} \tag{4.61}$$

$$\underline{\underline{Q}}(t) = \frac{Cov(\underline{\hat{\theta}}(t))}{\sigma_e^2} \tag{4.62}$$

Equation 4.57 is similar in structure to the *EKF* equation 4.52. $\underline{L}(t-1)$ and $\underline{K}(t)$ are both gain terms and $\varepsilon(t)$ and $\underline{y}(t) - \underline{\hat{y}}(t \mid t-1)$ are prediction errors. Like $\underline{P}(t \mid t)$ in equation 4.55, $\underline{\underline{Q}}(t)$ provides a measure of the covariance of the parameter estimates. The model linearization steps required for the *EKF* are replaced by the calculation of $\underline{Z}(t)$ whose elements are partial derivatives of the model with respect to the parameters.

To provide for time varying parameters, the *RPEM* has been formulated with an exponential forgetting factor, λ. Values of λ near 1 correspond to slow parameter updating whereas a smaller λ results in recent information being weighted more heavily than past data so that $\underline{\hat{\theta}}$ can change quickly. A constant value of λ can result in slow parameter updating after abrupt process changes and in covariance blow-up when too much old information is discarded during periods of steady

operation. To prevent these problems, Fortescue et al. (1981) have developed a variable forgetting factor algorithm which adapts λ according to the information content of the data. Their algorithm shown below results in a small λ after abrupt process changes and a λ near unity during periods when prediction errors are small:

$$\lambda(t) = 1 - \frac{1 - \underline{Z}^T(t)\underline{L}(t-1)}{\gamma}\varepsilon^2(t) \tag{4.63}$$

Just as the rate at which parameters change is influenced by the elements of $\underline{R}_w$ in the *EKF*, γ is a tuning factor which influences the rate of parameter change when the *RPEM* is used. The latter approach, however, lacks some of the flexibility of the *EKF* when more than one parameter is being updated. The elements of $\underline{R}_w$ can be specified independently to influence individual parameters. Changes to γ, however, cause a similar effect in the rates of change of all of the parameters.

Unlike the *EKF*, *RPE* methods provide updated estimates of the model parameters whenever new observations are made, however, they do not simultaneously provide updated estimates of the state variables ($MI_c^{-0.286}$, $1/\rho_c$) at these instances. Obviously by updating the model parameters recursively, the prediction errors of these states are kept small over time. However, to evaluate the model equations 4.45 and 4.46 over each product sampling interval, initial conditions at the start of the interval must be given for MI_c and ρ_c. These initial conditions could be taken as the measured values at $t-1$, the predicted values at $t-1$ or some compromise between the two. A benefit of the *EKF* is that it automatically provides the optimal estimates as part of the update vector $\hat{\underline{x}}(t \mid t)$. To solve this problem, the *RPE* algorithm can be augmented with an empirical filter of the form:

$$\underline{\hat{x}}^*(t \mid t) = \underline{\hat{x}}^*(t \mid t-1) + \underline{K}^*(\underline{y}(t) - \underline{\hat{y}}(t \mid t-1)) \tag{4.64}$$

where $\underline{x}^* = (MI_c^{-0.286}, 1/\rho_c)^T$. This state filtering equation is of the same form as the Kalman Filter equation 4.52, except that $\underline{K}^*$ is assumed to be a constant matrix which is estimated from a representative record of plant data so as to minimize the sum of squared prediction errors. In general, for measurements with very little noise, the diagonal elements of $\underline{K}^*$ will approach unity, while for noisy measurements, these elements will be smaller.

4.3 APPLICATION OF RECURSIVE ESTIMATION FOR PRODUCT QUALITY INFERENCE

Before a recursive estimation scheme can be implemented, one must choose which parameter values should be adapted on-line and which should remain constant. If the recursive technique is used to fit data from a well-designed dynamic experiment, then a number of parameters can be successfully updated simultaneously. However, if the parameter estimator is applied to happenstance data, it is better to fix most of the parameter values off-line and estimate only a few on-line. If the input to the estimator lacks sufficient information on some of the model parameters, the resulting parameter estimates will have a large covariance and will be highly correlated with the estimates of other parameters. Such correlation can be determined from the elements of $\underline{P}$ or $\underline{Q}$. While a model with poorly known and highly correlated parameters can track the process successfully during periods of ordinary plant operation, when a change in operating conditions occurs, the poor parameter estimates will initially lead to poor model predictions. Updating only a few essential parameters can help to alleviate this problem.

For the melt index and density models, the candidates for on-line updating are parameters k_1 to k_7 in equation 4.26 and p_0 to p_4 in equation 4.35. Since many different unmeasured impurities affect the instantaneous melt index, the entire $k_5[I]/[M_1]$ term is a good candidate for on-line updating. Equation 4.26 can be rewritten as:

$$\ln(MI) = k_7\left(\frac{1}{T} - \frac{1}{T_0}\right) + 3.5\ln\left(k_0 + k_1\frac{[M_2]}{[M_1]} + k_2\frac{[M_3]}{[M_1]} + k_3\frac{[H_2]}{[M_1]} + k_4\frac{[R]}{[M_1]}\right) \tag{4.65}$$

where $k_5[I]/[M_1]$ and k_6 have been collapsed into a single term, k_0. Updating k_0 on-line has intuitive appeal because it accounts for the effects of changing impurity levels on *MI*. Since low-level impurities have very little effect on density, there is no corresponding impurity term in equation 4.35 which should be automatically chosen for on-line estimation. If only one parameter is to be updated on-line, it must affect the model predictions, regardless of which comonomer is being used and the *MI* of the polymer being produced. For this reason, p_0 should be updated recursively. If necessary, additional parameters in either the melt index or density models could also be chosen for on-line adaptation. In the interest of simplicity, however, it was decided that only k_0 and p_0 would be updated on-line. This choice of a single parameter for each model avoids the problem of parameter correlation in the case of non-informative data and also makes the application simple to implement and maintain. Since instantaneous and cumulative properties are identical at steady state, parameters k_1 to k_4, k_7 and p_1 to p_4 were estimated off-line using steady state plant data.

In this study, the *RPEM* was chosen over the *EKF* approach. The reasons for this choice are that the *RPEM* is easier to implement, has fewer parameters to specifiy and the potential benefits of the *EKF* are not realized in this simple estimation problem. To implement an *EKF*, the user must supply: initial estimates of the state variables and

parameters, an initial covariance matrix $\underline{P}_0$, a linearized version of the model equations as shown in equation 4.47, and covariance matrices R_v and R_w. The only requirements for implementation of the RPEM are initial estimates of the parameters k_0 and p_0, initial estimates of their variances, expressions for the partial derivatives in equation 4.61, and a single tuning factor, γ, for each time varying parameter. Although the *RPEM* approach is recommended in this situation, the added flexibility of the EKF would be beneficial for more complex estimation problems. The potential benefits of the *EKF* over the *RPEM* include: the ability to estimate unmeasured model states, the potential for estimating several time varying parameters simultaneously while controlling the relative rate of change of each parameter, the ability to estimate parameters which appear simultaneously in several highly coupled models, and a means of optimally accounting for errors in the measured model inputs. These benefits are not realized in the estimation problem under consideration because our goal is to estimate only two time varying parmaters, k_0 and p_0 which appear in two essentially uncoupled equations. There is no requirement for the estimation of unmeasured model states nor is there any need to incorporate information on the gas composition or temperature measurement errors into the scheme. The measurement errors in these inputs are sufficiently small that they can be neglected, especially since the integration step of equations 4.45 and 4.46 has an averaging effect on the individual errors. Since none of the potential benefits of the *EKF* are realized in this estimation problem, the two approaches should give almost identical results.

A diagram illustrating the on-line product quality inference scheme for melt index is shown in Figure 4.1. An analogous diagram can be drawn for density. When a new melt index measurement becomes available from the laboratory, the measurement is compared with the model prediction which corresponds to the time at which the sample was taken from the reactor. Since the sample analysis delay may be as long as one hour,

a table containing past temperature and gas composition data at h minute intervals must be stored on-line. After the parameter update calculation, the current melt index estimate can be updated by applying equation 4.45 with the new value of k_0 over each h minute interval of the analysis delay, starting from the new measured value of MI. The prediction error used in the recursive estimation algorithm in Figure 4.1 is the difference between the logarithms of the measured and predicted MI's. This transformation is used because the variance of the melt index laboratory measurement increases with the melt index level. The error variance in $\ln(MI)$, however, does not depend on the magnitude of the MI measurement. A constant error variance assumption is implicit in least squares type estimators, which include both the *EKF* and *RPEM*. No transformation is required for density because the measurement error variance is not level dependent. Thus, y in equation 4.56 is either $\ln(MI)$ or ρ and $\underline{\hat{\theta}}$ in equation 4.57 is either k_0 or p_0 depending on which model is being updated. The partial derivatives required in equation 4.61 can be determined either numerically or analytically. Initial parameter estimates and variances were provided from the off-line parameter identification. γ, the forgetting factor tuning parameter, was tuned to achieve the desired trade-off between information content and the speed of the parameter update.

The *RPE* algorithm was also augmented with the fixed gain observer equation 4.63, where the gains in $\underline{K}^*$ were estimated from some plant data to minimize the sum or squared prediction errors. Estimates of these gains were close to unity. Consequently, the measured values were used as initial conditions in integrating the prediction equations over the next step.

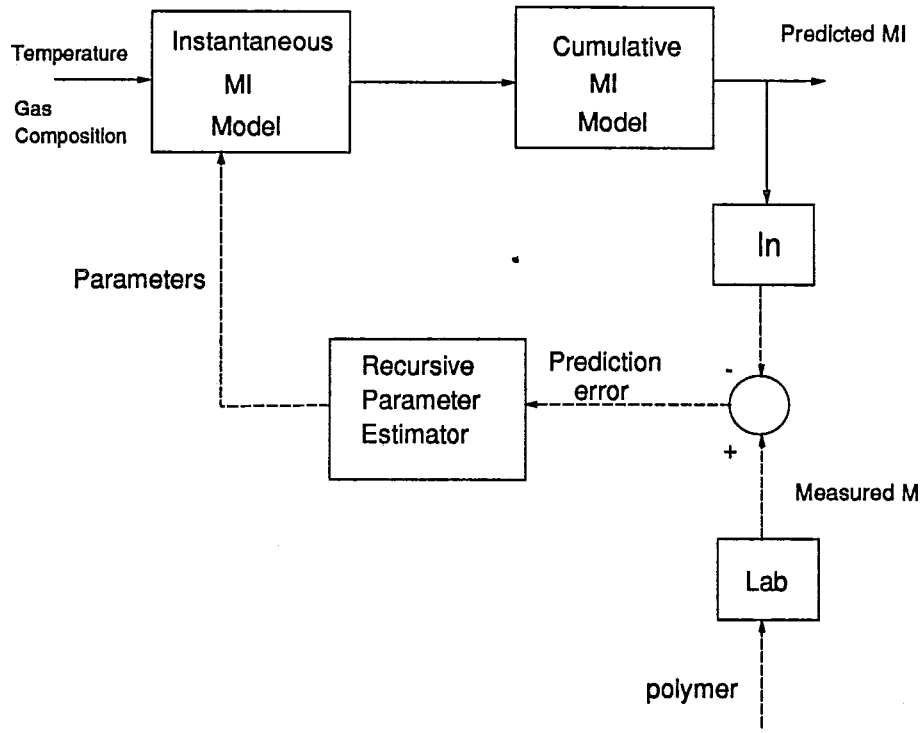

Figure 4.1 Melt index prediction scheme

4.4 RESULTS AND DISCUSSION

Typical results from the melt index and density inference scheme during a grade transition are shown in Figures 4.2a) to 4.2g). The model parameters and the γ settings required to produce these results are given in Table 4.1. Note that the values in Table 4.1 and the industrial results shown in the figures are scaled to keep actual reactor operating conditions and model parameters proprietary. Since the reactor was operated isothermally during the grade transition, a scaled value of $\exp\{k_7(1/T_0 - 1/T)\}$ is shown in Table 4.1 rather than k_7, itself. For most reactor operating conditions, $k_4[R]/[M_1]$ is very small and can be neglected. As shown in Figure 4.2a), the product quality inference

scheme is able to successfully track a density change from 9 to 13 scaled units. The density measurements, indicated by open circles, were performed several hours apart at irregular intervals. Any scheme used to update *MI* and ρ models on-line must account for this sporadic sampling period, as does the current *RPE* scheme. The small dots on the graph, which are often close enough together that they appear to form a line, represent the model predictions between the laboratory data. One dot was plotted each time the on-line gas composition measurements were made. The vertical distance between the predictions and the measurements is the density prediction error. After each laboratory measurement, the new model prediction starts at the measured value of ρ. Thereafter equation 4.46 is used to recursively calculate each new model prediction. The density change in Figure 4.2a) occurs in response to a reduction in the gas phase butene to ethylene ratio shown in 4.2b). During this 70 time period interval, the density update parameter plotted in 4.2c), remained constant within 0.1 scaled density units, indicating that the density model was able to account for the density behavior of the industrial reactor.

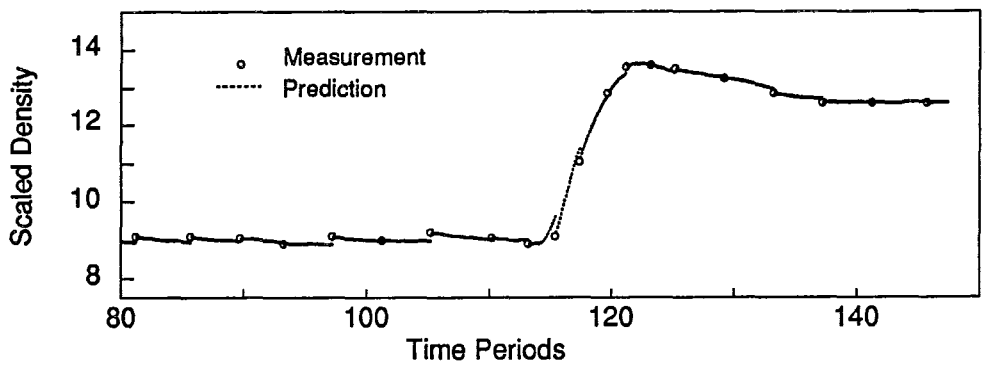

Figure 4.2a) Density predictions: Transition 1

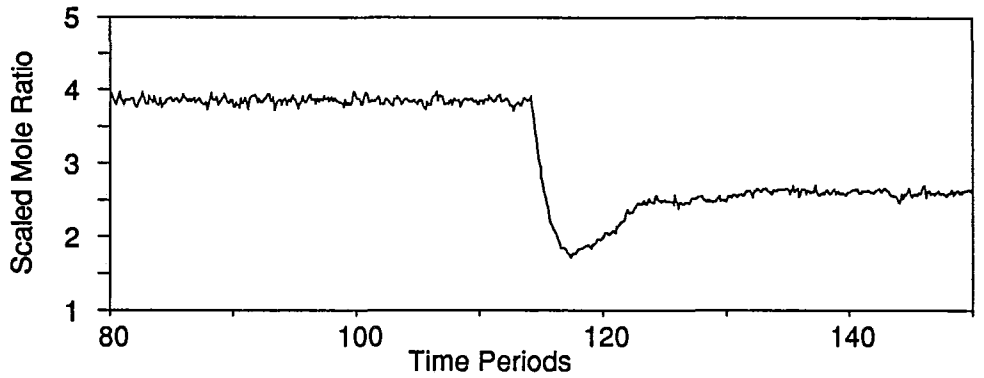

Figure 4.2b) Scaled butene to ethylene mole ratio: Transition 1

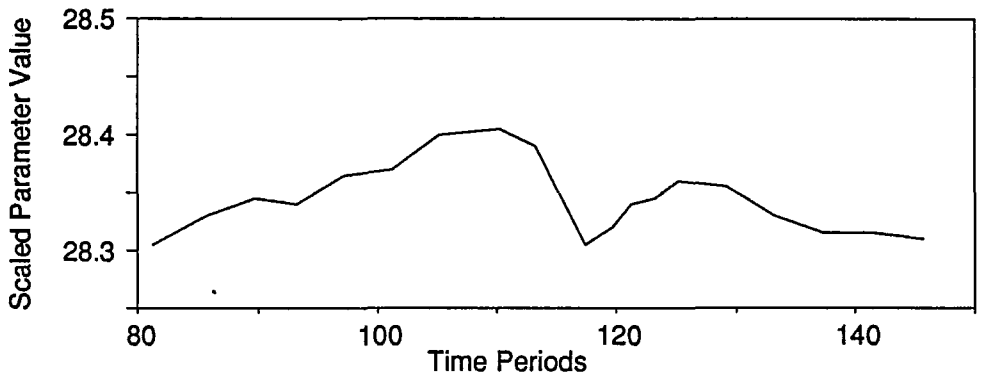

Figure 4.2c) Scaled density update parameter : Transition 1

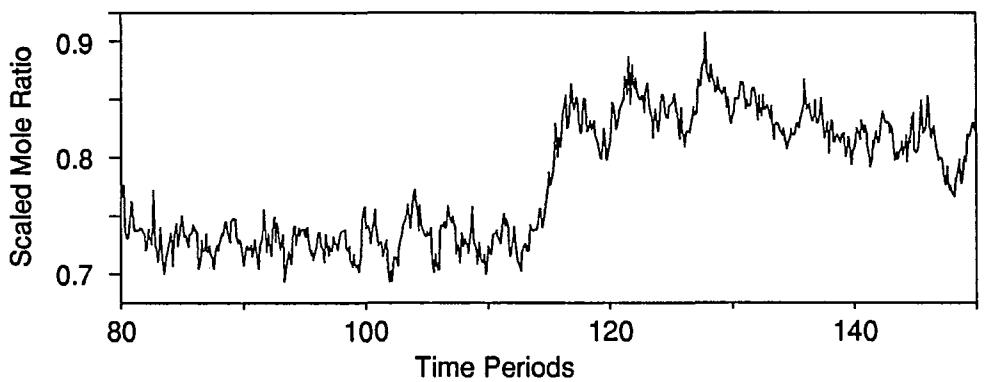

Figure 4.2d) Scaled hydrogen to ethylene ratio: Transition 1

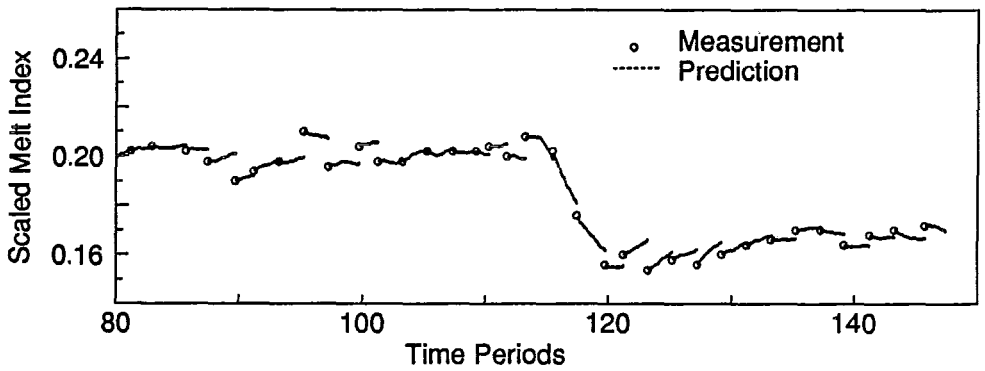

Figure 4.2e) Scaled melt index predictions: Transition 1

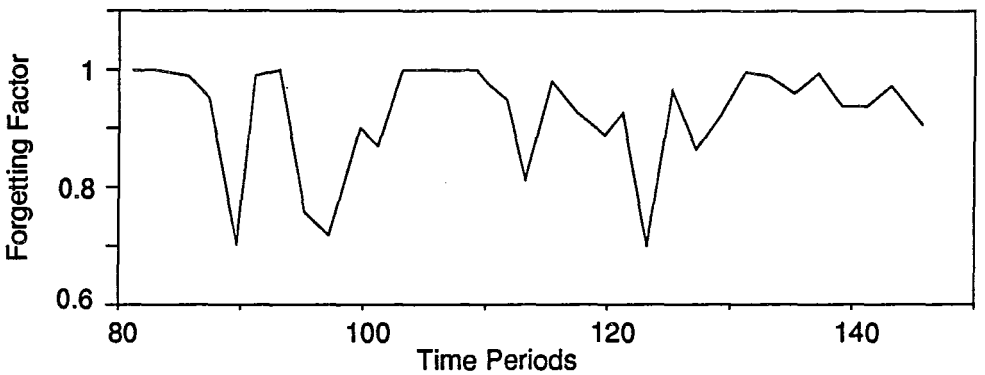

Figure 4.2f) Melt index forgetting factor: Transition 1

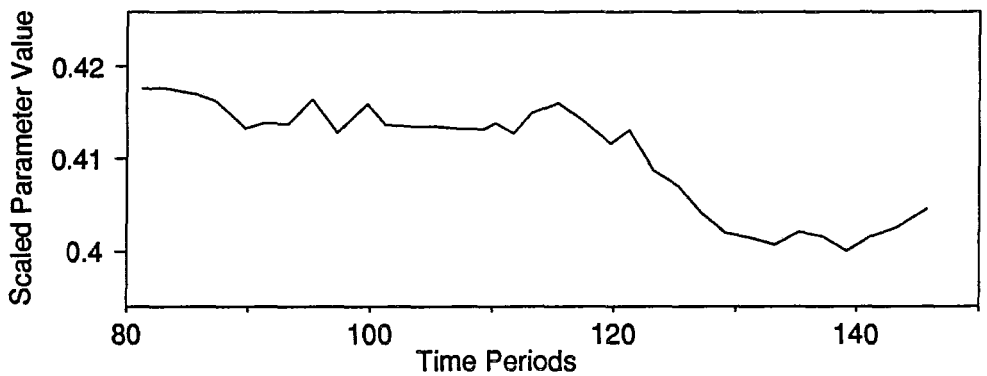

Figure 4.2g) Scaled melt index update parameter: Transition 1

Table 4.1 Scaled Parameters Required for Inference Scheme

Parameter	Scaled Value
$\exp\{k_7(1/T_0 - 1/T)\}$	0.1660
k_1	0.0726
k_3	0.3298
p_1	1.227
p_2	85.29
p_4	0.5292
γ for k_0	0.01
γ for p_0	0.25

The decrease in the butene to ethylene ratio at time period 112 in Figure 4.2b) was also accompanied by an increase in the hydrogen to ethylene ratio, shown in Figure 4.2d). Since both hydrogen and butene act as chain transfer agents, increases in their concentrations result in lower molecular weight polymer and, thus, in a higher melt index. Hence, the simultaneous decrease in butene and increase in hydrogen have opposite effects on *MI*, and it would be difficult to predict the resulting *MI* response without a model. As shown in Figure 4.2e), the on-line inference scheme was able to predict the resulting small decrease in *MI*. The prediction errors are more apparent in Figure 4.2e) than in 4.2a) because the ordinate scale is larger relative to the standard deviation of the laboratory measurement error. The behavior of the exponential forgetting factor, λ is shown in 4.2f). After time period 120, the on-line model predicts *MI* values in Figure

4.2e) which are too high for four consecutive measurements. The *RPEM* algorithm responds to the first large prediction error by reducing the forgetting factor so that k_0 can be adapted quickly. As the prediction errors become smaller, λ is then allowed to increase. During this period the value of k_0 adapts to a lower level as shown in Figure 4.2g). This small adjustment in k_0 is required to force the model to track the process after the change in reactor operating conditions. The necessity of a change in k_0 could be attributable to any of a number of possible causes: a change in impurity levels; a drift in the gas composition analysers; a change in catalyst properties; uncertainty in the other fixed model parameters, or a slight structural inadequacy of the model. Regardless of the cause, the on-line model was able to capture the main effects of the gas composition changes and the recursive parameter estimation scheme was able to quickly adapt k_0 to eliminate any offset.

Although the density change shown in Transition 1 is quite large, the melt index change is small compared with the range of *MI*'s produced in the reactor. Figures 4.3a) to 4.3i) show that the recursive updating scheme can successfully track a grade transition involving a large change in *MI* and only a slight density change. The transition from 10 to 4 scaled *MI* units shown in Figure 4.3a) occurs in response to changes in the hydrogen and butene concentrations shown in 4.3b) and 4.3c) and to a slight change in the reactor temperature shown in 4.3d). Between time periods 225 and 240, the *MI* update parameter k_0 undergoes small rapid changes due to *MI* prediction errors encountered during the grade transition. These prediction errors reduce the variable forgetting factor which allows the estimate of k_0 to change quickly. After time period 250, when the *MI* in the reactor reaches steady state, the value of k_0 stabilizes near the value calculated before the transition, indicating that little parameter adjustment was required to eliminate offset from the model.

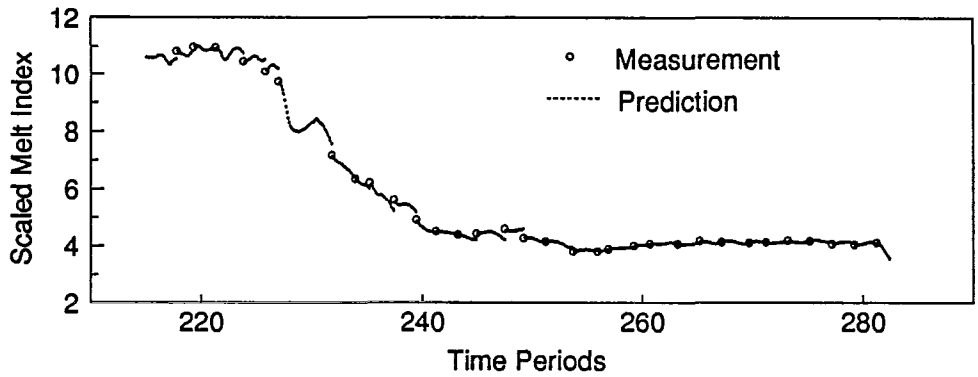

Figure 4.3a) Scaled melt index: Transition 2

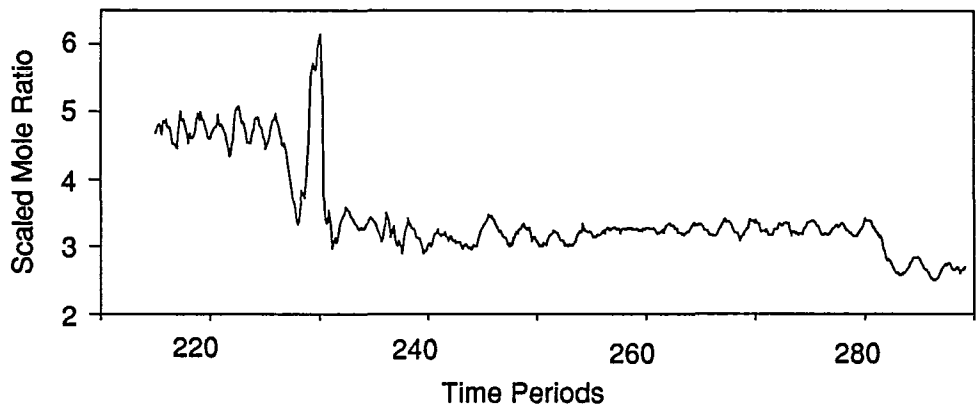

Figure 4.3b) Scaled hydrogen to ethylene ratio: Transition 2

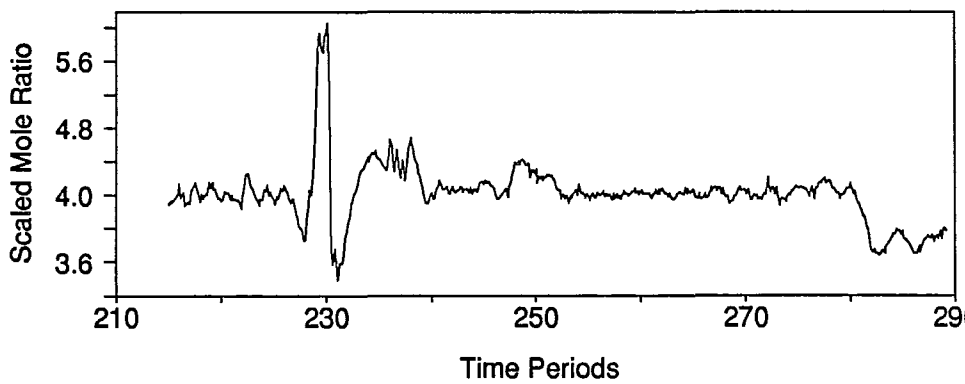

Figure 4.3c) Scaled butene to ethylene ratio: Transition 2

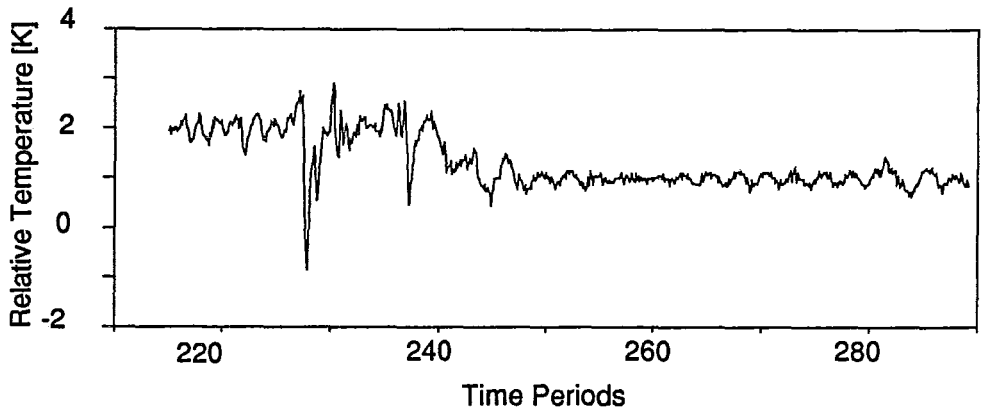

Figure 4.3d) Reactor temperature deviation from reference: Transition 2

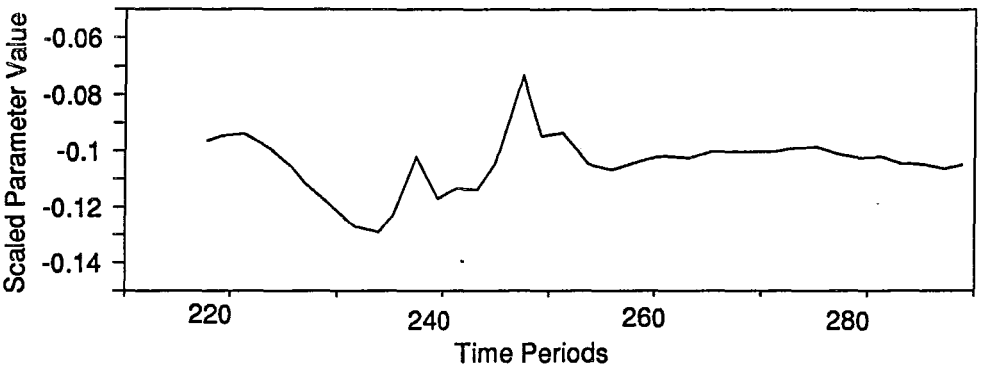

Figure 4.3e) Scaled melt index update parameter k0: Transition 2

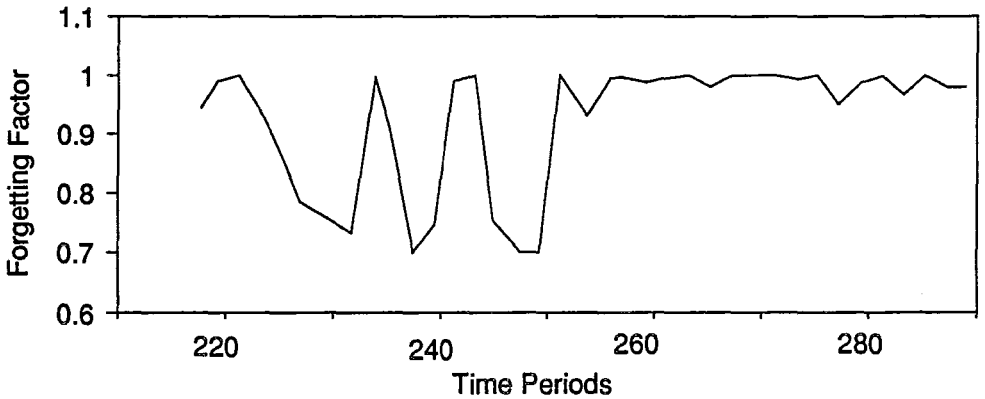

Figure 4.3f) Melt index forgetting factor: Transition 2

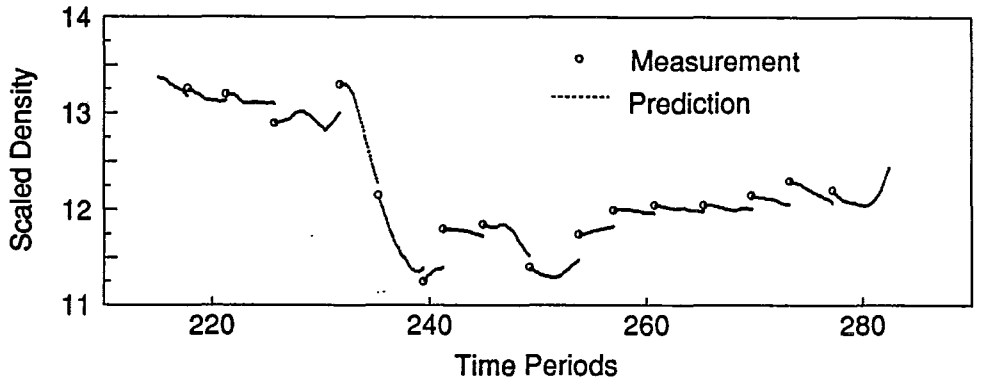

Figure 4.3g) Scaled density predictions: Transition 2

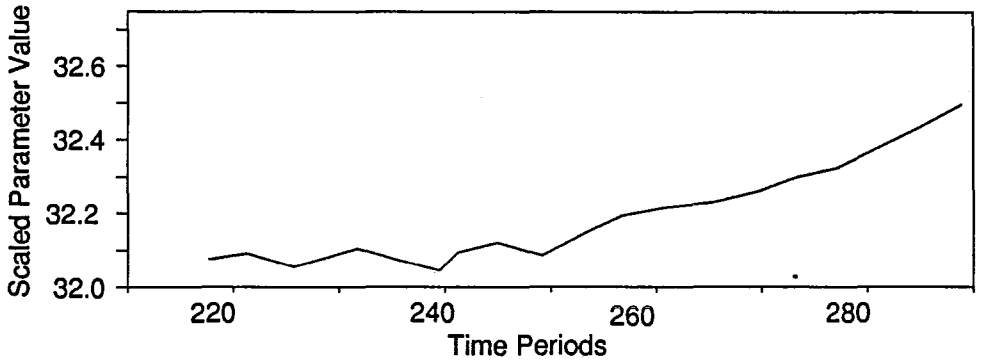

Figure 4.3h) Scaled density update parameter p0: Transition 2

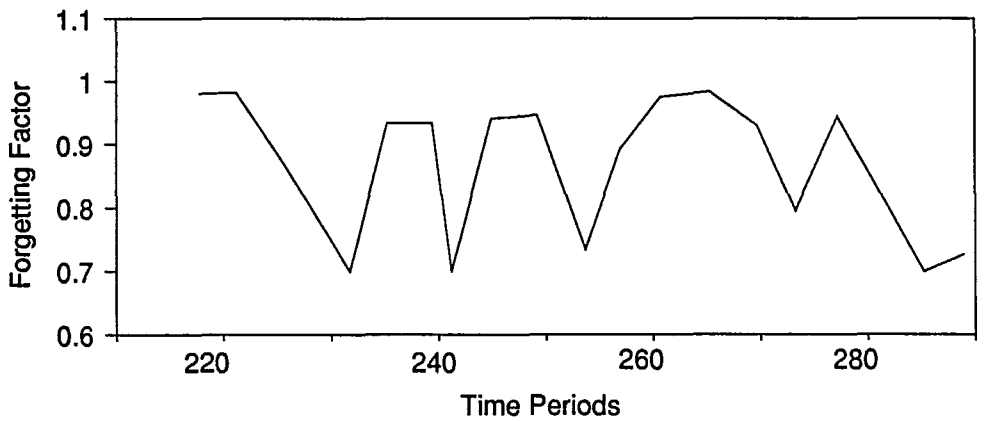

Figure 4.3i) Density forgetting factor: Transition 2

The density response to the change in reactor conditions is shown in Figure 4.3a). Between time periods 230 and 240, the density change was well-predicted by the simplified model. After time period 250, however, it is apparent that predictions from the density model are consistently too low. The recursive estimator responds by slowly increasing the value of p_0 to alleviate the mismatch.

Several different industrial catalyst formulations are used to produce different grades of polymer. It was suggested in section 4.1.2 that each catalyst grade contains a different distribution of active site types which can have a significant effect on product quality. To investigate this effect, the parameters in equations 4.26 and 4.35 were fitted separately for each catalyst type. It was shown that catalyst formulation has a significant effect on *MI* model parameters, but no significant difference between density model parameters was discernible from the steady state data available. As a result, it was proposed that a single density model should be used for all of the catalyst grades and that separate melt index models should be evaluated as a means to improve on-line predictions. Using reactor data for each catalyst type, it was determined that better *MI* predictions are obtained during grade transitions when individual catalyst-specific models are used to predict *MI*, rather than global model parameters determined using melt index data for all of the catalyst types .The results shown in Figures 4.2 and 4.3 were developed using the individual melt index models which matched the catalyst grades used in the reactor.

A problem arises when separate catalyst-specific models are used during transitions involving a catalyst changeover. To demonstrate how separate models can be incorporated into the on-line inference scheme, both *MI* and density have been predicted during two grade transitions with catalyst changeovers. The results are shown in Figures 4.4 and 4.5. In Figure 4.4, the catalyst change occurs at approximately time

period 90. The density response to the change in catalyst and in reactor conditions was predicted by the inference scheme, with only a small parameter adjustment required. When a single model was used to predict *MI* throughout the operating period, good results were obtained, but the parameter estimate k_0 required significant updating. Good results were also obtained when separate sets of *MI* model parameters were used before and after the catalyst change. To accomodate the use of two separate models, the on-line model parameters were switched when the feed of new catalyst to the reactor began. An initial value of k_0 for the new model was calculated so that the new and old models would give the same prediction of instantaneous *MI* at the time of the catalyst changeover. The reinitialization of k_0 results in the jump in the value of k_0 shown in Figure 4.4l). Thereafter, only a slight adjustment to k_0 was required to eliminate steady state offset.

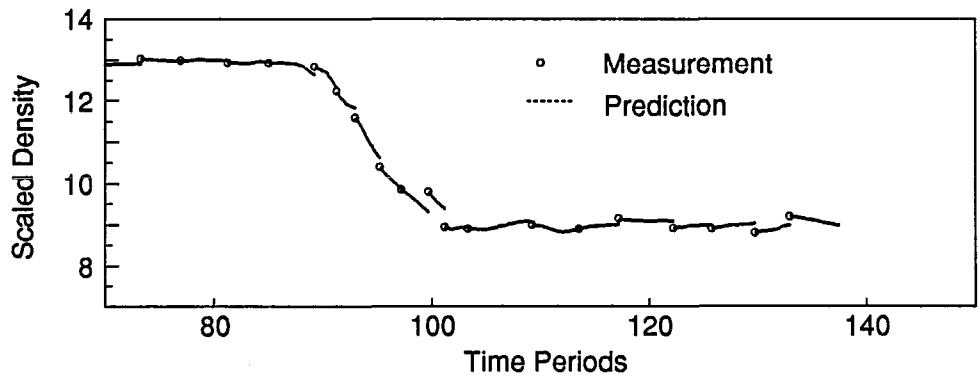

Figure 4.4a) Scaled density prediction: Transition 3

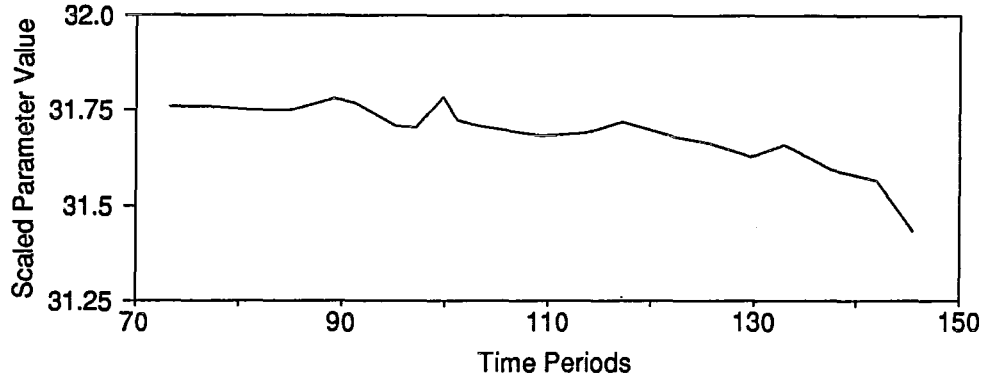

Figure 4.4b) Scaled density update parameter p0: Transition 3

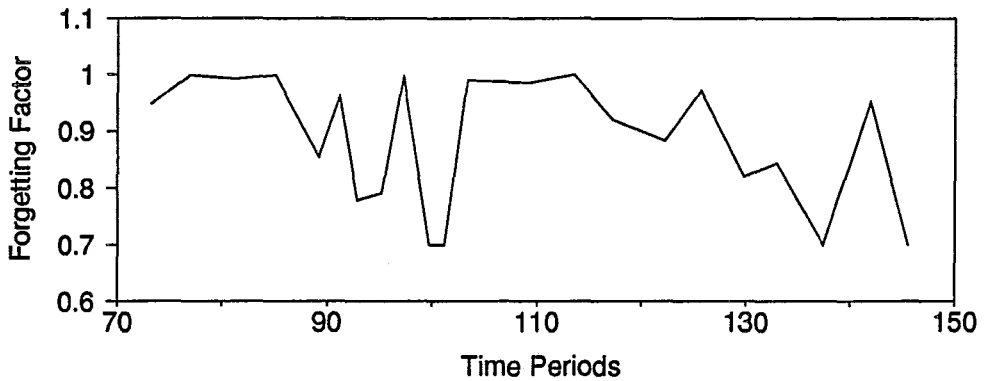

Figure 4.4c) Density forgetting factor: Transition 3

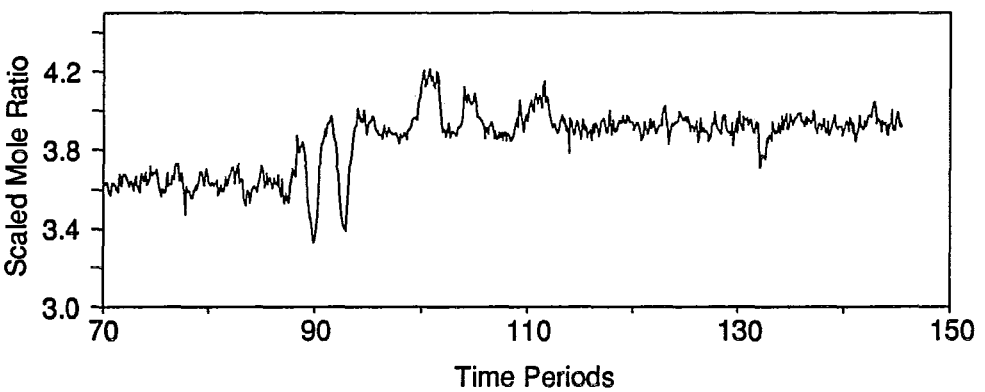

Figure 4.4d) Scaled butene to ethylene ratio: Transition 3

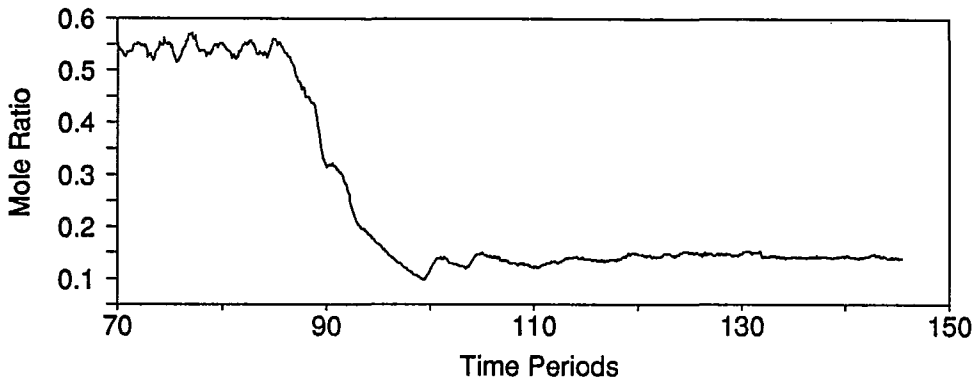

Figure 4.4e) Scaled hydrogen to ethylene ratio: Transition 3

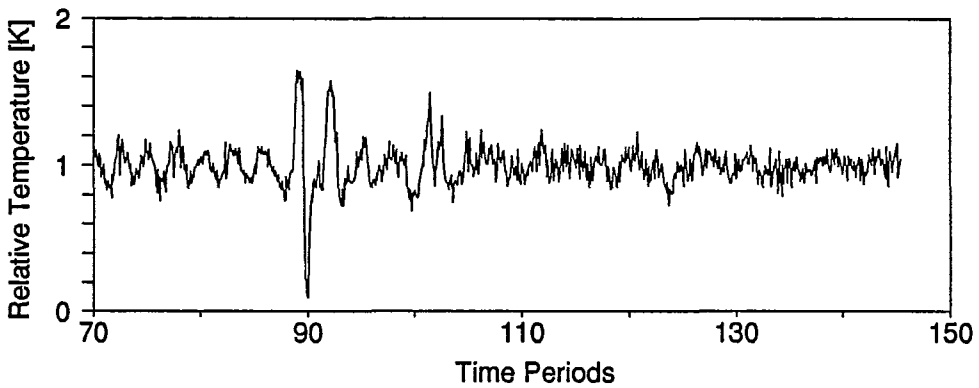

Figure 4.4f) Reactor temperature deviation from reference: Transition 3

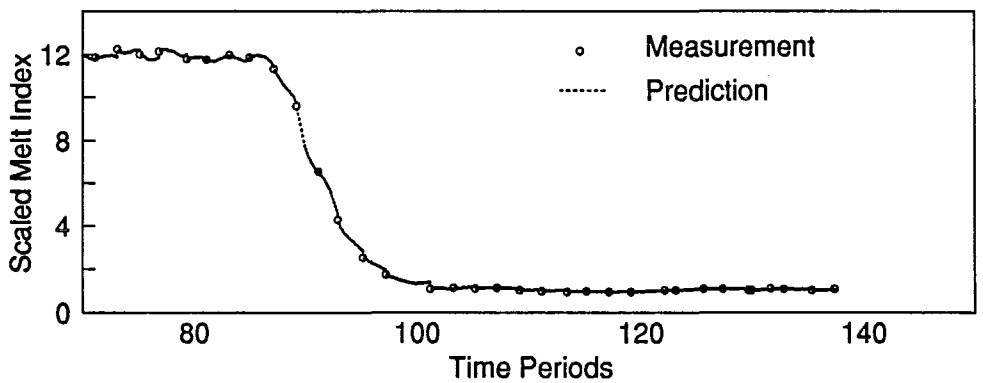

Figure 4.4g) Scaled MI predictions using a single model: Transition 3

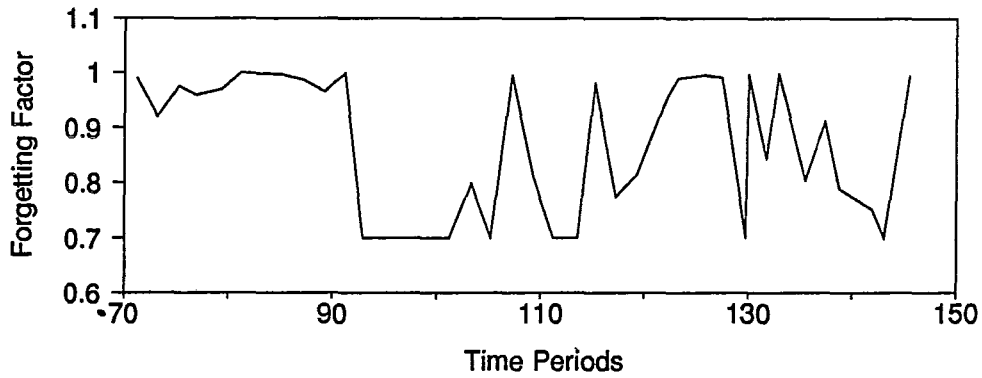

Figure 4.4h) MI forgetting factor using a single model: Transition 3

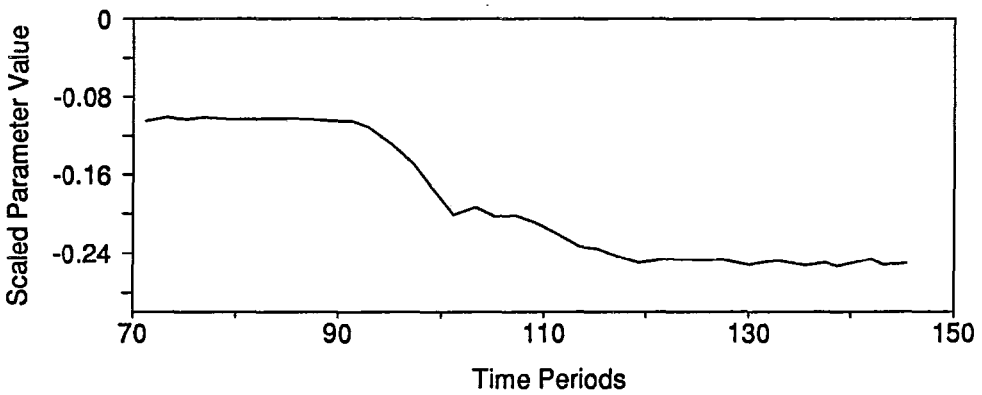

Figure 4.4i) Scaled MI update parameter k0 using a single model: Transition 3

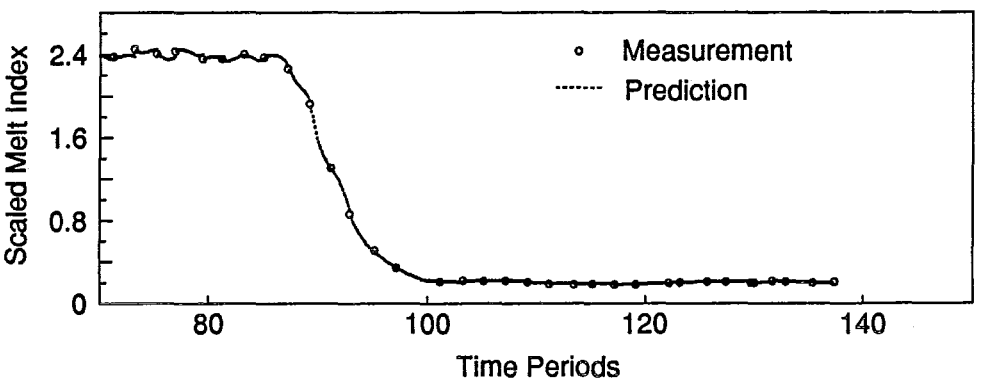

Figure 4.4j) Scaled MI predictions using specific models: Transition 3

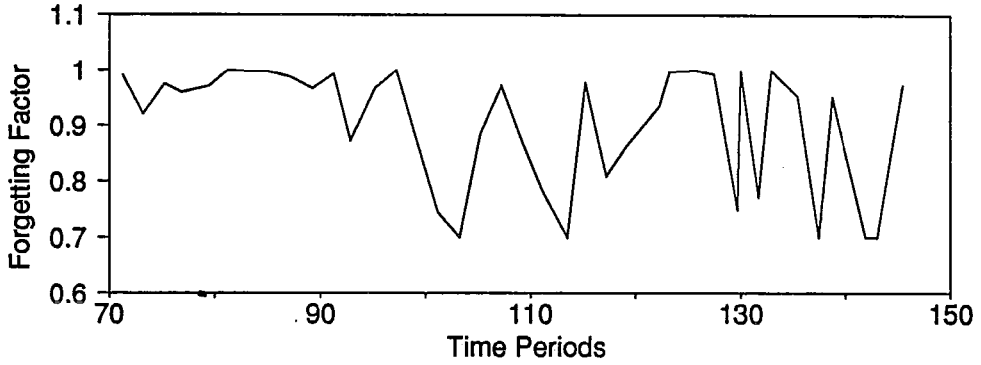

Figure 4.4k) MI forgetting factor using specific models: Transition 3

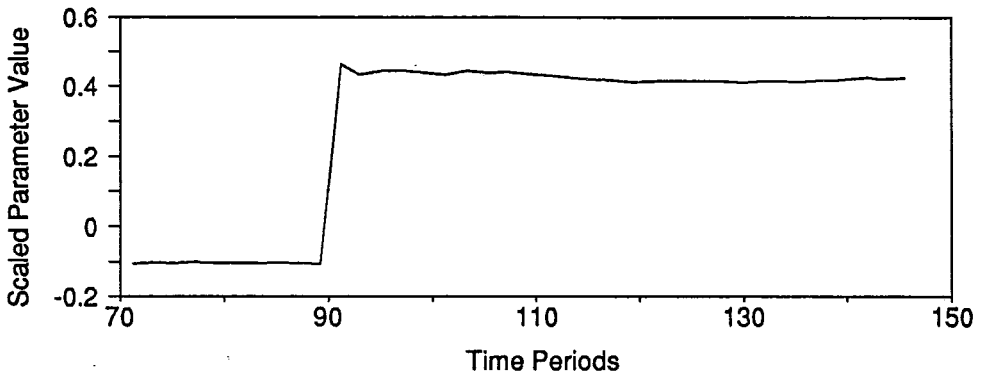

Figure 4.4l) Scaled MI update parameter k0 using specific models: Transition 3

From Figure 4.4g), it would seem that separate *MI* models may not be needed for different catalysts and that recursive estimation part of the inference scheme can adapt to account for different catalyst formulations. Nevertheless, this observation cannot be generalized for all grade transitions. As in the previous case, use of a single density model gave good predictions during grade transition 4, as shown in Figure 4.5a). However, if a single

MI

model is used both before and after the catalyst change, as shown in Figure 4.5g), the resulting *MI* predictions are poor. After the catalyst change, the *MI* model continues to predict *MI*'s which are too low and the parameter updating scheme reponds by increasing k_0 in Figure 4.5i) substantially between time periods 220 and 240. When the catalyst change at time period 220 is accounted for by changing the model parameters, the MI predictions are greatly improved (Figure 4.5j)). The main reason that the new model performs so much better is that it has the correct value for k_3, the hydrogen to ethylene ratio coefficient in equation 4.26. If the wrong model is used after the catalyst changeover, there is significant mismatch in terms of the effect of hydrogen concentration on *MI*. If the model parameters are not changed to reflect the new catalyst, the recursive prediction error scheme must eliminate the offset by changing k_0.

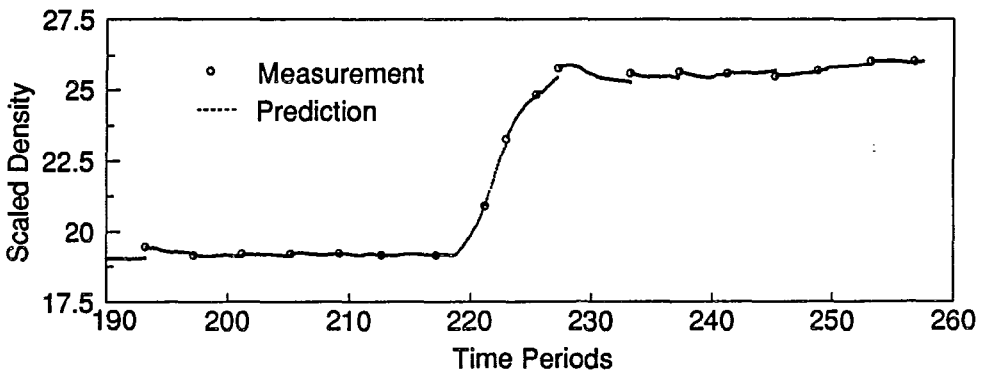

Figure 4.5a) Scaled density prediction: Transition 4

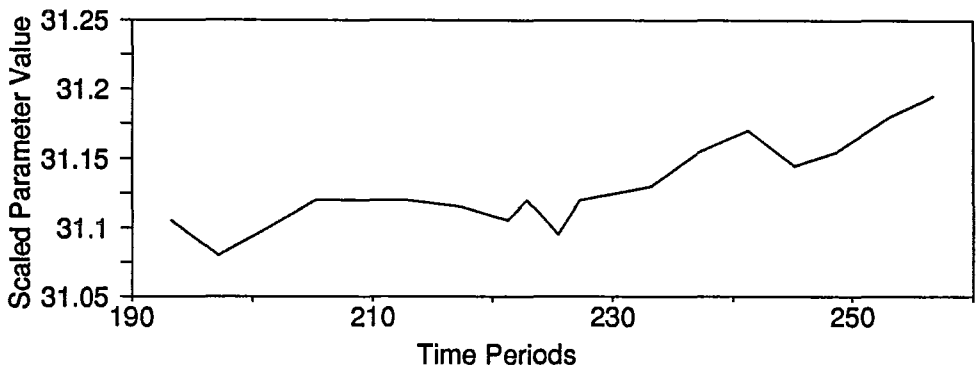

Figure 4.5b) Scaled density update parameter p0: Transition 4

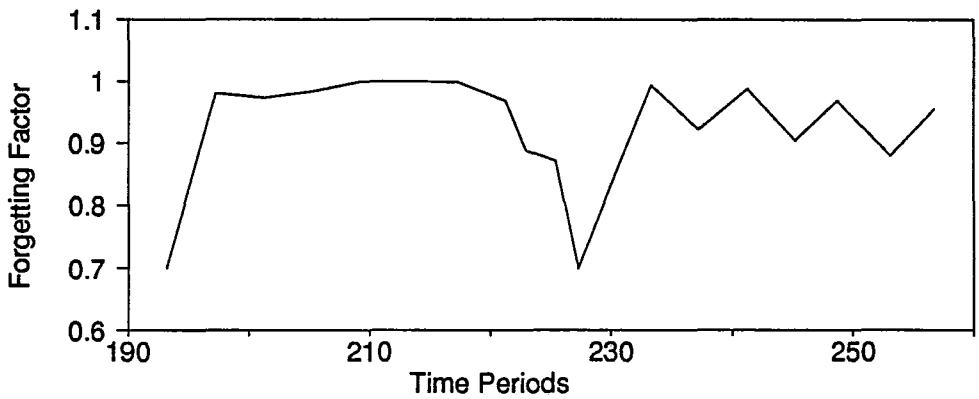

Figure 4.5c) Density forgetting factor: Transition 4

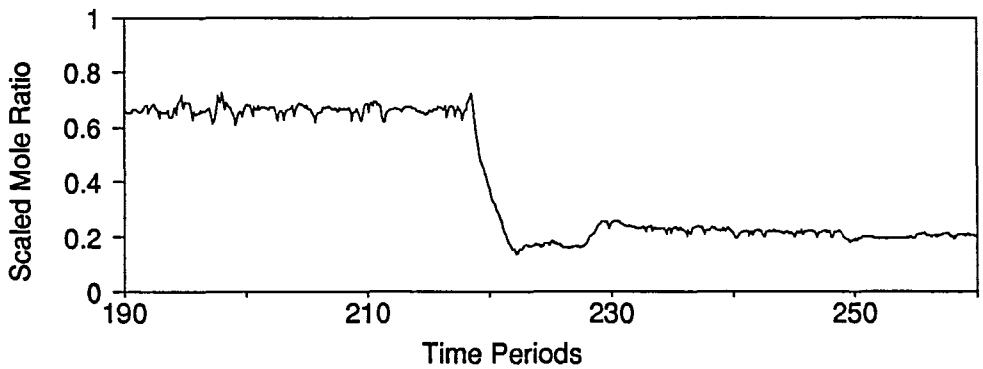

Figure 4.5d) Scaled HAO to ethylene ratio: Transition 4

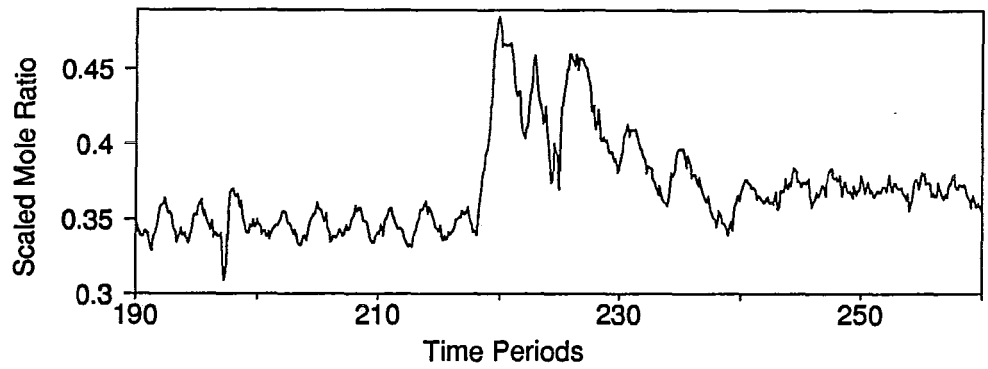

Figure 4.5e) Scaled hydrogen to ethylene ratio: Transition 4

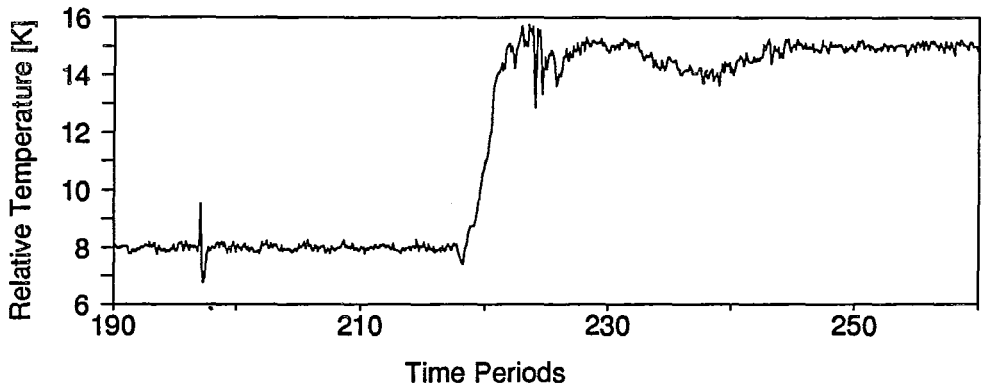

Figure 4.5f) Reactor temperature deviation from reference: Transition 4

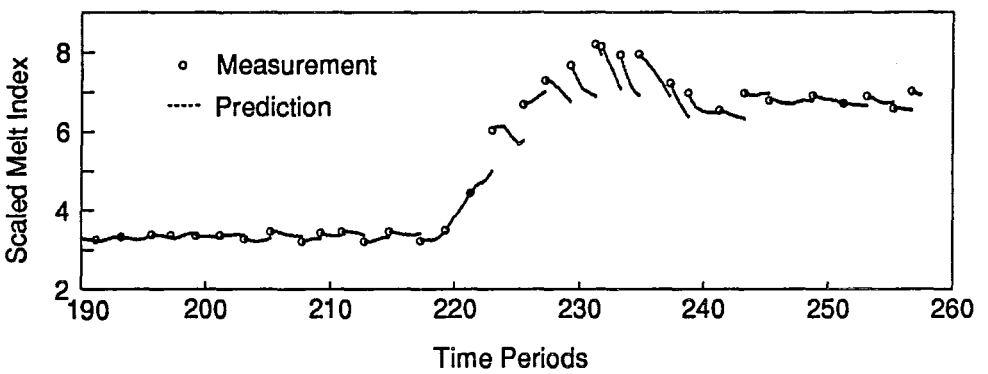

Figure 4.5g) Scaled MI predictions using a single model: Transition 4

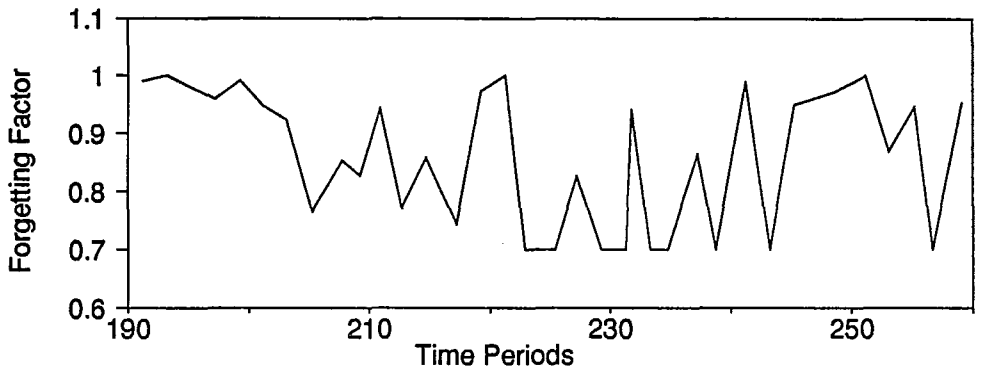

Figure 4.5h) MI forgetting factor using a single model: Transition 4

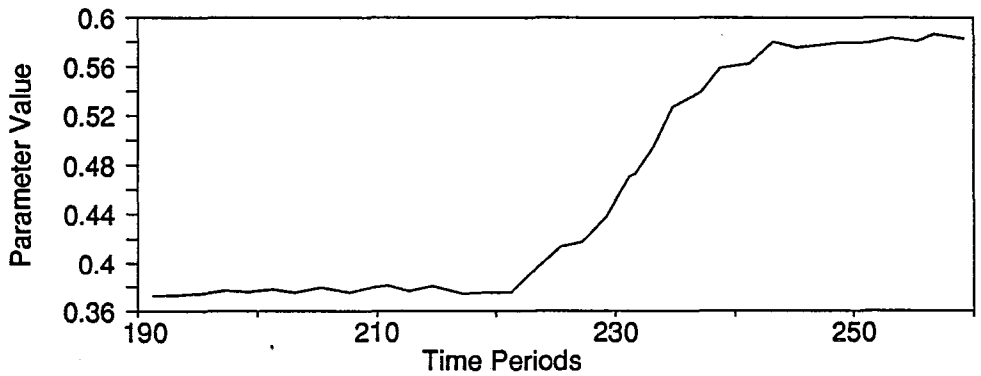

Figure 4.5i) Scaled MI update parameter k0 using a single model: Transition 4

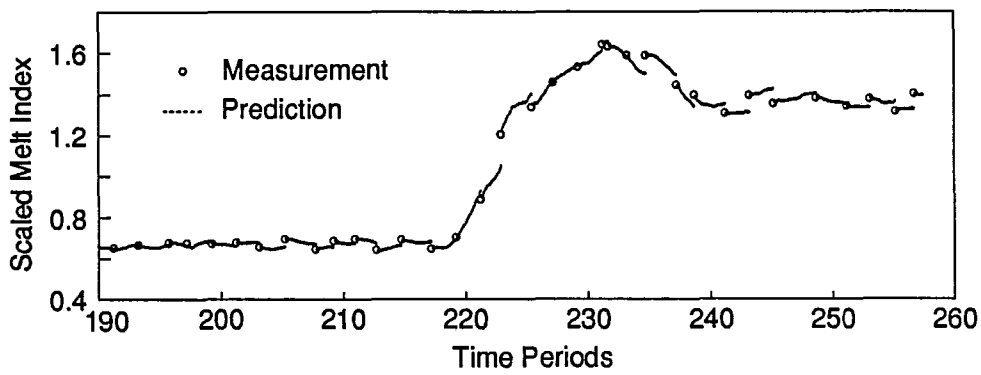

Figure 4.5j) Scaled MI predictions using specific models: Transition 4

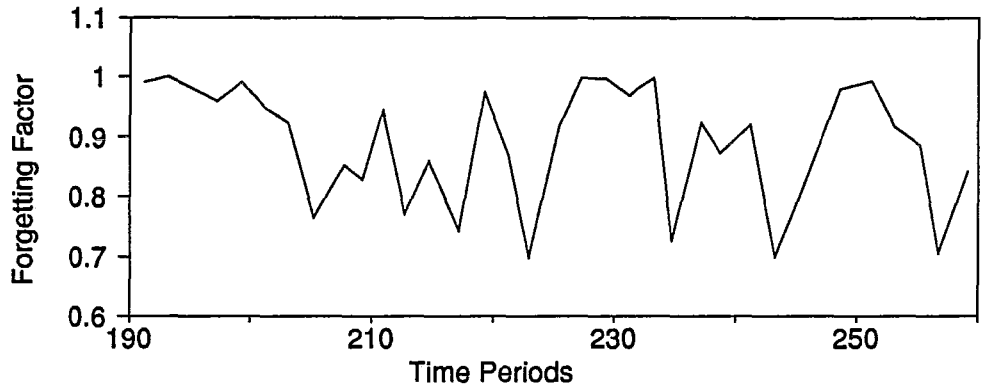

Figure 4.5k) MI forgetting factor using specific models: Transition 4

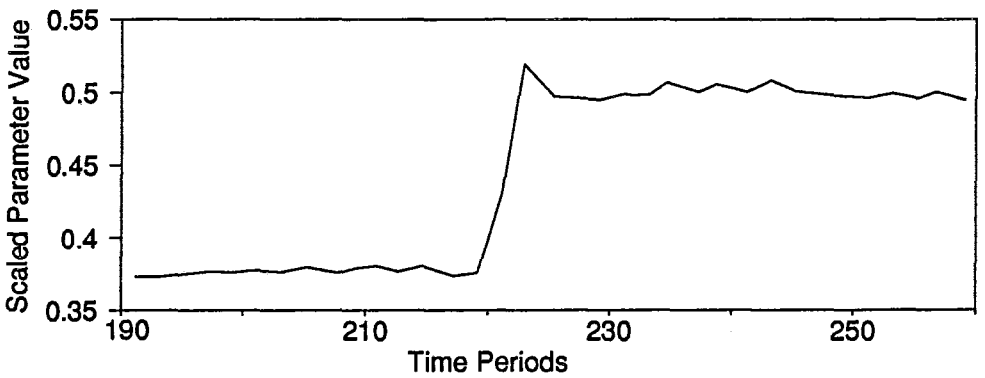

Figure 4.5l) Scaled MI update parameter k0 using specific models: Transition 4

4.5 CONCLUSIONS

A methodology for on-line melt index and density prediction in an industrial fluidized bed polyethylene reactor has been presented. This scheme consists of theoretically-based models which relate melt index and density to reactor operating conditions. Adjustable parameters in the models are updated on-line by a recursive prediction error method when the results of laboratory analyses become available. It has been demonstrated that this technique is capable of successfully predicting both *MI* and ρ. It has also been determined that melt index predictions can be improved by using

specific model parameters for each catalyst type. Changeovers between models are easily handled by changing model parameters when the feed of the new catalyst is started, and by reinitiating k_0 in order to keep the instantaneous melt index prediction constant at the changeover point. A single set of parameters for the density model is capable of predicting density during grade transitions for all of the catalyst types used in the reactor. These on-line predictions of melt index and density provide essential information to the polyethylene manufacturer so that a more consistent polymer can be produced.

4.6 NOTATION

a	Exponent in equation 4.1
$\underline{A}$	Coefficient matrix in linearized process model
a_2, a_3	Parameters in equation 4.27
c	Subscript indicating a cumulative property
C^*	Number of moles of active catalyst sites in the reactor
Ea_p	Activation energy for propagation reactions
Ea_{tr}	Activation energy for chain transfer and deactivation reactions
EKF	Extendend Kalman Filter
$\underline{G}$	Coefficient matrix in linearized process model
h	Gas composition sampling interval
$\underline{H}$	Matrix relating state variables to measured variables
$[H_2]$	Gas phase hydrogen concentration
$[I]$	Gas phase impurity concentration
i	Subscript indicating an instantaneous property
j	Type of active site on the catalyst
$\underline{K}$	Kalman gain
$k_0, k_1, ..k_7$	Parameters in instantaneous melt index model
kf_{iH}	Rate constant for chain transfer to hydrogen by an active site with terminal monomer i
kf_{im}	Rate constant for chain transfer to monomer m by an active site with terminal monomer i

kf_{iR}	Rate constant for chain transfer to cocatalyst by an active site with terminal monomer i
kp_{im}	Propagation rate constant for the addition of monomer m to an active site with terminal monomer i
$\underline{L}$	Gain matrix in equation 4.54
M_1, M_2, M_3	Ethylene, butene and higher alpha-olefin
mf_i	Mole fraction of monomer i incorporated in the polymer chains
MI	Melt Index
$\overline{M}_n$	Number average molecular weight
M_p	Mass of polymer in the reactor
$\overline{M}_w$	Weight average molecular weight
$\underline{P}$	Covariance matrix of state and parameter estimates
$p_0, p_1, ..p_4$	Parameters in the instantaneous density model
P_R	Polymer production rate
$\underline{Q}$	Matrix in equation 4.57
$[R]$	Gas phase cocatalyst concentration
R_{dI}	Rate of active site deactivation by impurities
R_{fH}	Rate of chain transfer to hydrogen
R_{ϕ}	Rate of chain transfer to monomer i
R_{fR}	Rate of chain transfer to cocatalyst
r_n	Number average degree of polymerization
R_p	Rate of propagation of living polymer chains
$RPEM$	Recursive prediction error method

R_{π}	Rate of consumption of monomer i by propagation
R_{tr}	Rate of production of dead polymer chains
$\underline{R}_v$	Covariance matrix for measurement errors
$\underline{R}_w$	Covariance matrix for modelling errors
t	Time
T	Absolute reactor temperature
T_0	Reference temperature
$\underline{u}$	Vector of input variables in equation 4.45
$\underline{v}$	Vector of measurement errors in equation 4.46
$\underline{w}$	Vector of modelling errors in equation 4.45
w_j	weight fraction of polymer produced at site type j
$\underline{x}$	Vector of state variables
$\underline{y}$	Vector of measurements
y	Model prediction
y_{meas}	Measurement corresponding to model prediction
$\underline{Z}$	Vector of partial derivatives in equation 4.60
ε	Prediction error
η	Viscosity of a polymer melt at low shear rates
λ	Variable forgetting factor
γ	Tuning parameter for variable forgetting factor
σ_e^2	Variance of prediction errors
$\underline{\theta}$	Vector of parameters

ϕ_i	Fraction of active sites with terminal monomer *i*
τ	Polymer phase time constant in the fluidized bed
ρ	Density

OPTIMAL GRADE TRANSITION POLICIES

5 OPTIMAL GRADE TRANSITION POLICIES

5.1 INTRODUCTION

It is essential to produce polyethylenes with a given melt index and density or, alternatively, with a specified average molecular weight and composition. Different polyethylene applications such as injection and roto-moulded products, wire coating and film, require different properties. The melt index and density of polyethylene are associated with both processing and end-use characteristics. Melt index is related to the rheological processing properties of the polymer as well as impact strength, stress crack resistance, tensile strength and elasticity. Density is related to stiffness, tensile strength, heat resistance, hardness, permeability, transparency, impact strength and flexibility (Foster, 1990). Reactor grade transitions from one melt index and density to the next are required to change products so that many types of polyethylene can be produced in a single reactor. The frequency and magnitude of grade changes is determined by both prices and market demand.

The major focus of Chapter 6 is the development of an algorithm for on-line product property control. The purpose of this controller is two-fold: to regulate *MI* and ρ over the wide range of polyethylene grades produced in the reactor, and to manipulate reactor operating conditions during grade transitions so that the quantity of off-specification product is minimized. Before designing such a controller, it is important

to investigate the types of grade transition trajectories which can be achieved in the reactor and to understand the consequences of adopting a specific grade transition policy for on-line implementation.

In this chapter, the best open-loop policies for accomplishing grade change-overs are determined using dynamic model-based optimization; the models employed are those developed in Chapters 2,3 and 4. First, the goals of the study are introduced, followed by a review of dynamic optimization techniques. The issues involved in formulating and solving the optimal grade transition problem are then discussed and optimal grade transition trajectories are shown for a typical progression of grade changes. Finally, the problems associated with implementing optimal off-line transitions without feedback are demonstrated. Industrially relevant operating limits are used in the optimal changeover problems solved in this chapter, so that process data can be used to validate the results. Hence, scaling is required to prevent disclosure of confidential operating information. All scaling is consistent with that used in Chapter 4.

Goals of the Optimal Grade Transition Study

The goals of this optimization study are:

a) To formulate a set of dynamic optimization problems for grade transitions involved in producing a typical series of polyethylene products. The products studied are shown in Table 5.1. The specific transitions studied are $A \rightarrow B$, $B \rightarrow C$, $C \rightarrow B$ and $B \rightarrow A$. This set of transitions represents a production schedule which might be followed in an industrial reactor. Change-overs $A \rightarrow B$ and $B \rightarrow A$ involve a small change in the *MI* specification and a relatively large density transition. In transitions $B \rightarrow C$ and $C \rightarrow B$, a large change in *MI* is required but the desired density remains constant.

b) To solve the optimization problems in a) in order to determine optimal policies for manipulating the reactor inputs and to determine the types of optimal *MI* and ρ trajectories achievable.

c) To determine the effects of problem formulation on the optimal solution. The factors considered include: the set of manipulated variables used to accomplish the change-over, the bounds on the manipulated variables and the tuning of the objective function.

d) To determine which of the optimal trajectories might be desirable for on-line implementation.

In order to accomplish these goals, a thorough understanding of both current dynamic optimization techniques and reactor operating strategies is required.

Table 5.1 Polyethylene Grades Considered in Transition Study

Grade	Scaled Melt Index Target	Scaled Density Target
A	0.2	9
B	0.16	13
C	2.4	13

5.2 DYNAMIC OPTIMIZATION TECHNIQUES AND APPLICATIONS

Dynamic systems modelled by nonlinear differential/algebraic equations (*DAE's*) arise in many aspects of chemical engineering. Optimization of these dynamic models is commonly used to solve kinetic parameter estimation problems (Biegler et al., 1986) and optimal control problems (Bryson and Ho, 1970; Ray, 1981; Farber and

Laurence, 1986). Such optimization problems are more difficult to solve than steady state nonlinear programming (*NLP*) problems because some of the equality constraints are given by differential equations.

An example of a typical optimal control problem for a dynamic system is shown below:

$$\begin{aligned} \underset{\underline{u}(t)}{\text{Min}} \quad & F(\underline{u}(t),\underline{x}(t)) && t \in [t_0, t_f] \\ s.t. \quad & c(\underline{u}(t),\underline{x}(t)) = 0 && (5.1) \\ & \dot{\underline{x}}(t) = \underline{f}(\underline{u}(t),\underline{x}(t)) && (5.2) \\ & \underline{x}(t_0) = \underline{x}_0 && (5.3) \\ & \underline{u}_* \le \underline{u}(t) \le u^* && (5.4) \\ & \underline{x}_* \le \underline{x}(t) \le \underline{x}^* && (5.5) \end{aligned}$$

where

F : objective function

$\underline{c}$: vector of algebraic equality constraints

$\underline{x}(t)$: vector of state variables

$\underline{f}$: vector of state derivatives

$\underline{u}(t)$: vector of manipulated variables

$\underline{u}_*$, $\underline{u}^*$: lower and upper bounds on manipulated variables

$\underline{x}_*$, $\underline{x}^*$: lower and upper bounds on state variables

The optimizer must choose the manipulated variable profile $\underline{u}(t)$ to minimize the performance index $F(\underline{x}(t),\underline{u}(t))$ so that the constraint equations 5.1 and 5.2 are obeyed and the manipulated variables and state variables do no move beyond the bounds in 5.4 and 5.5.

Biegler (1990) divides the solution methods for optimal control problems into three basic categories:

i) iterative methods based on variational calculus

ii) feasible path or sequential nonlinear programming methods

iii) simultaneous nonlinear programming methods

These methods are discussed in sections 5.2.1 to 5.2.3.

5.2.1 Variational Methods

These methods involve the extension of analytical solution techniques for small design problems to iterative algorithms based on variational conditions. Variational methods include the well-known control vector iteration algorithms (Bryson and Ho, 1975) which are based on Pontryagin's maximum principle. According to Biegler (1990), variational methods require excessive model and adjoint equation evaluations and are effective only when applied to the simplest optimal control problems.

5.2.2 Nonlinear Programming Methods with an Embedded Model

If the manipulated variable profile, $\underline{u}(t)$, is discretized or expressed as a polynomial or piecewise constant function, the optimal control problem can be solved as an *NLP*. This control parameterization approach is advantageous in that standard nonlinear optimization algorithms can be used to determine the parameters $\underline{p}$ required to specify $\underline{u}(t)$ (Ray, 1981). A diagram outlining this approach is shown in Figure 5.1. First, an initial set of parameters, $\underline{p}$, is used to construct the manipulated variable trajectories $\underline{u}(t)$. These trajectories provide input to the dynamic model which is integrated to determine the resulting trajectories of the state variables. Next, the

performance index, J, is calculated from the state trajectories. The optimizer then chooses a new set of parameters and the process is repeated until the optimum is reached. The number of iterations required to obtain a suitable solution can be greatly reduced if accurate sensitivity information is provided to a gradient based optimizer. This type of sensitivity information can be calculated by integrating a set of adjoint equations along with the model differential equations (Leis and Kramer, 1988).

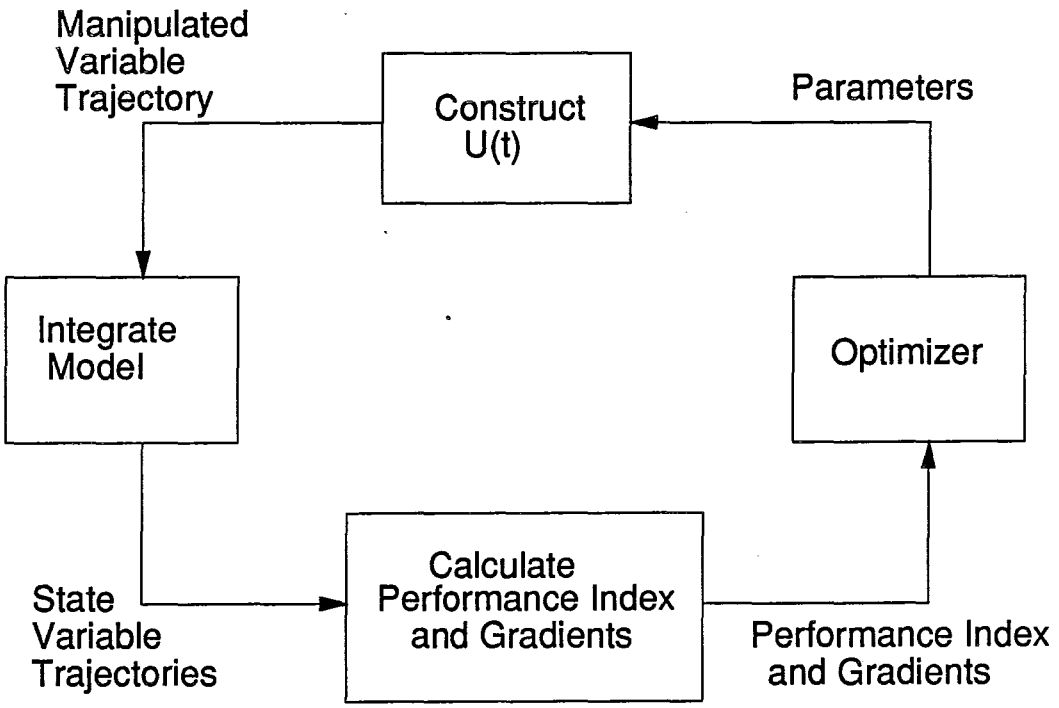

Figure 5.1 Embedded Model Approach to Dynamic Optimization

The major disadvantages of imbedded model techniques are that bounds on state variables as shown in equation 5.5 are difficult to handle (Biegler, 1990) and the optimal solution to the original problem is not obtained if $\underline{u}(t)$ is poorly parameterized (Ray, 1981). Recently, these problems have been studied by Goh and Teo (1988) and by Chen and Hwang (1990). Embedded model approaches have been very successful in solving large scale dynamic optimization problems (Sargent and Sullivan, 1979; Mujitaba and Macchietto, 1988).

5.2.3 Simultaneous Nonlinear Programming Methods

In this technique, both the manipulated variable profile and the state equations are parameterized simultaneously to form an *NLP* problem with only algebraic equation constraints. This type of formulation makes the handling of bounds on state variables relatively simple (Li and Biegler, 1988; Eaton and Rawlings, 1990; Tjoa and Biegler, 1991). However, simultaneous approaches lead to much larger *NLP's* than imbedded model methods and extreme care must be taken in the parameterization step to ensure that an accurate algebraic representation of the solution to the differential equations is obtained. As yet simultaneous optimization and integration approaches have been used only to solve small dynamic optimization problems, but they provide a promising research area for the future (Biegler, 1990).

5.3 THE OPTIMAL GRADE TRANSITION PROBLEM

Many issues must be considered when formulating an optimal grade transition problem. One must know which features distinguish a good grade transition from a bad one, and also have an idea of the relative importance of the competing goals embodied in the notion of an *optimal* policy. Several questions which must be considered are:

a) Which is more desirable, reducing the *quantity* of off-specification material produced, or reducing the *time* required to reach the new property target?

b) How much overshoot in instantaneous *MI* and ρ should be used to bring the cumulative properties to their targets quickly?

The answer to a) depends on economic conditions. During periods of high market demand, it may be better to adopt a policy which produces more off-specification polymer, but reaches the new target faster. Conversely, in periods of low demand, a policy which produces less off-target material at the expense of a longer transition time may be preferable. The answer to b) depends on the use to which the polymer will be put, and on the importance of consistency in the molecular weight and composition distribution in that application. Once the goals, trade-offs and opportunities are understood, these ideas must be translated into a tractable mathematical problem.

5.3.1 Features of an Desirable Grade Transition

A desirable grade transition policy is one which:

a) drives the product properties to their new target values in a short period of time, producing only a small quantity of off-specification polymer.

b) ensures that the reactor operates safely during the changeover. Excursions above the sticking temperature of the polymer and disruptions of fluidization, heat transfer and mixing in the bed cannot be tolerated.

c) results in economically desirable steady state reactor conditions at the end of the transition. Reactor temperature, bed level, polymer production rate and gas bleed rate should all settle at pre-specified final values.

d) does not adversely affect the quality or consistency of the on-specification polymer product in the reactor at the end of the transition period.

While items a) and b) are straightforward, c) and d) are not as obvious. In this thesis, it is assumed that the desired steady state conditions for the next grade, which are

required in item c) are known, either from experience, or from the solution to a separate steady state optimization problem. Whenever the optimal steady state conditions change due to economic decisions, the optimal dynamic grade transition policies will also change. The potential effects of grade transition policies on product quality is not a simple issue. Further explanation of iteme d) is given in section 5.3.2

5.3.2 Effects of Grade Transition Strategies on Polymer Properties

Knowing the values of the melt index and density measurements is not sufficient to give a complete prediction of the properties of a linear polyethylene sample. *MI* and ρ are only reflections of an average molecular weight and average composition of the copolymer. The breadths of the molecular weight and composition distributions also affect polymer properties. A continuous gas phase reactor operating at steady state with a given catalyst produces polymer with a certain *MI* and ρ and a fixed molecular weight and composition distribution. However, during grade transitions, the old polymer contained in the reactor is mixed with new instantaneous polymer produced at different conditions, leading to potential broadening of both the molecular weight and composition distributions. While the *MI* and ρ of this transition material may be within the specifications of a certain commercial grade of polyethylene, the properties of the transition polymer can differ substantially from those of polyethylene with the same *MI* and ρ produced under steady state reactor conditions.

For some polyethylene products such as wire and cable coating, broad molecular weight distributions are desirable. Resins with broad *MWD* show enhanced shear thinning compared to narrow *MWD* resins and, therefore, tend to flow more easily at the high shear rates prevailing in coating operations (Sinclair, 1983).

However, for the applications considered in this study (polyethylene film and injection moulded products), a narrow *MWD* is preferred. Narrow *MWD* polymers are used for injection moulding applications because they crystallize faster and the melt viscosity is less sensitive to melt flow conditions than for broad *MWD* polymers (Sinclair, 1983). In addition, a narrow *MWD* leads to higher impact strength (Williamson, 1970) and less shrinkage in the mould (Sinclair, 1983). The breadth of the *MWD* can also affect the optical properties of the polymer; narrow *MWD* films have higher transparency but are susceptible to higher haze and lower gloss than broad *MWD* films. In addition, a narrow *MWD* is associated with better resistance to environmental stress cracking and brittleness at low temperatures as well as higher tensile strength and resistance to creep (Sinclair, 1983).

High and low molecular weight tails in the *MWD* can be responsible for certain undesirable product characteristics. High molecular weight tails affect melt strength and the elasticity of the polymer (Foster, 1990) and can lead to melt fracture. In film applications, high molecular weight tails are responsible for high die swell which leads to low impact strength and lower machine direction tear strength (Williamson, 1970). Low molecular weight tails with high comonomer content are associated with waxes or extractables which adversely affect film blocking and heat seal properties (Foster, 1990; Sinclair, 1983). Thus, when performing grade transitions, it is important to consider the implications of a transition policy on the breadth of both the molecular weight and composition distributions of the transition material. Transition material which has an on-specification *MI* and ρ, but a *MWD* which differs significantly from steady state material, could lead to customer processing problems and deficiencies in the final product.

5.3.3 Problem Formulation

Many issues must be considered when formulating dynamic optimization problems to study grade transitions. The manipulated variables available for on-line control and their associated bounds must be known, as well as any constraints on state variables in the dynamic model. Choosing an objective function can be a difficult task; the implications of the objective function structure and tuning on reactor operability, economics and product quality should be considered.

5.3.3.1 Manipulated Variables and their Bounds

The variables which are manipulated in this study to obtain optimal grade transitions are shown in Table 5.2 along with lower and upper bounds. The butene feed rate, hydrogen feed rate and reactor vent position affect product properties by changing the gas composition in the reactor. The effects of gas composition and reactor temperature on both instantaneous *MI* and ρ have been discussed in Chapter 4. The catalyst feed rate and the quantity of polymer in the bed influence the production rate and the solid phase time constant, thereby affecting the rate at which cumulative *MI* and ρ change in response to changes in the instantaneous properties. The upper bounds on the gas feed and catalyst feed rates are fixed by the physical size of valves and catalyst injection equipment. The temperature setpoint must remain above the lower limit to ensure adequate catalyst activity, and below the upper limit to prevent sticking of the polymer particles. The vent position is held below its upper bound to prevent excessive bleeding of gas from the reactor. The mass of polymer in the bed must remain between the limits shown to ensure proper fluidization and mixing in the bed. The scaled bounds in Table 5.2 are indicative of the types of limits encountered in industrial gas phase

polyethylene reactors. The actual values of the bounds encountered by specific industrial reactors depend on the grades of polymer being produced and on the physical design of the reactor.

An additional variable which could be manipulated by the optimizer is the feed rate of nitrogen to the reactor. Nitrogen addition could be used to increase the pressure in the reactor, and thereby flush other gas phase components out of the reactor in the bleed stream. This action would have much the same effect as opening the bleed valve. Since the bleed valve position is already included as a manipulated variable in the optimization study, nitrogen feed flow manipulations have not been considered.

Table 5.2 Scaled Manipulated Variables and their Bounds

Manipulated Variable	Scaled Lower Bound	Scaled Upper Bound
Butene feed rate	0	1
Hydrogen feed rate	0	1
Reactor temperature setpoint	-7	8
Reactor vent valve position	0	1
Catalyst feed rate	0	1
Bed level setpoint	-1	1

5.3.3.2 Dynamic Reactor Model

The dynamic reactor model used in this study is described in Chapters 2 and 3, with one minor change. Melt index and density are not predicted using equations 2.66 and 2.70. Rather, differential equations 4.42 and 4.43 are included

in the state space model. As a result, equations 2.33, 2.34, 2.35 and 2.49, which describe the moments of the chain length distribution and the composition of the copolymer are not required for the *MI* and ρ predictions and can be removed from the model used by the optimizer. This reduction in model complexity provides for a faster and more efficient solution of the optimization problem. Once the optimal policy has been determined, a simulation is conducted using the full model so that the resulting polydispersity of the polymer can be calculated.

5.3.3.3 Objective Function and Constraints

Integral quadratic objective functions are commonly used both in process control designs and in dynamic optimization problems. The reason for their popularity is that they are an effective and simple way of penalizing deviations from targets over the time period of interest. Perhaps the simplest objective which could be conceived for the grade transition trajectory problem is to minimize $F(\underline{u})$ where:

$$F(\underline{u}) = \int_{t_0}^{t_f} w_1 (\ln MI_c - \ln MI_{sp})^2 + w_2 (\rho_c - \rho_{sp})^2 \, dt \tag{5.6}$$

t_0 is the time at which the grade transition begins and t_f is a time in the future at which the reactor will have reached steady state. w_1 and w_2 are weighting factors related to the relative costs of deviations of MI_c and ρ_c from their respective target values, MI_{sp} and ρ_{sp}. Objective function 5.6 penalizes deviations of the logarithm of MI_c from setpoint rather than raw MI_c deviations, so that the same percentage error in cumulative melt index is penalized equally, regardless of the level of MI_c.

Minimization of objective function 5.6 will result in a transition policy which satisfies item a) in section 5.3.1. So long as t_f is chosen to be sufficiently large, MI_c and ρ_c will be forced toward their setpoints and maintained there at steady state. By satisfying the bounds given in Table 5.2, item b) will also be satisfied. However, without further penalties or constraints, the solution to this simple problem will not necessarily meet criteria c) and d). Some means is required to ensure that the final steady state is an economically desirable one and that the resulting molecular weight and composition distributions at the end of the grade transition are not too broad.

Constraints or penalties on model states can be incorporated in several ways. Hard bounds can be defined for functions of the state variables, or penalty terms can be added to the objective function to ensure that no constraints are violated by the optimal solution. As discussed in 5.3.2, high and low molecular weight tails and broad molecular weight and composition distributions can lead to undesirable product properties. Excessive overshoots of the instantaneous melt index and density cannot be allowed during a transition, even though they can assist in quickly bringing the cumulative melt index and density to their target values. Two alternative approaches are discussed below which could be used to force the optimizer to consider the trade-off between fast transitions and narrow distributions. They are specification of hard bounds on instantaneous MI and ρ, and the use of quadratic penalty terms in the performance index.

Consider a melt index transition from an initial value MI_0 to a new, higher target value. An upper allowable limit on the instantaneous melt index, MI_i^* could be specified so that during the transition, the instantaneous MI is forced to have values less than or equal to this upper limit:

$$MI_i(t) \leq MI_i^* \tag{5.7}$$

Equation 5.7 could be included as a constraint in the optimization problem. Formulation of the problem in this way would mean that if $MI_i^* = 25 dg/\min$, then a sustained instantaneous melt index of 24.9 dg/min would be acceptable in the optimal solution, but an infinite penalty would be placed on an instantaneous melt index of 25.1 dg/min, for even a short time. While this type of hard constraint makes sense for the bounded manipulated variables, it is a far from perfect description of the desire to trade-off fast transitions against the formation of low molecular weight tails. This type of state variable constraint is difficult to handle using an embedded model technique, so a more difficult simultaneous solution approach might be in order.

A second method of handling the trade-off between fast transitions and narrow molecular weight distributions involves the addition of a quadratic penalty function to the original performance index $F(\underline{U})$. An objective function of the form:

$$J = F(\underline{u}) + w_3 \int_{t_0}^{t_f} (\ln MI_i - \ln MI_{sp})^2 dt \tag{5.8}$$

penalizes large deviations of the instantaneous MI from the target, including those beyond the desired upper limit. The relative importance of the original performance index, involving the cumulative properties, and the importance of limiting the tails of the molecular weight distribution, is influenced by the choice of the weighting factor, w_3. The quadratic penalty function in equation 5.8 results in a smoothly increasing penalty on instantaneous polymer properties which deviate from the target, and is easily handled using an embedded model approach. A similar term can be added to the model to penalize large over-shoots in instantaneous density:

$$w_4 \int_{t_0}^{t_f} (\rho_i - \rho_{sp})^2 dt \tag{5.9}$$

Depending on market conditions, the steady state production of a given grade of polyethylene is associated with economically optimal settings for temperature, vent flow rate, bed level and catalyst feed rate. While these variables can and should be allowed to deviate from these desired values in the short-run, the long-term tendency of the control system should be to drive these variables toward the desired positions. Only two degrees of freedom, the hydrogen and butene feed rates are required to achieve the desired polyethylene properties at steady state. Thus, the extra manipulated variables can be forced to settle near the desired values without causing offset in the product properties. The following simple quadratic penalty term will make certain that T_{fsp}, the final steady state temperature setpoint, is driven to its desired value T_{des}:

$$w_5(T_{fsp} - T_{des})^2 \tag{5.10}$$

No integration of this penalty term is required because both T_{fsp} and T_{des} are constants which do not change with time. Addition of:

$$\int_{t_0}^{t_f} w_6(v_p - v_{pdes})^2 dt \tag{5.11}$$

to the objective function ensures that the vent position v_p settles at the desired value v_{pdes}. Note that in 5.10 only the steady state value of the temperature setpoint has been penalized, whereas in 5.11 the deviation of the vent position is penalized over the entire duration of the transition. Costs associated with leaving the temperature setpoint near its limits for several hours are minimal. However, it is important to ensure that the vent does not unnecessarily remain near its limits for a sustained period of time. Excessive venting is expensive, and leaving the vent closed for a long period of time can result in the accumulation of poisons in the system. The weighting factors w_5 and w_6 can be used to weight the relative importance of moving toward the desired settling positions of manipulated variables against minimizing the other terms in the objective function.

If only the butene and hydrogen feed rates, the reactor temperature and the vent position are used as manipulated variables, the effects on production rate during the grade transition are relatively minor. In this case, an objective function containing terms from 5.6, 5.8, 5.9, 5.10 and 5.11 expresses all of the desired features of a good grade transition. If, however, the catalyst feed rate and the bed level are also manipulated, marked changes in production rate can occur. Thus, when the catalyst feed rate and bed level are included as manipulated variables, the objective function should be amended to account for changing production rate and its potential implications on the desirability of grade transition policies.

Production of off-specification polymer results in a cost or, alternatively, a loss of potential profit for the polyethylene producer. Polymer which does not fall between the specification limits of commercial grades must be sold at a discount because their is little market for it. There are also costs associated with polymer which is within specification limits but which is off-target. Customers prefer the polyethylene they purchase to have consistent properties both within a shipment and between successive shipments. Inconsistent polymer can cause increased processing equipment setup costs, and can ultimately lead to loss of market share for the polyethylene producer.

If one assumes that C, the cost per unit mass of polymer produced in the reactor associated with poor quality, is a quadratic function of both cumulative and instantaneous properties, then C can be expressed as:

$$C = a_1(\ln MI_c - \ln MI_{sp})^2 + a_2(\rho_c - \rho_{sp})^2 + a_3(\ln MI_i - \ln MI_{sp})^2 + a_4(\rho_i - \rho_{sp})^2 \qquad (5.12)$$

The coefficients, a_i, are weighting factors denoting the relative costs of deviations in the respective polymer properties. For an entire grade transition, then, the total cost of off-target production is:

$$\int_{t_0}^{t_f} P_R C \, dt = \int_{t_0}^{t_f} P_R [a_1(\ln MI_c - \ln MI_{sp})^2 + a_2(\rho_c - \rho_{sp})^2 + a_3(\ln MI_i - \ln MI_{sp})^2 + a_4(\rho_i - \rho_{sp})^2] \, dt \qquad (5.13)$$

where P_R is the instantaneous polymer production rate. An objective function which minimizes the cost of off-specification production, while ensuring an economically desirable final temperature setpoint, bleed position, final bed level, B_w, and production rate is:

$$\int_{t_0}^{t_f} P_R C \, dt + w_5(T_{fsp} - T_{des})^2 + w_7(B_{wfsp} - B_{wdes})^2 + \int_{t_0}^{t_f} w_6(v_p - v_{pdes})^2 + w_8(P_R - P_{Rdes})^2 dt \qquad (5.14)$$

Near the beginning of a grade transition when the polymer properties are far from target, the first term in 5.14 will dominate the objective function and the optimizer will take action to simultaneously bring the properties closer to their setpoints and to reduce the production rate so that not much off-specification polymer is produced. Near the end of the transition, when the product properties are near the targets, the first term in the objective function will be small relative to the final term, so that the optimizer will choose the manipulated variables to achieve the desired steady state production rate.

5.3.4 Method of Solution

Since hard constraints on state variables are not required in the problem formulation, an embedded model approach has been adopted. The manipulated variable profiles are parameterized by approximating the optimal policies as a series of ramps, as shown in Figure 5.2. The decision variables chosen by the optimizer are the values of the manipulated variable trajectories at the end points of the ramps. For each manipulated variable, the trajectory is specified by 12 decision variables. Three different sets of switching times corresponding to the end-points of the ramps were chosen arbitrarily and are show in Table 5.3

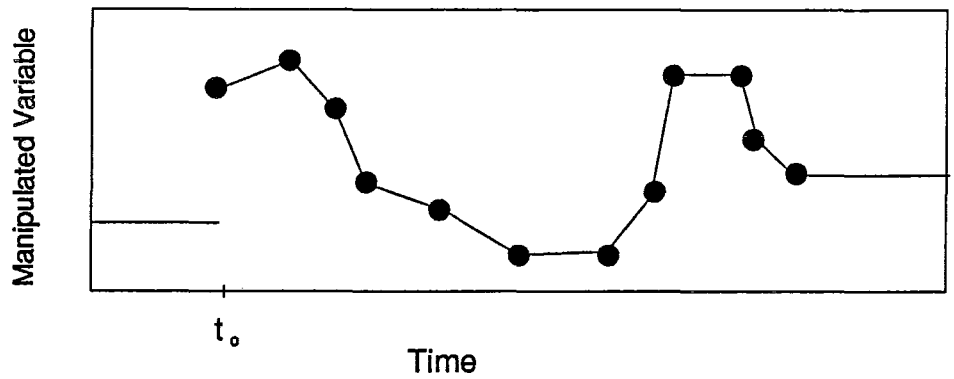

Figure 5.2 Manipulated Variable Trajectory Parameterization

Table 5.3 Switching Times Used to Parameterize Manipulated Variable Trajectories

	Switching Times [Scaled Time Units]											
Case I	0	0.33	0.67	1	1.5	2	2.5	3	4	5	6	7
Case II	0	1	2	3	4	5	6	7	8	9	10	11
Case III	0	1	2	3	4	6	8	10	12	14	16	18

For grade transitions $A \rightarrow B$ and $B \rightarrow A$, which required approximately 10 time periods to reach their new targets, Case I, was used to specify the switching times for the decision variables. For $B \rightarrow C$ transitions, which required approximately 15 time periods, Case II was used. Case III was used to parameterize $C \rightarrow B$ transitions which required approximately 20 time periods to reach the new target setpoints. In all cases, a final time, t_f, of 60 time periods was used for the dynamic model and objective function calculations to ensure that steady state would be reached.

A commercial nonlinear programming package, MINOS 5.1 (Murtagh and Saunders, 1987) was used to solve for the optimal decision variables. A set of adjoint equations was integrated, along with the model equations and the objective function, in order to supply the optimizer with accurate gradient information.

5.4 RESULTS

A series of optimal trajectories has been determined for the grade schedule $A \rightarrow B \rightarrow C \rightarrow B \rightarrow A$. The settings of the manipulated variables at the start of this set of transitions is given in Table 5.4. During all of the transitions shown in this chapter, the ethylene partial pressure set point was 0.3835 scaled pressure units and the feed rate of inerts (nitrogen) to the reactor was held constant. Each of the transitions ($A \rightarrow B, B \rightarrow C, C \rightarrow B, B \rightarrow A$) was optimized over 60 time periods. However, some steady state segments have been removed from the figures so that more attention can be focussed on the interesting phenomena which occur during the first 20 to 30 time periods of each transition. The optimal trajectory corresponding to the simplest objective function, Equation 5.6, is presented in section 5.4.1, with only hydrogen and butene feed rates as manipulated variables. The effect of incorporating penalties on instantaneous *MI* and ρ in the objective function, in order to narrow the molecular weight and composition distributions, is discussed in section 5.4.2. In section 5.4.3, the reactor temperature setpoint is added to the set of manipulated variables and expression 5.10 is included in the objective function to ensure that the temperature settles at the desired final value. The potential for improving the optimal trajectory by manipulating the vent position is investigated in section 5.4.4. In this case, expression 5.11 is included in the objective function. In section 5.4.5, the sensitivity of the $B \rightarrow C$ transition to the upper bound on the hydrogen feed rate is determined and, in 5.4.6, the effect of manipulated

variable discretization on the optimal trajectory is discussed. Grade transitions which incorporate both catalyst feed rate changes and bed level changes are shown in section 5.4.7. Finally, in section 5.4.8, the importance of feedback control during on-line implementation of optimal transition policies is discussed.

Table 5.4 Initial Conditions for Scaled Manipulated Variables

Hydrogen Feed Rate	0.10259
Butene Feed Rate	0.62714
Temperature Setpoint	0
Vent Position	0.6
Catalyst Feed Rate	0.8
Bed Level	0

5.4.1 Base Case: Policy I

The simplest optimal grade changeover policy is one in which only the hydrogen and butene feed rates are manipulated to accomplish the transition. Such a changeover is shown in Figures 5.3 a) to g). Note that scaled *MI* is plotted on a log scale, and that all other variables are plotted on standard linear scales. The objective function resulting in this set of trajectories was Equation 5.6, wherein w_1 and w_2 were set to 1.0 and 0.04 so that a deviation of 1% in *MI* and 0.5 scaled density units are penalized equally.

In Figure 5.3, the $A \rightarrow B$ transition begins at time period 5, followed by $B \rightarrow C$ at period 25, $C \rightarrow B$ at period 55 and $B \rightarrow A$ at period 85. The $A \rightarrow B$ transition involves a small downward change in scaled *MI* from 0.2 to 0.16, and a large scaled density change from 9 to 13 units. This transition is accomplished by

turning off the butene feed for 1.5 time periods, then overshooting to 0.92 units before returning to the steady state position of 0.40. Some oscillations in the hydrogen feed rate, followed by a drop to 0 are used to bring *MI* to its new setpoint. Note that the final settling positions of the hydrogen feed rate and concentration are very near to their positions before the transition. At steady state the grade change is mainly achieved by the reduction in butene concentration which causes *MI* to decrease and ρ to increase.

Large overshoots in the instantaneous *MI* and ρ are used to bring the cumulative properties to their new targets very quickly. The large deviation of instantaneous density from the setpoint may lead to undesirable properties of the polymer leaving the reactor between time periods 7 and 13. Even though the cumulative polymer appears to be on target, it is a mixture of instantaneous polymer with scaled ρ_i ranging from 9 to 20, and will have different physical properties from polymer produced at steady state with a scaled density of 13. The overshoot in instantaneous *MI*, however, is less pronounced and does not appear to cause a problem with the polydispersity of the polymer as shown in Figure 5.3 g). The steady state polydispersity of grade *B* is lower than that of *A*, and the effect of the optimal transition policy is a smooth, monotonically decreasing response in the polydispersity.

The $B \rightarrow C$ transition, beginning at time period 25, involves a large change in scaled *MI* from 0.16 to 2.4 units, and no change in the density setpoint. The optimizer accomplishes this transition by initially increasing both the hydrogen and butene feed rates to their upper bounds in order to increase *MI*. This action causes the density to deviate significantly from its setpoint. The accompanying overshoot in instantaneous *MI* results in broadening of the molecular weight distribution, which

is evident from the rise in polydispersity. Note that the $B \rightarrow C$ transition results in a decrease in the steady production rate, due to a hydrogen inhibition effect. As discussed in Chapter 2, after a chain transfer to hydrogen reaction, the active site must be reinitiated before propagation can commence. If this reinitiation step is slow, then the number of growing polymer chains in the reactor is diminished.

An interesting facet of the reactor control problem is revealed in Figures 5.3 c) and d). During the $B \rightarrow C$ transition, the butene concentration responds rapidly to the step in the butene feed rate, whereas the response of the hydrogen concentration to the hydrogen feed step is much more sluggish. Another complication which must be addressed by the on-line quality control scheme is revealed in the $C \rightarrow B$ transition which begins at time period 55. The hydrogen concentration response, associated with the downward step in the hydrogen feed rate, is even more sluggish than the response to the upward step. This slow change in the hydrogen concentration is responsible for the slow *MI* response during the $C \rightarrow B$ transition. Note that the optimal trajectories and manipulated variable policies for the upward and downward steps are very different, reflecting the inherent nonlinearity of the quality control problem.

In the $B \rightarrow A$ transition at time period 85, the grade change is accomplished primarily through an increase in the butene concentration. During this transition, scaled density drops as low as 5 units. This high level of comonomer incorporation may be unacceptable, depending on the quality requirements of the customer.

Although the vent valve position remains constant throughout the series of transitions, the scaled bleed rate ranges between 3.5 and 6.5 in response to reactor pressure fluctuations (Figure 5.3 e)). The polymer production rate remains relatively steady throughout the production schedule, ranging from 0.95 to 1.1 scaled units.

Figure 5.3 Transition Policy I

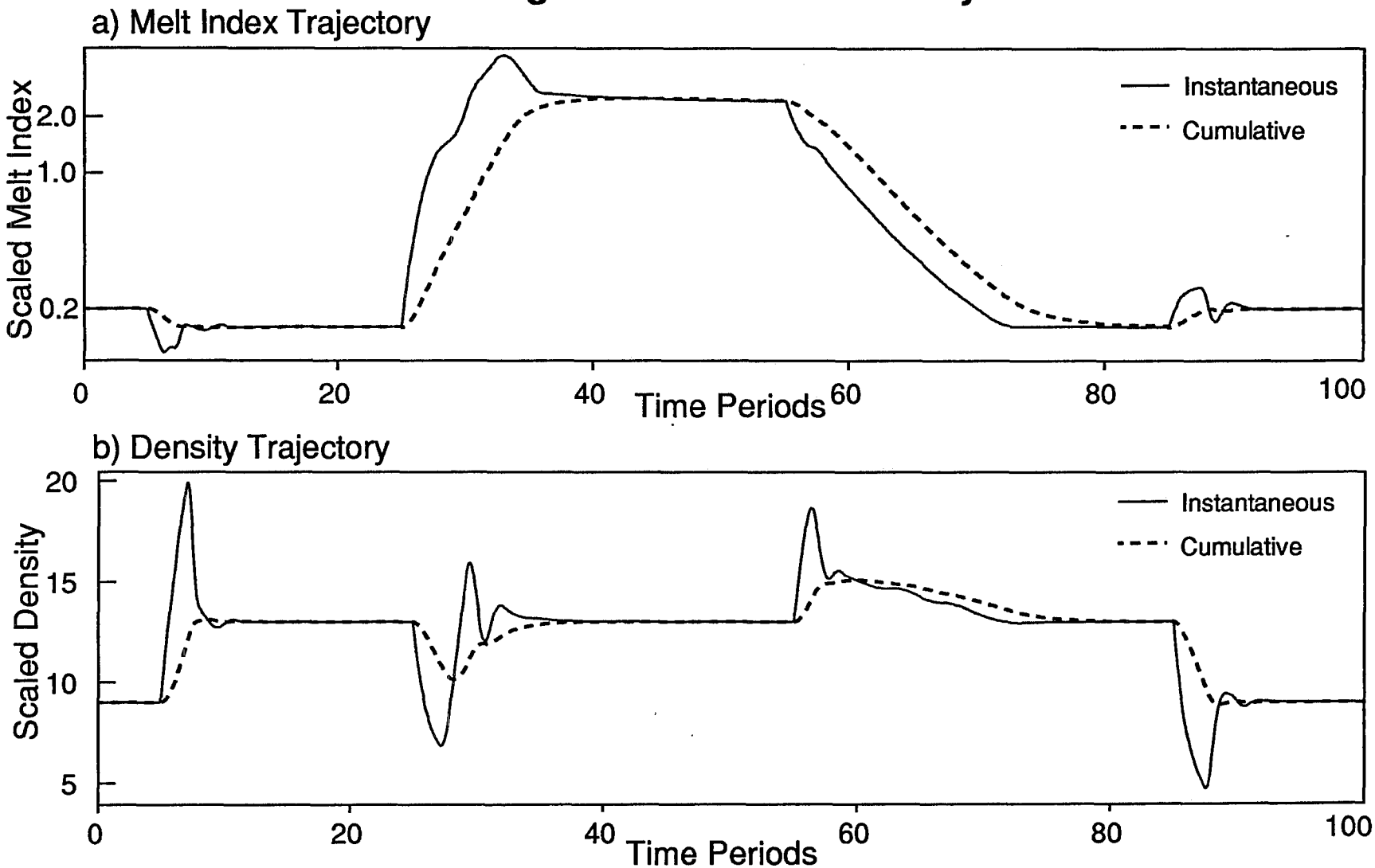

Figure 5.3 Transition Policy I

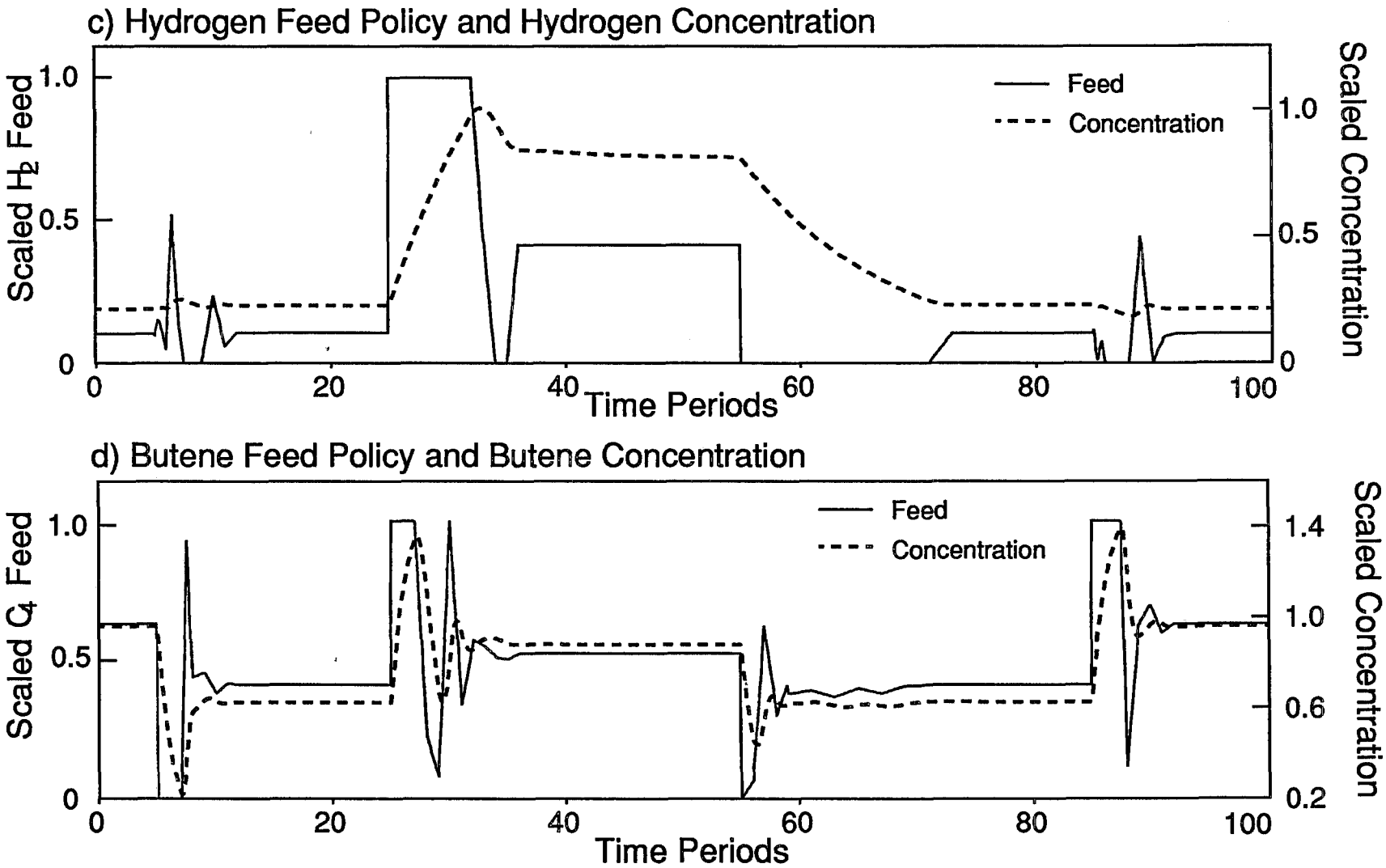

Figure 5.3 Transition Policy I

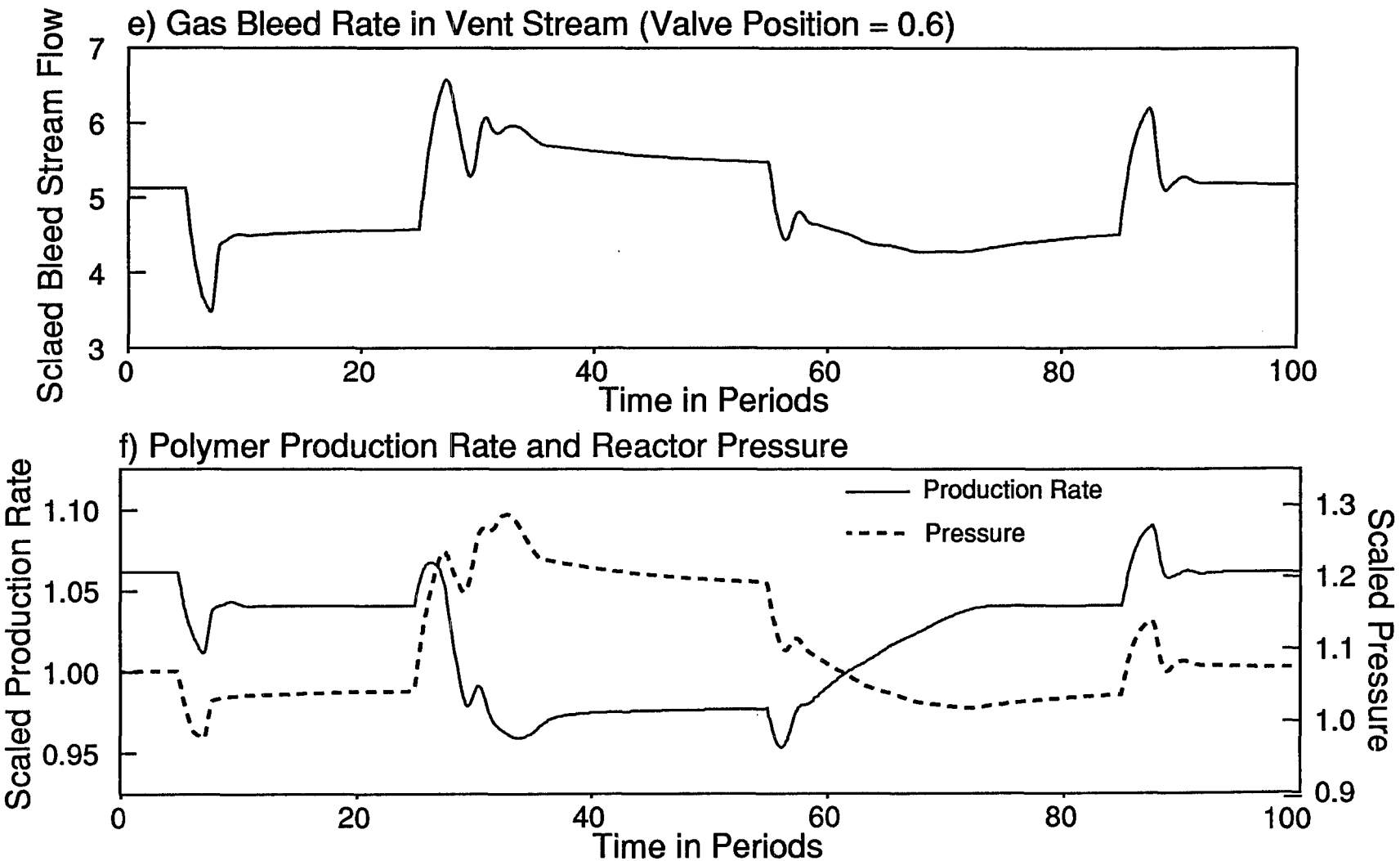

Figure 5.3 Transition Policy I

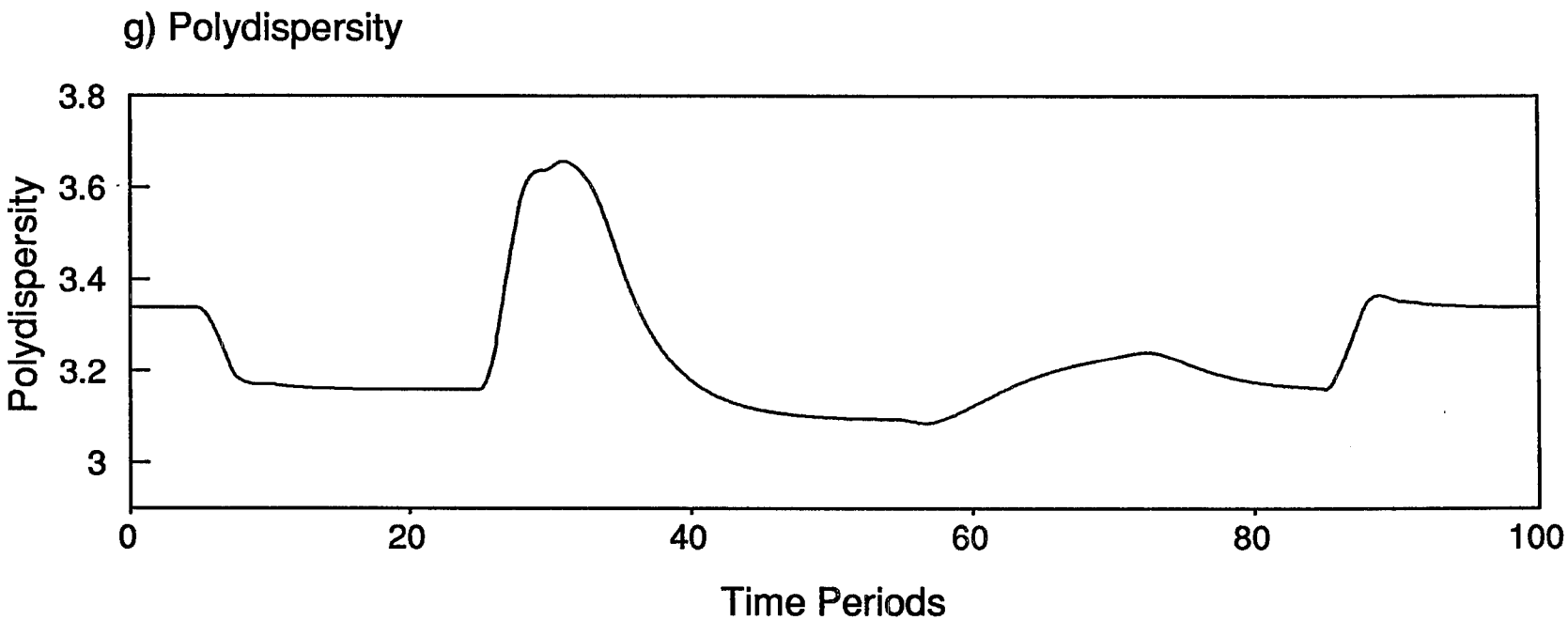

5.4.2 Penalties on Instantaneous Property Deviations: Policy II

Because overshoots in MI_i and ρ_i can result in a degradation in polymer quality, a similar set of optimal grade transitions was determined with expressions 5.8 and 5.9 included in the objective function. The weighting factors used were $w_3 = 0.25$ and $w_4 = 0.01$, so that deviations in instantaneous properties would be penalized half as much as cumulative property deviations. The resulting transitions are shown in Figure 5.4. As expected, the over shoots in MI_i and ρ_i are less pronounced than they were for Policy I. The optimal manipulated variable trajectories are less extreme than those in section 5.4.1. The most pronounced changes are in the butene feed rate policy which is less oscillatory and remains at its upper and lower bounds for shorter periods of time than in Policy I. Although the maximum polydispersity for the $B \rightarrow A$ transition is lower for Policy II than for Policy I, the $B \rightarrow C$ polydispersity remains unchanged, because the
corresponding optimal hydrogen feed policy does not change significantly. The Policy II transitions result in similar reactor pressures, vent rates and production rates as Policy I, except the changes are somewhat smoother.

While improving the instantaneous property trajectories, the penalties on MI_i and ρ_i deviations do result in considerably longer transition times and in the production of more cumulative polymer which deviates from the MI and ρ targets. A summary of the changeover times and amounts of off-target material produced for all of the transition policies studied is given in Table 5.5. In order to calculate the quantity of off-specification polymer produced, the following simple rule was used. Prime polymer was defined as any material which had both a value of MI_c within ±5% and a value of ρ_c within ±0.25 scaled density units of one of the target grade

specifications. All other polymer was considered to be off-prime. Similarly, the transition time was the time interval commencing when the polymer first left the specification range of the previous grade, and lasting until the cumulative properties entered, and stayed within, the specification range of the new target material. Obviously, this method of segregating good polymer from off-target material does not include any criterion for judging the breadth of the molecular weight or composition distribution, and, as such, is not being promoted as a means of classifying prime and non-prime polymer to sell to customers. These results are merely tabulated as one means of comparing the grade transitions resulting from different types of problem formulations.

Table 5.5 Comparison of Optimal Transition Policies

			Transition Time and Quantity of Off-Spec			
	Manipulated Variables		$A \rightarrow B$	$B \rightarrow C$	$C \rightarrow B$	$B \rightarrow A$
Policy I	H,B	Time Mass	2.0 2.043	10.9 10.845	24.1 24.492	2.4 2.594
Policy II	H,B	Time Mass	4.1 4.237	11.8 11.717	24.1 24.499	4.1 4.389
Policy III	H,B,T	Time Mass	3.6 4.209	9.6 10.839	32.7 31.626	4.1 4.642
Policy IV	H,B,T,V	Time Mass	3.6 4.240	9.5 10.576	17.5 16.043	4.1 4.649
Policy IV High H2feed	H,B,T,V	Time Mass		9.0 10.149		
Policy IV Case IIC $\rightarrow B$	H,B,T,V	Time Mass			33.3 33	
Policy V	H,B,T,V,C, W	Time Mass	3.6 3.666	10.0 9.484	17.1 9.510	3.7 3.878

Figure 5.4 Transition Policy II

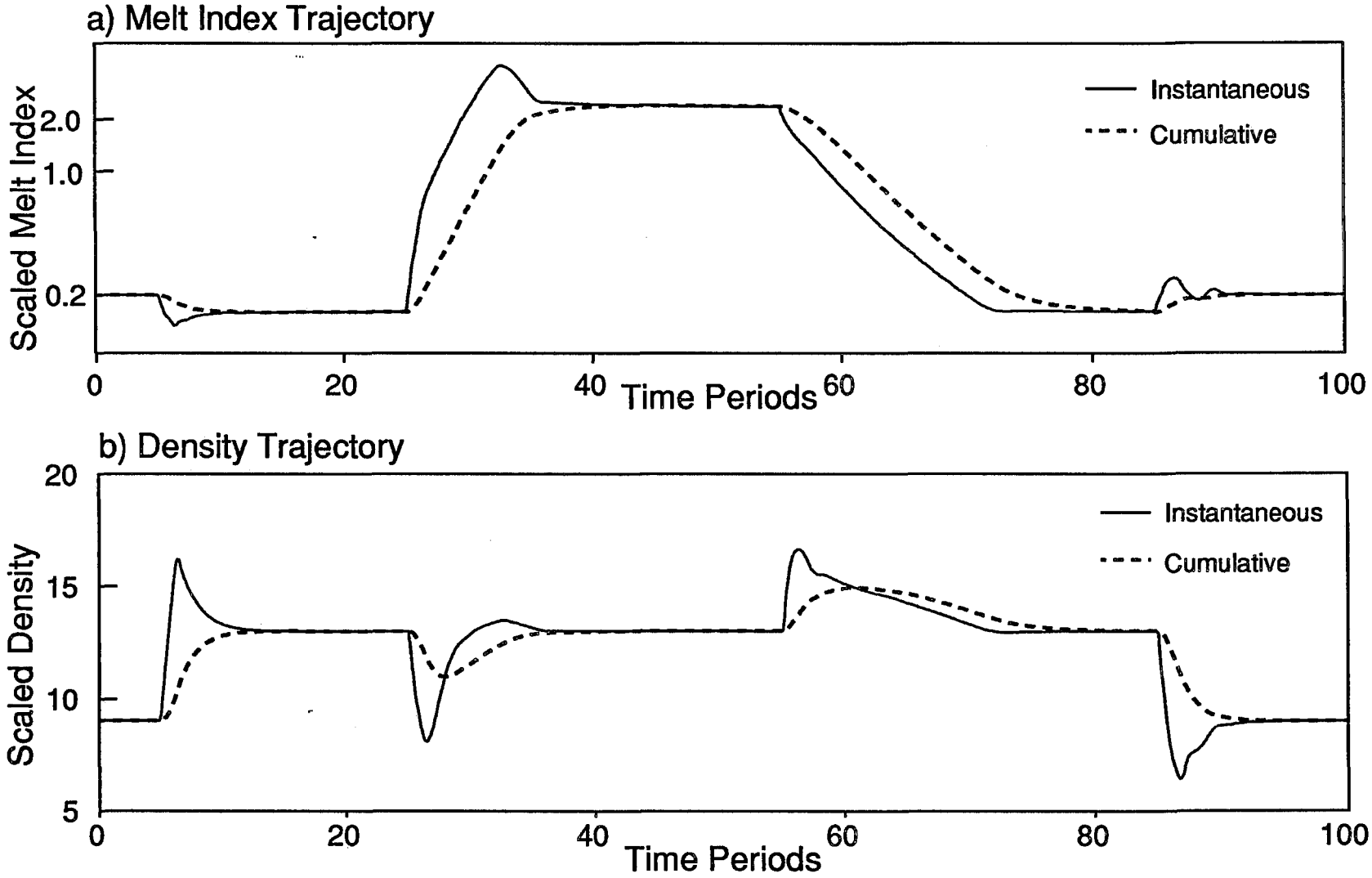

Figure 5.4 Transition Policy II

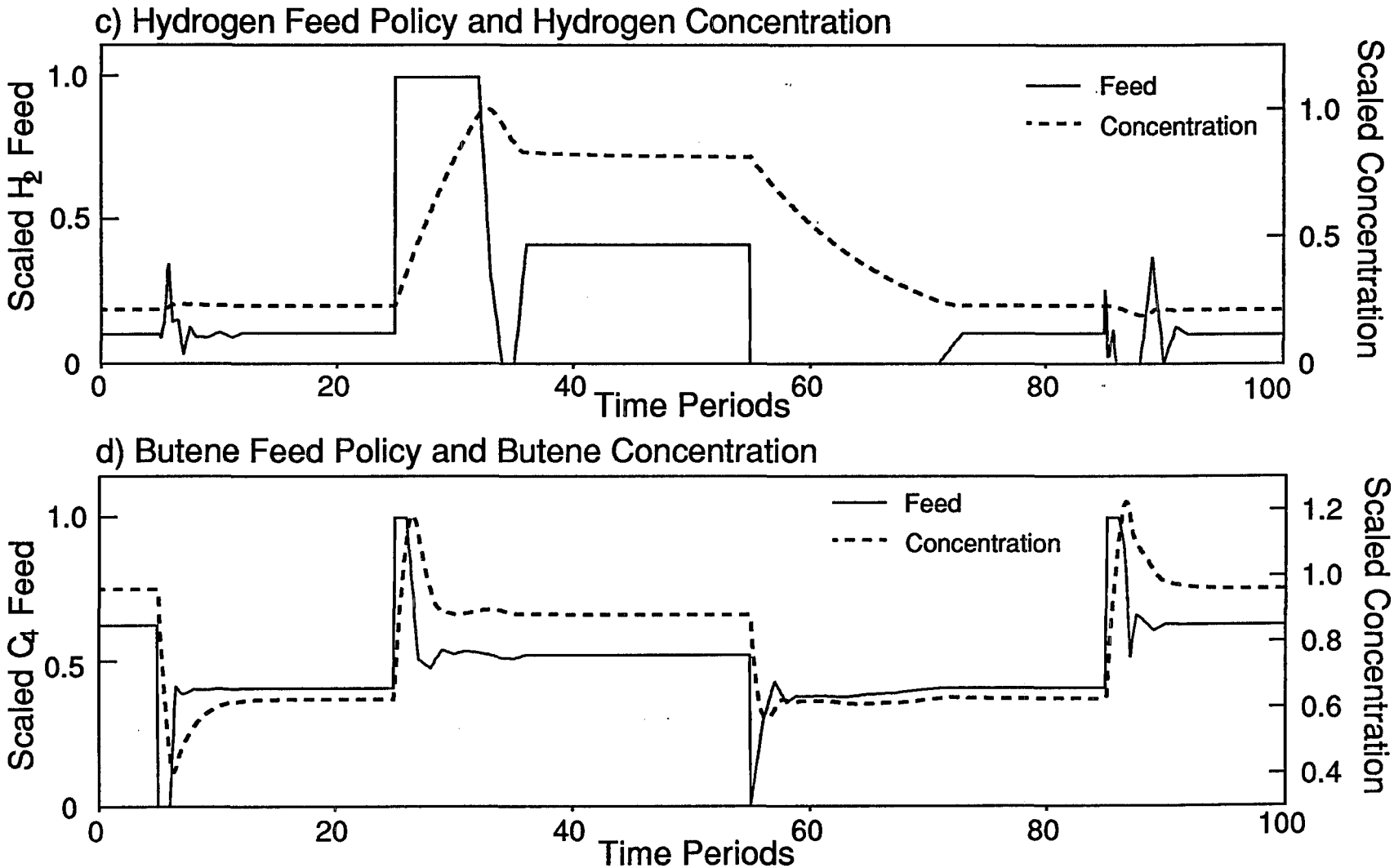

Figure 5.4 Transition Policy II

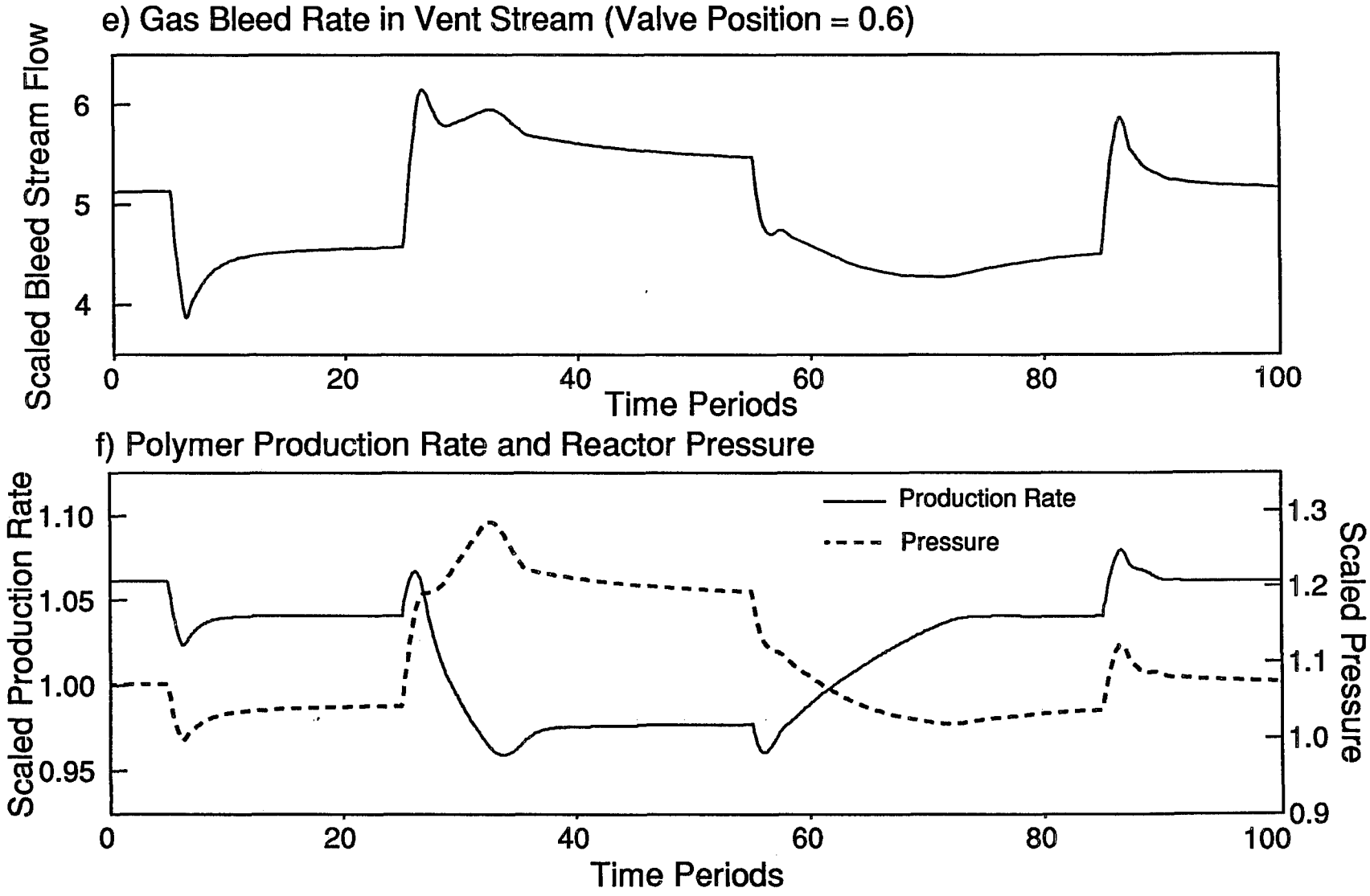

Figure 5.4 Transition Policy II

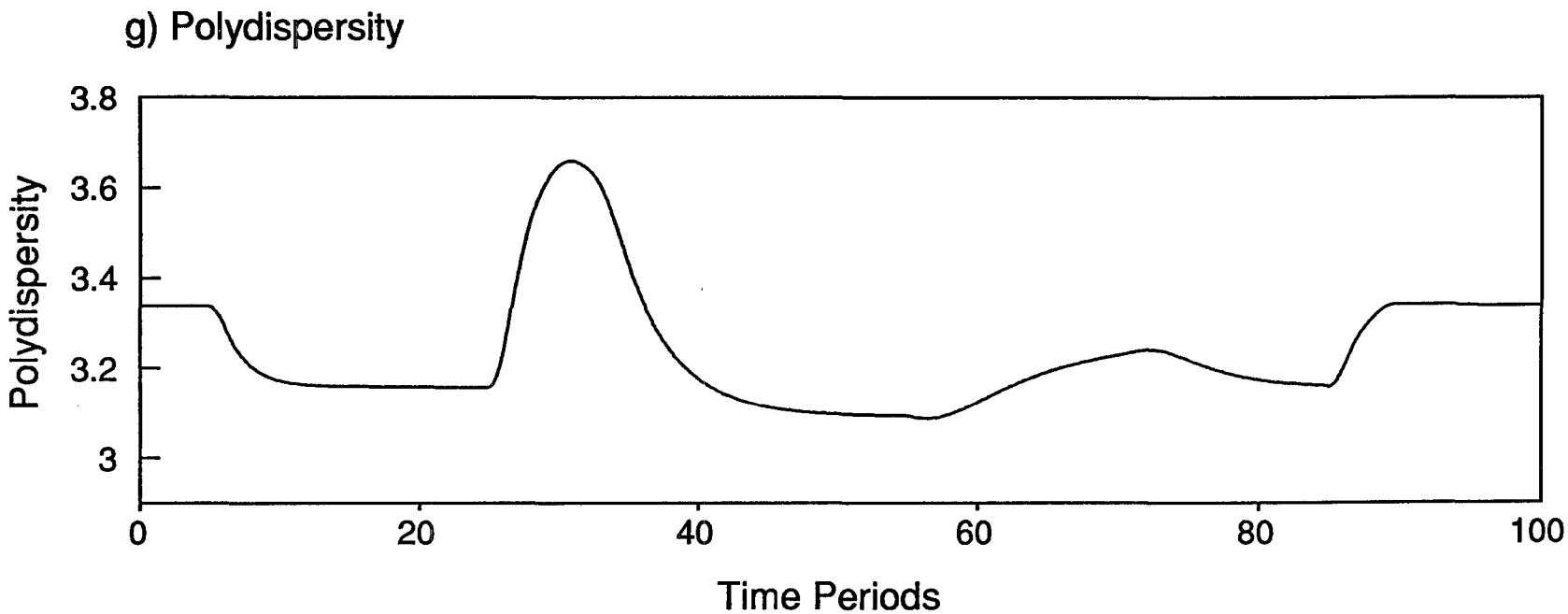

5.4.3 Benefits of Manipulating Reactor Temperature: Policy III

In this set of transitions, the reactor temperature setpoint was included ,along with the hydrogen and butene feed rates, in the set of manipulated variables. Expression 5.10 with $w_5 = 12$ was added to the objective function of Policy II, so that the final temperature would settle at or near the desired value. Note that only the twelfth temperature setpoint decision variables chosen by the optimizer was penalized. The density trajectories in Figure 5.5 are very similar to those of Policy II. The greatest benefit of manipulating the temperature is observed in the *MI* trajectories. As shown in Figure 5.5 e), the response of the reactor temperature to setpoint changes is very fast. One potential problem with these temperature responses is the temperature overshoot. If the $B \rightarrow C$ transition is unacceptable because the initial temperature spike might lead to particle sticking and agglomeration, then the bound on the first temperature setpoint decision variable should be reduced by several degrees and the optimization repeated. The fast changes in temperature result in equally fast changes to the instantaneous melt index, making temperature a desirable manipulated variable for *MI* control during grade transitions. Nevertheless, several problems can result from using temperature to control *MI* in the long run. The range of allowable temperatures at which the reactor can be run is very narrow, and operating the reactor below the desired value results in lower catalyst activity, leading to higher operating costs and increased catalyst residue in the product. Operation above the desired temperature reduces the margin of safety for defending against temperature disturbances and for preventing particle agglomeration.

A peculiar result shown in Figure 5.5 e) is that both the $A \rightarrow B$ and $B \rightarrow A$ transitions make use of an increase in the reactor temperature above the initial value.

One explanation of why this action is optimal is that a higher temperature leads to a higher production rate and a smaller solid phase residence time. This smaller residence time allows for a faster changeover of cumulative properties in the reactor. The faster MI response for the $B \rightarrow C$ transition results in a higher maximum for the polydispersity than for Policy II. This is not a major concern, because the rate at which the polydispersity falls is also much larger for Policy III than for Policy II, so that by the time the cumulative MI reaches its target, the polydispersities resulting from the two policies are essentially the same.

As shown in Table 5.5, both the quantity of off-specification polymer and the transition time were significantly reduced for the $B \rightarrow C$ transitions. However, for the $C \rightarrow B$ transition, including temperature as a manipulated variable actually results in an increase in transition time for the optimal policy. This result is somewhat unexpected, but can be readily explained. The optimizer is best able to reduce the objective function by holding the temperature setpoint at its lower bound for 16 time periods and then increasing the temperature setpoint so that it is at its desired value at the final switching time. While this reduction in temperature results in a very fast reduction in instantaneous MI at the start of the transition, it also results in a lower reactor pressure and, therefore, in a lower hydrogen bleed flow rate. The hydrogen concentration in the reactor at time period 71 is significantly higher than it was for Policy II, so that when the temperature reaches its desired final setpoint at time period 73, the instantaneous MI is outside of the melt index specification range. Once the manipulated variables have been fixed at their steady state values, the rate at which MI_i, and in turn MI_c fall toward the specification limit is determined by the rate at which the hydrogen concentration falls toward its steady state level. Reparameterization of the manipulated variable policies would help in reducing the

time required to reach the specification limit. If the optimizer were allowed to hold the temperature at the lower limit and the hydrogen feed rate at zero while more hydrogen was vented from the reactor, then MI_c would move within the specification limits sooner.

This grade transition illustrates an important point. Minimization of the objective function does not necessarily imply that the resulting grade transition produces either the minimum possible quantity of off-specification polymer, or that the grade transition is accomplished in the minimum amount of time. If one really wants to solve the minimum time or minimum quantity problem, then the optimization problem must be reformulated to include knowledge of the positions of the grade specification limits, rather than of the targets alone.

Another important result which can be observed from Figure 5.5 is that little benefit results from including temperature as a manipulated variable in the $A -> B$ and $B \rightarrow A$ changeovers. In fact, the quantity of off-specification polymer produced during the $B \rightarrow A$ transition was actually higher for Policy III than for Policy II, due to the higher production rate of off-specification material induced by the higher reaction temperature. Including temperature as a manipulated variable is more beneficial in transitions involving a major melt index change than it is for transitions which are mainly concerned with density, because temperature has a major influence on MI_i and very little effect on ρ_i. Therefore, for transitions like $A \rightarrow B$ and $B \rightarrow A$, it may be better to simplify the changeover, by adopting an optimal policy which does not include temperature setpoint as a manipulated variable.

Figure 5.5 Transition Policy III

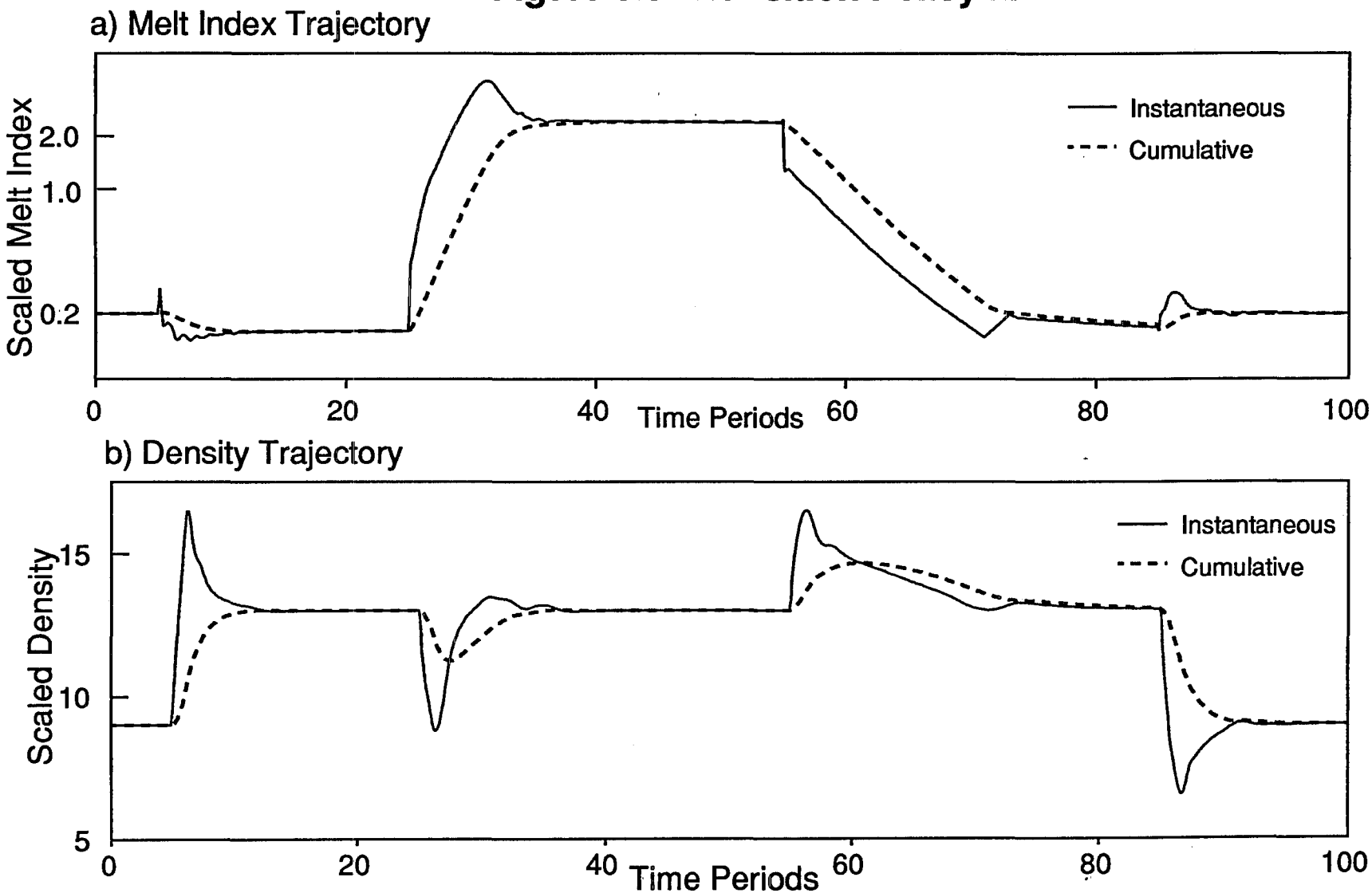

Figure 5.5 Transition Policy III

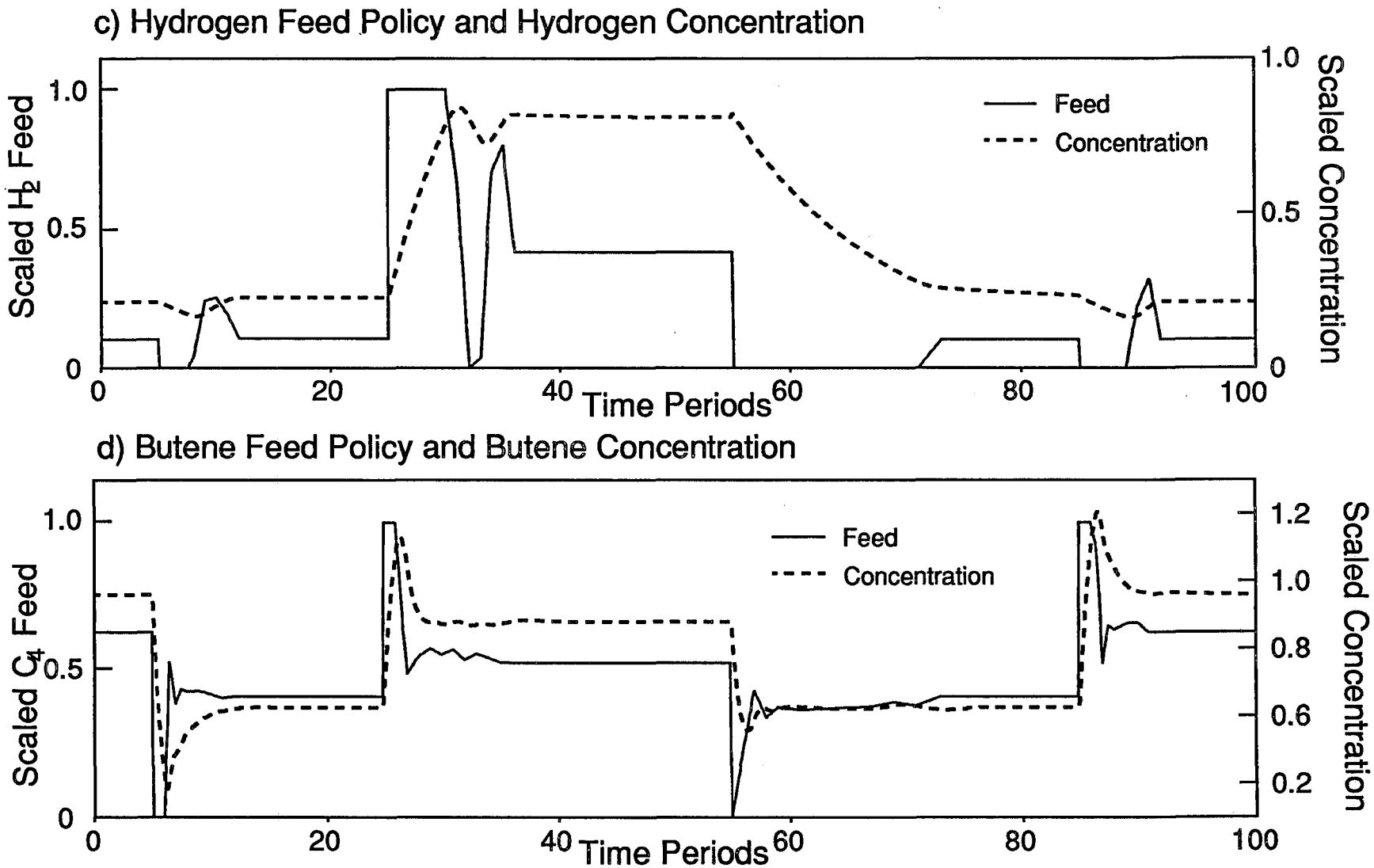

Figure 5.5 Transition Policy III

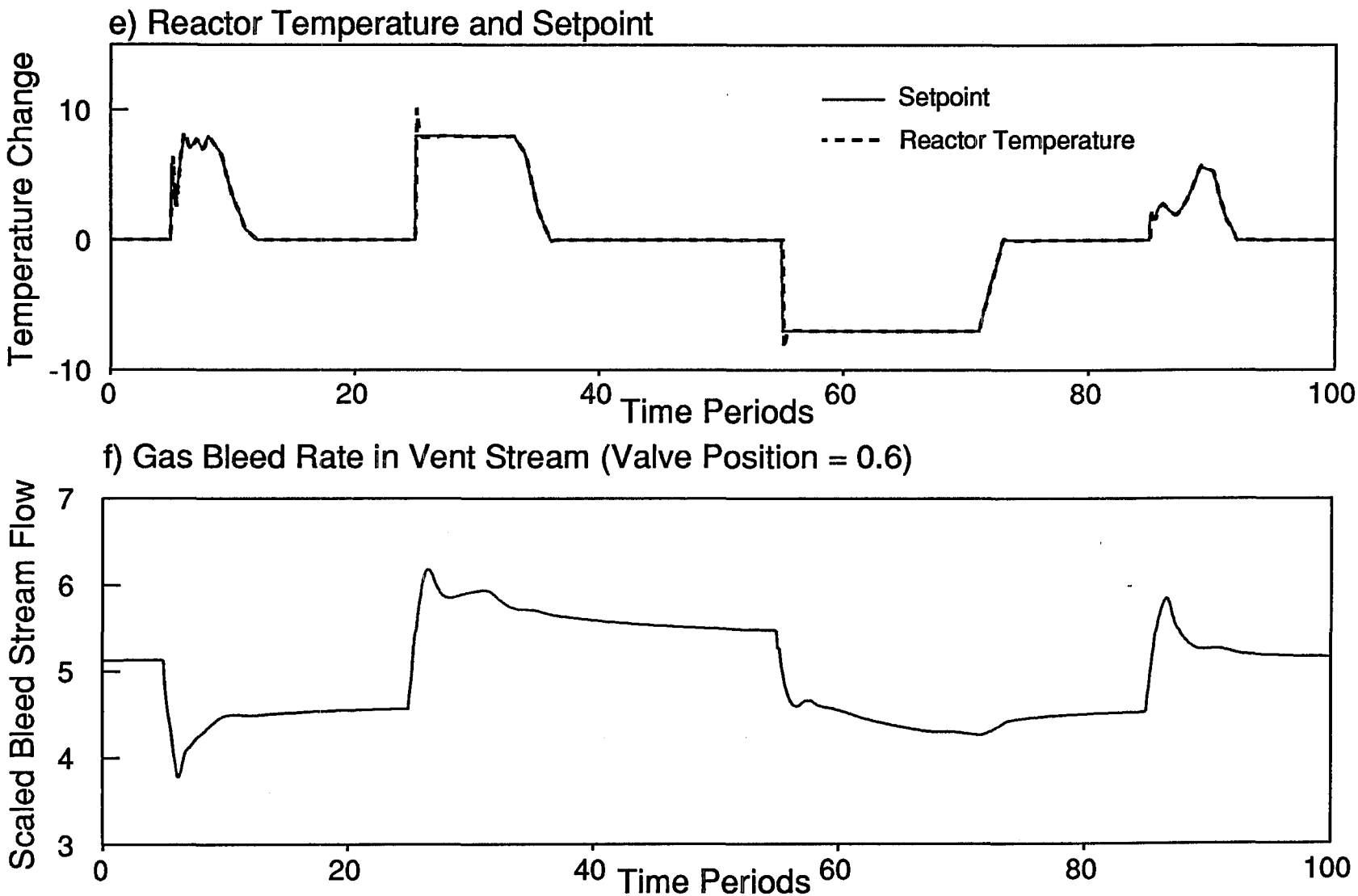

Figure 5.5 Transition Policy III

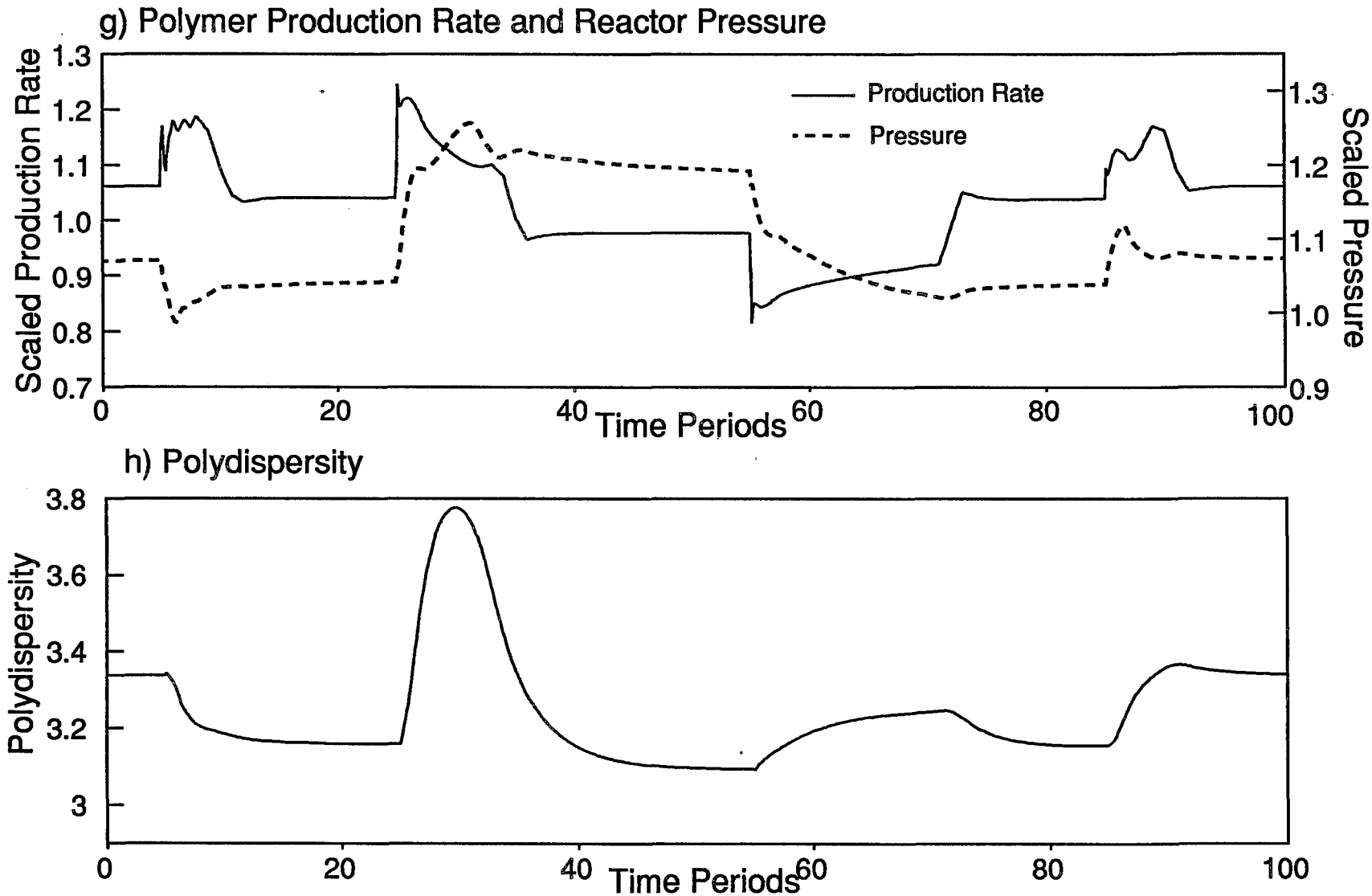

5.4.4 Benefits of Manipulating the Bleed Rate: Policy IV

In this set of grade transitions, the bleed rate, temperature setpoint, and hydrogen and butene feed rates were manipulated to achieve optimal grade transition policies. The objective function used was the same as in section 5.4.3, except that expression 5.11 was added with $w_6 = 0.125$ to ensure that the final bleed valve position settles near the desired value and to prevent excessive venting during transitions. As shown in Figure 5.6 f), the optimizer closes the vent for 3 time periods during the $B \rightarrow C$ transition in order to increase the rate of hydrogen accumulation in the reactor. As a result, the hydrogen concentration in Figure 5.6 c) climbs more quickly than in 5.5 c). Hence MI_i rises more quickly and reaches a slightly higher maximum value, leading ultimately to a higher maximum polydispersity. However, the polydispersity at time period 35, when the cumulative polymer first comes within the specification limits, is almost unchanged from Policy III.

The grade transition wherein venting is most beneficial is $C \rightarrow B$. The optimizer holds the vent position at its upper limit for 10 time periods during the changeover. Opening the vent allows hydrogen in the reactor to escape, causing the hydrogen concentration to fall more quickly than in policy III. As a result, the duration of the grade transition is reduced from 32.7 to 17.5 time periods. This faster changeover results in an increased polydispersity, even after time period 73 when the polymer is within the grade limits (Figure 5.6 h)). Although the polymer produced between time periods 73 and 78 is prime according to the definition used in Table 5.5, it will have slightly different physical properties than polymer produced after

time period 80. Use of bleed stream manipulations has very little benefit for transitions $A \rightarrow B$ and $B \rightarrow A$. Perhaps both venting and temperature setpoint changes should be reserved for grade transitions involving a large change in MI.

Figure 5.6 Transition Policy IV

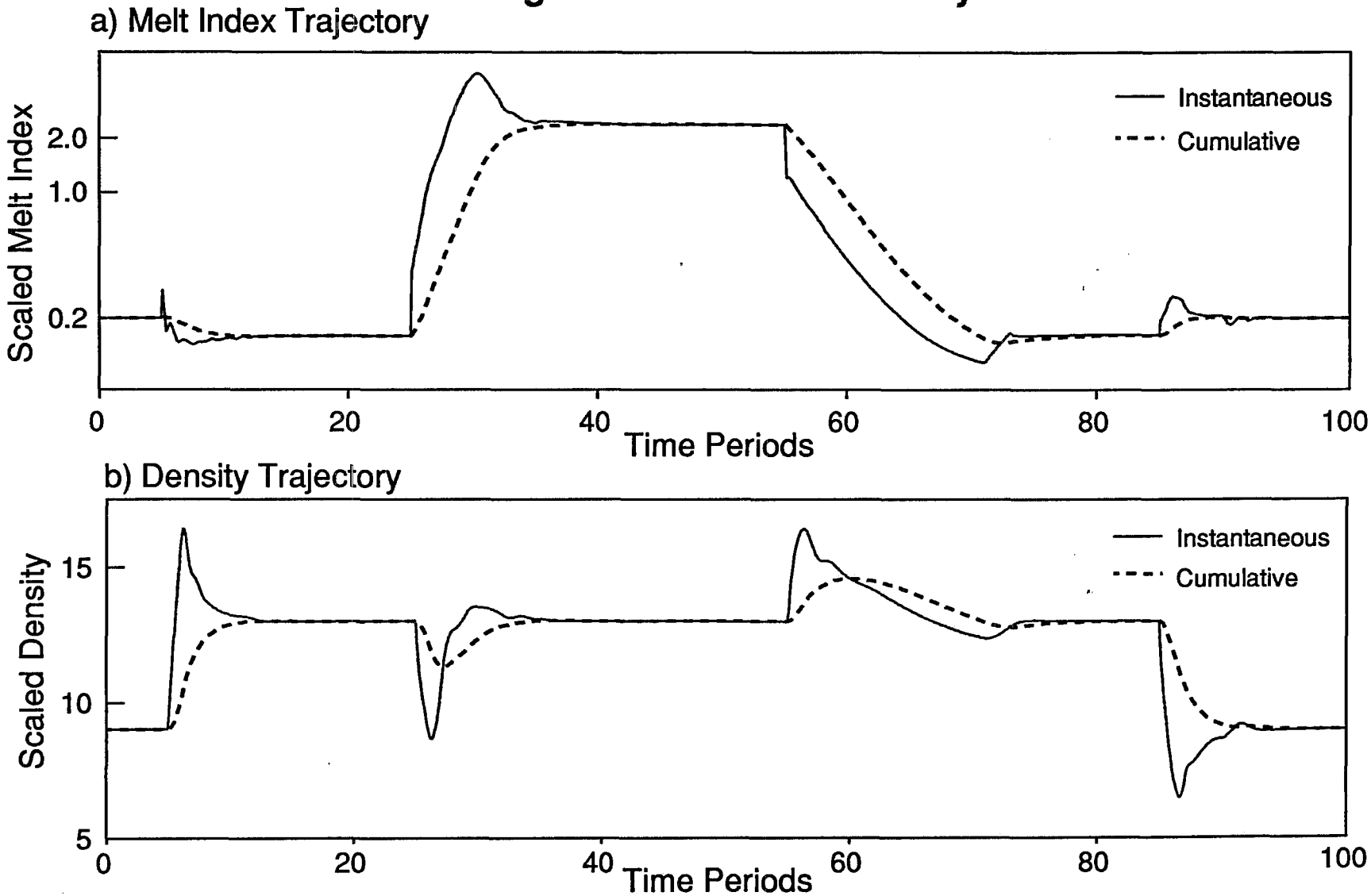

Figure 5.6 Transition Policy IV

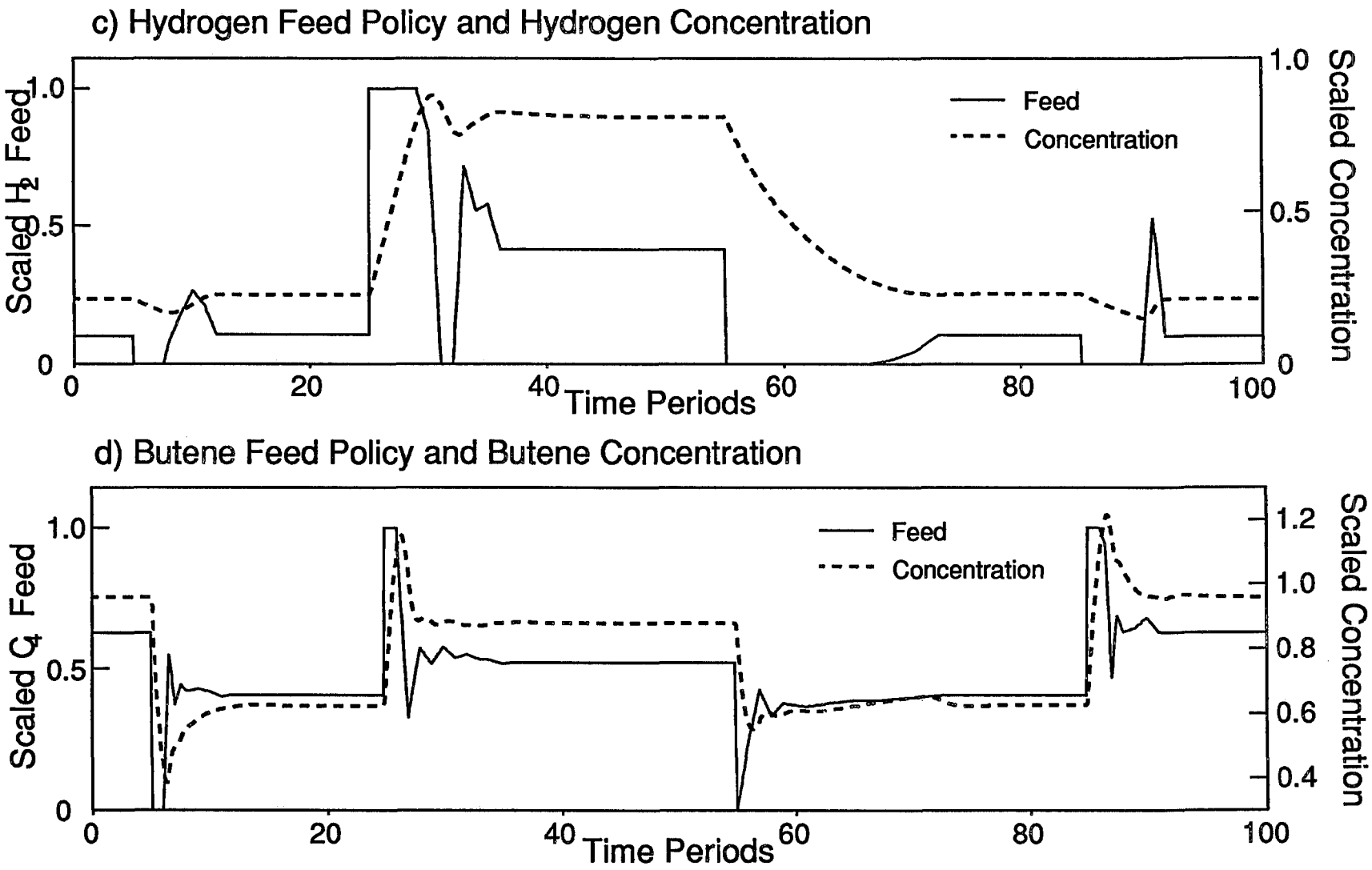

Figure 5.6 Transition Policy IV

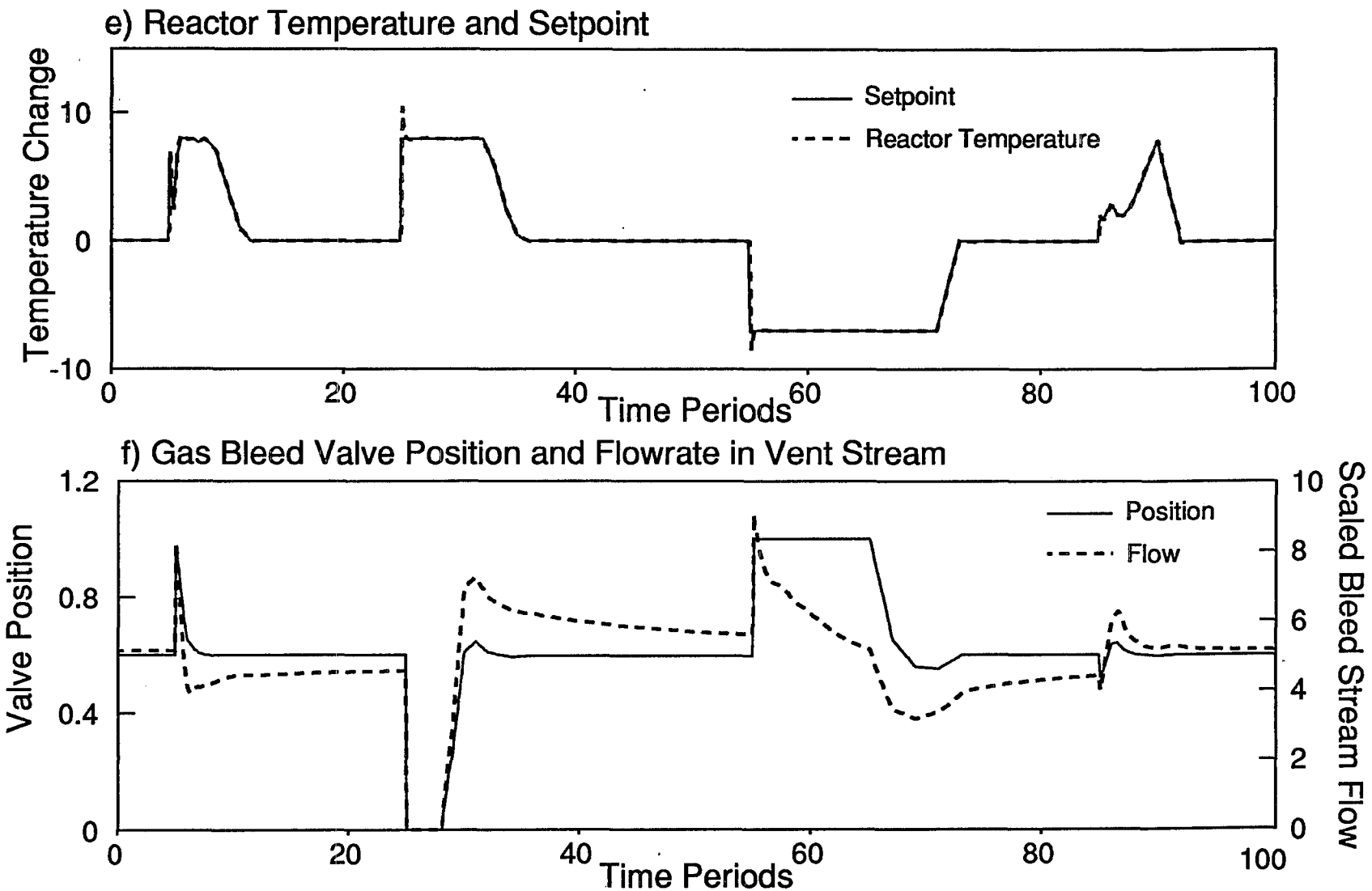

Figure 5.6 Transition Policy IV

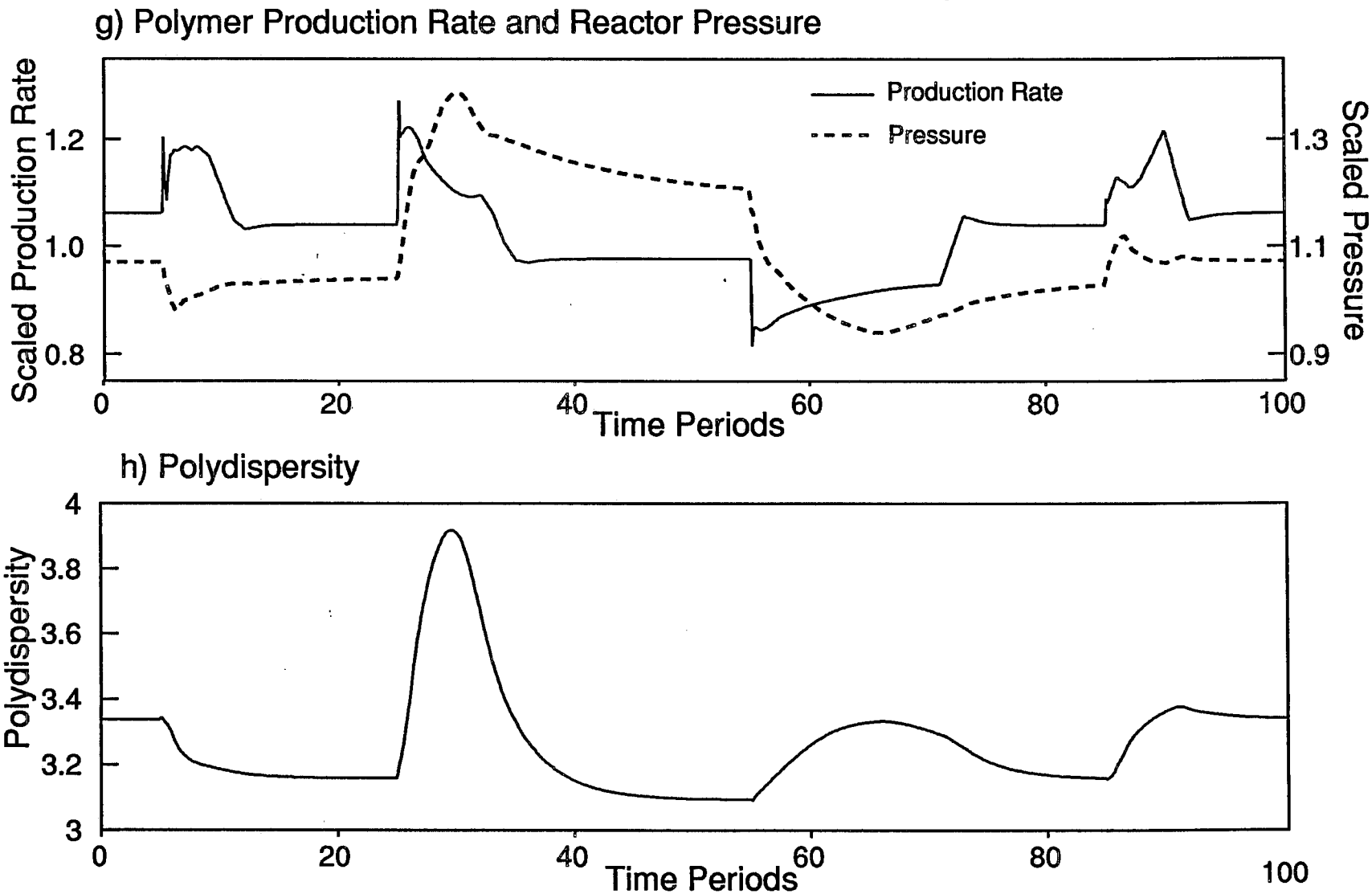

5.4.5 Sensitivity of the $B \rightarrow C$ Transition to the Maximum Hydrogen Feed Rate

One of the bounds imposed on the optimization problem, which could be changed by a design change in the plant, is the upper bound on the hydrogen feed rate. A larger valve would allow more hydrogen to flow into the reactor in a shorter period of time. To assess the potential benefit of such a change, the optimization problem in section 5.4.4 was rerun with the upper hydrogen feed rate bound increased by 11.1 %. The results are shown in Figure 5.7. The optimal policy is much the same as that shown in Figure 5.7, except that the hydrogen concentration and MI_i climb faster than they did in Figure 5.6, resulting in a faster transition, less off-target material, a higher overshoot in MI_i, and a higher maximum polydispersity. The resulting savings in off-spec production and in transition time are shown in Table 5.5.

5.4.6 Effect of Manipulated Variable Discretization

Since the manipulated variable profiles have been parameterized as shown in Figure 5.2, the grade transitions determined in this study are actually slightly suboptimal. The true optimal manipulated variable trajectories which would minimize the objective function are curves rather than a series of ramps. The reason that the ramp approximation was adopted is that the resulting optimization problem is much easier to solve than that involving determination of the true optimal curves for the manipulated variables. While approximation of the true optimal solution could be improved by finer discretization of the manipulated variable policies, addition of more decision variables makes solution of the optimization problem more time

consuming. Each additional decision variable increases the number of degrees of freedom considered by the optimizer, but the main reason for the increase in solution time is that more adjoint equations must be added
to the model integration stage so that the required gradient information can be provided to the optimizer. Since a set of eleven ramps joining twelve points is capable of approximating a great many curves, no more decision variables were added to the optimization problem.

A more important factor which can lead to sub-optimality is the position of the decision variables in time. Three sets of switching times corresponding to the end-points of the ramps are shown in Table 5.3. These arbitrary switching times were chosen after an initial trial and error study. An important result of this initial study is that the times corresponding to the final switching intervals must be sufficiently large compared with the time for the optimal trajectory to reach its new target. Otherwise, the resulting grade transition can take a long time. An example of this phenomenon is shown for a $C \rightarrow B$ transition in Figures 5.8 a) to h).

The transition time for the $C \rightarrow B$ transition using Case III discretization and transition policy IV was 17.5 time periods (Figure 5.6). This transition time is similar to the final Case III switching time of 18 periods. There is no reason to extend the final switching point beyond period 18 because the optimizer can do little to improve the objective function by moving the manipulated variables after steady state has been reached. However, if the Case II discretization policy is used, there is a dramatic effect on the "optimal" policy. Since the final switching time is now 11 time periods after the start of the transition, the optimizer is not able to hold the hydrogen feed rate, the vent position and the temperature setpoint at their bounds for as long as required to give a good transition. As a result, the total transition time is

greatly extended from 17.5 to 33.3 time periods, and the quantity of off-spNcification polymer produced is more than doubled. The reason for this increase in transition time is obvious from Figures 5.8 a) and c). After period 11, the hydrogen feed rate is set to its steady state value and the rate at which the melt index approaches the new specification range is determined by the slow dynamics of the falling hydrogen concentration. Since the final time for integrating the objective function is only 60 time periods, the bleed valve position does not settle at its desired value of 0.60, but remains at 0.62824. This indicates that the optimizer is trading off the deviation in the final vent position

against a smaller hydrogen reactor residence, in order to bring the cumulative *MI* on-specification sooner. The results in Figure 5.8 demonstrate the importance of choosing a sufficiently long time interval for optimization of the manipulated variable trajectory.

Figure 5.7 BC Transition Policy IV (Maximum Hydrogen Feed Rate = 1.11)

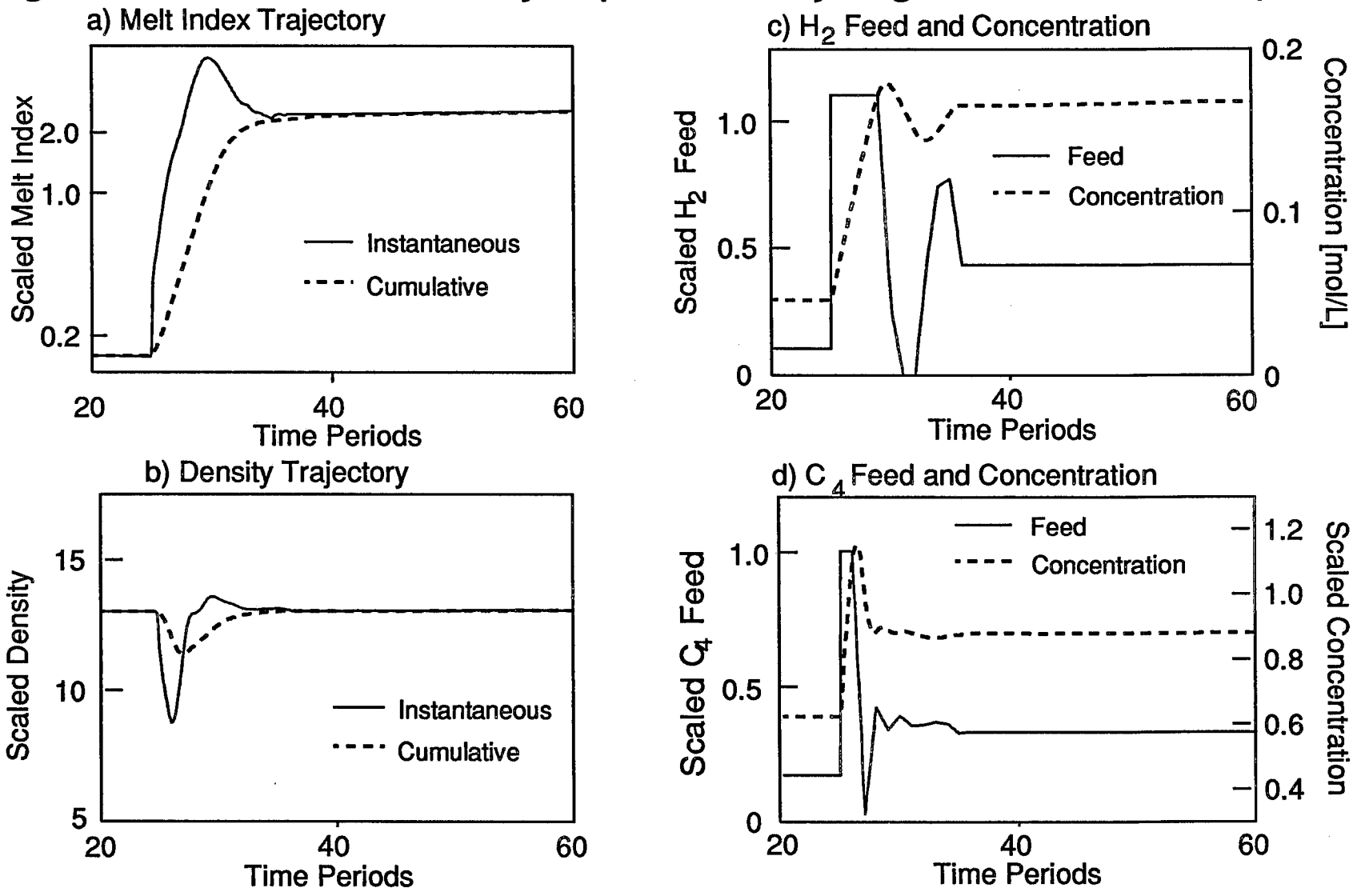

Figure 5.7 BC Transition Policy IV (Maximum Hydrogen Feed Rate = 1.11)

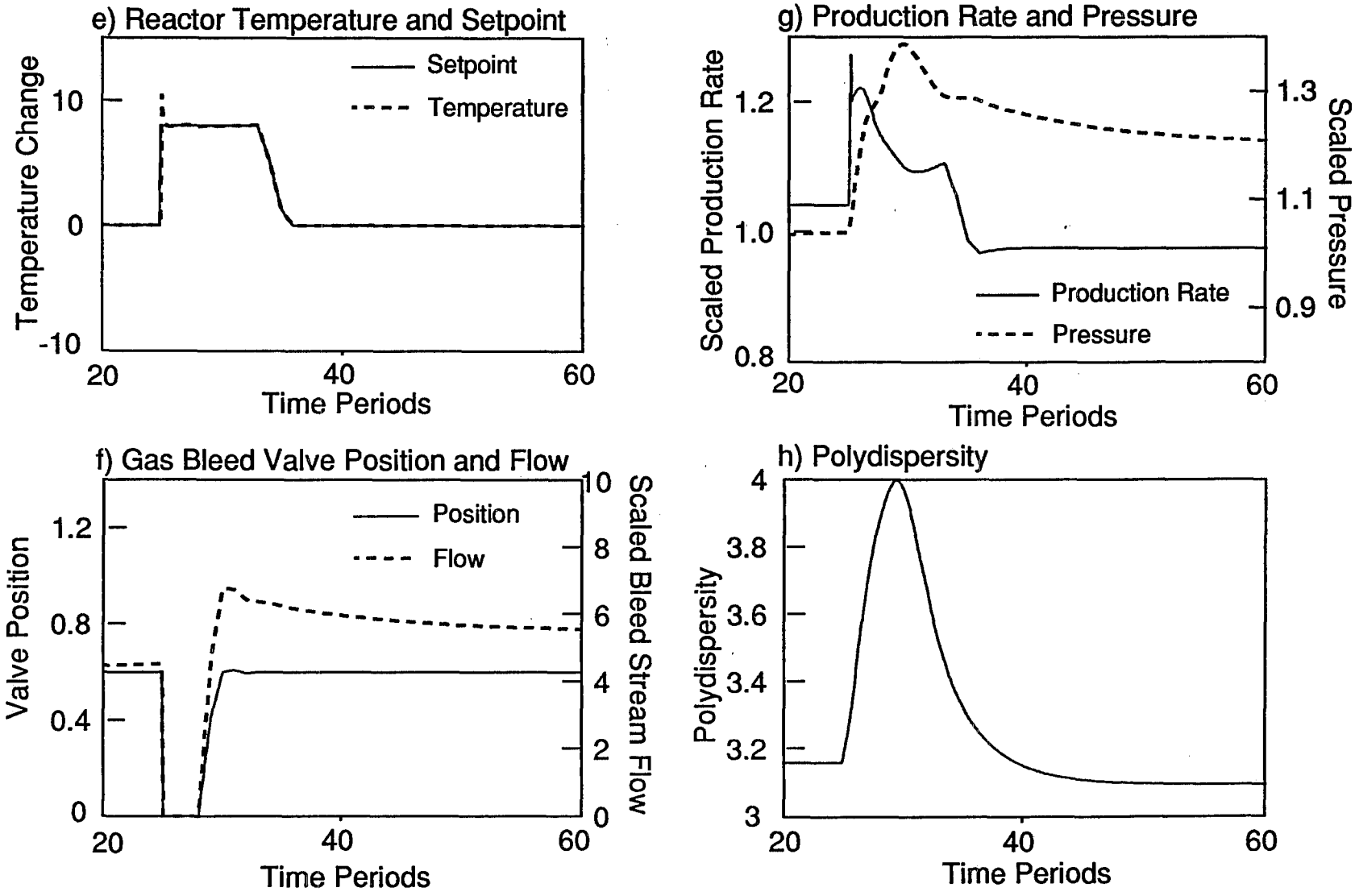

Figure 5.8 CB Transition Policy IV with Case II Discretization

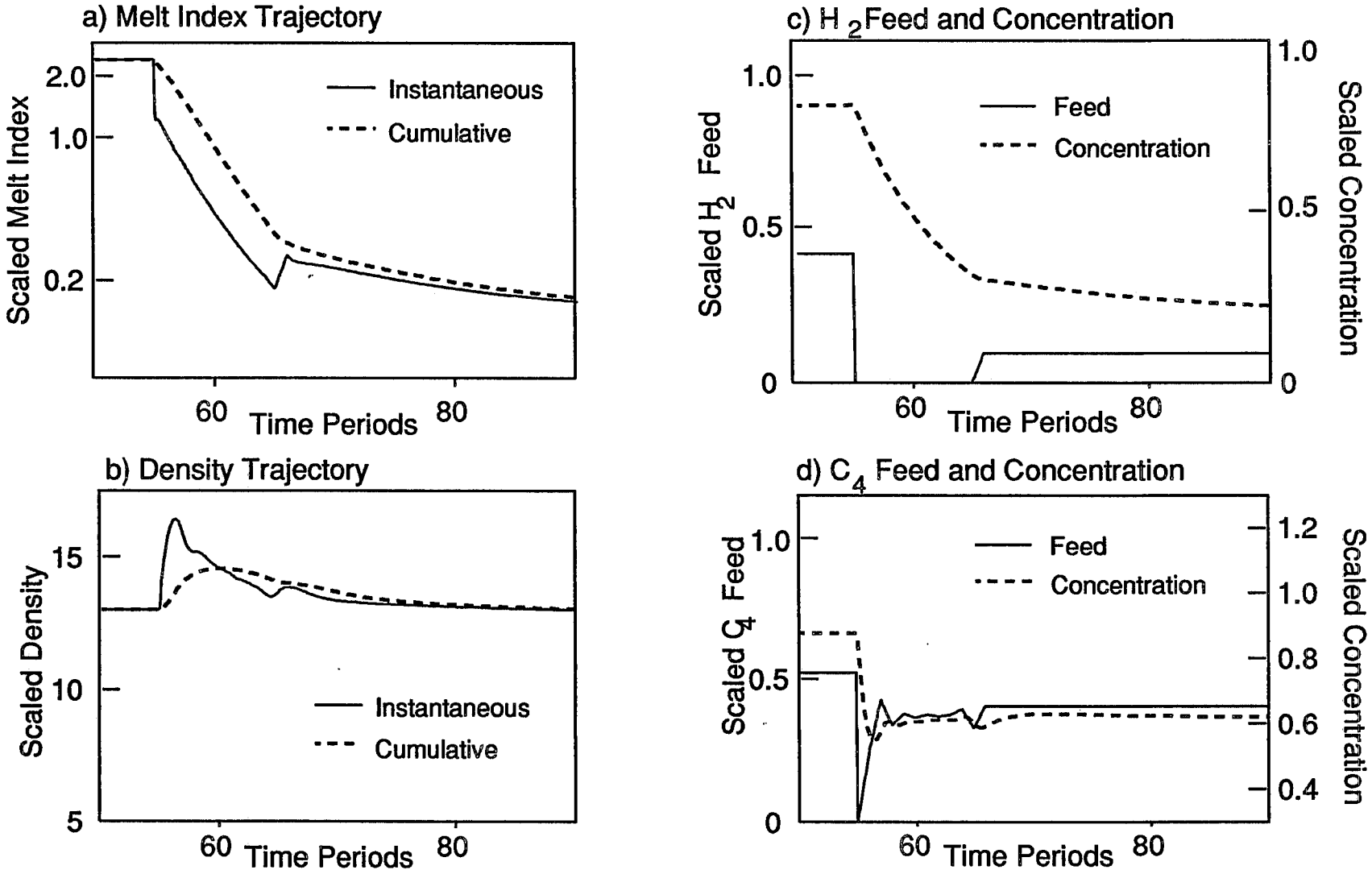

Figure 5.8 C→B Transition Policy IV with Case II Discretization

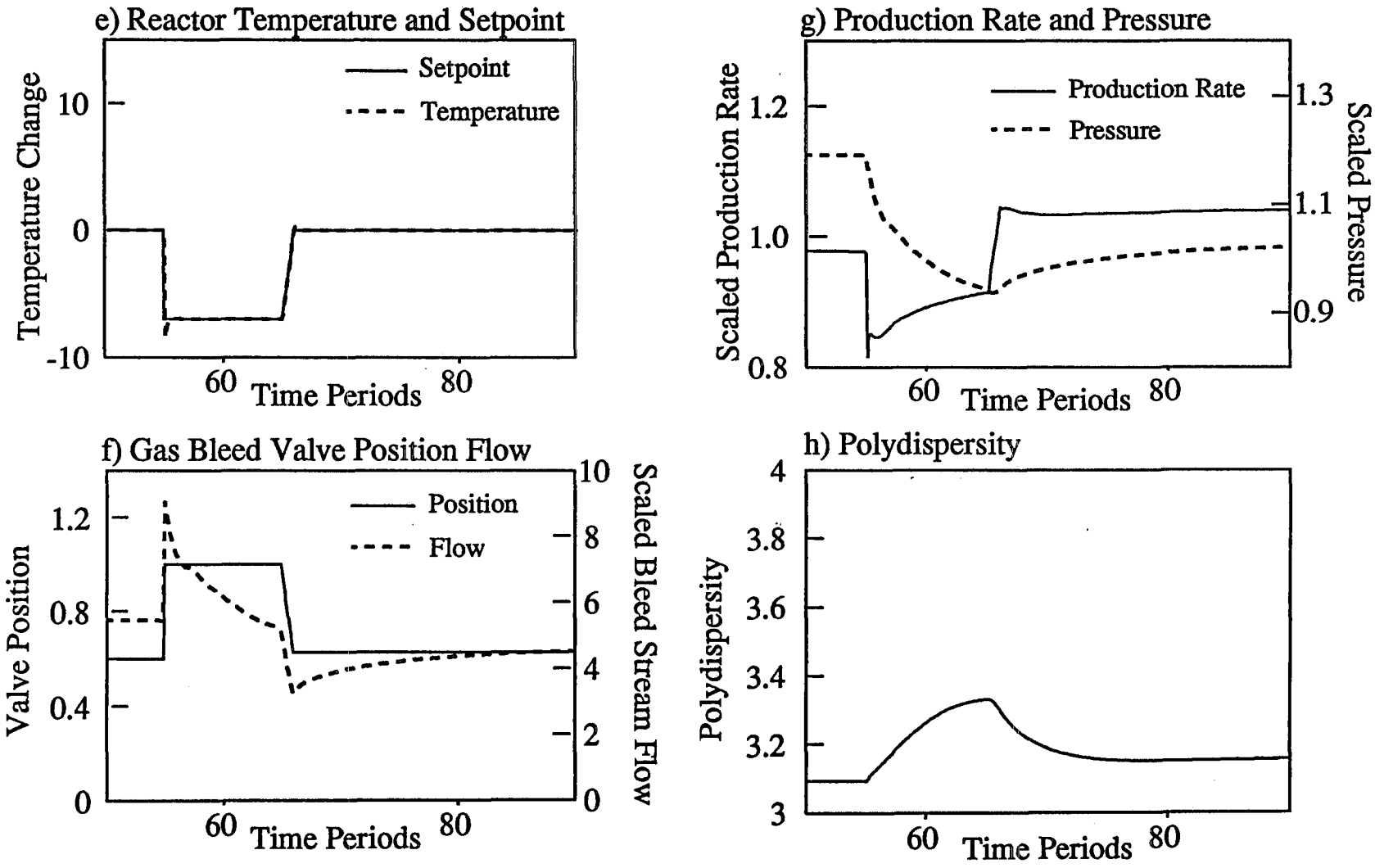

5.4.7 Benefits of Manipulating Catalyst Feed and Bed Level: Policy V

In the transition policies discussed in sections 5.4.1 to 5.4.6, no attempt is made to improve the grade changeovers by manipulating either the catalyst feed rate or the bed level setpoint. As a result, the production rate remains relatively constant throughout the grade changeovers. In this section, the catalyst feed rate and the bed level are manipulated so that less off-specification polymer is produced early in the transitions, when the instantaneous product properties are far from their targets. Since the production rate can fluctuate significantly during such changeovers, the objective function in expression 5.14 has been adopted. The values of a_1 to a_4 in expression 5.13 have been set equal to w_1 to w_4 in earlier objective functions. Since the scaled production rate in Policies I to IV always remained near unity, this choice of weighting factors will result in the same trade-offs between *MI* and ρ and between cumulative and instantaneous properties as in the earlier optimization studies. In addition, the values of w_5 and w_6 are kept at 12 and 0.125, respectively, to ensure consistency with previous policies. w_7 and w_8, the penalty coefficients for the final bed level and for production rate deviations, have been set at 33.75 and 2.0, respectively. The optimal policies which result from objective function 5.14 are show in Figures 5.9 a) to h). The corresponding transition times and quantities of off-specification material are given in Table 5.5.

For the $A \rightarrow B$ transition, incorporating catalyst feed and bed level manipulations resulted in a similar transition time as compared to policy IV, but in a 13.5% reduction in the quantity of off-specification product. The reduction in non-prime polymer results from a drop in the bed level and the initial catalyst feed rate, which causes a reduction in the production rate at the start of the transition.

Also, dropping the reactor bed level allows more of the polymer initially in the bed to be classified within the product A grade specification, rather than having it remain in the reactor to be mixed with new instantaneous polymer. While the optimal trajectories for ρ_i and ρ_c are very similar to those in Figure 5.6, the melt index trajectories are very different. The instantaneous *MI* does not experience an initial upward spike as in Figure 5.6. The new optimal temperature profile, which involves a decrease in the temperature setpoint, rather than an increase, is responsible for this downward fluctuation in MI_i. The hydrogen feed profile is also very different from Policy IV. The optimizer uses an increase, rather than a decrease, in hydrogen concentration during the transition in order to accomplish the changeover. As before, the steady state hydrogen concentrations before and after the transition are nearly identical. Note that the production rate, bed level, and bleed valve position all settle at their final values. If one could tolerate a slightly longer transition time in exchange for the production of less off-specification material, then a slightly lower value of w_8, the coefficient of the production rate deviation term in the objective function, could be adopted. A smaller penalty on production rate deviations from setpoint would result in a lower catalyst feed rate and a lower production rate of off-specification material during the initial stages of the transition. In that way, less off-specification polymer would be produced until the butene concentration in the gas had reached its new lower level.

Compared with Policy IV, the $B \rightarrow C$ transition shown in Figure 5.9 results in a 10.3% reduction in the quantity of off-specification material produced, but in a 10% increase in transition time. The reason for the smaller amount of off-target polymer is that much of the Grade B polymer initially in the bed is dumped out at the start of the transition, rather than remaining inside to be blended with

off-specification instantaneous polymer. In addition, the production rate falls to about 70% of its steady state level so that less polymer is produced when the instantaneous properties are far from the new target. The reason for the longer transition time is that the solid phase residence time in the reactor between periods 32 and 38 is larger than in Policy IV because the bed level is climbing.

The $C \rightarrow B$ transition requires 17.1 time periods, which is marginally less time than in Policy IV. However, the quantity of off-target material is reduced by over 40%. By shutting off the catalyst feed, the optimizer is able to almost stop the production of off-specification material while waiting for sufficient hydrogen to be vented from the reactor. During this transition, the optimal bed level policy in Figure 5.9 is somewhat unexpected. Instead of decreasing the bed level setpoint to its lower limit, the optimizer increases the bed level. This results in a very large solid phase residence time between periods 55 and 60 and in a very slow change in both ρ_c and MI_c. By keeping the bed level high and the production rate low, the optimizer is able to use a low butene concentration to reduce MI_i quickly, without producing a large deviation in the cumulative density. After several hours, this material is dumped from the reactor and new instantaneous polymer with properties nearer to the targets is used to refill the bed to the desired level. The $C \rightarrow B$ changeover policy in Figure 5.9 gives only a slight reduction in the objective function ($< 2\%$) compared with the more intuitive approach wherein the bed level is initially set to its lowest value. Therefore, the type of policy determined by the optimizer is very sensitive to the relative values of a_1, a_2, a_3 and a_4 in the objective function. A smaller penalty on ρ_c or a larger penalty on MI_c will result in an optimal initial bed level setpoint at the

lower rather than the upper bound. In either case, the reduction in production rate, while MI_i is moving toward the new target, is an effective means of reducing the quantity of off-specification polymer.

Manipulation of the catalyst feed and bed level for the $B \rightarrow A$ transition results in a significant reduction in both transition time and off-specification product. Since much of the old polymer in the reactor is dumped out early in the transition, less instantaneous polymer with properties at or beyond the new target values is required to bring the cumulative properties within the specification limits.

Figure 5.9 Transition Policy V

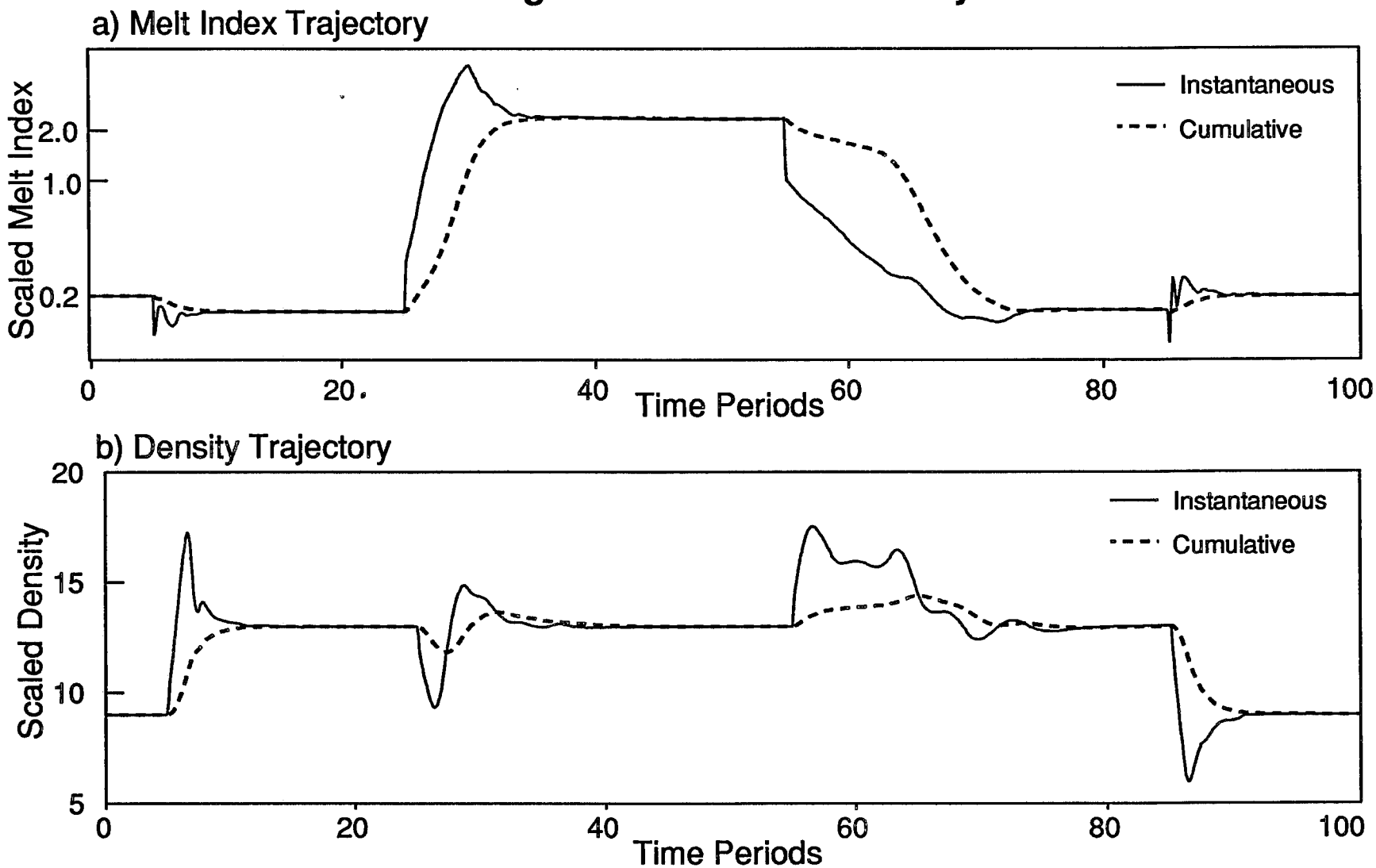

Figure 5.9 Transition Policy V

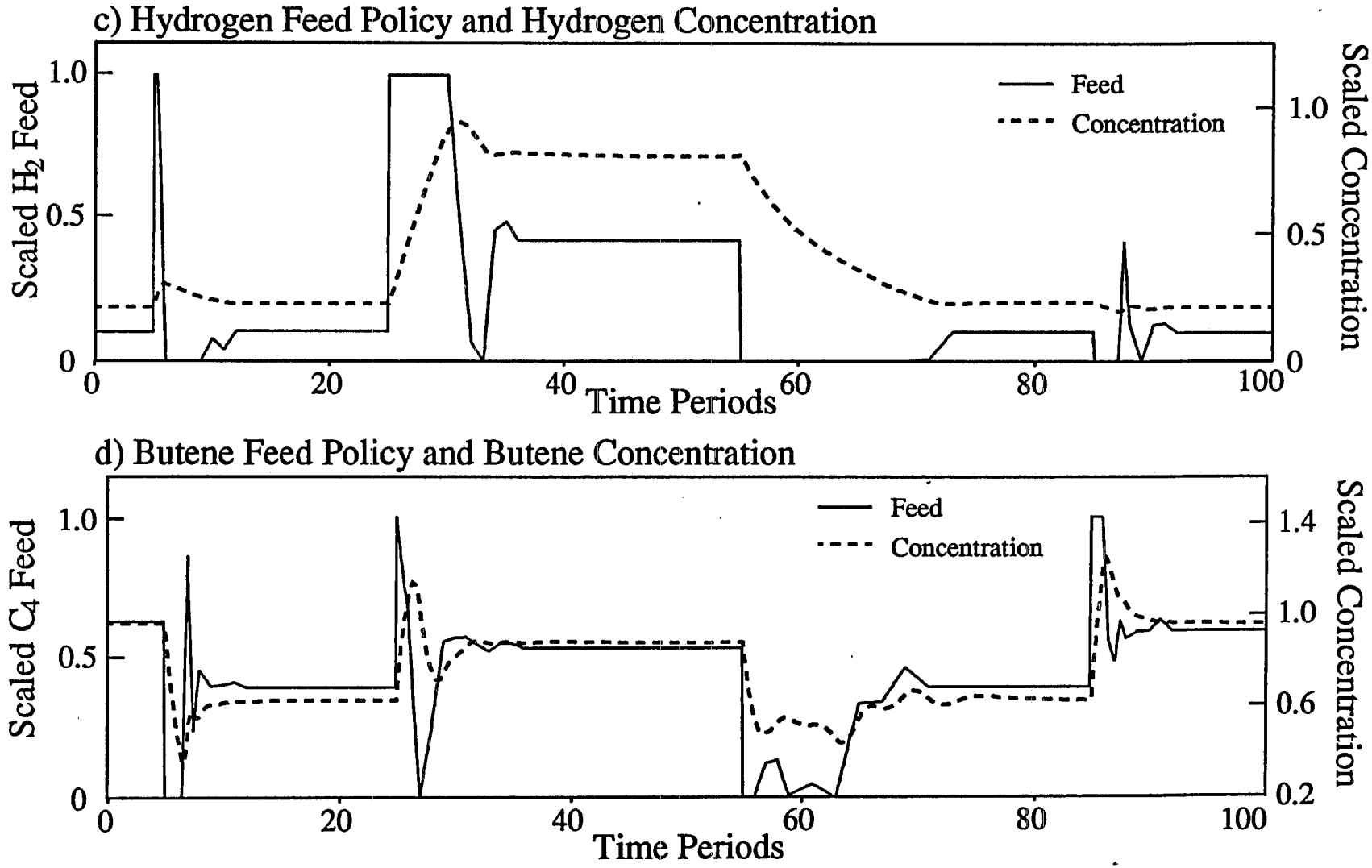

Figure 5.9 Transition Policy V

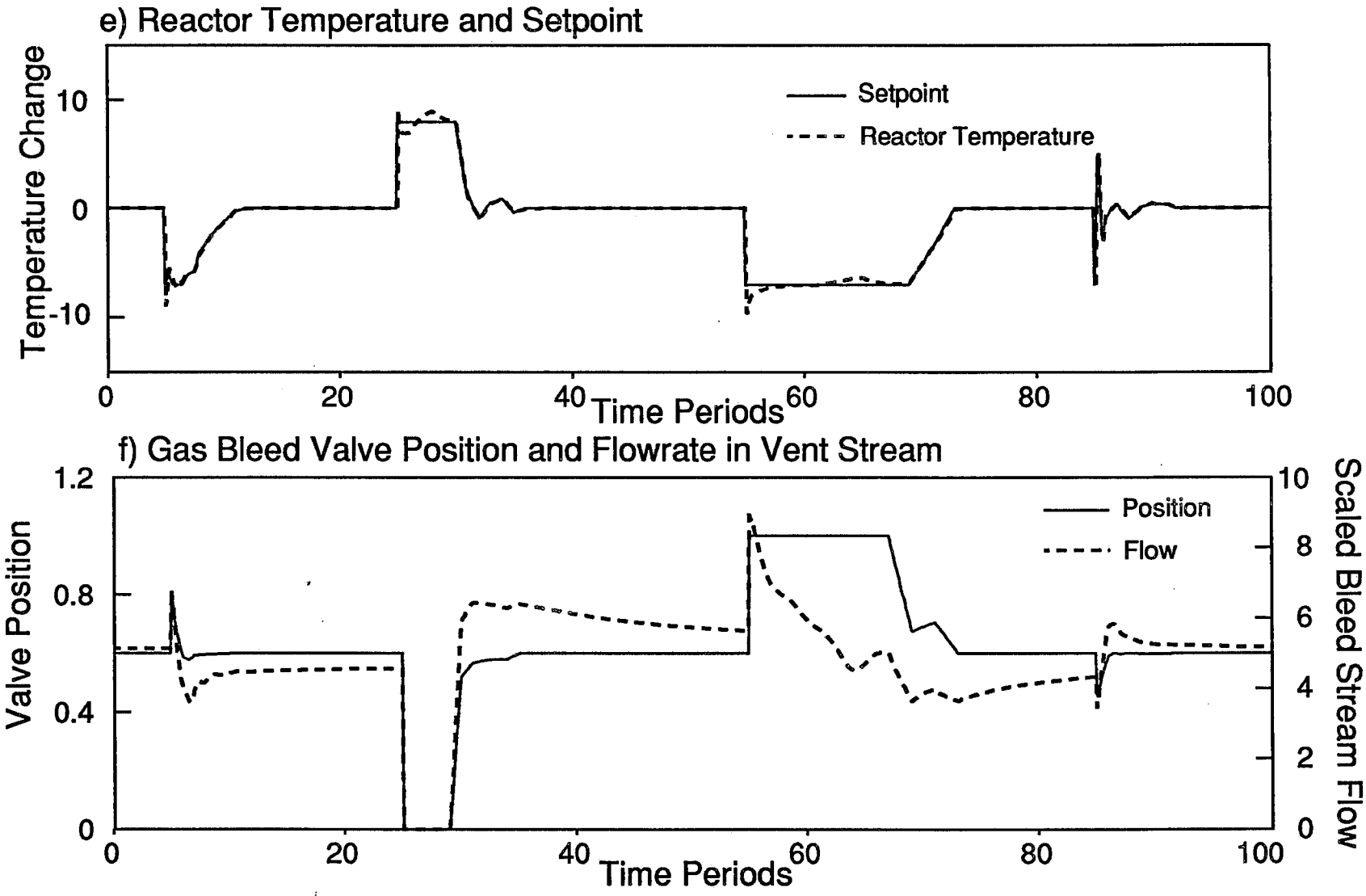

Figure 5.9 Transition Policy V

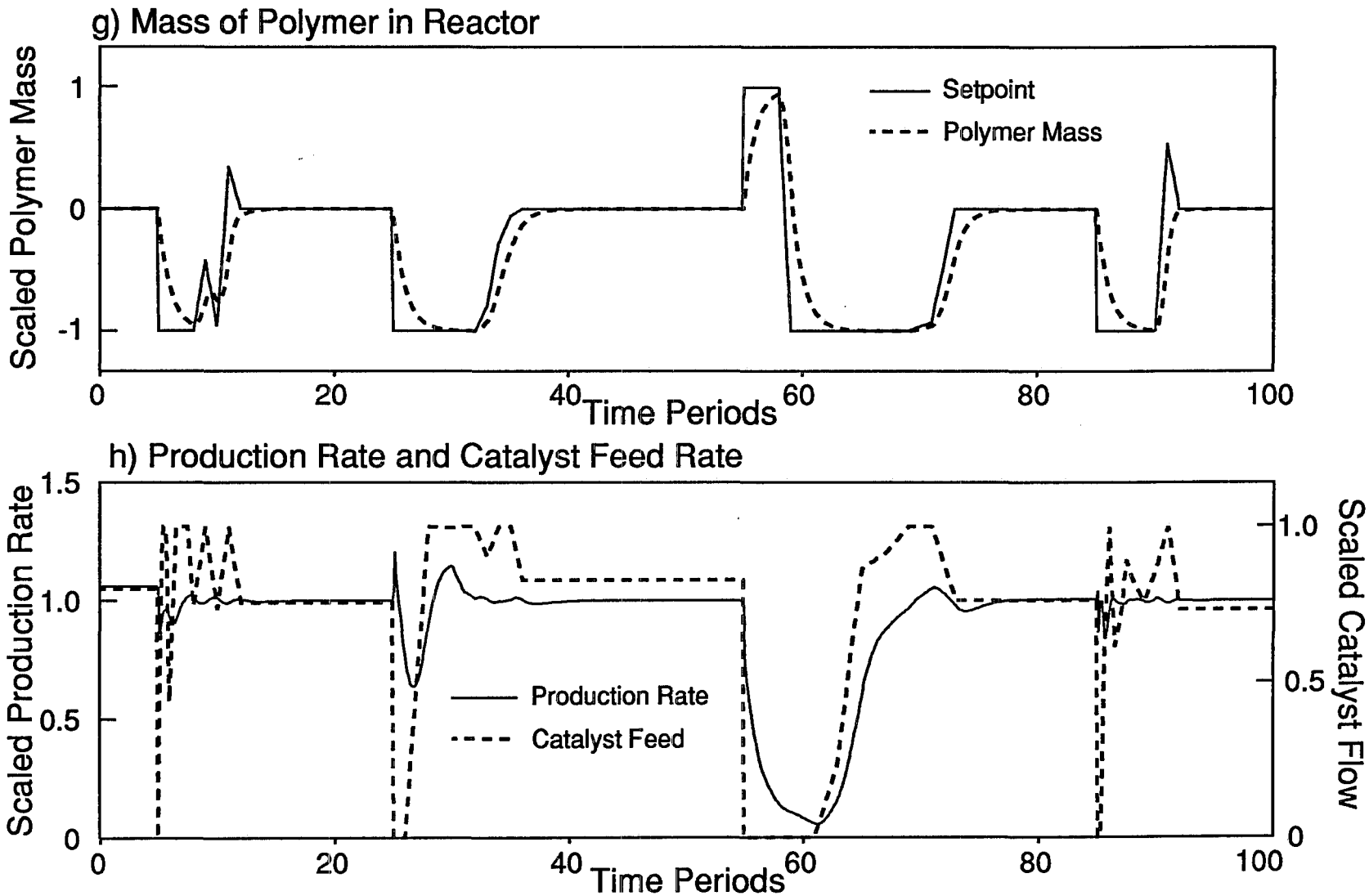

Figure 5.9 Transition Policy V

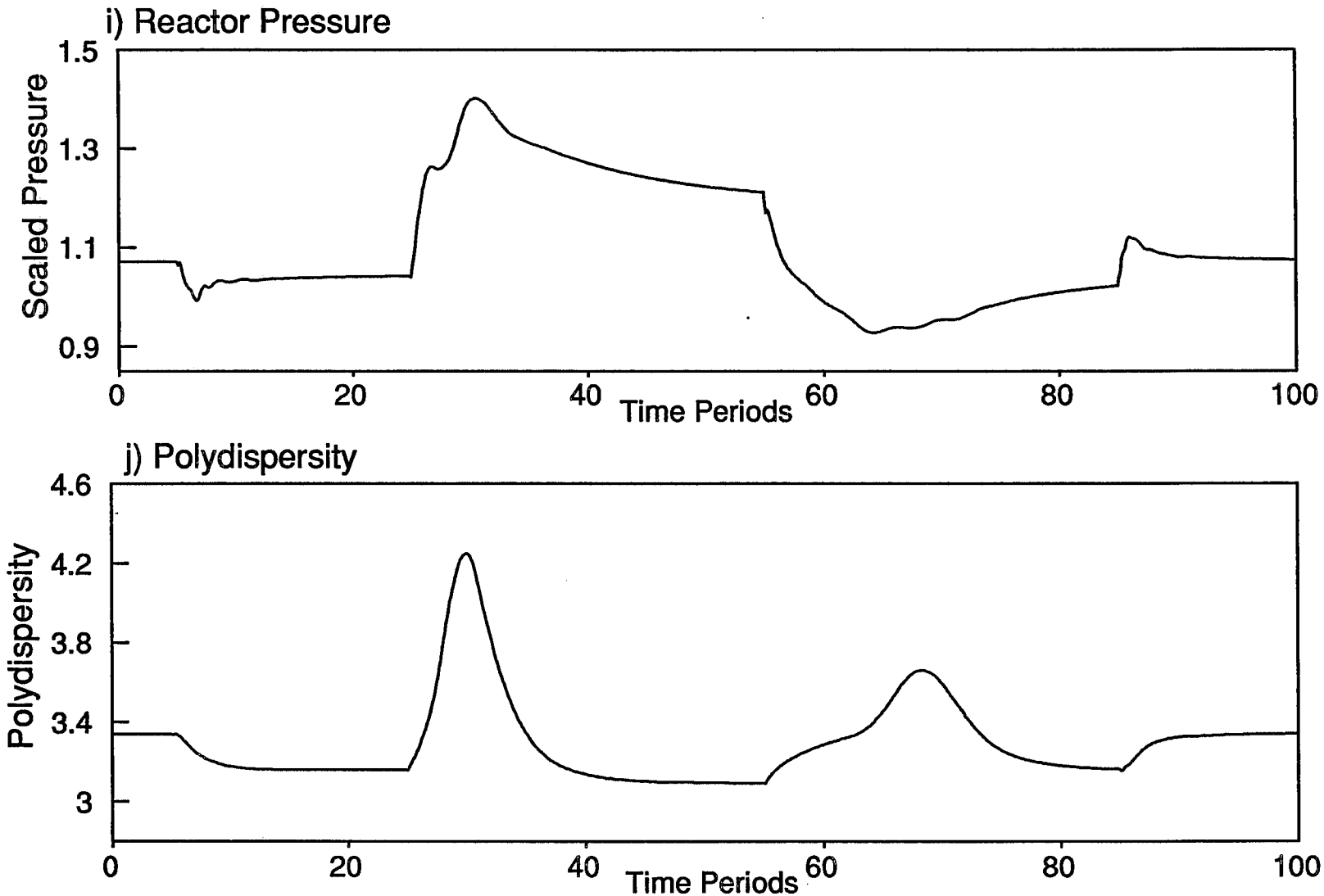

5.5 IMPLEMENTATION OF OPTIMAL POLICIES WITHOUT FEEDBACK

When implementing an optimal grade transition policy on-line, it is essential to account for mismatch between the predictions of the model used in the optimization study and the true behaviour of the plant. Otherwise, steady state offset can occur between the desired *MI* and ρ, and the actual product properties achieved. Even if the model used to determine the optimal transition is an exact description of plant behaviour at the time when the optimal policies are determined, small disturbances in catalyst properties and in impurity levels in the reactor can lead to mismatch during future changeovers.

The potential effects of model mismatch are illustrated in Figure 5.10, which shows the simulated open-loop implementation of optimal policy IV for the $C \rightarrow B$ transition. At the beginning of the transition there is no mismatch, however, at time period 67, a new batch of catalyst is introduced into the catalyst feed stream. This catalyst batch has the same distribution of catalyst sites as the previous batch, but has 10 % fewer active sites per unit mass of catalyst. As a result, the production rate, shown in Figure 5.10 d), begins to fall at period 67. It remains lower than the production rate shown in Figure 5.6 which was achieved with the nominal catalyst. The reduction in catalyst sites in the reactor leads to a lower butene consumption rate, and to an increase in the butene concentration in the reactor, compared to the nominal transition. The higher than optimal butene concentration results in a final scaled *MI* and ρ of 0.1716 and 12.455, respectively. Therefore, implementation of the optimal nominal policy without accounting for the catalyst site concentration mismatch results, not only in a suboptimal grade transition trajectory, but also in the production of off-specification polymer during the steady state period following the transition. Feedback control actions during the grade changeover

could prevent deviations from the nominal optimal product property trajectory, and, thereby, prevent the production of off-specification polyethylene. Appropriate feedback control strategies for on-line implementation of the optimal policies developed in this chapter are presented in Chapter 6.

Figure 5.10 CB Transition Policy IV with Low Catalyst Site Concentration

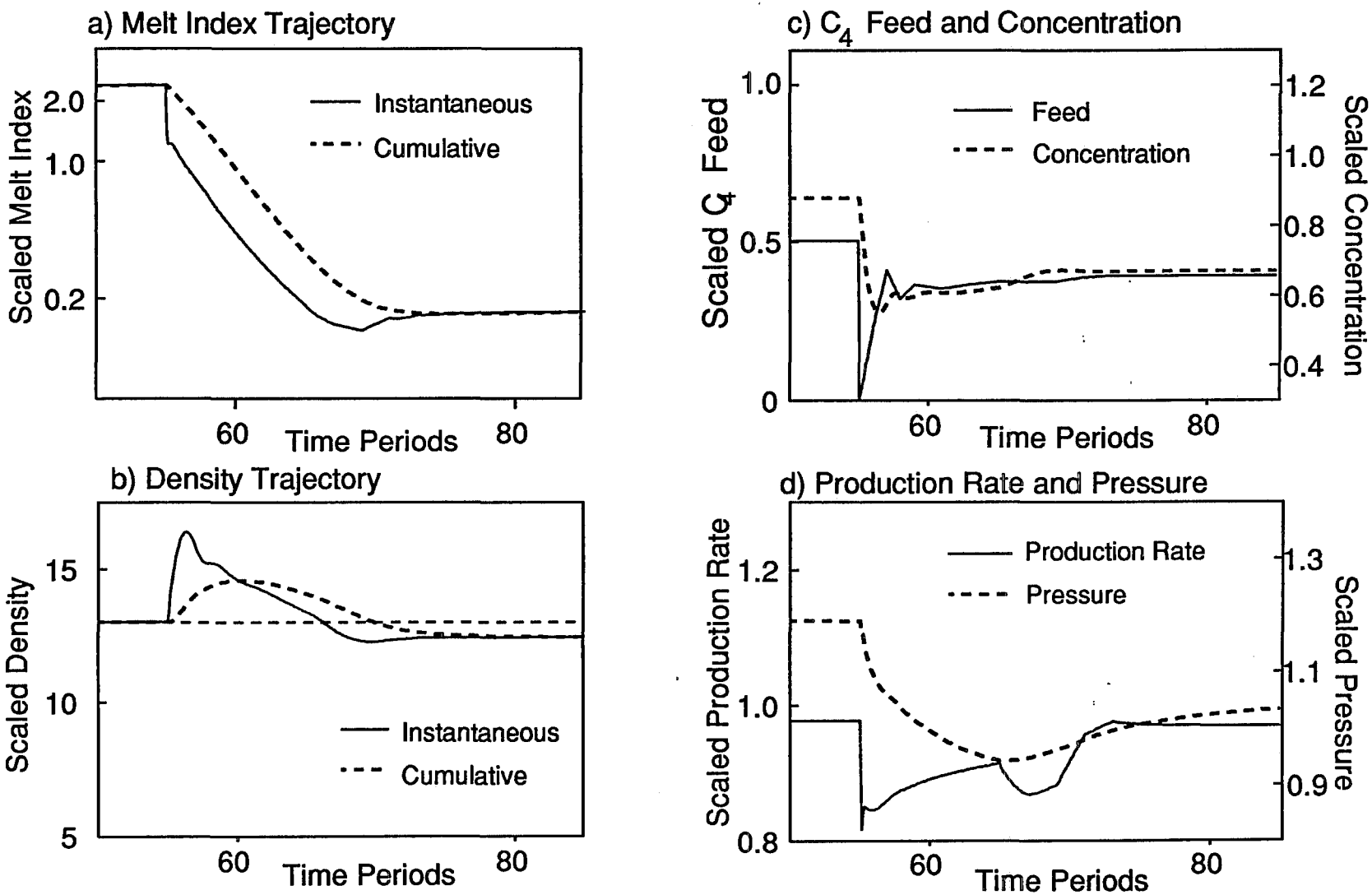

5.6 CONCLUSIONS

A set of optimal grade transition trajectories has been determined for a series of grade changes between three commercially relevant polyethylene grades. It was concluded that:

1. An embedded model approach to dynamic optimization, using commercially available optimization software, provides a simple and effective method for solving dynamic optimization problems.
2. Use of an embedded model approach requires parameterization of the manipulated variable trajectories. If the parameterization chosen does not allow enough variation in the manipulated variable policy throughout the time interval when the transition occurs, then the solution to the parameterized problem may be very different from the solution to the true unparameterized optimization problem.
3. Quadratic penalty terms can be included in the objective function to prevent large undesirable overshoots in instantaneous *MI* and ρ, and to ensure that the reactor temperature, bed level, bleed rate and production rate settle at economically desirable levels.
4. Reactor temperature and gas vent rate are important manipulated variables for transitions which involve large changes in the *MI* target. Less benefit is realized during transitions dominated by a density change.
5. Large transitions in *MI* are hampered by the slow hydrogen dynamics in the gas phase. As a result, an 11% increase in the maximum allowable hydrogen feed rate leads to a significant reduction in the transition time required for a transition to lower melt index.
6. When the instantaneous polymer being produced is far from the target, decreasing the catalyst feed rate and the bed level in the reactor can be used to reduce the production rate of off-specification material during the initial stages of a grade transition.

7. The type of optimal manipulated variable profile determined can be very sensitive to small changes in the structure of the objective function and to the relative sizes of the weighting parameters, especially when many variables are manipulated to achieve the optimal trajectory.

8. The optimization problems solved in this study minimize neither the transition time, nor the quantity of off-specification material produced. To solve either of these related problems, a new objective function must be adopted which includes information on the sizes of the grade specification limits for both the previous grade and the target grade.

9. Implementation of nominal optimal manipulated variable policies, without accounting for disturbances or model mismatch, can lead to product property trajectories which differ significantly from the associated nominal optimal property trajectories. Feedback control during grade changeovers is required to ensure than large quantities of off-specification material are not produced.

5.7 NOTATION

a_i	Cost coefficient for deviation of property i from target
B_{wdes}	Desired final mass of polymer in the fluidized bed
B_{wfsp}	Final bed weight setpoint
$\underline{c}$	Vector of algebraic inequality constraints
C	Cost per unit mass of polymer due to deviations from property targets
C_4	Butene
F	Value of objective function
$\underline{f}$	Vector of functions describing state time derivatives
H_2	Hydrogen
J	Objective function
MI, ρ	Melt index and density
MI_c, ρ_c	Cumulative melt index and density
MI_i, ρ_i	Instantaneous melt index and density
MI_{sp}, ρ_{sp}	Melt index and density setpoints
P_R	Production Rate
P_{Rdes}	Desired Production Rate
t	Time
t_0	Time at which the grade transition begins

t_f	Final time for integrating the performance index
T_{des}	Desired steady state temperature after the transition
T_{fsp}	Final temperature setpoint
$\underline{u}$	Trajectories of manipulated variables
$\underline{u}_*, \underline{u}^*$	Lower and upper bounds on manipulated variables
v_p	Valve position
v_{pdes}	Desired valve position
w_i	Objective function weighting factors
$\underline{x}$	State variables in the dynamic model
$\dot{\underline{x}}$	Time derivatives of state variables
$\underline{x}_*, \underline{x}^*$	Lower and upper bounds on state variables

NONLINEAR CONTROLLER DESIGN

6 ON-LINE PRODUCT PROPERTY CONTROL

6.1 INTRODUCTION

In this chapter an on-line product property control algorithm is proposed for polyethylene production in a gas phase reactor. Important results from previous chapters are used in the controller design: the instantaneous melt index and density models developed in Chapter 4 are used to model the effects of reactor operating conditions on product properties, and the optimal grade transition policies determined in Chapter 5 provide the target trajectories tracked by the feedback controller. The actual operation and testing of the control scheme also requires results developed earlier in this thesis: the controller is tested using the reactor simulation developed in Chapters 2 and 3, and on-line estimates of *MI* and ρ from the property inference scheme described in Chapter 4 are used in lieu of on-line measurements.

A block diagram showing the flow of information among the property inference scheme, the reactor, and the controller is shown in Figure 6.1. Every few hours, a polymer sample is collected from the reactor and analyzed in the quality control laboratory. After a measurement delay, typically ranging from 20 minutes to 1 hour, the measured values of cumulative *MI* and ρ are provided to the product property inference scheme. The inference scheme uses these measured values, along with on-line measurements of temperature, gas composition, bed level, and production rate to update parameters in the on-line product property models. The parameter values and the estimates of melt index

and density are provided to the on-line property controller. Between laboratory measurements, the property inference scheme predicts $\hat{MI}$ and $\hat{\rho}$ using parameter estimates from the previous update step. The product property control algorithm uses the inferred values of MI and ρ, the setpoints, model parameters and on-line measurements to calculate control actions. The control actions effect changes in reactor operation, bringing the product properties to their desired settings. This chapter is concerned both with the design of the product property control algorithm box in Figure 6.1, and with implementing and testing the entire control scheme.

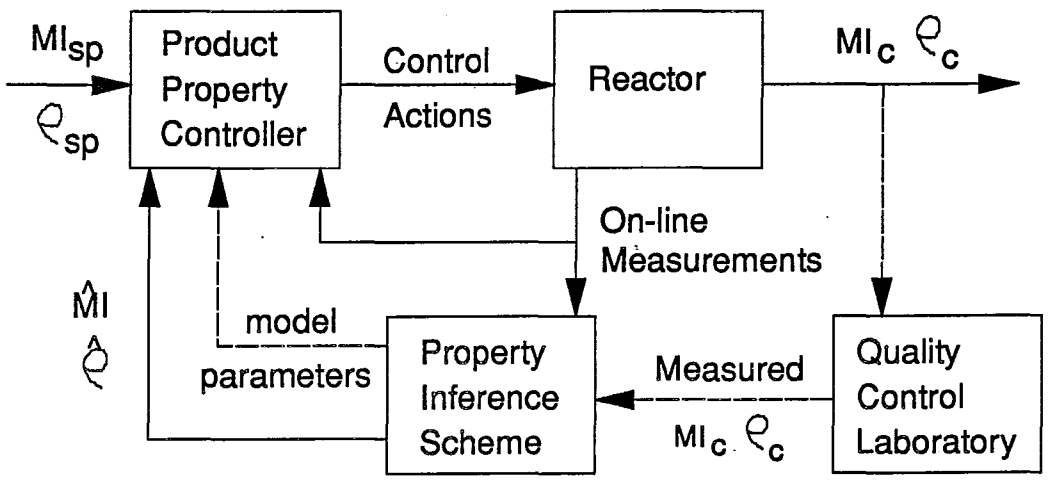

Figure 6.1 Product Property Controller Information Flow Diagram

In this chapter, the objectives of the control scheme are outlined, followed by a brief discussion of nonlinear control techniques. Next, a model-based control strategy and a means of updating the controller model are proposed. The control algorithm is tested for both grade transitions and disturbance rejection, and the controller performance

is compared with that of a linear internal model control (IMC) design. An optimal means of handling manipulated variable saturation is presented, and an alternative control structure which could be used during input saturation is discussed. Finally, simulations are shown which illustrate how the entire controller and property inference scheme of Figure 6.1 might behave on an industrial reactor.

6.2 CONTROLLER REQUIREMENTS

The on-line property controller developed in this chapter must satisfy certain basic requirements. It must be capable of both implementing grade transition policies and of providing effective regulatory control over the full range of polyethylene grades produced in the reactor. In addition, the computing power required to implement the control algorithm must be reasonable. Since the reactor behaviour is very nonlinear, no single linear controller would be capable of providing effective control performance over the entire range of grades. As such, a nonlinear model-based control algorithm is required.

6.3 NONLINEAR MODEL-BASED CONTROL TECHNIQUES

Current nonlinear model-based control techniques can be divided into two categories: nonlinear programming approaches and model inverse-based controllers. These techniques have been reviewed extensively by Garcia et al. (1989), Bequette (1990a,1990b) and McLellan et al. (1990).

6.3.1 Model-Based Control Using Nonlinear Programming

Nonlinear programming (*NLP*) approaches to model-based control provide a direct extension of the linear model predictive control concepts used in Quadratic Dynamic Matrix Control (*QDMC*) (Garcia and Morshedi, 1986) to nonlinear control problems. *NLP* control techniques involve solving a constrained nonlinear dynamic

optimization problem on-line at each control interval. For example, using a suitably fast computer, the optimal grade transition trajectory problem discussed in Chapter 5 could be solved on-line at the start of each control interval to determine the best set of future control actions for implementation. Feedback to the control system would be provided by the on-line measurements and the estimates of cumulative *MI* and ρ from the property estimator. Examples of *NLP*-based control algorithms and their application have been presented by Li and Biegler (1988), Brengel and Seider (1989) and by Bequette (1991).

The main benefits of this approach are that the problem statement is relatively easy to write and understand, and that systems which exhibit inverse responses are readily handled. Non-square systems and bounds on manipulated variables can also be handled using this approach. Nevertheless, on-line dynamic optimization is frought with problems. The computational requirements can be inordinately large, and the time required to solve the optimization problem grows quickly as the number of controlled and manipulated variables increases. The reason for the large computational load is that a solution to the full *NLP* must be obtained at each control interval. Although the solution from the previous control calculation often provides a good starting point for the next optimization step, there is no guarantee that the optimizer will determine a suitable set of control actions within a reasonable amount of time. In the event that the solution fails to converge within the time allotted, some form of on-line diagnostics and a fallback control action must be included in the control scheme. While *NLP*-based controllers may be practical for systems with slow dynamics and and a long sampling time, the speed of current computing technology prohibits widespread application in the chemical industry.

When using an *NLP* controller, the assumption that the time to compute the control action is negligible may not be valid; in fact, the computing time can add significant deadtime to the system.

6.3.2 Nonlinear Feedback Controllers Based on Model Inversion

In order to determine manipulated variable profiles which will force the state or output variables to follow a desired trajectory, nonlinear control laws based on model inverses require inversion of the process model. The tools for performing this model inversion and for analyzing the stability and controllability of nonlinear dynamic systems are provided by a field of nonlinear mathematics called differential geometry. Nonlinear geometrical techniques and their applicability to chemical process control have been reviewed by Kantor (1987) and by Kravaris and Kantor (1990a, 1990b).

6.3.2.1 Important Concepts in Nonlinear Model Inverse-Based Control

A useful concept for designing, comparing and analysing nonlinear control laws is that of the tracking error trajectory (McLellan et al., 1991). The closed loop error trajectory for any process can be defined as:

$$e(t) = \underline{Y}_{sp}(t) - \underline{Y}(t) \tag{6.1}$$

where $\underline{Y}(t)$ is the vector of output variable trajectories and $\underline{Y}_{sp}(t)$ is the set of desired trajectories. Many control laws, both linear and nonlinear alike, can be derived by specifying the type of closed loop error trajectory which the system will follow. For example, the design criterion for a Dahlin (1965) controller is

that the closed loop step response of the system to setpoint changes is first-order plus deadtime, with a closed loop time constant, τ. This specification can be written in terms of the error trajectory function:

$$\dot{e}(t) = -\frac{1}{\tau} e(t) \qquad \forall \quad t - t_0 > t_d \tag{6.2}$$

where t_d is the deadtime and t_0 is the time of the setpoint change. Similarly, the choice of tuning factors for the first order filters in the decoupled internal model control (*IMC*) designs of Garcia and Morari (1982), is equivalent to specifying the following error trajectory function in response to setpoint changes:

$$\underline{\dot{e}}(t) = -\underline{K}\,\underline{e}(t) \qquad \forall \quad t - t_0 > t_d \tag{6.3}$$

where the diagonal matrix $\underline{K}$ contains the reciprocals of the desired closed loop time constants for the decoupled error trajectories. This type of error trajectory specification has been used to extend linear *IMC* designs to accomodate nonlinear models (Economou et al., 1986). Freund (1973, 1975, 1982) and Kozub (1989) have used first-order error trajectory descriptions, without deadtime, to design nonlinear input/output linearizing controllers. The error trajectory specification used in generic model control (*GMC*) (Lee and Sullivan, 1988) contains an additional integral term and, thus produces a second-order closed loop error trajectory. The type of error trajectory which can be specified for a nonlinear model-inverse controller depends on the structure of the nonlinear model, and on whether forecasts of the model states are available to compensate for deadtime in the system.

Another important concept in the design of nonlinear controllers is the relative order of the process model. The relative order, or alternatively the

differential order, of a nonlinear dynamic system can be explained intuitively as the inherent integration between the process input and output (McLellan et al., 1990). For example, if one uses the hydrogen feed rate to control the instantaneous melt index in the polyethylene property control problem, then the relative order of the system is one. The hydrogen feed rate is integrated once in equation 3.5 to yield the hydrogen concentration which directly affects the instantaneous melt index. If, however, the hydrogen feed rate is used to control the cumulative melt index, then the corresponding relative order is two, because MI_i is integrated in equation 4.4 in order to determine MI_c. Generally, the smaller the relative order of the process, the simpler it is to design an appropriate nonlinear controller.

6.3.2.2 Benefits of Nonlinear Model Inverse-Based Control

The benefit of using a nonlinear inverse-based controller over the *NLP* approach is that, using model inverse techniques, an analytical expression can be derived for the manipulated variable policy. Computation of control actions from this analytical expression is fast, simple and the time required to perform the computation will be consistent from interval to interval. In special cases, explicit expressions for the control actions, $\underline{u}(t)$, can be written, making the control algorithm calculations trivial. The major disadvantage of the model-inverse approach is that nonsquare systems, systems exhibiting inverse responses, and constraints on state and manipulated variables are not easily handled. However, where these issues can be overcome, the nonlinear model inverse techniques are superior to *NLP*-based controllers due to their relative ease of implementation and on-line maintenance.

6.3.2.3 Application of Nonlinear Model Inverse Controllers to Chemical Engineering Problems

Some of the earliest nonlinear control laws were developed for robotics applications. Freund (1973, 1975, 1982) developed decoupling control laws for systems of arbitrary relative order in which the manipulated variables entered the state equations linearly, as shown below:

$$\dot{\underline{x}}(t) = \underline{\underline{A}}(\underline{x}, t) + \underline{\underline{B}}(\underline{x}, t)\underline{u}(t) \tag{6.4}$$

In the chemical engineering literature, several approaches to nonlinear model inverse control design have been developed. Like the earlier work of Freund, the global linearizing control (*GLC*) technique of Kravaris and Chung (1987) can control systems of high relative order in which the control action enters linearly. Internal decoupling (Balchen et al., 1988), generic model control (Lee and Sullivan, 1988) and reference system synthesis (Bartusiak et al., 1989) can all be used to control systems wherein the control actions enter nonlinearly, but they are limited to systems of relative order one. Recently, Henson and Seborg (1990) have proposed control techniques for higher relative order problems wherein the manipulated variables enter nonlinearly. Other advances include the addition of nonlinear feedforward control to account for measured disturbances (Daoutidis et al., 1990).

Examples of nonlinear chemical process control problems which have been solved using inverse based controllers include: temperature control in a CSTR (Balchen et al., 1988), pH control (Jayadeve at al., 1990), semibatch emulsion polymerization of styrene butadiene rubber (Kozub, 1989), continuous methyl methacrylate solution polymerization (Adebekun and Schork, 1989) and

semibatch compolymerization of styrene and methylmethacrylate (Kravaris and Soroush, 1990). Nonlinear inverse based controllers are especially useful for square, invertible, nonlinear problems with fast dynamics wherein accounting for the nonlinearity is more important than the optimal handling of constraints. For very slow nonlinear systems in which performance is dominated by the ability to optimally account for constraints, an *NLP*-based approach is preferable. Regardless of which technique is used, the appropriate choice of a dynamic model and a means of accounting for process/model mismatch are important concerns.

6.3.3 Accounting for Process/Model Mismatch

The development of a mathematical representation of the process is the most important part of a nonlinear model-based control scheme. To provide for good control performance, the model must adequately predict the effects of the manipulated variables on the controlled variables. Yet, the model structure should be simple, because a reduced process model can lead to improved controller robustness (Gilles, 1987), and a simple model is easier to implement and solve on-line.

An issue which must be faced in model-based controller design is the effect of model mismatch on controller performance. If no action is taken to correct the process model, some nonlinear control designs can lead to steady state offset. Even if there is integral action in the control law, so that offset at steady state is not an issue, mismatch in the dynamic behaviour of the process model can lead to degraded control performance. To solve model mismatch problems, extended Kalman filters (*EKF*'s) and other state variable observers have been implemented as part of the control scheme (Gilles, 1987; Parrish and Brosilow, 1988; Kozub, 1989; Adebekun and Schork, 1989b; Lee et al. 1989; Bequette, 1991).

Many benefits are associated with using a state observer in conjunction with the model-based control scheme. An *EKF* provides filtered estimates of the state variables, thereby reducing the effect of measurement noise on the control scheme. If some of the controlled variables, or the states required to calculate them, are not measured, then the *EKF* can often observe these states from the available measurements. If some of the measured values are delayed, as is often the case for chromatographic measurements of gas composition, the *EKF* can be used to forecast the states required by the control algorithm. Perhaps the main benefit of an *EKF* for model-based control is that incorporation of meaningful disturbance or model mismatch states allows the model to accurately track the process. Many of the physical parameters of a chemical process, such as kinetic rate parameters, catalyst activities and heat transfer coefficients, can change as a function of time or operating conditions. Use of an *EKF* permits on-line estimation and updating of these time varying parameters.

Since there are frequently more sources of disturbances than there are process measurements, the estimator design problem is often one of choosing a consistent set of parameters for updating, in order to yield a unique estimation problem (Parrish and Brosilow, 1988). If too many parameters are chosen for on-line updating, the system will be unobservable. If too few are updated, then sustained offset between model predictions and plant measurements can result. Issues of state observability and estimator constistency are discussed in more detail by Kozub (1989). The *EKF* algorithm was presented and discussed in Chapter 4.

6.4 PROPOSED CONTROL SCHEME

A convenient choice of a control interval for the product property controller is h, the sampling interval for the gas chromatograph system. It is proposed that an *EKF* be used to update the controller model each time a new set of concentration measurements becomes available, and that the control actions be calculated using a model forecast of the reactor conditions. In this way, the deadtime due to the composition measurement delay can be easily accounted for in the control scheme. h, which is typically between 5 and 10 minutes for industrial installations, is too short of a time to ensure that an on-line *NLP* will converge. Hence, it is proposed that a model inverse-based control design be evaluated.

The two manipulated variables which have the best range for achieving different steady state levels of *MI* and ρ are the hydrogen and butene feed rates. At steady state, the other manipulated variables, reactor temperature, vent rate, catalyst feed rate and bed level, should be held near specific levels, in the interests of favourable process economics and reactor operability. However, it was shown in Chapter 5, that short-term manipulation of these four additional manipulated variables can lead to a great reduction in both transition time and the quantity of off-specification material produced. Therefore, the following feedforward/feedback control scheme is proposed. During grade transitions, the optimal open-loop policies for temperature setpoint, bleed valve position, catalyst feed rate and bed level will be implemented. To account for disturbances and for mismatch between the actual plant behaviour and that of the model used in the off-line optimization studies, the hydrogen and butene feed rates will be used for feedback control. The objective of the feedback controller will be to force the instantaneous melt index and density onto the nominal trajectory determined from the off-line transition studies. For regulation about a desired steady state, only the feedback portion of the controller

will be used. A potential drawback associated with the choice of the hydrogen and butene feed as the only feedback variables is that the response of the hydrogen concentration and, hence, of MI_i to hydrogen feed flow changes can be very sluggish, especially when the hydrogen feed rate is saturated at its upper or lower bound. Therefore, an alternative, variable-structure, feedback control law which also incorporates the bleed flow rate as a manipulated variable is discussed in section 6.9.

The reason for choosing instantaneous MI and ρ as controlled variables, rather than the cumulative properties, is to improve the consistency of the polymer produced in the reactor. Consider the regulation problem shown in Figure 6.2, wherein the reactor is currently operating away from the setpoint at the point marked *. A product property regulator with the cumulative density as the controlled variable could bring ρ_c back to the target quickly by producing some polymer with an instantaneous density on the other side of the target, leading to the trajectories for ρ_i and ρ_c shown in Figure 6.2. In the petroleum industry, such a response might be desirable for the composition of a liquid stream which is fed to a downstream tank, because alternating deviations from the setpoint are eliminated by mixing the off-specification product. However, for polymer production, this type of control strategy is not desirable because it leads to increased variability of the final product. Off-specification product on either side of a target cannot be blended together to get end-use and processing properties which are identical to those of polymer made at the target conditions. A better philosophy for getting back to the target is shown in Figure 6.3. With the instantaneous property as the controlled variable, the controller responds to the deviation by driving the ρ_i back to its setpoint. No additional off-target material is produced to compensate for off-target polymer produced in the past.

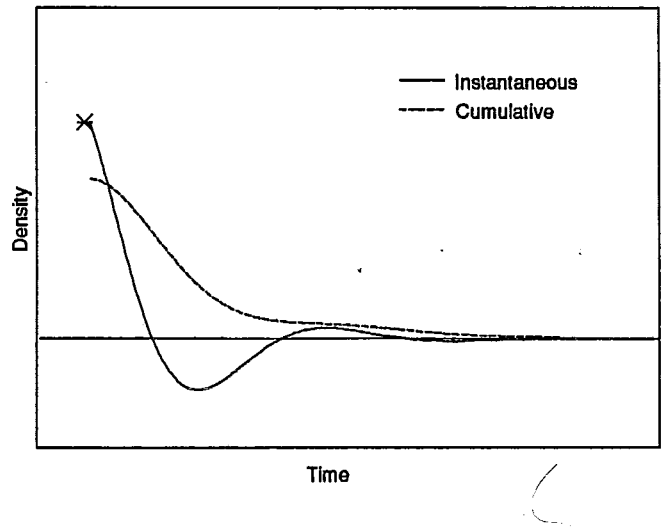

Figure 6.2 Strategy for Cumulative Product Property Regulation

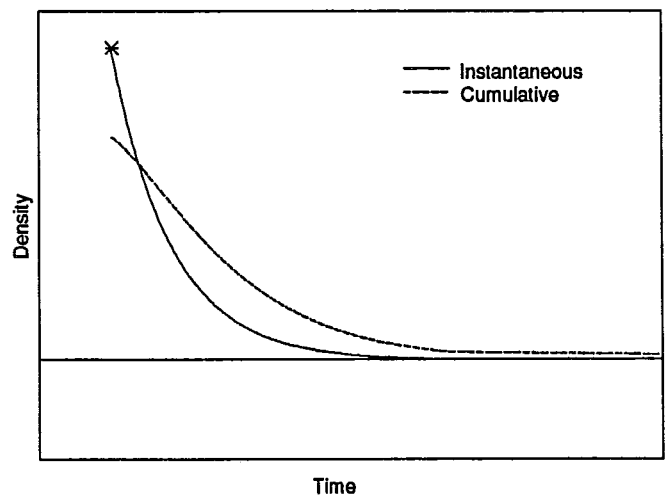

Figure 6.3 Strategy for Instantaneous Product Property Regulation

During grade changeovers, deviations from the precomputed optimal trajectory can be handled in the same manner. The nonlinear inverse-based controller can compute the required hydrogen and butene feed policies to force the instantaneous properties back onto the desired non-stationary path, as shown in Figure 6.4. In this way, the same nonlinear feedback controller can be used for both grade transition control and for regulation over the entire range of grades produced in the reactor. One disadvantage of this approach is that, due to disturbances, the precomputed trajectory will not always be the optimal changeover policy. Driving the system back onto the nominal path may not lead to the best grade transition trajectory possible. Use of an *NLP*-based controller would allow the optimal policy to be updated on-line as disturbances are detected. It is believed, however, that the simplicity and reliability of the proposed approach will more than compensate for the resulting suboptimality.

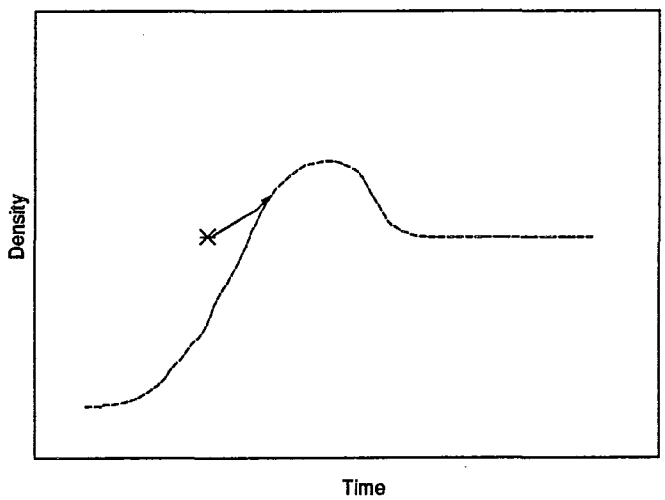

Figure 6.4 Strategy for Return to Optimal Trajectory

6.5 MODEL STRUCTURE

The model used in the nonlinear controller design must be capable of predicting the effects of hydrogen and butene feed rates on instantaneous *MI* and ρ. The model should also account for the effects of reactor temperature, vent flow rate, catalyst feed rate, and bed level on product properties because these variables change quickly during grade transitions. Additional disturbances which must be accounted for in the model, or in the updating process, include changes in impurity levels and in the concentration and distribution of the catalyst sites in the catalyst feed.

The proposed model consists of dynamic mass balances on hydrogen, butene, catalyst sites and polymer:

$$V_g \frac{d[H_2]}{dt} = \frac{F_H}{mw(H)} - kh\, Y[H_2] - \frac{[H_2]b_T}{[C_T]} - gl[H_2] \tag{6.5}$$

$$(V_g + V_s)\frac{d[M_2]}{dt} = \frac{F_{M2}}{mw(M_2)} - kp2\, Y[M_2] - \frac{[M_2]b_T}{[C_T]} - S(M_2)[M_2]O_p \tag{6.6}$$

$$\frac{dY}{dt} = F_{cat}a_{cat} - \frac{Y\,O_p}{B_w} - kd\, Y \tag{6.7}$$

$$\frac{d\,B_w}{dt} = Y\{kp1\,[M_1]mw(M_1) + kp2\,[M_2]mw(M_2)\} - O_p \tag{6.8}$$

V_g is the volume of gas in the reactor, calculated from:

$$V_g = V_T - \frac{B_w}{\rho_c} \tag{6.9}$$

where V_T is the total volume of the reactor, and B_w is the mass of the polymer bed. F_H, F_{M2} and F_{cat} are the hydrogen, butene and catalyst feed rates, respectively. $kh, kp1$ and $kp2$ are the respective pseudo rate constants for the consumption of hydrogen, ethylene and

butene by reaction. Y is the total number of moles of active catalyst sites in the reactor. b_T is the total gas bleed rate in the vent stream, and $[C_T]$ is the total gas phase concentration in mol/L, calculated from the reactor temperature and pressure using the ideal gas law:

$$[C_T] = \frac{P_T}{RT} \tag{6.10}$$

gl in equation 6.5 is a hydrogen gas loss coefficient which accounts for mismatch in the hydrogen mass balance. V_s in equation 6.6 is the equivalent gas volume of butene dissolved in the polymer bed, which is calculated using Henry's Law:

$$V_s = \frac{\alpha_v k_H^* V_p P_T}{[C_T]} \tag{6.11}$$

α_v, k_H^*, and V_p are defined in Chapter 3. $S(M_2)$ is a solubility coefficient for butene sorption in the polymer, also determined using Henry's Law:

$$S(M_2) = \frac{\alpha_v k_H^* P_T}{[C_T]\rho_c} \tag{6.12}$$

O_p is the outflow rate of polymer from the reactor, and a_{cat} in equation 6.7 is the number of moles of active sites per unit mass of catalyst in the catalyst feed stream. kd is a catalyst deactivation rate constant which includes both spontaneous deactivation and deactivation by impurities. From this model, the hydrogen and butene concentrations in the reactor can be determined, given the feed rates of hydrogen and butene, the reactor temperature and pressure, the catalyst feed rate, the bleed flow rate, the ethylene concentration, the polymer outflow rate, the hydrogen gas loss parameter, and the rate constants $kh, kp1, kp2$ and kd. In turn, the instantaneous melt index and density can be calculated from equations 4.65 and 4.35. The model in equations 6.5 to 6.8 was chosen

to predict hydrogen and butene concentrations because it is simple in structure, yet it describes how the manipulated variables and reactor operating conditions affect the gas compostion and hence the instantaneous product properties.

6.5.1 Parameters to Update On-line

Variables in model equations 6.5 to 6.8, for which direct measurements are available on-line, include: the reactor temperature and pressure, the concentration of ethylene, and the vent flow rate. An on-line estimate of ρ_c can be obtained from the on-line property estimator. Since filtered estimates of these quantities are not required in the control scheme, the raw measurements are used directly in the model predictions. Four other on-line measurements: the gas phase hydrogen and butene concentrations, the weight of polymer in the bed, and the production rate are used for updating parameters in the mass balance model. These four measurements allow the following set of four observable parameters to be updated on-line: $gl, kp2, kd$ and O_p. These parameters have been chosen for updating over other candidate parameters because they form a consistent set of parameters to eliminate mismatch between the model and the measurements, and their true values are expected to change with changing reactor operating conditions.

gl is updated to account for unmeasured hydrogen losses in the reactor and for mismatch in the other terms in the hydrogen mass balance. The unmeasured hydrogen loss is due to the interstitial gas which leaves the reactor during each product discharge. While most of this gas is recycled to the reactor, a small portion is not recovered. The main source of error accounted for in the hydrogen mass balance is error in the total vent flow measurement. The loss term was chosen for updating, instead of kh which was fixed in the mass balance model, because very little hydrogen

in the reactor is actually consumed by reaction. Most of the hydrogen either exits in the vent stream or in the product discharge system. That is why the hydrogen dynamics in the reactor are so much slower than those of butene. Once hydrogen has been fed to the reactor, it takes a long time to get out. It is essential that mismatch be removed from the hydrogen mass balance so that proper dynamic information is contained in the model inverse.

Since the majority of the butene in the reactor is consumed by reaction, mismatch in the vent term and loss of unrecovered interstitial butene are not particularly important. The best way to prevent mismatch in the butene mass balance is by updating a parameter in the consumption by reaction term. Comparison of equation 6.6 with the butene mass balance in equation 3.8 reveals that *kp2* is really a pseudo rate constant which depends on temperature, the ratio of active site types in the catalyst, and the relative concentrations of butene and ethylene in the reactor. Hence, *kp2* should be updated on-line, both because it affects the rate of butene consumption and because its true value is expected to change with reactor operating conditions.

To ensure that the catalyst mass balance closes, and to achieve consistent predictions of the polymer production rate, the rate parameter *kd* has been chosen for updating. On-line updating of *kd* can be used to account for several different phenomena: spontaneous catalyst deactivation, catalyst deactivation by impurities, and changes in the active site concentration or distribution in the catalyst feed. Y, in equations 6.5 to 6.8, is the sum of both types of active catalyst sites in the reactor. Since each site type has its own set of propagation rate constants, either a change in the distribution of site types, or in the concentration of sites in the feed affects the polymer production rate. There are too few measurements available to distinguish

these effects from a change in the catalyst deactivation rate, so only one parameter in the catalyst mass balance can be updated on-line. *kd* was chosen over a_{cat} because changes in catalyst feed conditions can easily be accounted for by a change in *kd*. However, if a_{cat} is chosen for updating, and the system experiences poisoning of a portion of the active sites during a period of low catalyst feed rates, then unrealistic changes in the feed conditions would be required to account for the resulting change in production rate.

The polymer outflow rate, O_p, was chosen for updating because the actual removal rate of polymer from the system is not well measured. Calculation of the removal rate from the product discharge frequency is difficult, because product removal is performed in discrete batches which can vary in size. Updating O_p allows the *EKF* to calculate a smoothed estimate of the outflow rate based on the bed weight measurement.

6.6 MODEL UPDATING USING AN EXTENDED KALMAN FILTER

A discrete extended Kalman filter was implemented using h, the sampling interval and measurement delay for the gas composition measurements, as the discretization interval. The model predictions, $\hat{\underline{x}}(t \mid t-1)$, used in the EKF are obtained by integrating the following nonlinear state-space model over the discretization interval:

$$\begin{bmatrix} \dot{\underline{x}}_m \\ \dot{\underline{x}}_p \end{bmatrix} = \begin{bmatrix} \underline{f}(\underline{x}_m, \underline{x}_p, \underline{u}) \\ \underline{0} \end{bmatrix} \tag{6.13}$$

where $\underline{x}_m^T = \{\, [H_2] \quad [M_2] \quad Y \quad B_w \,\}$ is the set of state variables modelled in equations 6.5 to 6.8, and $\underline{x}_p^T = \{\, kp2 \quad gl \quad kd \quad O_p \,\}$ is the set of parameters updated by the *EKF*.

At each interval, this model is linearized about the new prediction, and discretized to obtain $\underline{A}(t)$ in equations 4.53 to 4.55. Similarly, $\hat{\underline{y}}(t \mid t-1)$, the measurement predictions required in equation 4.52, are obtained by substituting $\hat{\underline{x}}(t \mid t-1)$ into the following measurement equation:

$$y = \begin{bmatrix} [H_2] \\ [M_2] \\ P_R \\ B_w \end{bmatrix} = \begin{bmatrix} [H_2] \\ [M_2] \\ Y(kp1\ [M_1]\, mw_1 + kp2\ [M_2]\, mw_2) \\ B_w \end{bmatrix} \tag{6.14}$$

$\underline{H}(t)$ in equations 4.53 and 4.55 is obtained by linearizing equation 6.14 above about the predicted states.

6.6.1 Results

The operation of the discrete extended Kalman filter was tested both for a catalyst feed quality disturbance, and for the open loop implementation of several grade transitions determined in Chapter 5. The results are shown in Figures 6.5 and 6.6, respectively. In these simulations, the full reactor model described in Chapters 2 and 3, was used to simulate the actual plant operation. Normally distributed random errors were added to the variables shown in Table 6.1 in order to simulate the effects of measurement errors which would occur in an industrial setting. The discrete extended Kalman filter was tuned using the following covariance matrices for the scaled measurement errors and modelling errors errors, respectively:

$$\underline{R}_v = diag[\,4.0E-10,\quad 1.0E-10,\quad 2.5E-7,\quad 1.8E-4\,] \tag{6.15}$$

$$\underline{R}_w = diag[\,4.0E-12,\ \ 2.5E-9,\ \ 1.0E-2,\ \ 1.11E-3,\ \ 0.01,\ \ 1.0E-4,\ \ 1.0E-12,\ \ 0.025\,] \qquad (6.16)$$

Table 6.1 Measurement Errors Used in *EKF* Simulations

Measured Variable	**Standard Deviation of Error in Scaled Measurement**
Hydrogen concentration	$2.0E-5$
Butene concentration	$1.0E-5$
Production rate	$5.0E-4$
Bed weight	0.01333
Total bleed flow	$1.0E-5$
Ethylene concentration	$1.0E-4$
Temperature	0.01
Pressure	$5.0E-4$

In Figure 6.5, the *EKF* is able to detect and compensate for a step change in the catalyst feed quality. At time period 5, a new batch of catalyst is fed to the reactor. This new catalyst has 70% fewer active sites per unit mass than the original catalyst has. After 30 time periods, feed of the original catalyst is resumed. As shown in Figures 6.5 a) and b), this disturbance, and resulting change in gas composition, lead to an increase in MI_i and to a decrease in ρ_i. The disturbance has little influence on the hydrogen concentration, but a major effect on the butene concentration, as

revealed in Figures 6.5 c) and d). The on-line model is able to predict the behaviour of each of these component concentrations. While no change in *gl* is required to ensure that the model tracks the process, a small change in *kp2* is used. In the short term, the *EKF* reduces *kp2* to account for the increasing butene concentration. After a few hours *kp2* reaches a new steady state level. The steady state difference in *kp2* between time periods 5 and 30 is the result of the change in the steady state ethylene to butene concentration ratio, which causes the butene pseudo propagation rate constant in the full reactor model to change.

As shown in Figure 6.5 g), the catalyst feed disturbance results in a 20% reduction in the polymer production rate. The *EKF* tracks this production rate change by increasing the catalyst deactivation rate constant in Figure 6.5 j). This change in *kd* alllows for a decrease in Y, the predicted number of active catalyst sites in the reactor. In the short run, the mass balance model predicts a slight drop in the quantity of polymer in the reactor. The *EKF* alleviates this mismatch by decreasing the polymer outflow rate in Figure 6.5 i).

This simulation shows that the *EKF* is capable of quickly updating the nonlinear mass balance model in response to a major catalyst disturbance. The system response to this same catalyst disturbance, with a product property controller on-line, is discussed in section 6.7.4.

Figure 6.5 Kalman Filter Response to Catalyst Quality Step Change: Grade A

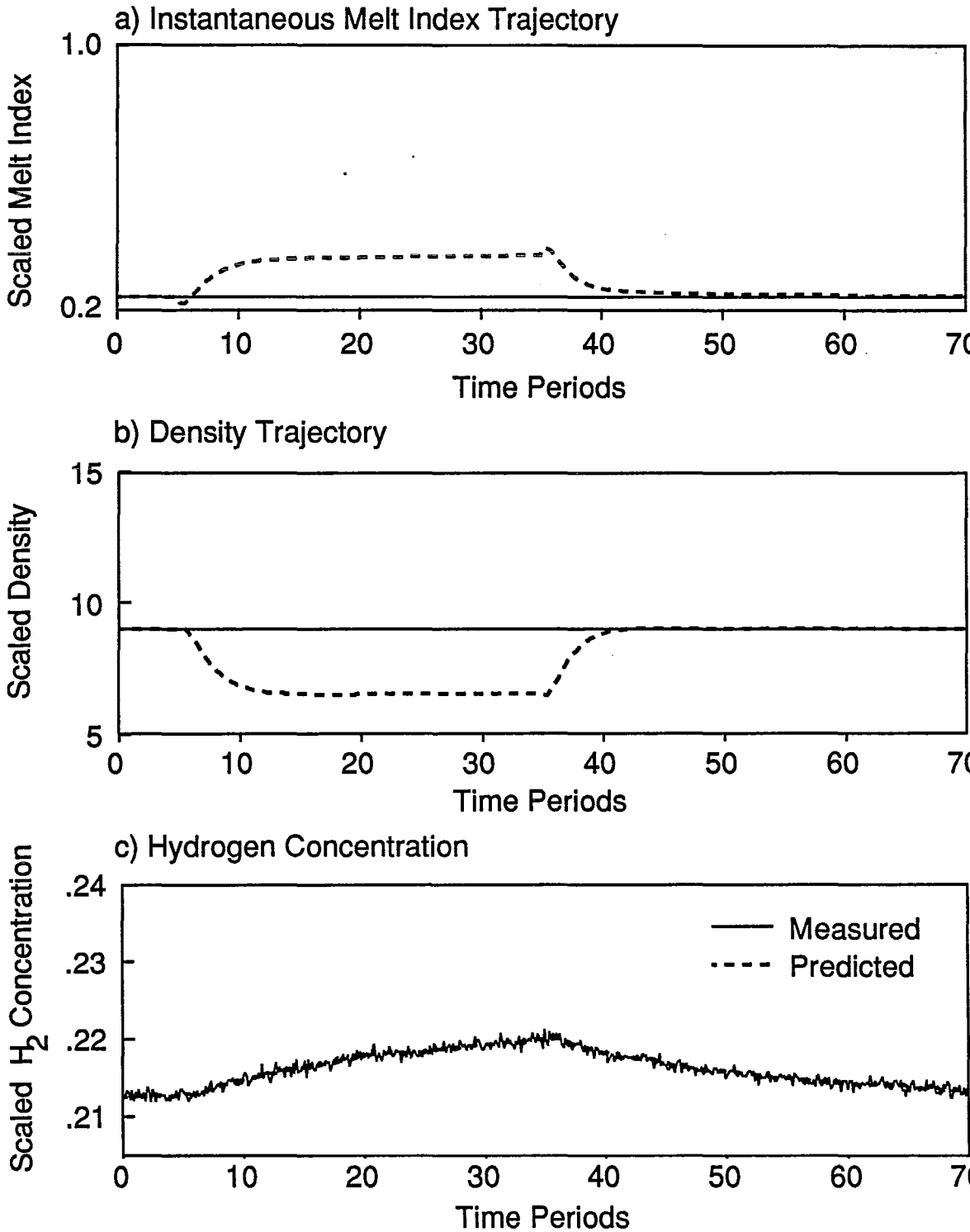

Figure 6.5 Kalman Filter Response to Catalyst Quality Step Change: Grade A

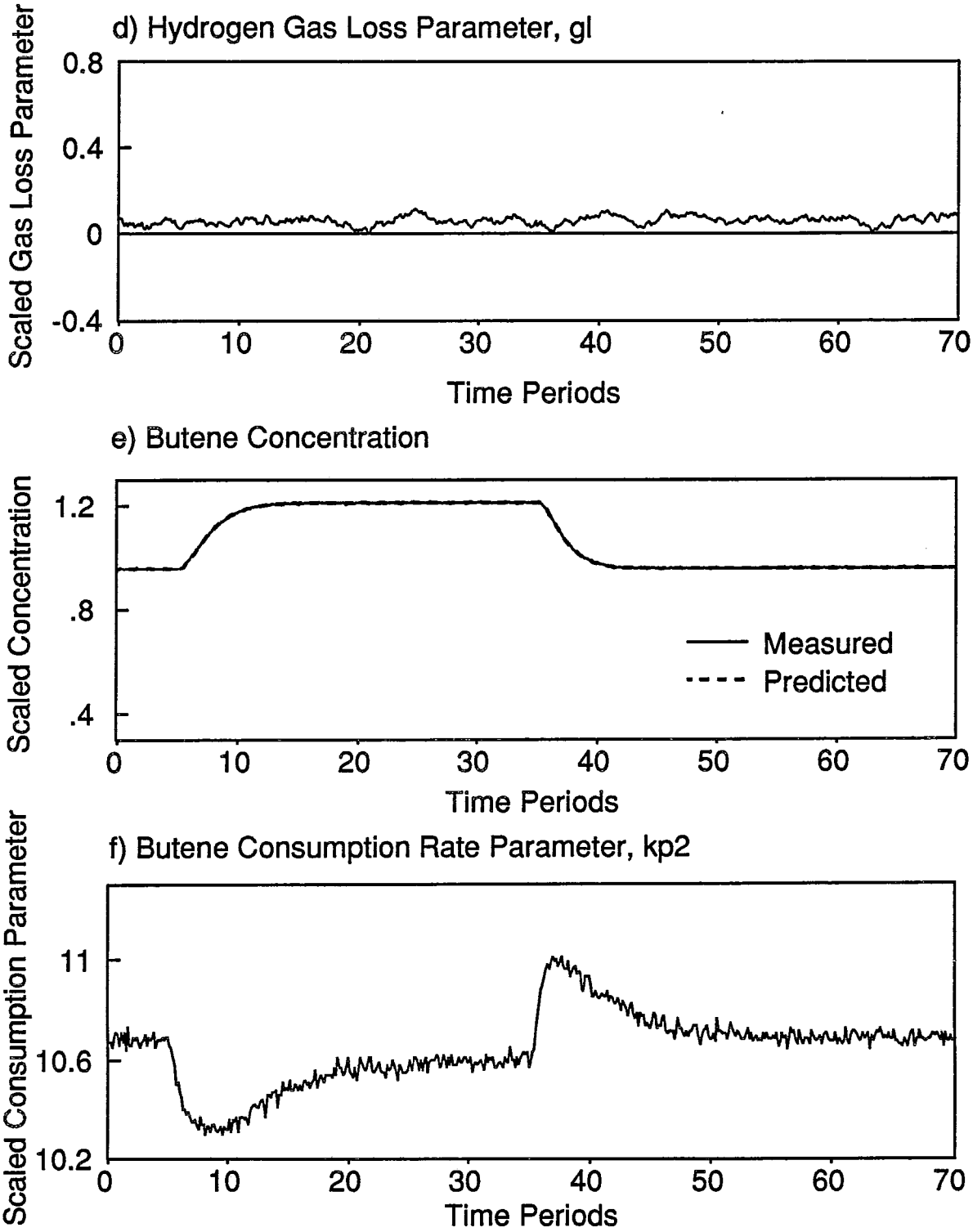

Figure 6.5 Kalman Filter Response to Catalyst Quality Step Change: Grade A

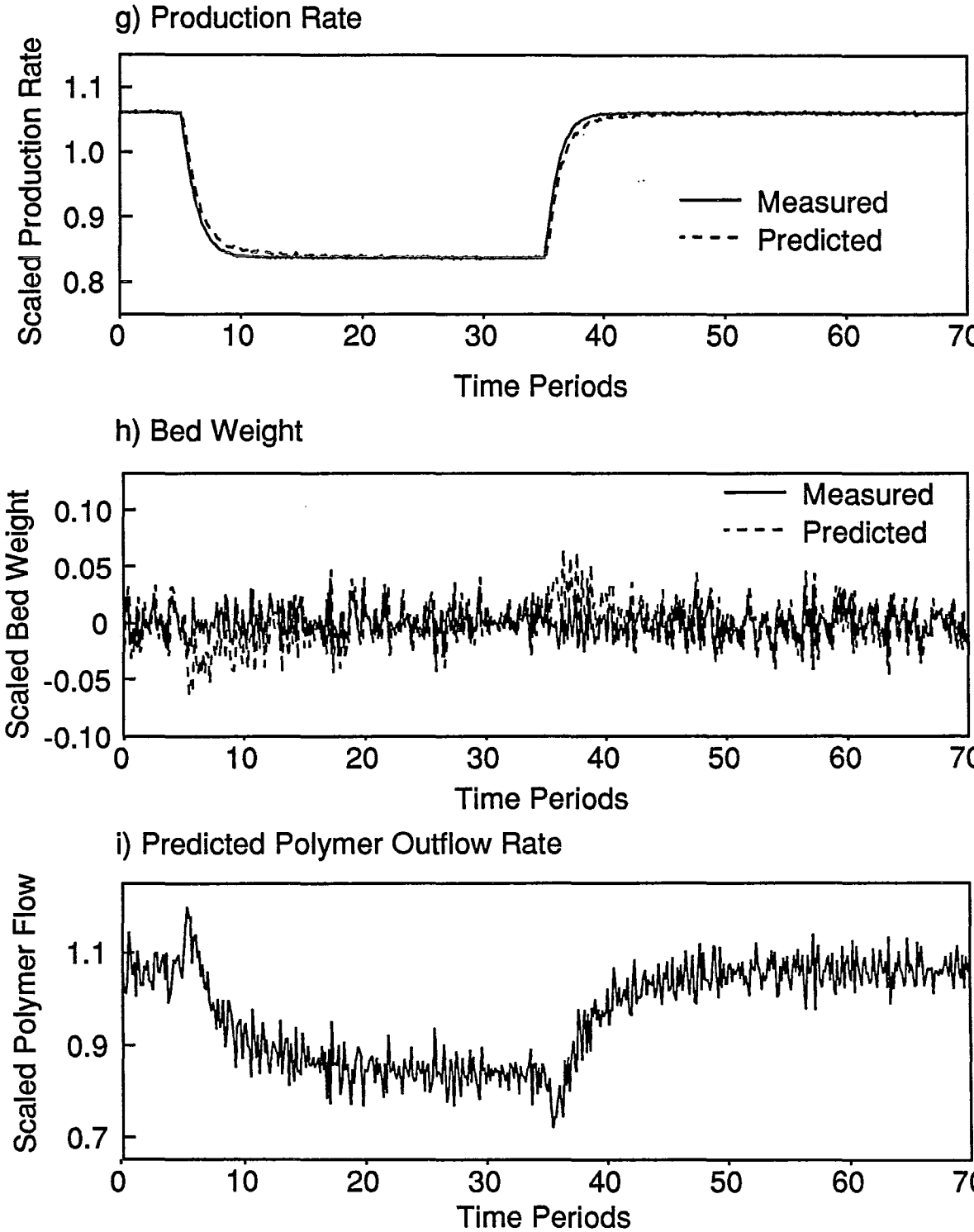

Figure 6.5 Kalman Filter Response to Catalyst Quality Step Change: Grade A

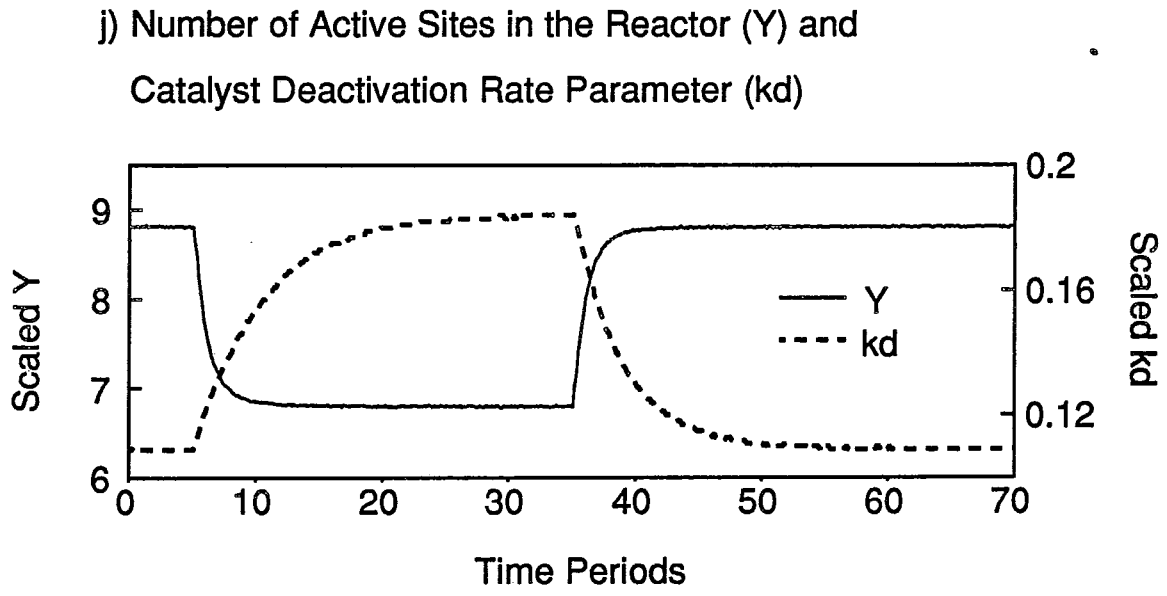

The *EKF*'s response to a series of grade transitions from Chapter 5 is shown in Figure 6.6. Optimal Policy II is used to accomplish both the $A \rightarrow B$ and $B \rightarrow A$ transitions. The $B \rightarrow C$ and $C \rightarrow B$ transitions make use of manipulated variable profiles from Policy IV. As shown in Figures 6.6 a), b), c), and e), the model and *EKF* successfully track the changes in MI_i, ρ_i, $[H_2]$, and $[C_4]$. The $B \rightarrow C$ and $C \rightarrow B$ transition policies in this simulation use the temperature setpoint changes shown in Figure 5.6 e) to assist in the grade changeovers. The *EKF* responds to the rise in temperature during the $B \rightarrow C$ transition by increasing gl, and to the temperature drop during the $C \rightarrow B$ transition by decreasing gl. The changes in gl shown in Figure 6.6 d) account for the effect of temperature on the true value of kh. High temperatures enhance the rate of chain transfer to hydrogen, and thus the rate of hydrogen consumption.

The *EKF* also tracks the changes in production rate shown in Figure 6.6 g). The major cause of the production rate changes during the $B \rightarrow C$ and $C \rightarrow B$ transitions is the reactor temperature. Since temperature effects on *kp1* and *kp2* are not included in the mass balance model, the *EKF* accounts for these production rate changes by manipulating *kd* and Y, as shown in Figure 6.6 j). The *EKF* also tries to compensate for the large, sudden changes in production rate by short-term spikes in the predicted polymer outflow rate, as illustrated in Figure 6.6 i). However, differences between the measured and predicted bed level in Figure 6.6 h) soon reveal that a change in the outflow rate is not responsible for the jump in production rate.

The behaviour of *kp2* during the $A \rightarrow B$ and $B \rightarrow A$ transitions is analogous to that caused by the catalyst disturbance in Figure 5.5 f). *kp2* responds both to changes in the ethylene to butene mole ratio in the reactor, and to changes in the polymer production rate. However, during the $B \rightarrow C$ and $C \rightarrow B$ transitions, the

direction of the changes in $kp2$ is less intuitive. During $B \rightarrow C$ transition, when the reactor temperature is high, the estimate of $kp2$ falls, whereas the Arrhenius dependency of rate parameters on temperature suggests that it should increase. This apparent contradiction can be explained as follows. The temperature rise causes the true values of both $kp1$ and $kp2$ to increase. Since Arrhenius effects are not built into the mass balance model, the *EKF* must increase Y to account for the increase in production rate. The increase in Y leads to an over-prediction of the butene consumption rate, given by the product $kp2\ Y\ [M_2]$, for a portion of the transition. During this time the *EKF* reacts by reducing $kp2$.

The results shown in Figure 6.6 illustrate that the model and *EKF* are capable of predicting reactor behaviour, and of accounting for the plant/model mismatch which occurs during grade transitions. The response of the *EKF* and nonlinear feedback control system to this same set of changeovers is discussed in section 6.7.4.

Figure 6.6 Kalman Filter Response to Open Loop Grade Transition Policies II and IV

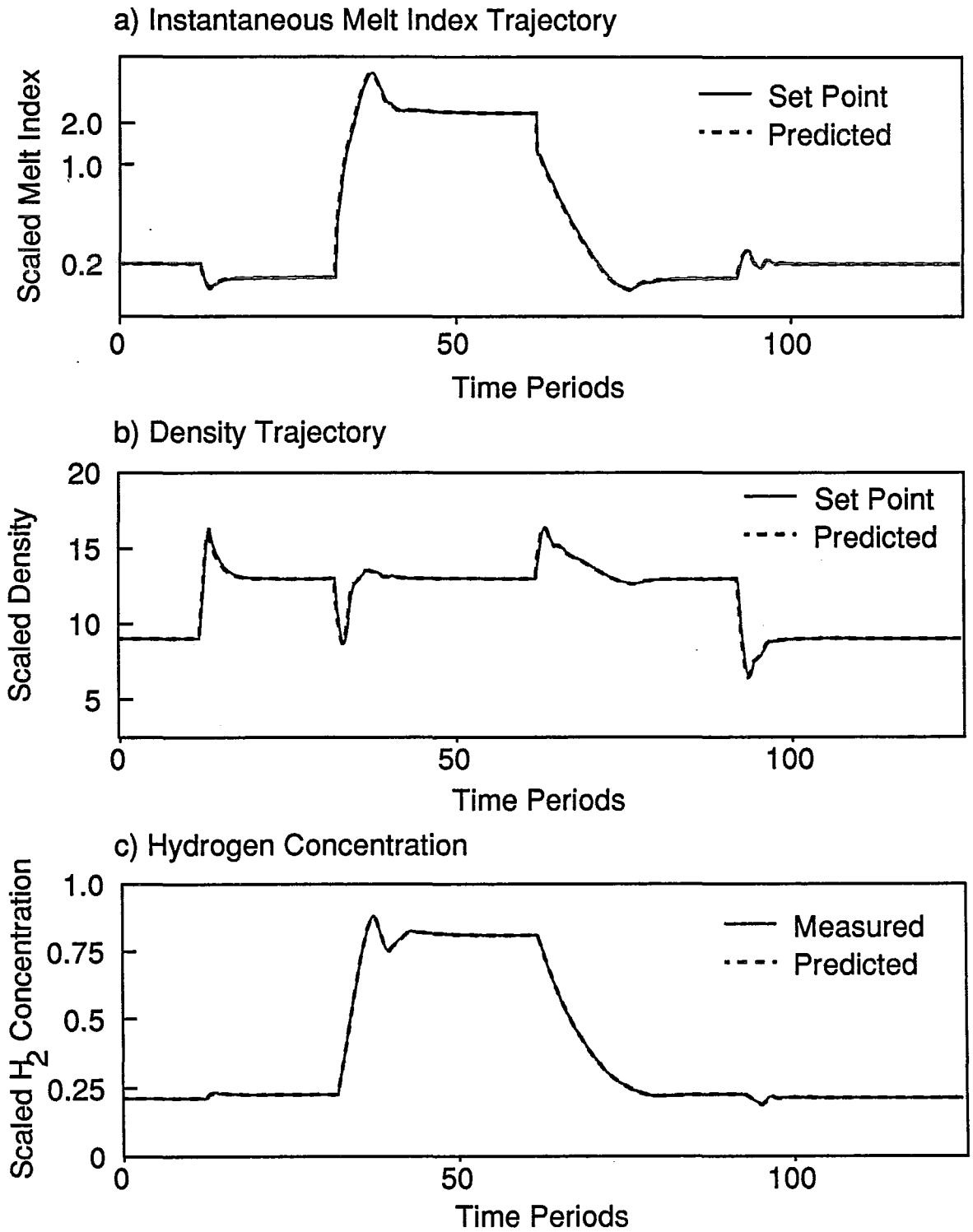

Figure 6.6 Kalman Filter Response to Open Loop Grade Transition Policies II and IV

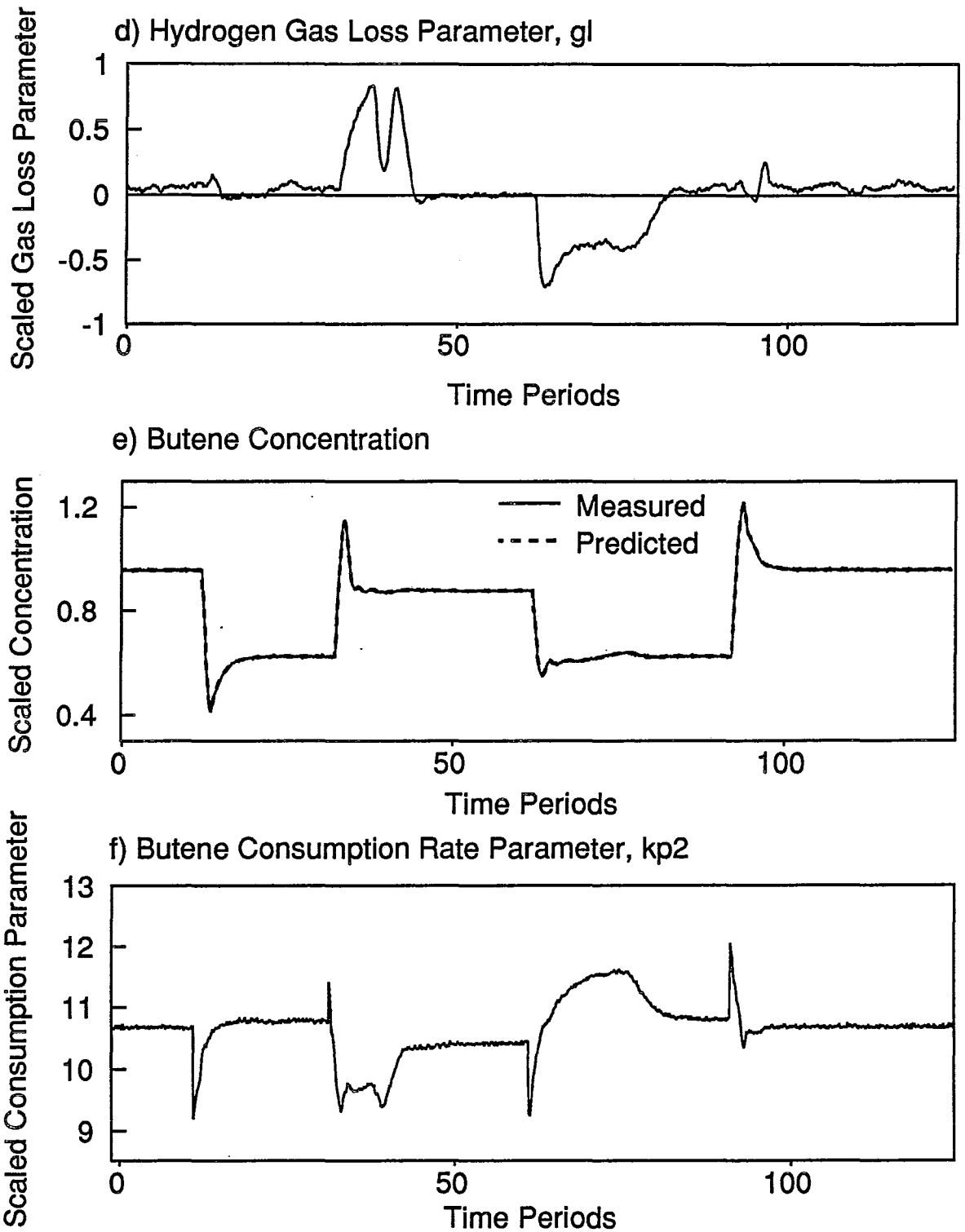

Figure 6.6 Kalman Filter Response to Open Loop Grade Transition Policies II and IV

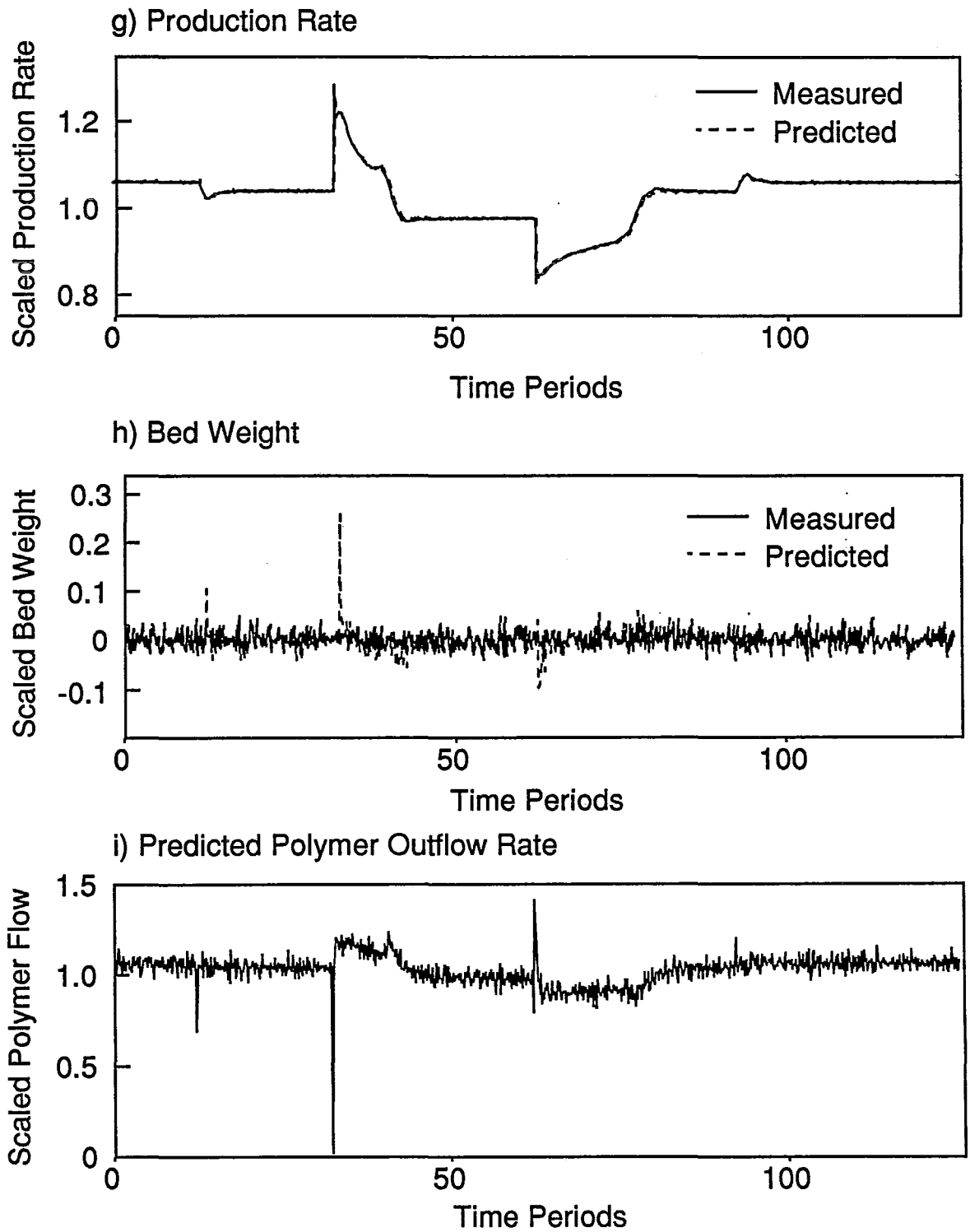

Figure 6.6 Feedback Control of Open Loop Grade Transition Policies 2 and 4

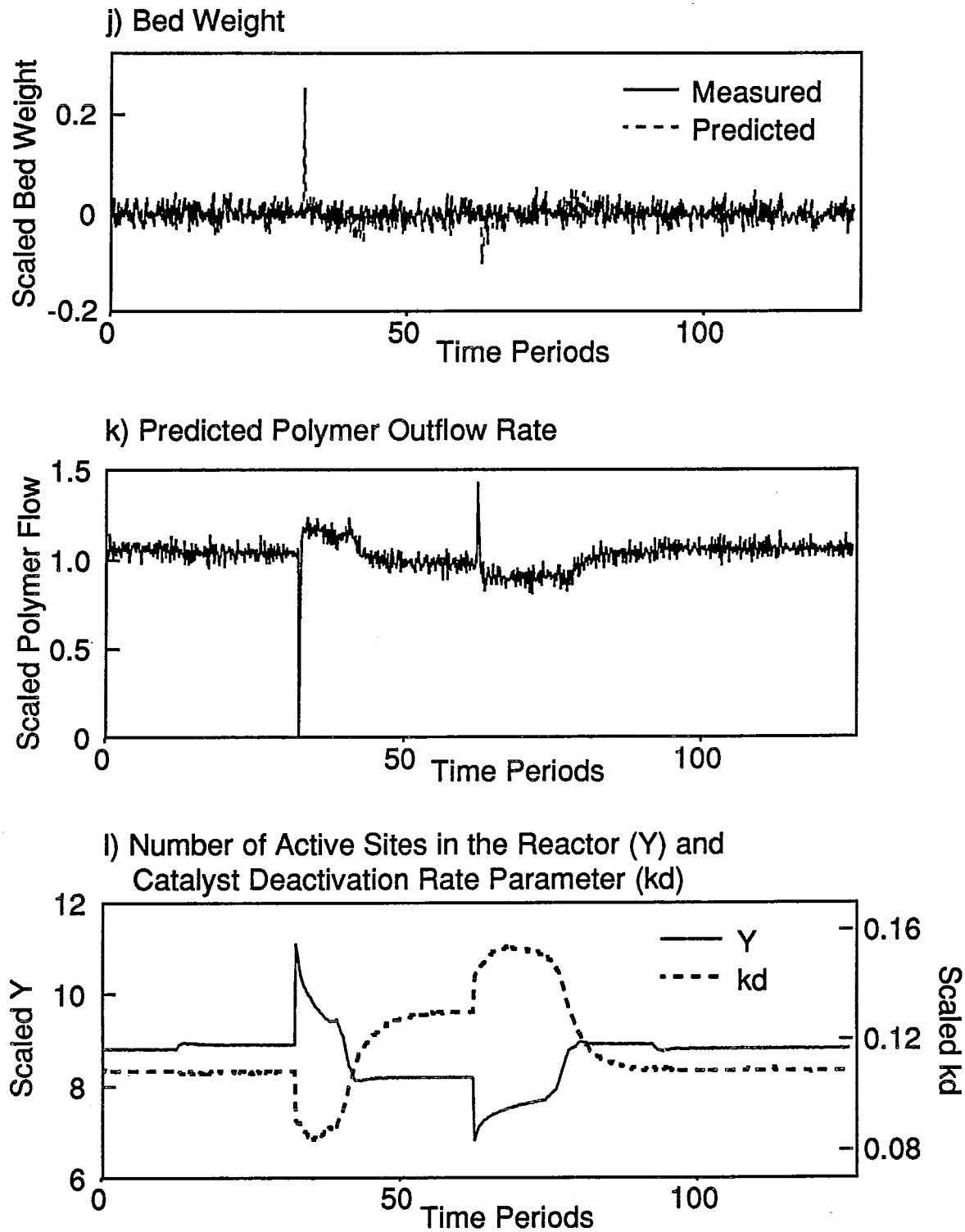

6.6.2 Conclusion

The mass balance model developed in section 6.5 is capable of predicting the way that butene and hydrogen feed rates affect hydrogen and butene concentration in the reactor. This model also directly accounts for catalyst feed and bleed flow rate changes. Using noisy on-line measurements, the *EKF* is able to adjust the model parameters in response to temperature changes, product outflow rate changes, catalyst quality disturbances, and changes in the quantity of polymer in the fluidized bed. The parameters chosen for on-line updating are consistent with the measurements used by the *EKF*, so that all states are observable, and no sustained mismatch between measurements and model predictions occurs. These properties of the model and filter, make them ideal for use in a model-based control scheme.

6.7 NONLINEAR FEEDBACK CONTROLLER DESIGN

Together, the mass balance model and the *EKF* provide a forecast of the delayed hydrogen and butene concentration measurements, account for disturbances, and prevent any sustained offset between model predictions and plant behaviour. As a result, the control law designed in this section is not required to compensate for measurement delay, nor must it contain integral action.

Using the gas composition forecasts calculated for the *EKF* and equations 6.5 and 6.6, one can write state equations of the form:

$$\dot{x}_1 = f_1(x_1, u_1) \tag{6.17}$$

$$\dot{x}_2 = f_1(x_2, u_2) \tag{6.18}$$

where $\dot{x}_1$ and $\dot{x}_2$ are the time derivatives of the hydrogen and butene concentrations, and u_1 and u_2 are the fresh feed rates of hydrogen and butene to the reactor. Equations 4.65 and 4.33 provide output equations of the form:

$$Y_1 = \ln(MI_i) = h_1(x_1, x_2, T) \tag{6.19}$$

$$Y_2 = \rho_i = h_2(x_1, x_2, T) \tag{6.20}$$

which describe how the controlled variables are influenced by temperature, and by the state variables which, in turn, are affected by the manipulated variables. Note that output equation 6.19 is written in terms of $\ln(MI_i)$ rather than MI_i. This choice is consistent with the objective functions in Chapter 5, which penalize deviations of $\ln(MI_i)$ and $\ln(MI_c)$ from their targets.

6.7.1 Choice of an Error Trajectory Description

Any number of nonlinear control laws could be derived for this relative order 1 system in which the manipulated variables enter linearly. One means of assessing the alternatives is by considering the closed loop error trajectory, which was introduced in section 6.3.2.1. The simplest error trajectory specification used in the design of input/output linearizing controllers is the following decoupled first-order specification:

$$\underline{\dot{e}}(t) = \underline{K}\, e(t) \tag{6.21}$$

wherein $\underline{K}$ is diagonal. This type of specification has been used by Freund(1973, 1975, 1982), by Kozub (1989), and by Adebekun and Schork (1989b), among others. This error trajectory specification results in an output response which approaches the nominal trajectory along a first-order path. Tuning of the response is accomplished by changing the elements of $\underline{K}$ which are the negative reciprocals of the first-order closed-loop time constants.

A second commonly used error trajectory specification is a decoupled second order response:

$$\underline{\dot{e}}(t) = \underline{K}_1 e(t) + \underline{K}_2 \int_{t_0}^{t} \underline{e}(\mu)\, d\mu \tag{6.22}$$

where $\underline{K}_1$ and $\underline{K}_2$ are both diagonal. This type of error trajectory specification is used in the design of *GMC* controllers (Lee and Sullivan, 1988). Whereas the first-order trajectory in equation 6.21 leads to an exponential decay of the error, and cannot be used to achieve overshoot in the closed-loop response, a second-order error specification is capable of producing either an over-damped or under-damped error response, depending on the choices of $\underline{K}_1$ and $\underline{K}_2$. Since overshoot is not desired in the control of instantaneous product properties, this added flexibility of a second-order specification provides no benefit in the current situation. Note that a controller designed using equation 6.22, requires twice as many tuning parameters as one employing equation 6.21.

Another important difference between nonlinear controllers with first and second-order error trajectory specifications is that controllers designed using equation 6.22 contain integral action. Thus, without model updating, a controller with a second-order error specification will automatically remove steady state offset caused by non-stationary disturbances. Conversely, controllers using first-order error specifications are prone to steady state off-set if no model updating step is included in the control system. Since the gas mass balance models in equations 6.5 to 6.8 are updated on-line, integral action in the controller is not required in order to eliminate offset. As such, the simpler first-order error trajectory specification is adopted in the controller design which follows.

6.7.2 Derivation of the Feedback Control Law

The first-order error trajectory specification in equations 6.19 can be rewritten as:

$$\dot{Y}_1 = \dot{Y}_{1sp} - \kappa_1 (Y_{1sp} - Y_1) \tag{6.23}$$

$$\dot{Y}_2 = \dot{Y}_{2sp} - \kappa_2 (Y_{2sp} - Y_2) \tag{6.24}$$

where κ_1 and κ_2 are the diagonal elements of $\underline{K}$. The entire right hand sides of equations 6.23 and 6.24 above are known quantities. During a grade changeover, the values of Y_{1sp}, Y_{2sp} and their time derivatives are specified by the optimal noniminal trajectories determined in Chapter 5. During regulation at a target grade, Y_{1sp} and Y_{2sp} are constants and $\dot{Y}_{1sp}$ and $\dot{Y}_{2sp}$ are both zero. Y_1 and Y_2 are the estimated values of $\ln(MI_i)$ and ρ_i, respectively, calculated using the current temperature measurement and the forecasted current gas concentrations which are provided by the *EKF*.

Differentiating the measurement equations 6.19 and 6.20 with respect to time gives:

$$\dot{Y}_1 = \frac{\partial h_1}{\partial x_1}\dot{x}_1 + \frac{\partial h_1}{\partial x_2}\dot{x}_2 + \frac{\partial h_1}{\partial T}\dot{T} \tag{6.25}$$

$$\dot{Y}_2 = \frac{\partial h_2}{\partial x_1}\dot{x}_1 + \frac{\partial h_2}{\partial x_2}\dot{x}_2 + \frac{\partial h_2}{\partial T}\dot{T} \tag{6.26}$$

If the cocatalyst term in equation 4.65 is neglected, the partial derivatives in equations 6.24 and 6.26 can be calculated as follows,

$$\frac{\partial h_1}{\partial x_1} = 3.5 \frac{k_3/[M_1]}{k_0 + k_1[M_2]/[M_1] + k_3[H_2]/[M_1]} \tag{6.27}$$

$$\frac{\partial h_1}{\partial x_2} = 3.5\frac{k_1/[M_1]}{k_0 + k_1[M_2]/[M_1] + k_3[H_2]/[M_1]} \tag{6.28}$$

$$\frac{\partial h_1}{\partial T} = \frac{k_7}{T^2} \tag{6.29}$$

$$\frac{\partial h_2}{\partial x_1} = p_1\frac{\partial h_1}{\partial x_1} \tag{6.30}$$

$$\frac{\partial h_2}{\partial x_2} = p_1\frac{\partial h_1}{\partial x_2} - p_4\left(p_2\frac{[M_2]}{[M_1]}\right)^{p_4-1}\frac{p_2}{[M_1]} \tag{6.31}$$

$$\frac{\partial h_2}{\partial T} = p_1\frac{\partial h_1}{\partial T} \tag{6.32}$$

The partial derivatives in equations 6.27 to 6.32 can be evaluated given the current temperature measurement, and the forecasted gas compositions. Since an ethylene partial pressure controller is operating on-line, the ethylene concentration in the reactor is relatively steady. Thus, the past measured value of $[M_1]$ is adequate for use in these calculations. A filtered estimate of $\dot{T}$ in equations 6.25 and 6.26 can be estimated from past on-line reactor temperature measurements.

Eliminating $\dot{Y}_1$ and $\dot{Y}_2$ from equations 6.23 to 6.26 and solving for $\dot{x}_1$ and $\dot{x}_2$ yields the following expressions:

$$\dot{x}_1 = \frac{\frac{\partial h_2}{\partial x_2}M - \frac{\partial h_1}{\partial x_2}N}{\frac{\partial h_2}{\partial x_2}\frac{\partial h_1}{\partial x_1} - \frac{\partial h_1}{\partial x_2}\frac{\partial h_2}{\partial x_1}} = P \tag{6.33}$$

$$\dot{x}_2 = \frac{M - \frac{\partial h_1}{\partial x_1}P}{\frac{\partial h_1}{\partial x_2}} = Q \tag{6.34}$$

where:

$$M = \dot{Y}_1 - \kappa_1(Y_{1sp} - Y_1) - \frac{\partial h_1}{\partial T}\dot{T} \tag{6.35}$$

$$N = \dot{Y}_2 - \kappa_2(Y_{2sp} - Y_2) - \frac{\partial h_2}{\partial T}\dot{T} \tag{6.36}$$

Eliminating $\dot{x}_1$ and $\dot{x}_2$ from equations 6.17, 6.18, 6.33 and 6.34 gives the following expressions for the manipulated variables in terms of known quantities:

$$u_1 = (P + L)\, mw(H_2)\, V_g \tag{6.37}$$

$$u_2 = (Q + W)\, mw(M_2)\, (V_g + V_s) \tag{6.38}$$

$$L = \frac{khY[H_2] + \frac{[H_2]b_T}{C_T} + gl\,[H_2]}{V_g} \tag{6.39}$$

$$W = \frac{kp2\; Y[M_2] + \frac{[M_2]b_T}{C_T} + S(M_2)\,[M_2]O_p}{V_g + V_s} \tag{6.40}$$

Equations 6.37 and 6.38 give the hydrogen and butene feed rates required to achieve the desired first-order error trajectory response. These simple analytical state feedback expressions for u_1 and u_2 make for a very simple calculation of the required control actions.

6.7.3 Controller Implementation

The feedback controller in equations 6.37 and 6.38 has been derived for continuous time implementation. However, due to the gas sampling interval, the measurement delay, and the discrete *EKF*, it makes more sense to implement a discrete time approximation of this control law. A discrete version of the control algorithm can be implemented as follows. Every h time units, when a new delayed gas composition measurement is available, these measurements are used by the *EKF* to

update the parameter and state estimates. Next, the model in equations 6.5 to 6.8 can be integrated over h time units, starting from the filtered values. The predictions from this integration step are saved so that they can be used for future *EKF* calculations. These predictions are also used in the control law calculation. Next, appropriate control actions u_1 and u_2 are calculated using the model predictions, so that they can be implemented during the control interval which follows. When new gas composition measurements become available, the process is repeated.

Since the sampling interval, h, is several minutes long, a significant change in both the butene and hydrogen concentrations can occur over that time interval. It may not be wise to merely calculate the values of u_1 and u_2 from the continuous control law that would be appropriate at the start of the interval, and then hold these values constant for h time units. A better discrete approximation of the continuous control law can be obtained if h is divided into smaller sub-intervals of length q, during which it is valid to assume that changes in $[H_2]$ and $[M_2]$ will be small. Initial values of u_1 and u_2 can be calculated from the continuous control law, and a difference equation approximation can be used to predict the resulting hydrogen and butene concentrations at the end of the sub-interval. These calculations are repeated for each sub-interval to obtain hydrogen and butene feed rate profiles. These manipulated variable profiles can be implemented during the next control interval, or alternatively, time average values of u_1 and u_2 can be calculated from the profiles. Implementation of these constant, average values over the next control interval results in the same total quantities of hydrogen and butene being fed to the reactor as is if the time varying profiles had been implemented. This approach is adopted in the examples shown in sections 6.74.

Due to disturbances and short-term model mismatch, the values of u_1 and u_2, calculated from the control law, can be beyond the physical bounds on the hydrogen and butene feed flow rates. When manipulated variable saturation occurs, the actual implemented value of the control action, rather than the calculated values of u_1 and u_2, should be used in model, *EKF*, and control calculations in order to prevent wind-up. Further discussion of the manipulated variable saturation problem is provided in section 6.9.

6.7.4 Control Scheme Testing

The nonlinear controller was tested using the same catalyst feed disturbance as in Figure 6.5. The results are shown in Figure 6.7. In Figure 6.5, no feed back action is taken to compensate for the catalyst feed disturbance, and as a result, significant deviations in both MI_i and ρ_i occur. In Figure 6.7, the feed back controller uses hydrogen and butene feed rate manipulations to alleviate the effects of the disturbance. Consequently, only minimal short-term deviations from the setpoints are observed in Figures 6.7 c) and d). The feedback control actions result in smaller changes in both $[M_2]$ and *kp2* than in the open-loop case. The responses in production rate, bed level, outflow rate, Y, and *kd* are nearly identical to those in Figure 6.5.

The favourable results in Figures 6.7 c) and d) indicate that the combination of the *EKF* and nonlinear controller is effective both for updating the model to predict the system behaviour, and for alleviating the effects of the disturbances on product quality. Due to the updating action of the *EKF*, there is no steady state offset between the product properties and their setpoints, even though the controller itself does not contain integral action. Another important feature of this controller is that it rejects

product quality disturbances equally well, no matter which polymer grade is being produced. This is verified in Figure 6.8, wherein the controller rejects the same catalyst disturbance while producing Grade C.

Figure 6.7 Closed Loop Response to Catalyst Feed Disturbance: Grade A

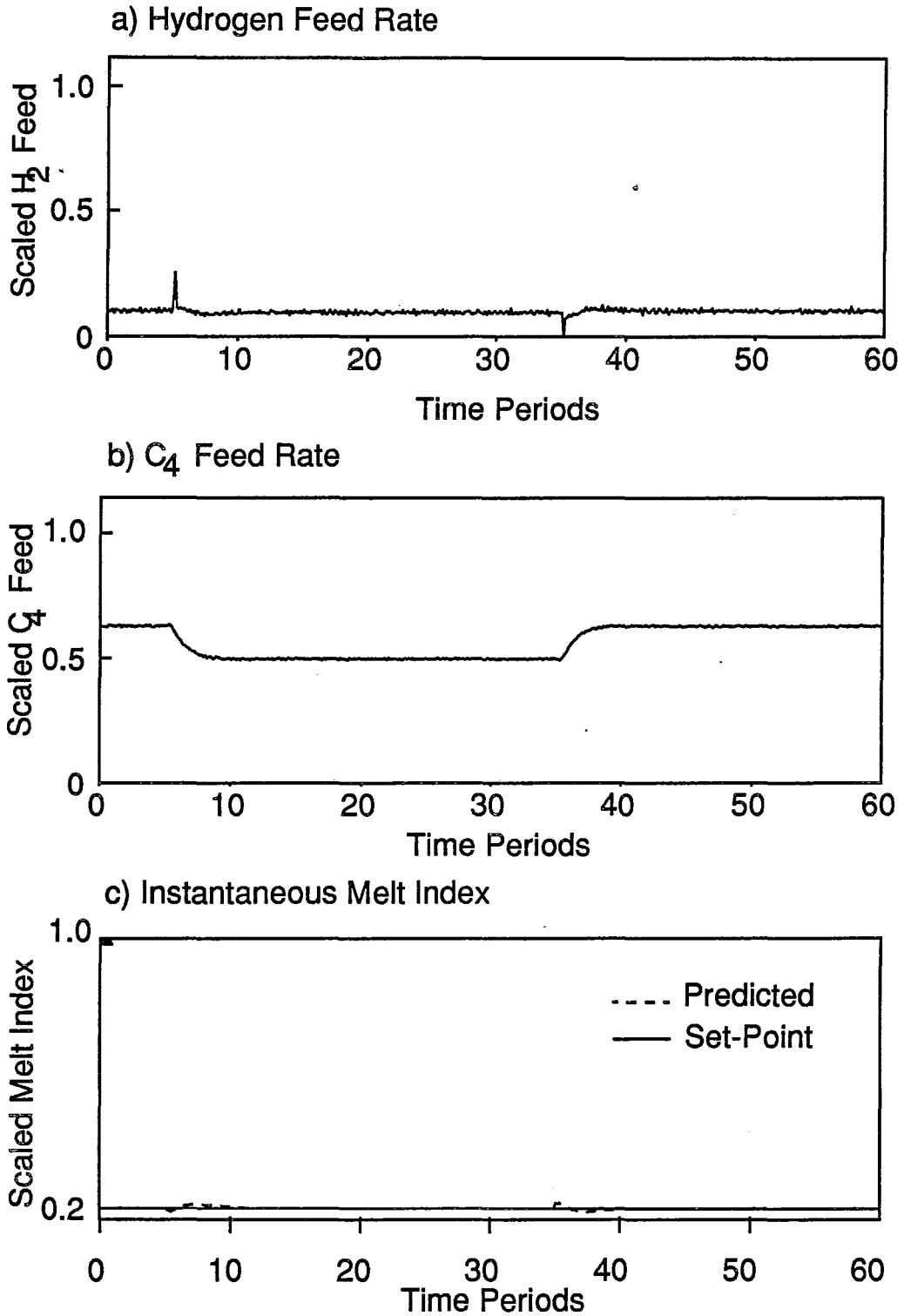

Figure 6.7 Closed Loop Response to Catalyst Feed Disturbance: Grade A

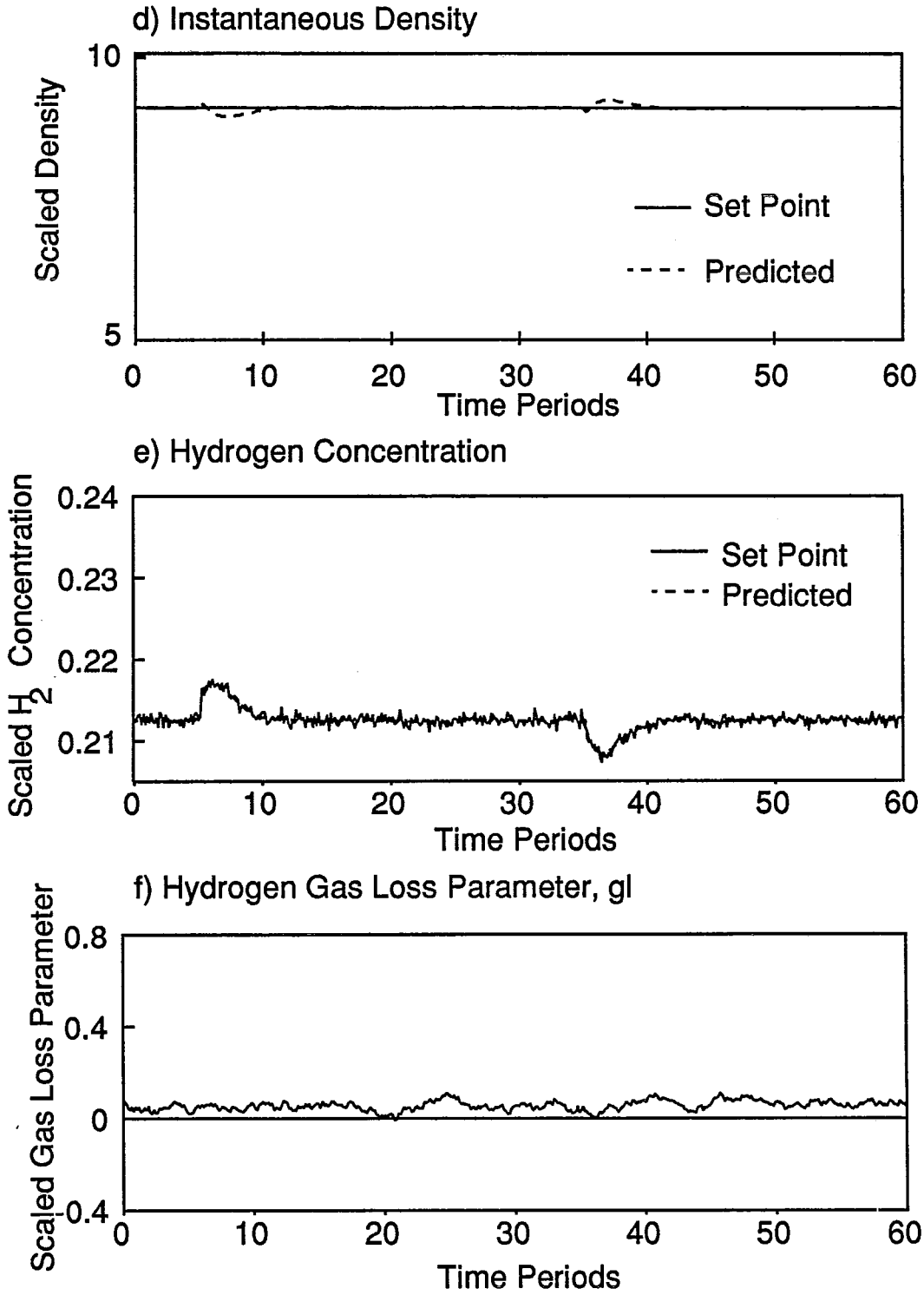

Figure 6.7 Closed Loop Response to Catalyst Feed Disturbance: Grade A

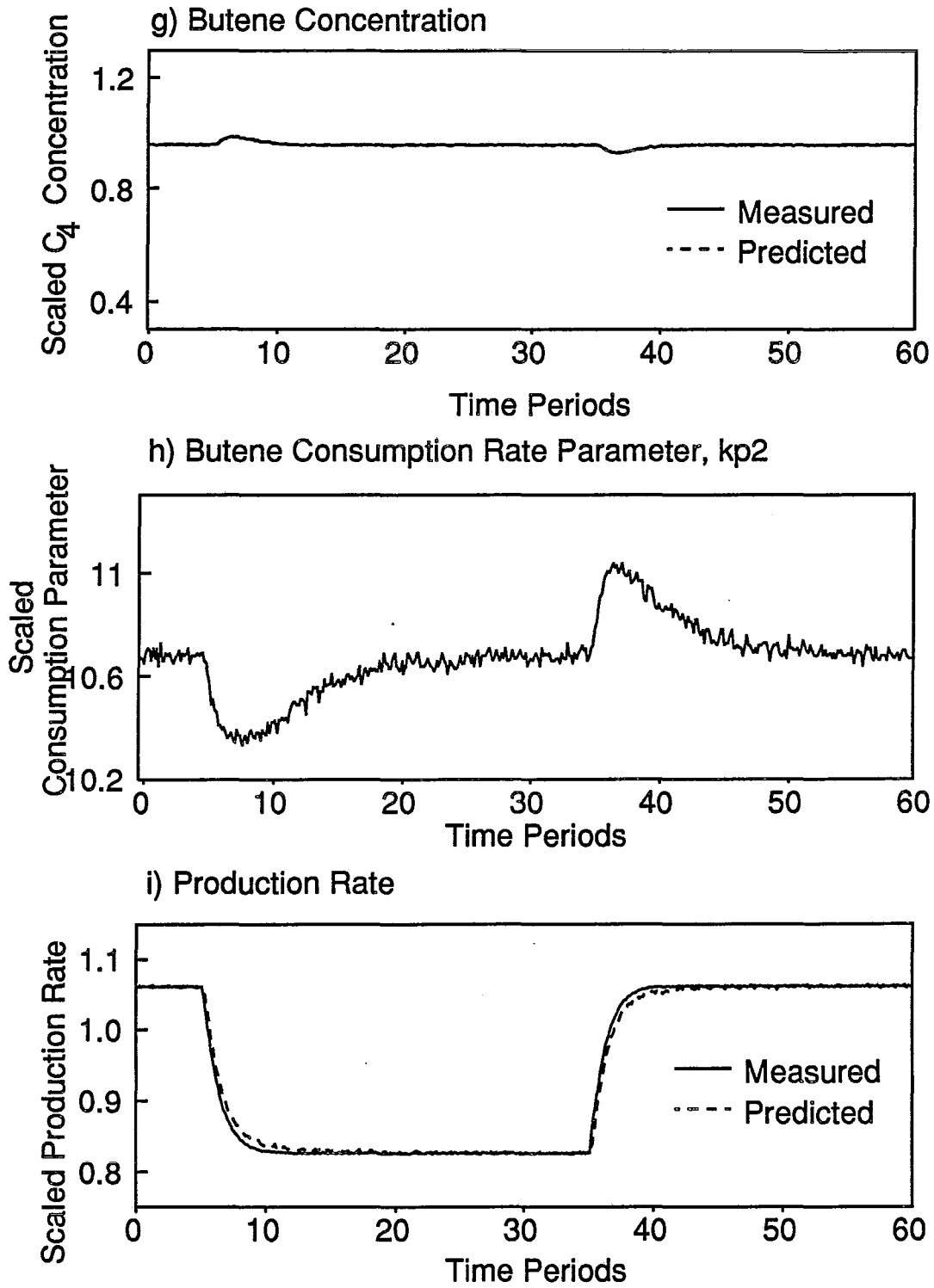

Figure 6.7 Closed Loop Response to Catalyst Feed Disturbance: Grade A

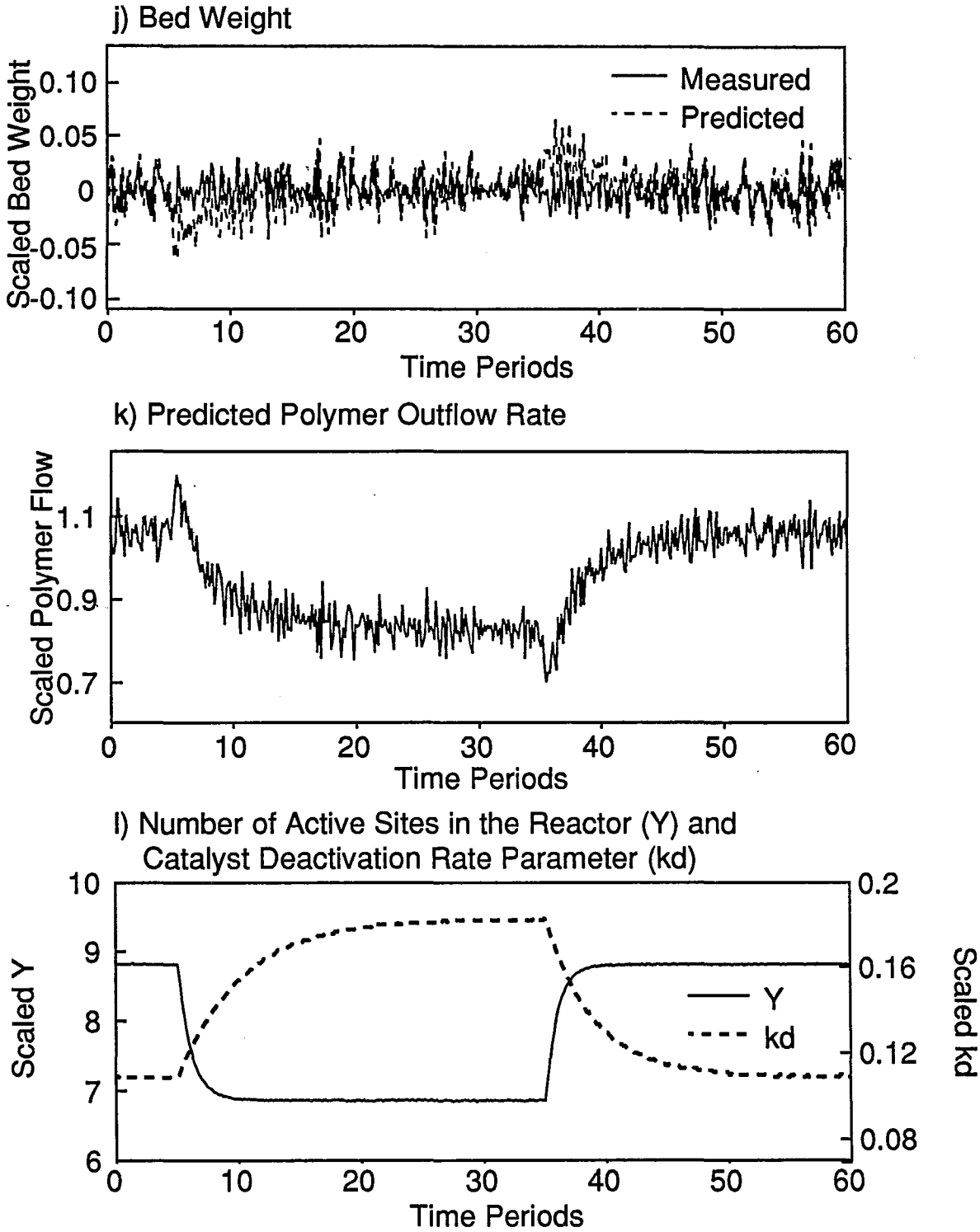

Figure 6.8 Closed Loop Response to Catalyst Feed Disturbance: Grade C

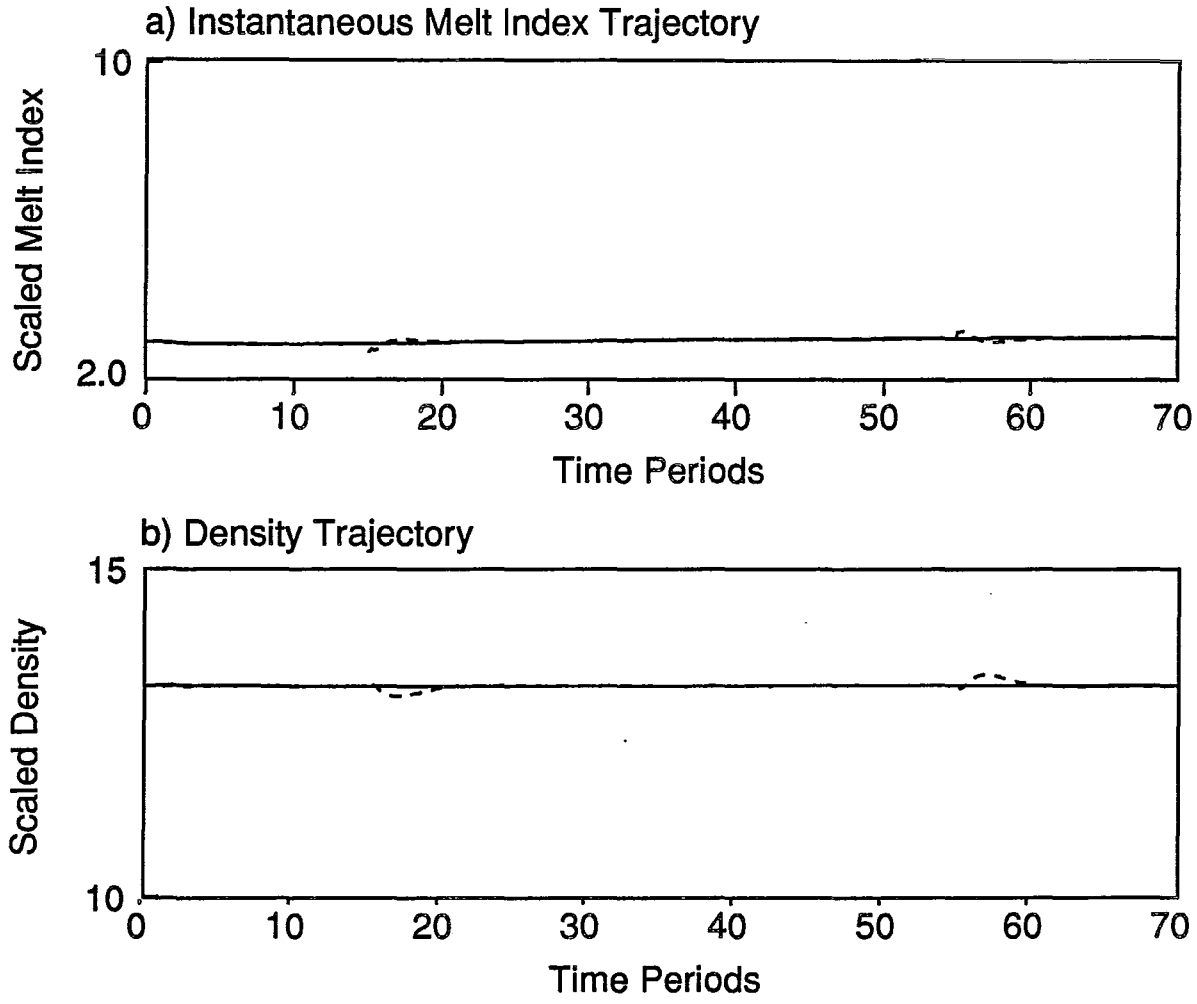

The ability of the nonlinear controller to follow several sets of optimal grade transition trajectories has been simulated, and the results are show in Figures 6.9 and 6.10. In Figure 6.9, the controller was used to follow the Policy II and IV grade changeovers which were studied in Figure 6.6. The resulting control actions and instantaneous product property trajectories are shown in Figures 6.9 a) to d). The feedback controller is able to follow the prespecified trajectories while the *EKF* updates the mass balance model. The butene and hydrogen feed policies calculated by the controller are nearly identical to those in the optimal policies in Chapter 5. This similarity indicates that the *EKF* is able to keep the model-inverse in the control law very close to the true inverse of the plant. There are minor differences in the closed loop *gl* and *kp2*, compared to those in Figure 6.6, due to the slightly different manipulated variable and concentration profiles. The responses of O_p, Y, and *kd*, are virtually indistinguishable from those in Figure 6.6, and have not been shown.

In the Policy II and IV transitions, changes in catalyst feed rates and bed level are not used to assist in the grade changeovers. To test the effects of these additional feed forward variables on the *EKF* and controller, the closed loop response to a series of Policy V transitions was simulated. The results are given in Figure 6.10. Even when faced by measurement noise and model mismatch, the feedback controller is able to follow the desired trajectories. As shown in Figures 6.10 c) and d), only slight deviations are observed between the desired and actual instantaneous product property trajectories. The control actions chosen by the controller in Figures 6.10 a) and b) are very similar to the corresponding open loop optimal policies from Chapter 5. Slight deviations are due to short-term model mismatch caused by the large temperature and outflow rate changes, which must be identified by the *EKF* because they don't enter the mass-balance model automatically. The changes in

gl, $kp2$, O_p, and kd, chosen by the *EKF*, are shown in Figures 6.10 f), h), k) and l), respectively. That the controller performance is robust under such extreme conditions, when the model used in the control calculations is changing quickly, is a positive sign that this control design can perform well in an actual industrial reactor.

Figure 6.9 Feedback Control for Transition Policies II and IV

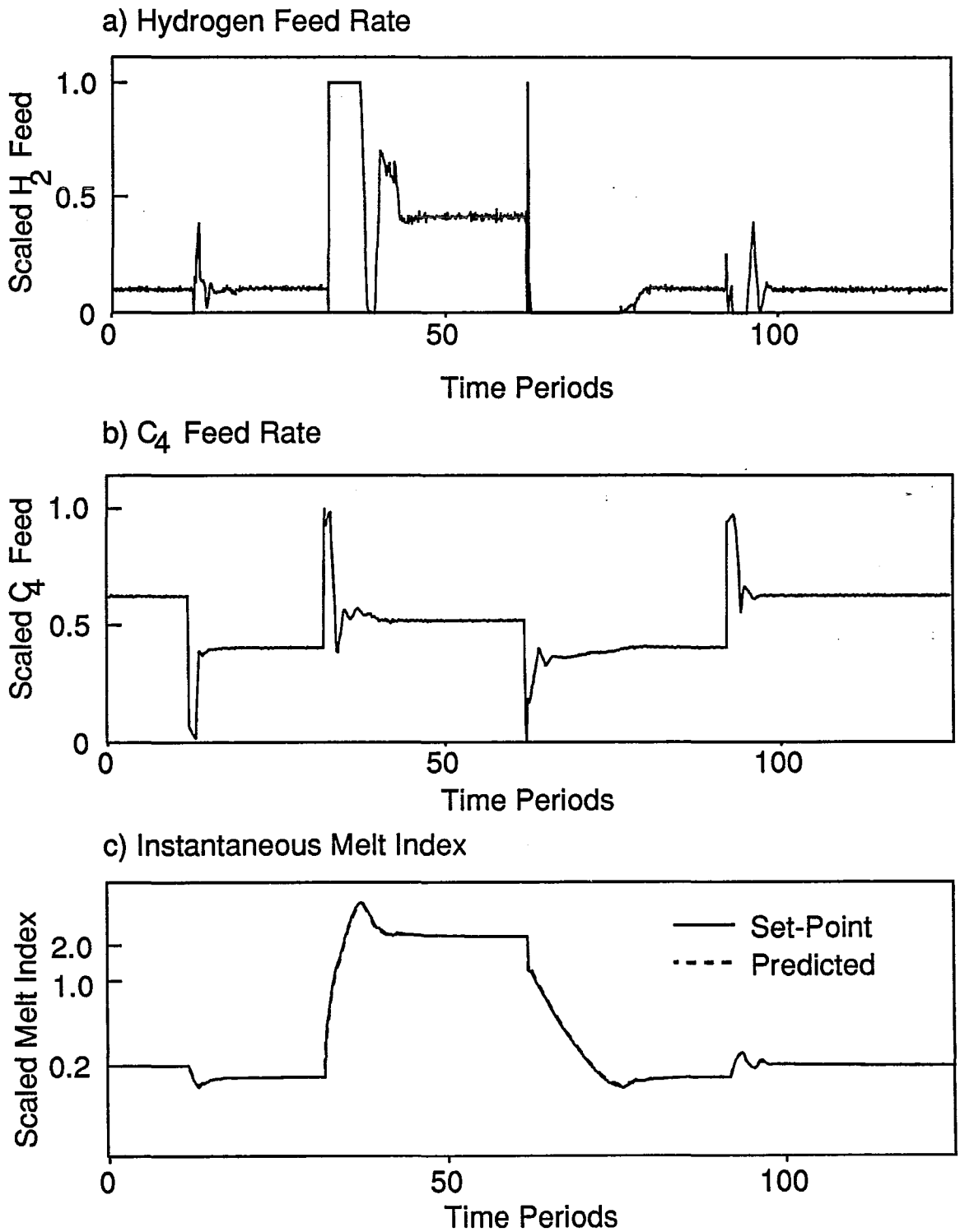

Figure 6.9 Feedback Control for Transition Policies II and IV

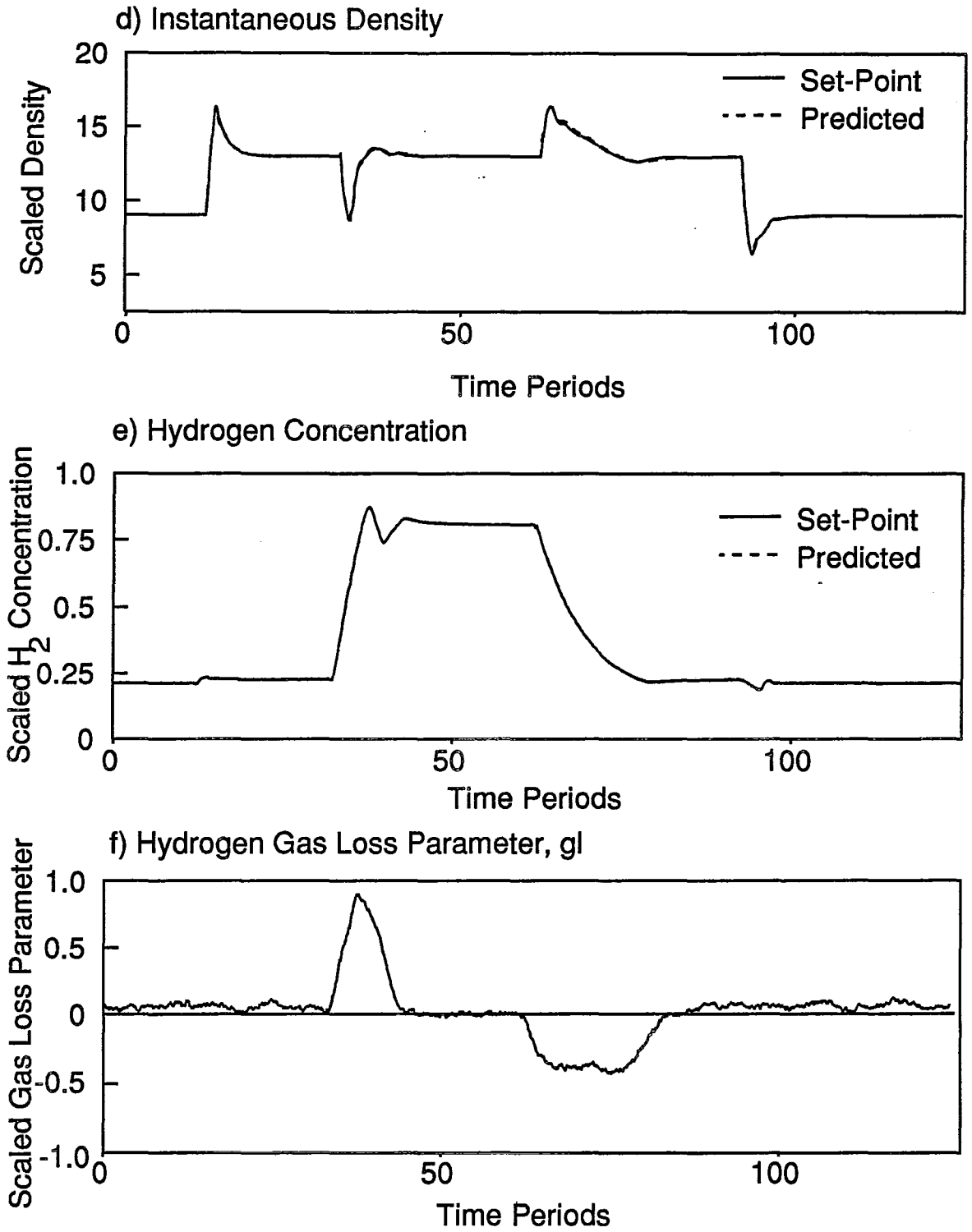

Figure 6.9 Feedback Control for Transition Policies II and IV

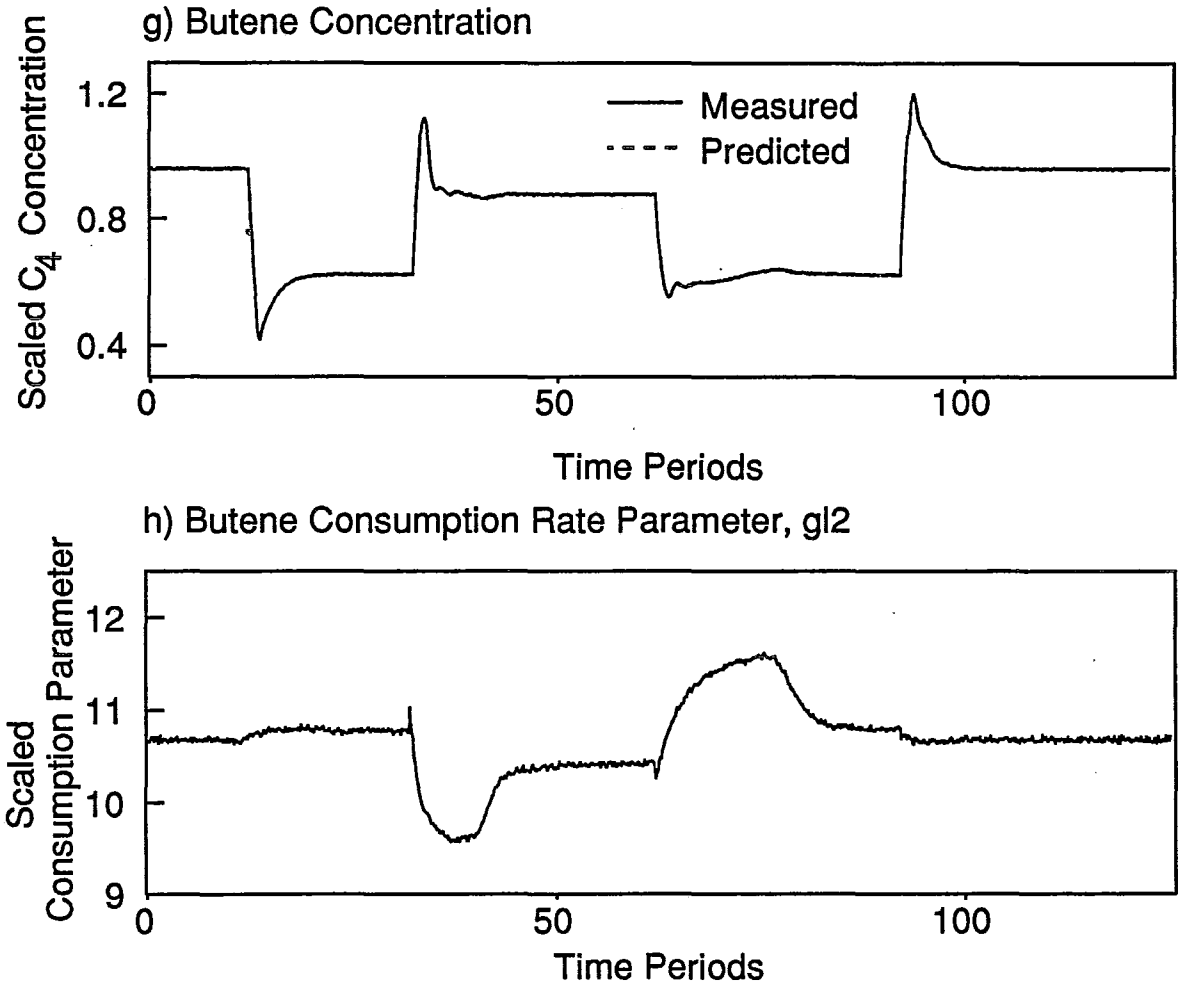

Figure 6.10 Feedback Control for Transition Policy V

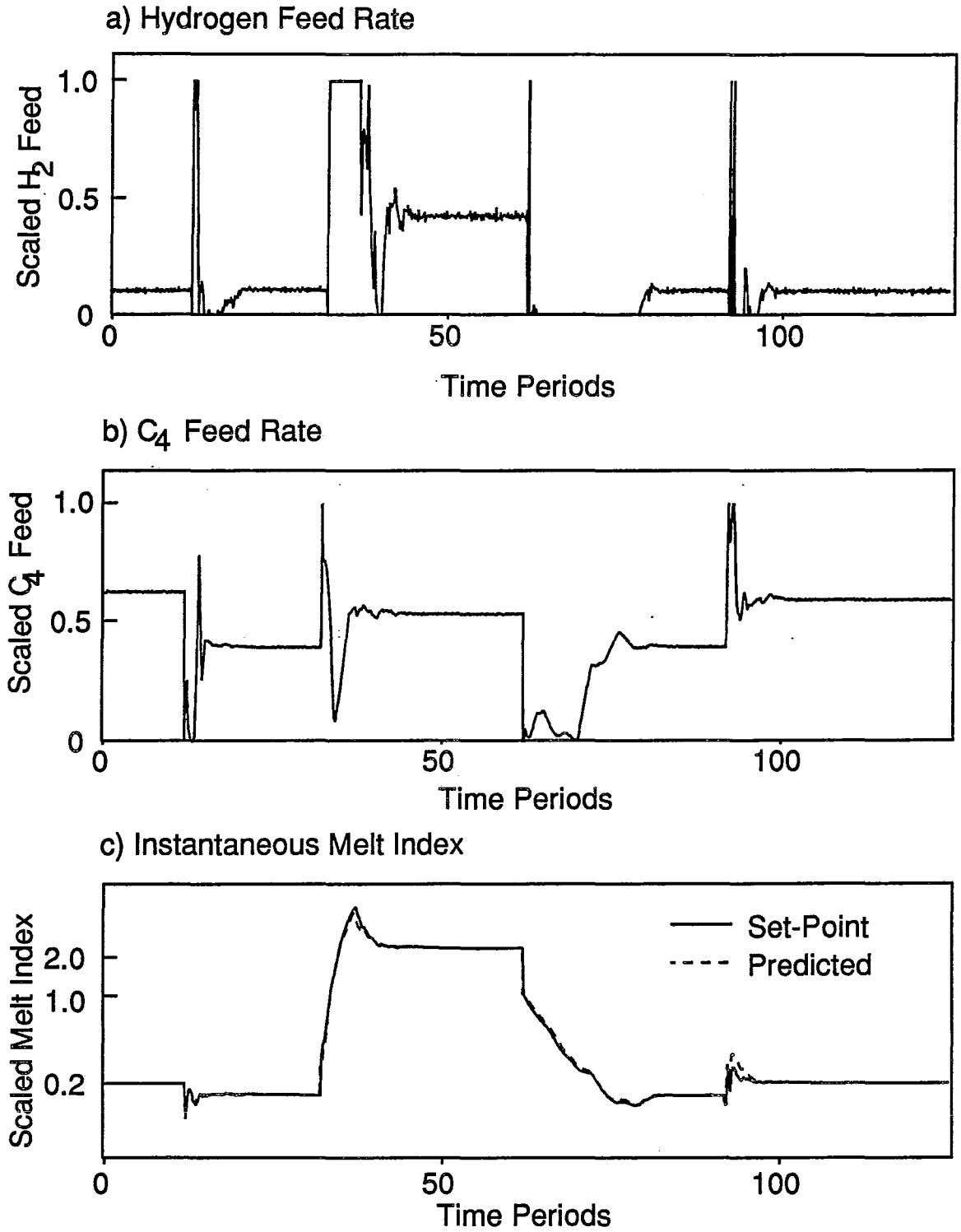

Figure 6.10 Feedback Control for Transition Policy V

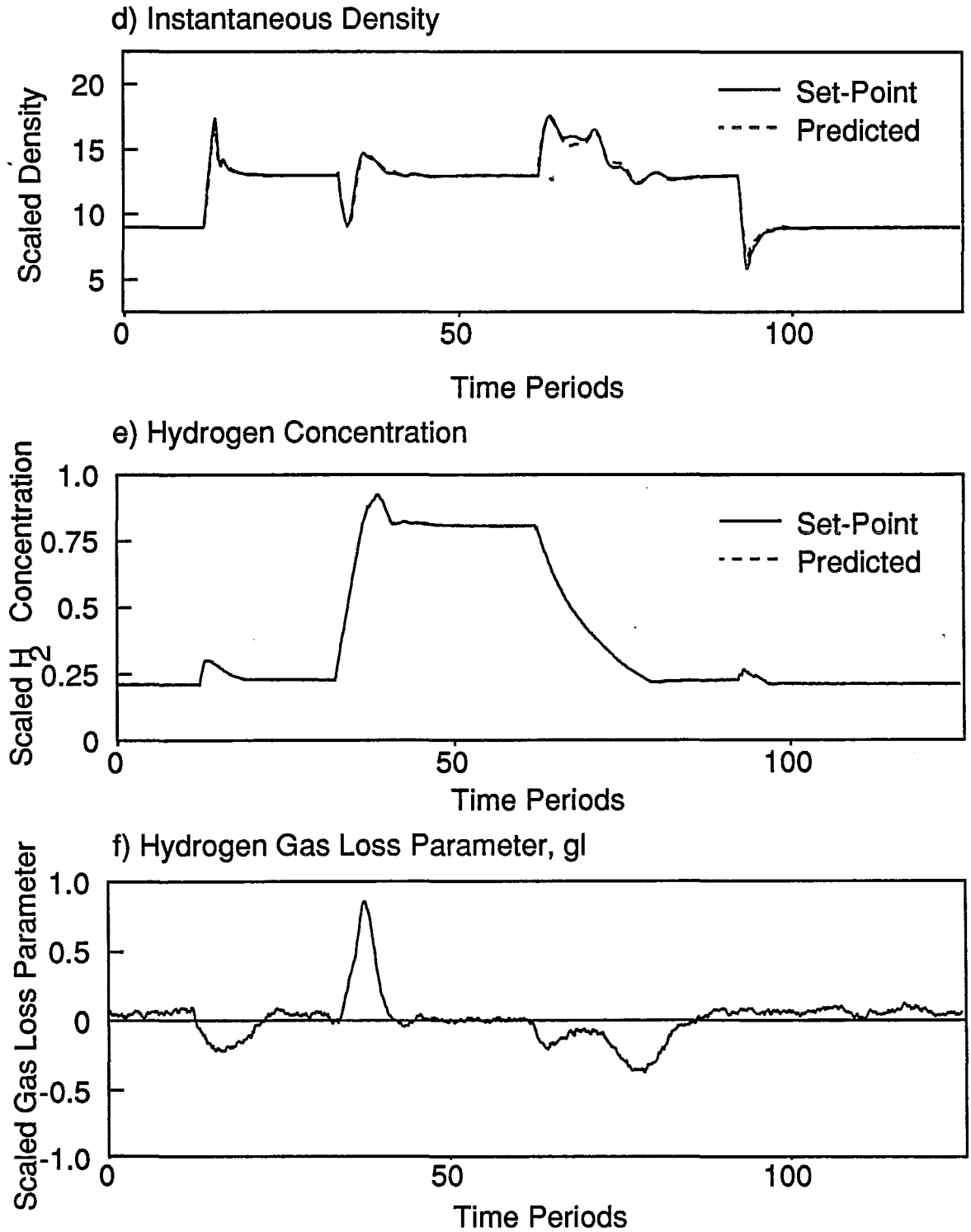

Figure 6.10 Feedback Control for Transition Policy V

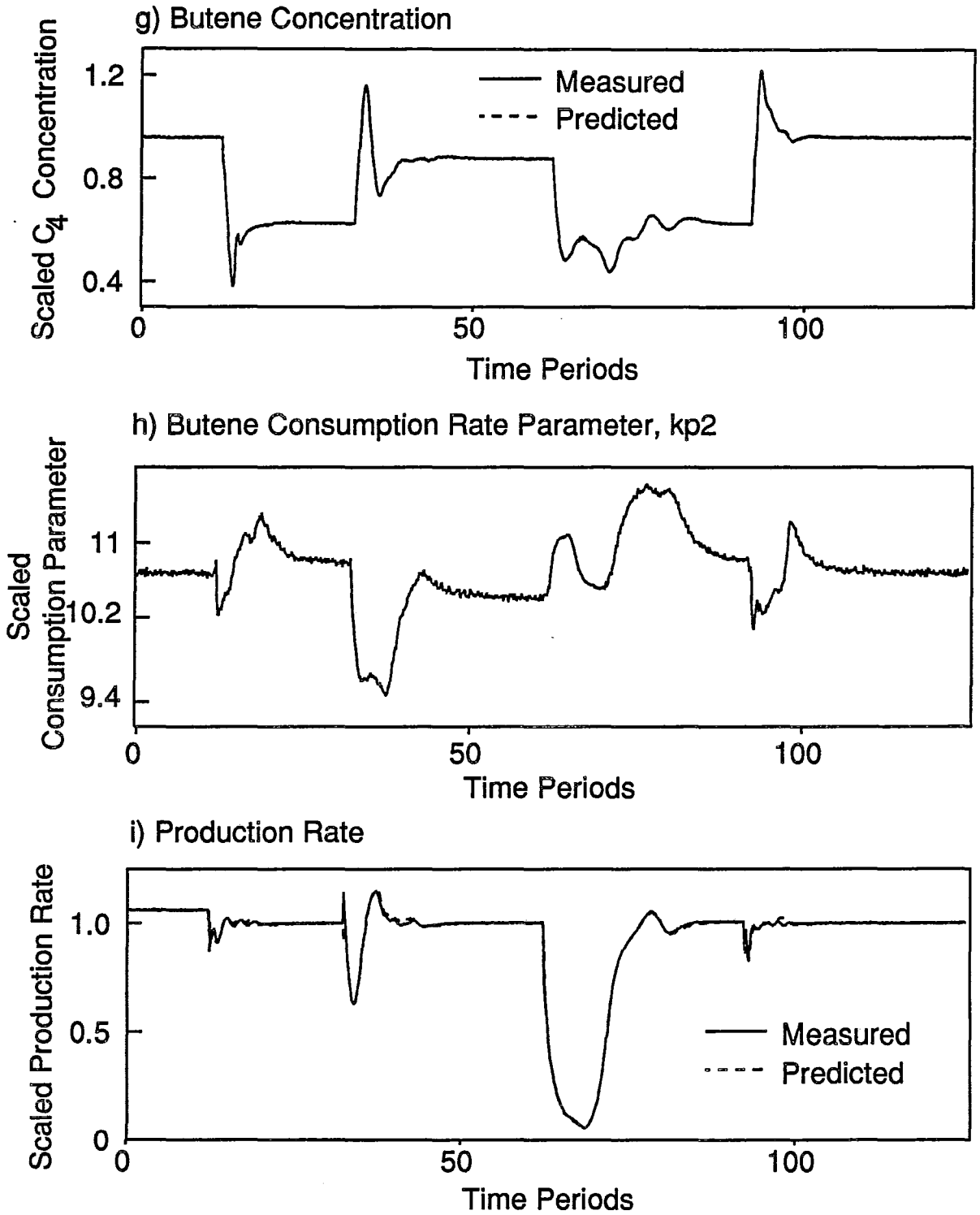

Figure 6.10 Feedback Control for Transition Policy V

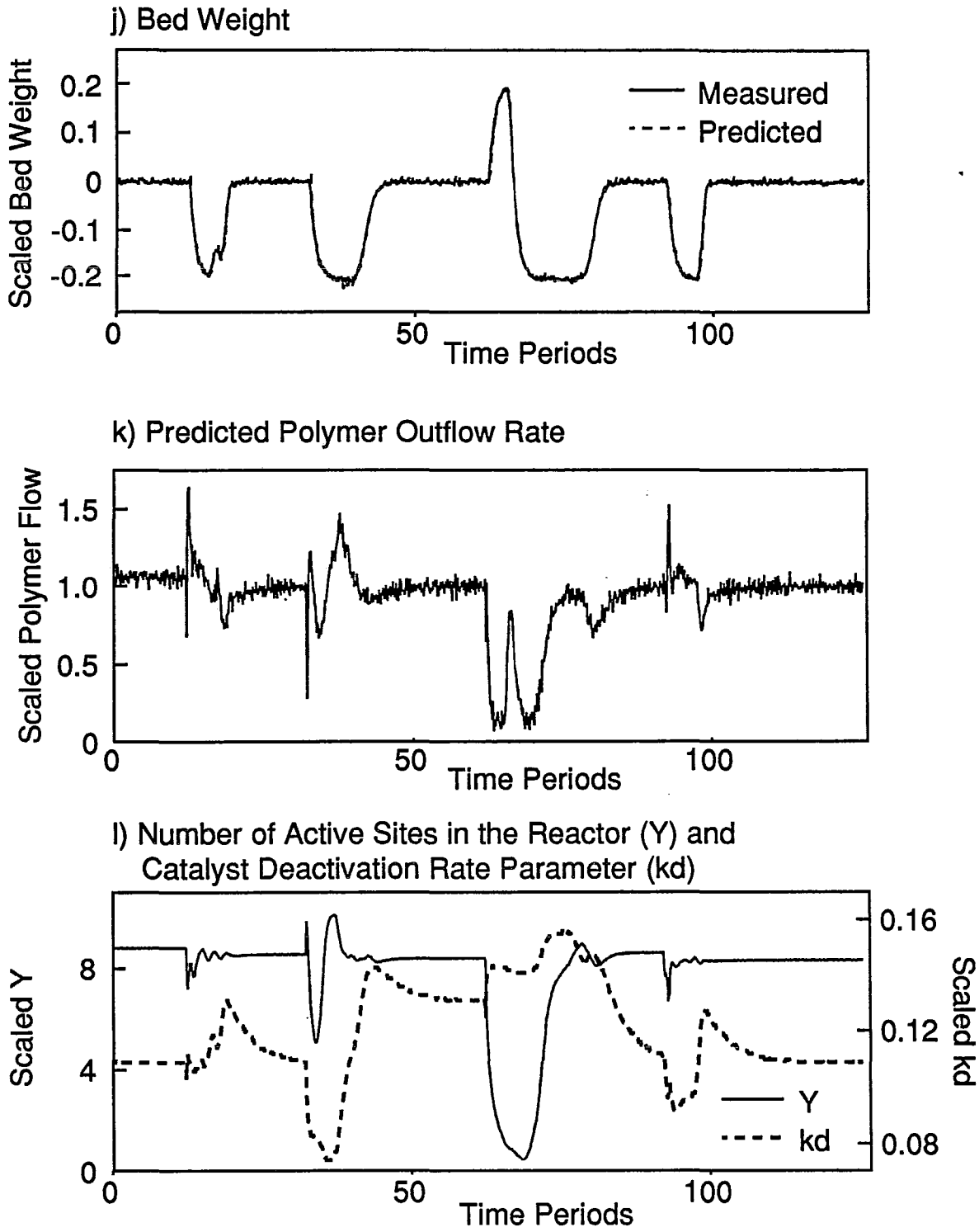

6.8 LINEAR ANALOG TO THE NONLINEAR FEEDFORWARD/FEEDBACK CONTROLLER

To truly illustrate the effectiveness of the combined *EKF* and nonlinear control law, its performance must be compared against that of a known standard controller. Fortunately, it can be shown that a linear decoupled internal model control (*IMC*) design provides a linear analog to the nonlinear control design in section 6.7.

6.8.1 Derivation of the IMC Controller

The first-order decoupled error trajectory in equation 6.21 corresponds to the following discrete time equivalent:

$$\underline{e}(t+h) = \underline{m}\,\underline{e}(t) \tag{6.41}$$

where h is the sampling time, and $\underline{m}$ is a diagonal matrix. The elements of $\underline{m}$ correspond to $\exp(-h/\tau_i)$ where τ_i is the desired first-order closed loop time constant of the i_{th} error response.

If time-invariant linear transfer function models are sufficient to predict the instantaneous product properties in the gas phase polyethylene reactor, then one can write:

$$\underline{Y}(t) = \underline{G}_p\underline{u}(t) + \underline{D}\,\underline{v}(t) + \underline{d}(t) \tag{6.42}$$

where $\underline{G}_p$ is a 2X2 discrete transfer function matrix which relates the manipulated variables u_1 and u_2 to the outputs Y_1 and Y_2. $\underline{D}$ is a 2X4 transfer function matrix which describes how the feedforward variables, $\underline{v}$, affect the output. The elements of $\underline{v}$ are the reactor temperature setpoint, the bleed valve position, the catalyst feed rate, and the bed level setpoint. $\underline{d}(t)$ is a vector of disturbances which are not accounted for in the transfer function models.

The error trajectory specification in equation 6.41 can be rewritten as:

$$\underline{Y}_{sp}(t+h) - \underline{Y}(t+h) = \underline{m}\{\underline{Y}_{sp}(t) - \underline{Y}(t)\} \tag{6.43}$$

Substituting for $\underline{Y}(t+h)$ and $\underline{Y}(t)$ from equation 6.42 gives:

$$\underline{Y}_{sp}(t+h) - \underline{G}_p(t+h) - \underline{D}\,\underline{v}(t+h) - \underline{d}(t+h) = \underline{m}\{\underline{Y}_{sp}(t) - \underline{G}_p\underline{u}(t) - \underline{D}\,\underline{v}(t) - \underline{d}(t)\} \tag{6.44}$$

If one assumes that the best forecast for future values of the disturbance, $\underline{d}(t)$, is that it will remain constant, that is $\underline{d}(t)$ is a random walk or step disturbance then, equation 6.44 can be rearranged to give:

$$\underline{m}\,\underline{G}_p\underline{u}(t) - \underline{G}_p\underline{u}(t+h) = \underline{m}\,\underline{Y}_{sp}(t) - \underline{Y}_{sp}(t+h) - \underline{m}\,\underline{D}\,\underline{v}(t) + \underline{D}\,\underline{v}(t+h) - (\underline{m}-\underline{I})\underline{d}(t+h) \tag{6.45}$$

In the model in equation 6.42, all of the terms in the $\underline{G}_p$ and $\underline{D}$ matrices contain two periods of delay, one for the zero-order hold, and one for the gas composition measurement deadtime. Each of these matrices can be factored as follows:

$$\underline{G}_p = z^{-2}\tilde{\underline{G}}_p \tag{6.46}$$

$$\underline{D} = z^{-2}\tilde{\underline{D}} \tag{6.47}$$

where $\tilde{\underline{G}}_p$, the undelayed portion of the transfer function model, is invertible. Since $\underline{u}(t) = z^{-1}\underline{u}(t+h)$, equation 6.45 can be rewritten as:

$$(\underline{m}z^{-1}-\underline{I})\tilde{\underline{G}}_p z^{-2}\underline{u}(t+h) = (\underline{m}z^{-1}-\underline{I})\underline{Y}_{sp}(t+h) - (\underline{m}z^{-1}-\underline{I})\tilde{\underline{D}}z^{-2}\underline{v}(t+h) - (\underline{m}-\underline{I})\underline{d}(t) \tag{6.48}$$

Right multiplication of both sides by $(\underline{m}z^{-1}-\underline{I})^{-1}$ and then by $\tilde{\underline{G}}_p^{-1}$ gives:

$$z^{-2}\underline{u}(t+h) = \tilde{\underline{G}}_p^{-1}z^{-1}\underline{Y}_{sp}(t+2h) - \tilde{\underline{G}}_p^{-1}\tilde{\underline{D}}z^{-2}\underline{v}(t+h) - \underline{F}z^{-1}\underline{d}(t+h) \tag{6.49}$$

where

$$\underline{F} = (\underline{I}-\underline{m}z^{-1})^{-1}(\underline{I}-\underline{m}) \tag{6.50}$$

Dividing both sides of equation 6.49 by z^{-1}, and assuming that $\underline{d}(t+h) = \underline{d}(t)$, leads to the following expression for the control law:

$$\underline{u}(t) = \tilde{\underline{G}}_p^{-1}\underline{Y}_{sp}(t+2h) - \tilde{\underline{G}}_p^{-1}\tilde{\underline{D}}\,\underline{v}(t) - \underline{F}\,\underline{d}(t) \tag{6.51}$$

This linear controller can be implemented in the *IMC* form shown in Figure 6.11 wherein $\underline{G}^*$ and $\underline{D}^*$ represent the true process. This is a standard *IMC* feedback control structure, with added feedforward action. $\underline{Y}_{sp}(t+2h)$ is constant for regulation at a single grade. During grade changeovers, the future setpoints can be obtained from the optimal grade transition trajectories of Chapter 5. Note that the setpoint trajectory is not filtered, but first-order filtering is performed along the disturbance and mismatch path. The identification of linear transfer function models for this *IMC* controller is discussed in section 6.8.2. The behaviour of the linear controller has been simulated for both disturbance rejection and grade changeovers. The results are shown in section 6.8.3.

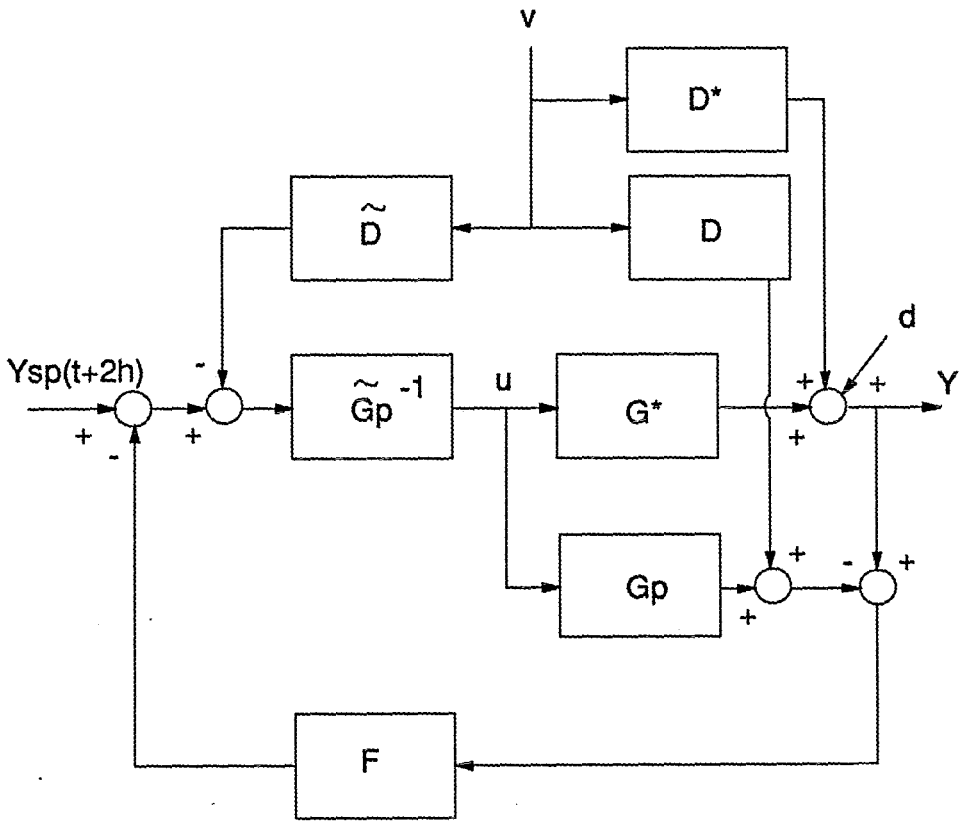

Figure 6.11 Linear IMC Analog of the Nonlinear Controller

6.8.2 Transfer Model Identification for the linear IMC Controller

A series of step tests was performed on the full nonlinear plant model to determine the set of discrete transfer function models shown in Table 6.1. The sampling interval for these models is $h = 0.141667$ time periods. Note that transfer function models relating the catalyst feed rate and the bed level setpoint to the instantaneous product properties are not included in the table. In section 6.8.3, the

feedforward/feedback controller is tested on Policy II and Policy IV transitions, only. As a result the additional four transfer function models are not required to perform the simulations. The transfer functions in Table 6.2 were identified from the full model response to small upward and downward step tests. These step tests were performed about the steady state conditions for Grade A. No measurement noise was used in the step test simulations. The magnitudes of the steps used in the model identification are given in Table 6.3.

Table 6.2 Transfer Function Models Used in IMC Design

	Scaled Output Deviation Variable	
Scaled Input Deviation Variable	Y_1 $\ln(MI_i)$	Y_2 ρ_i
u_1 Hydrogen Feed	$\frac{0.16054z^{-2}}{1 - 0.98561z^{-1}}$	$\frac{0.16443z^{-2}}{1 - 0.98351z^{-1}}$
u_2 Butene Feed	$\frac{0.15757z^{-2}}{1 - 0.8891z^{-2}}$	$\frac{-1.577625z^{-2}}{1-0.9023z^{-1}}$
v_1 Temperature Setpoint	$\frac{0.7596z^{-2}-0.8298z^{-3}-0.05152z^{-4}+0.1306z^{-5}}{1 - 0.9748z^{-1}}$	$\frac{-0.0044725z^{-2}+0.03579z^{-3}}{1 - 0.7091z^{-1}}$
v_2 Bleed Valve Position	$\frac{-0.02269z^{-2}}{1 - 0.9771z^{-1}}$	$\frac{0.00105425z^{-2}-0.00106525z^{-3}}{1 -1.728z^{-1} +0.7324z^{-2}}$

Table 6.3 Step Sizes for Transfer Function Identification

Manipulated Variable	Scaled Step Size in Scaled Units
u_1 Hydrogen Feed	± 0.01111
u_2 Butene Feed	± 0.0014286
v_1 Temperature Setpoint	± 0.5
v_2 Bleed Valve Position	± 0.2

6.8.3 Linear Controller Testing

The linear decoupled IMC controller shown in Figure 6.11 was designed using the models in Table 6.2. Both m_1 and m_2 were set at 0.86791 to correspond to the first-order closed loop time constant of 1 time period used in the nonlinear controller design.

6.8.3.1 Controller Performance without Model Mismatch

The nominal response of the controller was tested for setpoint changes, disturbance rejection, and changes in the feedforward variables. The linear transfer function models in Table 6.2 were used in place of the nonlinear plant

model to demonstrate the controller performance without plant/model mismatch. The simulation results are shown in Figure 6.12a) to d). During the first 5 time periods, step set point changes in both MI_i and ρ_i were performed. These steps are followed exactly by the outputs since there is no setpoint filter in the controller design. Also, the output response is perfectly decoupled. The response to a set of step disturbances was tested between time periods 5 and 15. As specified in the design, the output response, for both Y_1 and Y_2, is first-order with a closed loop time constant of 1 time period. Between time periods 15 and 30, the response to changes in the temperature and bleed valve position is shown. The controller compensates perfectly for changes in the feedforward variables by manipulating the hydrogen and butene feed rates. No change in either Y_1 or Y_2 occurs.

The simulations in Figure 6.12 were repeated with measurement noise added to MI_i and ρ_i. These simulation results, shown in Figure 6.13 are very similar. Ringing of the manipulated variables does not occur, even though the model-inverse used in the controller design has poles at -0.98368 and -0.89035.

Figure 6.12 Nominal Performance of Linear IMC Controller

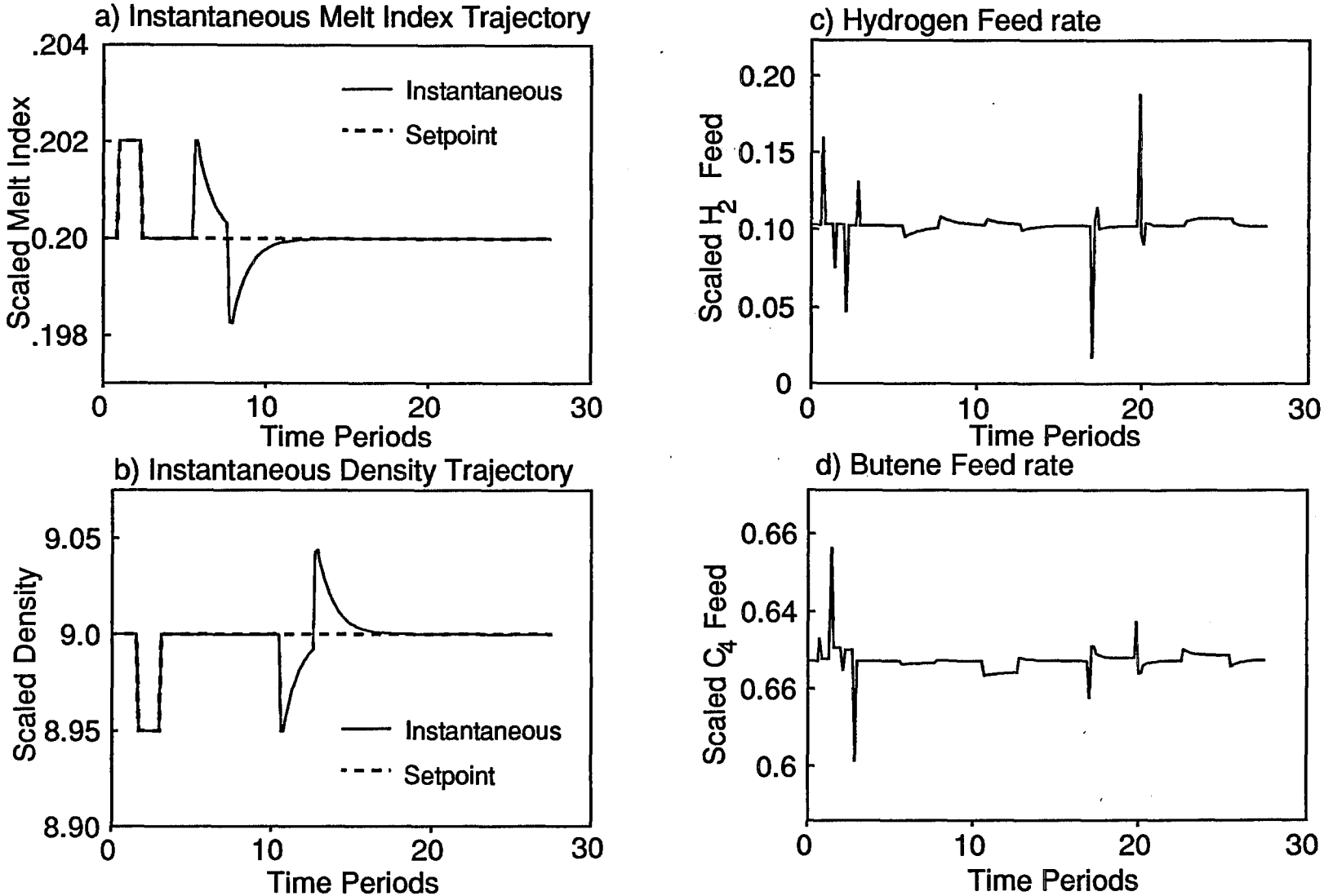

Figure 6.13 Nominal Linear Controller with Measurement Noise

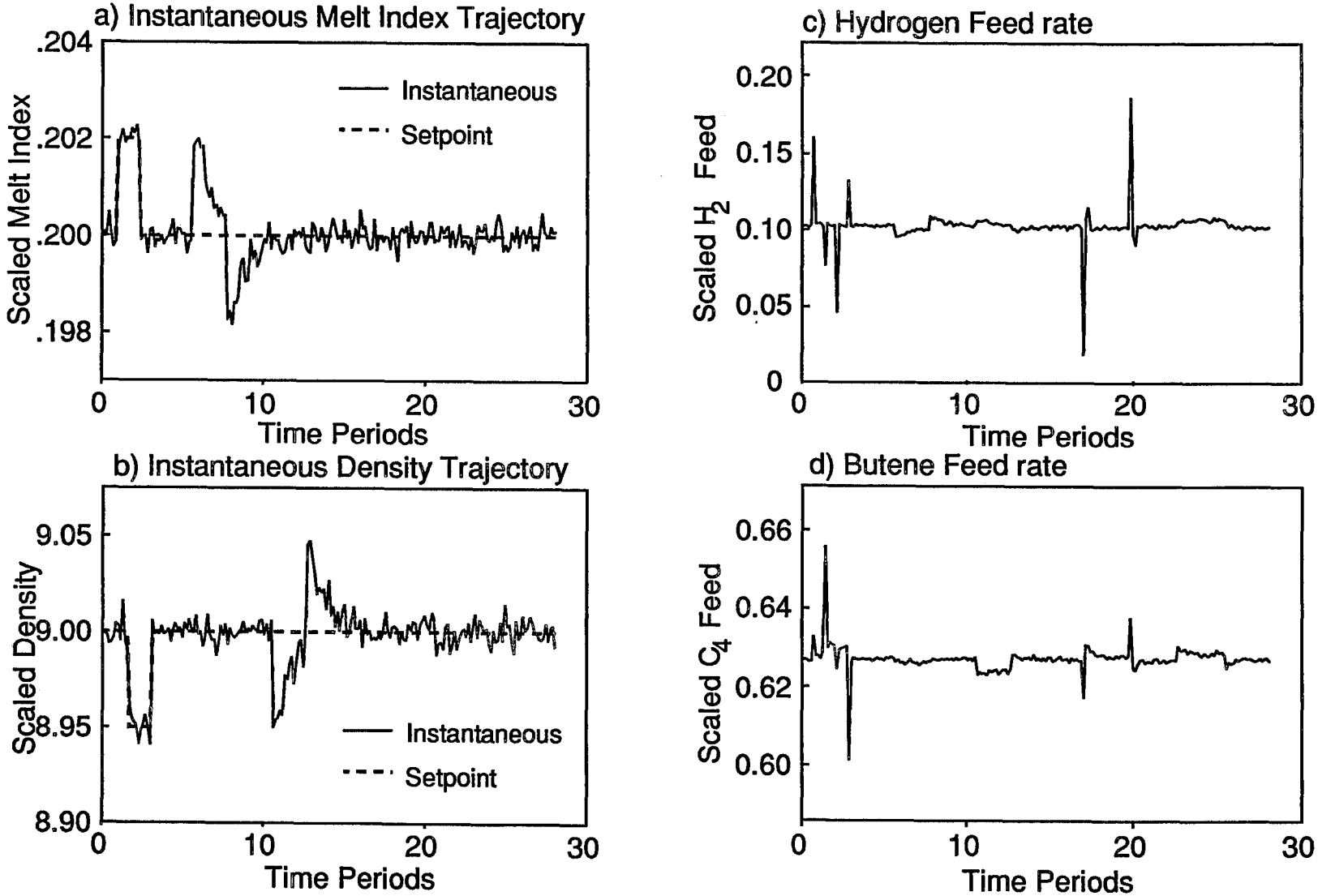

6.8.3.2 Controller Performance on the Full Nonlinear Plant Model

The linear controller was tested for small step setpoint changes from Grade A where the transfer function models were identified. As shown in Figure 6.14, the controller performed very well. To test the linear controller's disturbance rejection capabilities, catalyst feed quality changes, of the same size as those in section 6.7.4, were simulated for reactor operation at both Grades A and C. In Figure 6.15, which corresponds to the production of Grade A polymer, the controller performed well. However, when the same disturbance was simulated during Grade C production, the closed-loop response considerably worse. Due to mismatch between the linear models and the plant, the instantaneous melt index is away from its setpoint for a longer time (Figure 6.16).

To test how the linear controller might perform during grade changeovers, two sets of transitions were simulated. In the first, shown in Figure 6.17, very slow grade transitions are followed. The setpoint trajectories for Y_1 and Y_2 were determined by setting the hydrogen and butene feed rates at their steady state values for the next grade, and then holding them constant. The manipulated variable policies chosen by the linear controller are similar to the optimal step policies required to achieve the exact setpoint trajectories. While there is some mismatch between MI_i and its setpoint between time periods 100 and 150, in the long term, the controller is able to remove steady state offset. The offset persists for a long time due to mismatch between the linear model predictions and the nonlinear plant behaviour (Figures 6.17 e) and f)).

The feedback portion of the controller responds to this mismatch in the same manner as it does to disturbances The difference between the predicted and measured values of $\ln MI_i$ grows quickly between time periods 80 and 120, so that the mismatch seen by the controller is more like a ramp than a step disturbance. Since the controller has not been designed for this type of disturbance, its performance is poor between time periods 100 and 150.

In Figure 6.18, simulation results are shown for the *IMC* controller implementation, during a series of optimal grade transitions from Chapter 5. As in Figure 6.9, the $A \rightarrow B$ and $B \rightarrow A$ transitions correspond to transition policy II and the $B \rightarrow C$ and $C \rightarrow B$ transitions correspond to transition policy IV. As shown in Figures 6.18 a) and b), the manipulated variable trajectories determined by the controller are very different from the optimal trajectories. As a result, the output performance of the controller is very poor. Although offset is removed at steady state, the actual trajectories of MI_i and ρ_i are far from their respective setpoint trajectories throughout all four grade transitions.

The reason for this poor performance is model mismatch. Shown in Figure 6.18 e) and f) are the true behaviour of the nonlinear plant and the predicted responses of the true models. The reactor temperature setpoint and the bleed valve position were used as feed forward variables during the $B \rightarrow C$ and $C \rightarrow B$ transitions. Their contributions to the predicted responses are shown, as solid lines, in Figures 6.18 e) and f). Regardless of whether or not the feed forward variables are used to accomplish grade changeovers, the performance of the linear *IMC* controller is inadequate for following the optimal grade transition policies.

The behaviour of the process is too nonlinear to be adequately described by linear models and their inverses. A nonlinear design, like the one proposed in section 6.7, is far superior.

Figure 6.14 Controller Response for Small Step Setpoint Changes

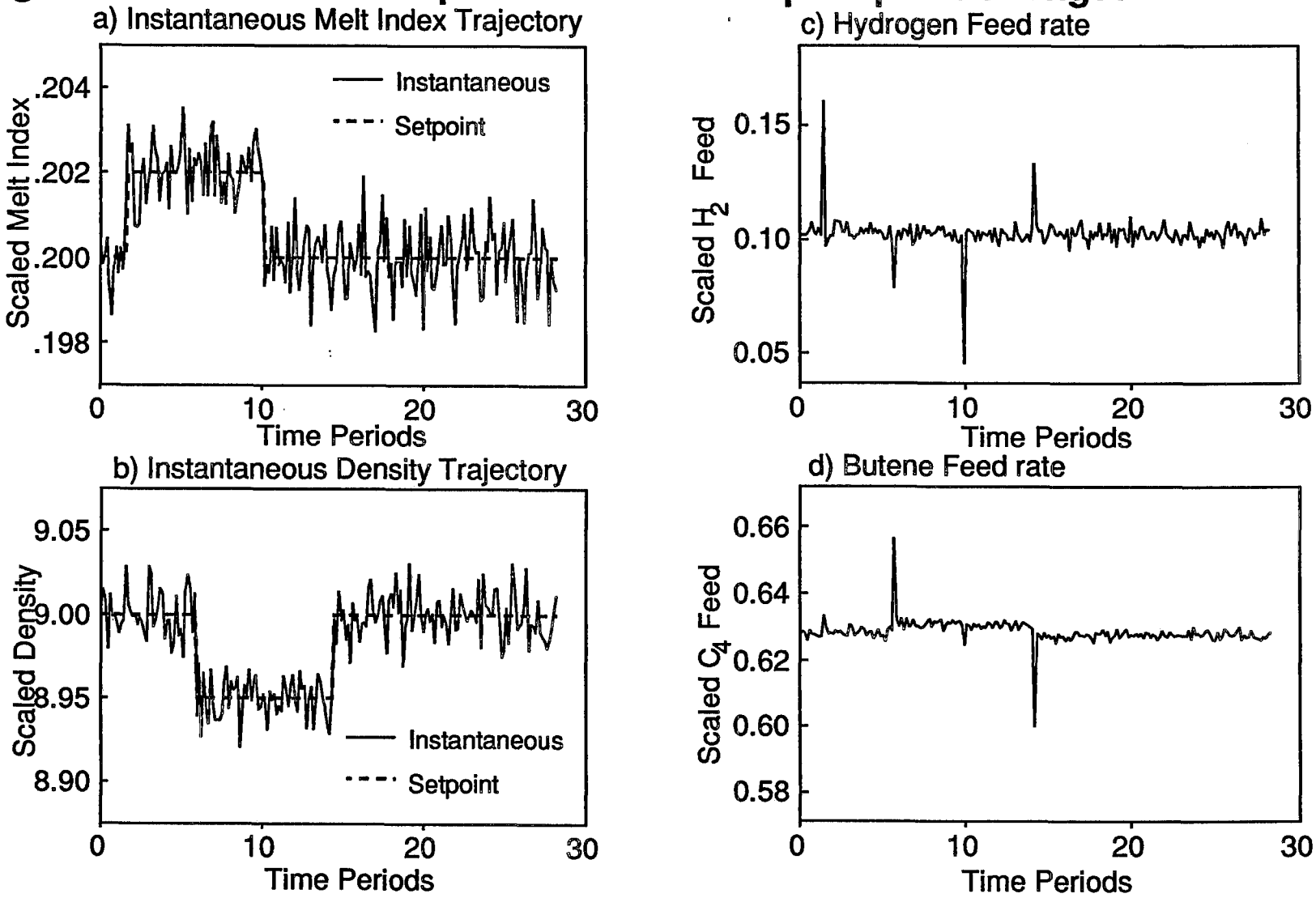

Figure 6.15 Controller Response to Catalyst Feed Quality Disturbance: Grade A

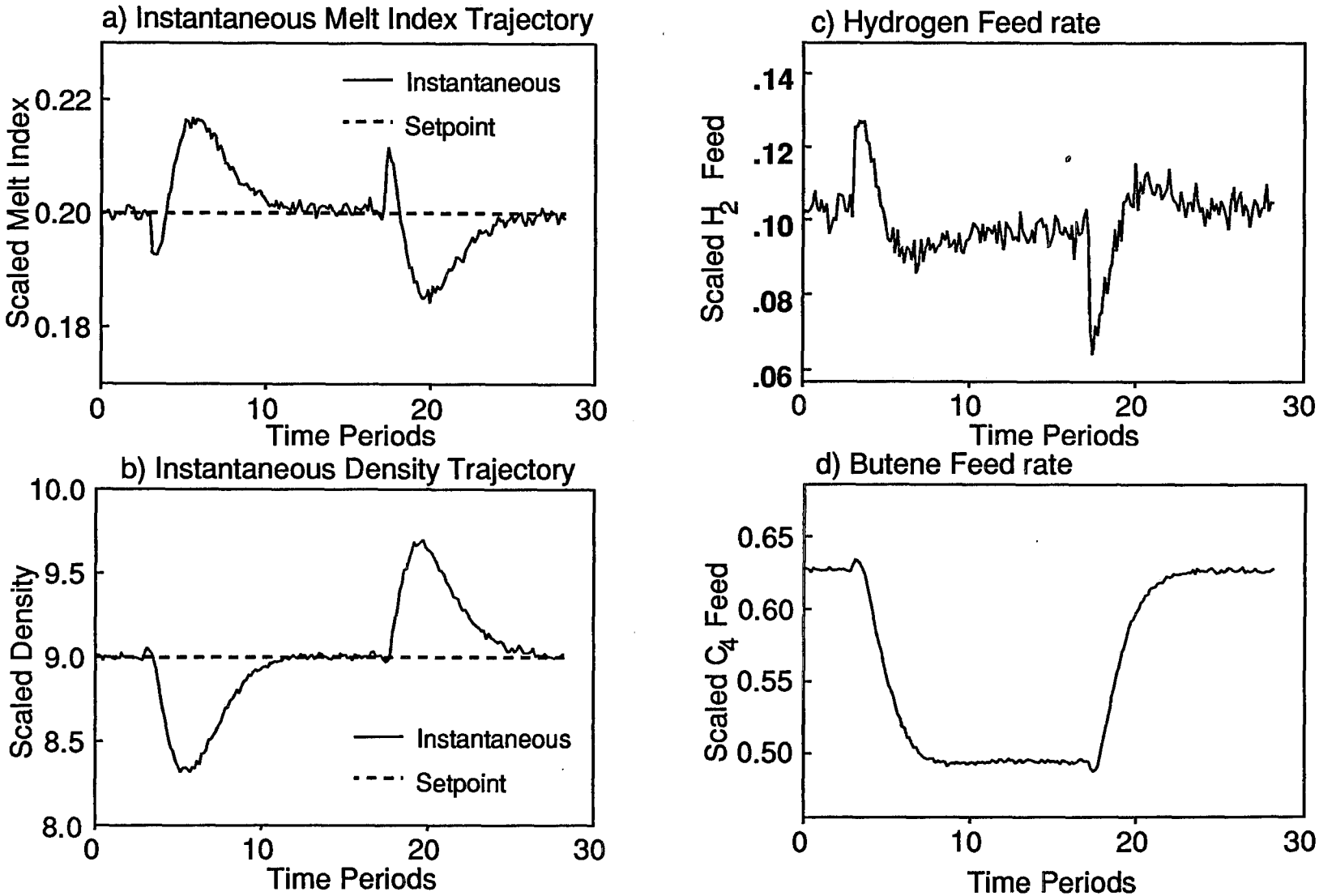

Figure 6.16 Controller Response to Catalyst Feed Quality Disturbance: Grade C

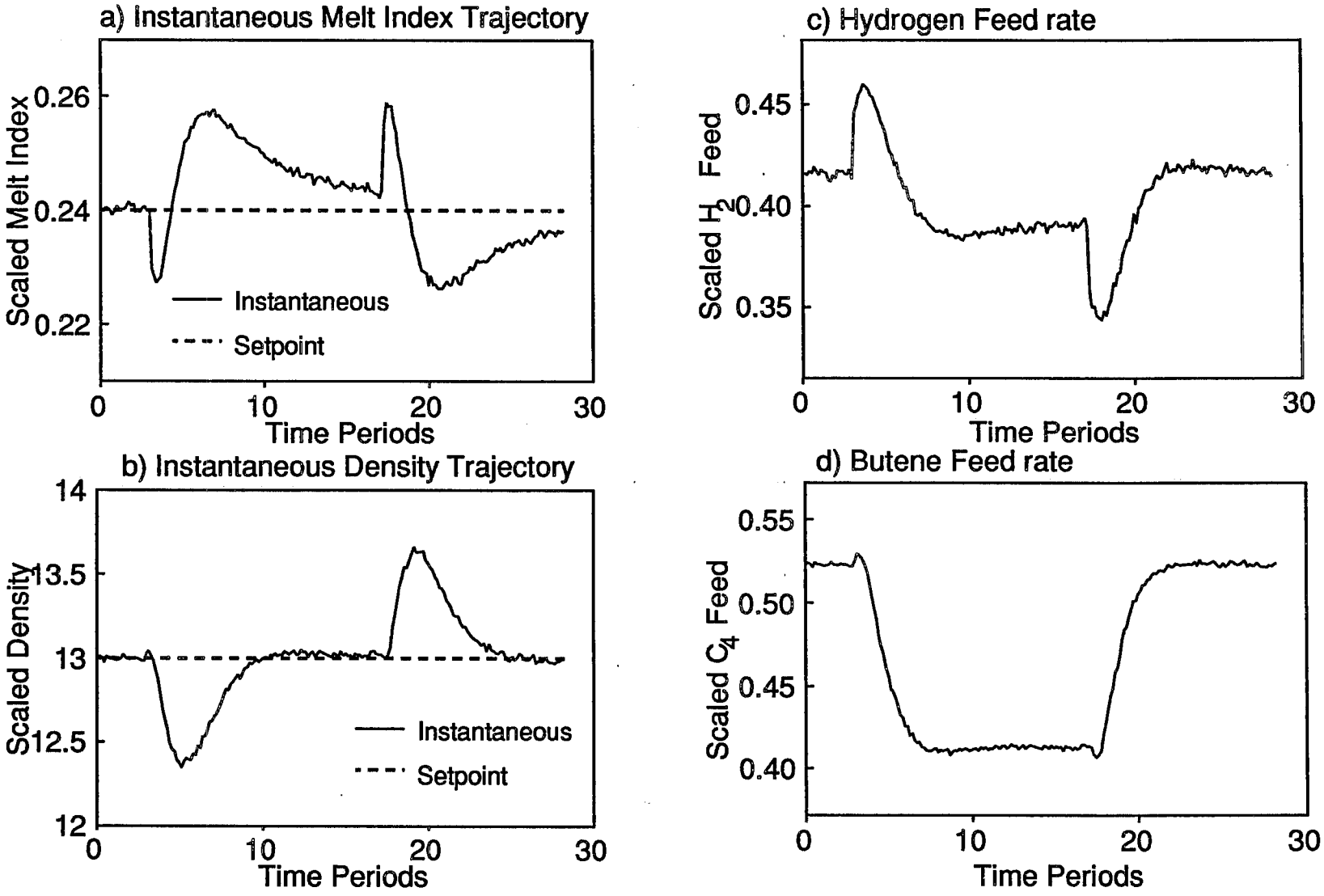

Figure 6.17 Following Simple Setpoint Trajectories with the Linear IMC Controller

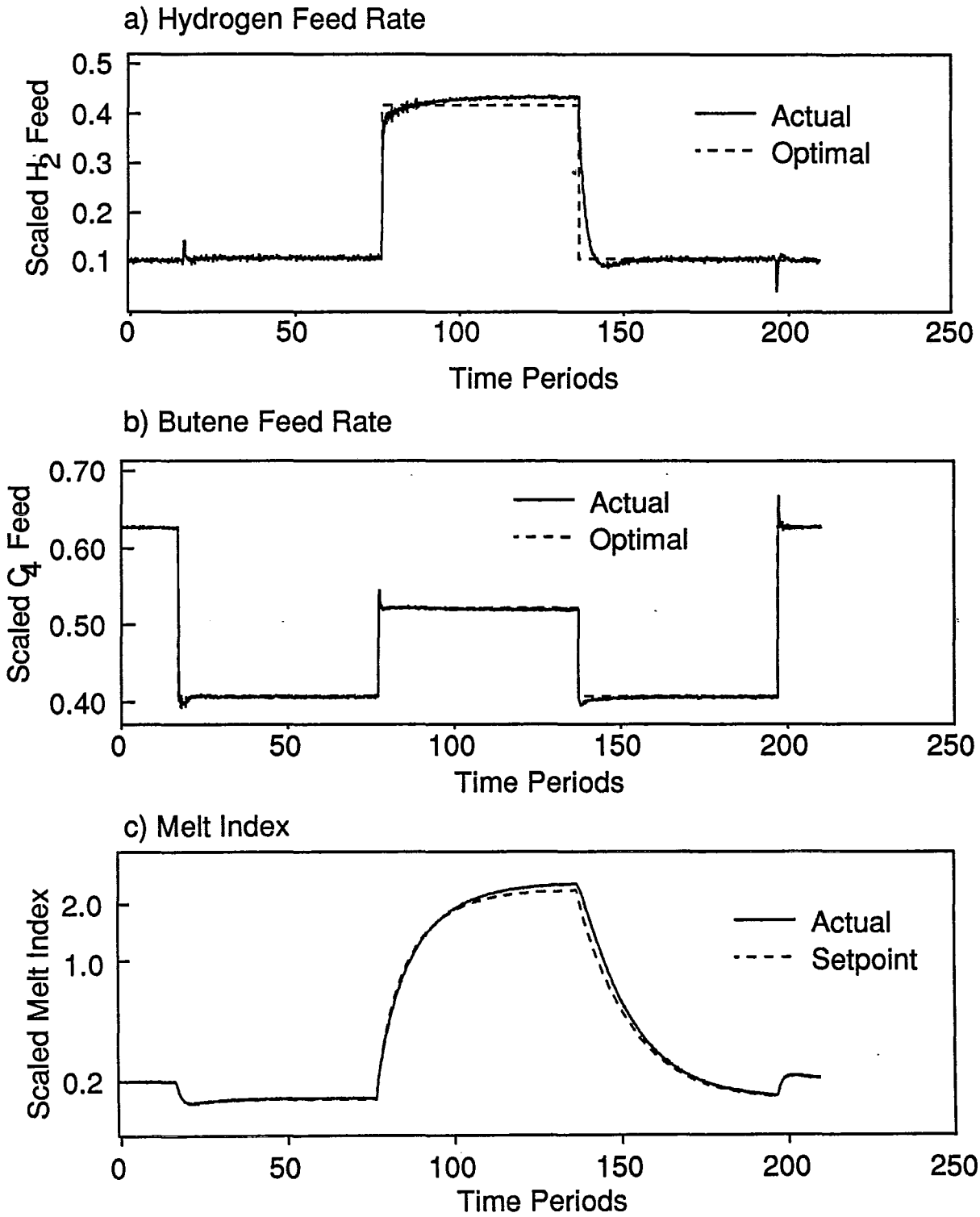

Figure 6.17 Following Simple Setpoint Trajectories with the Linear IMC Controller

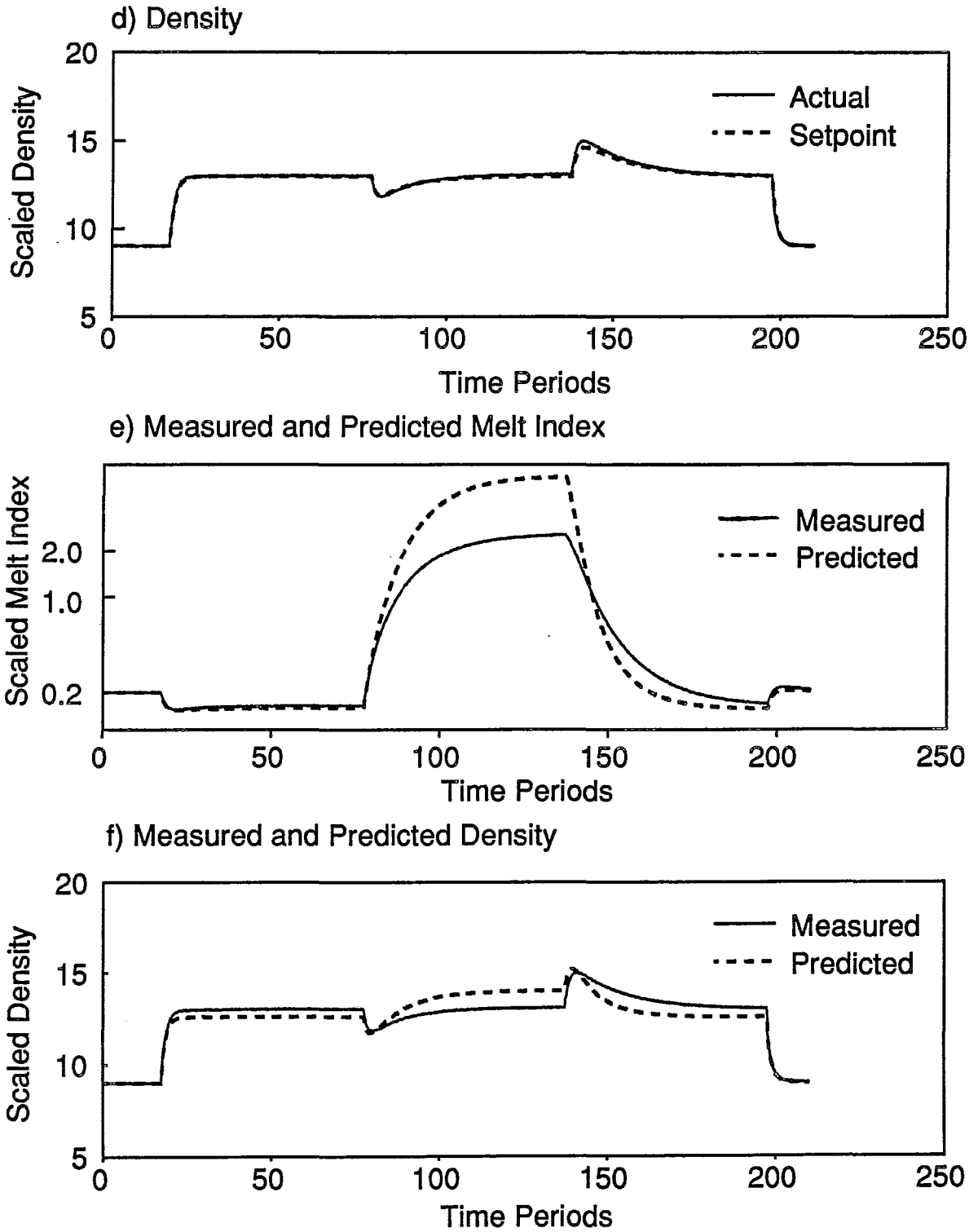

Figure 6.18 Implementation of Policies II and IV with the Linear IMC Controller

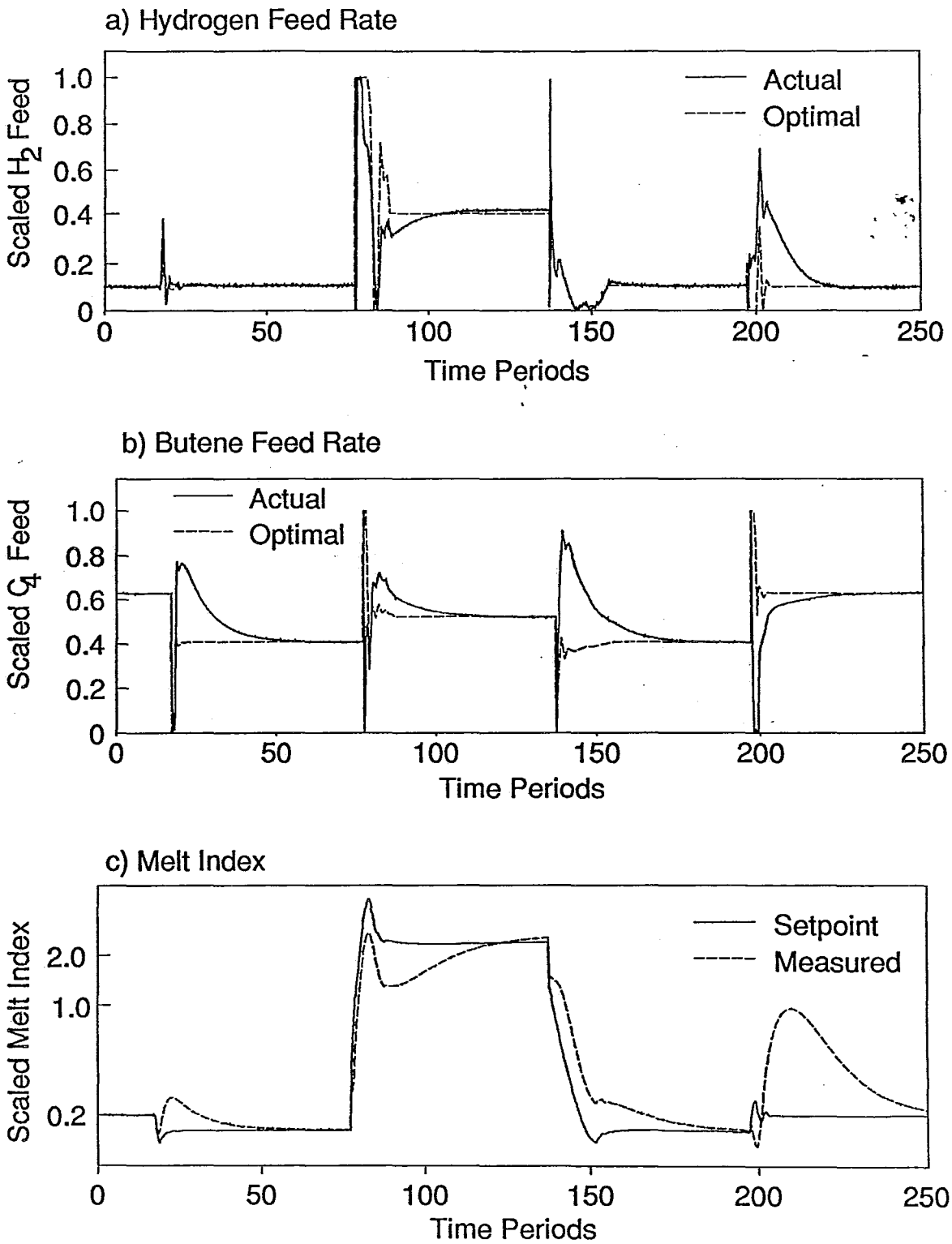

Figure 6.18 Implementation of Policies II and IV with the Linear IMC Controller

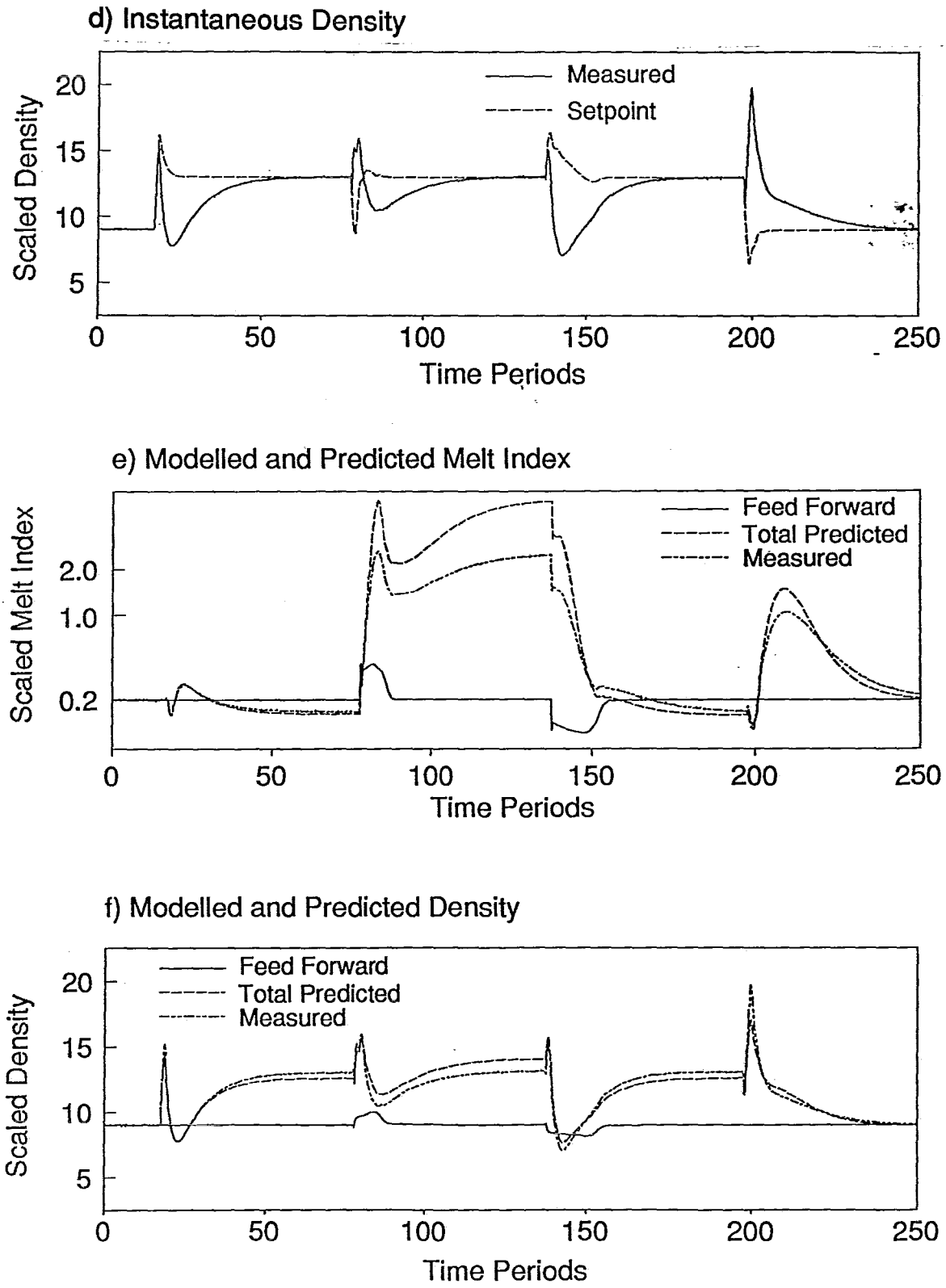

6.9 OPTIMAL HANDLING OF MANIPULATED VARIABLE SATURATION

In the optimal grade transition policies determined in Chapter 5, both the hydrogen and butene feed rates are held at their bounds for extended periods of time. Therefore, it is crucial that any feedback controller used to implement these policies must be able to deal adequately with manipulated variable saturation. The simulations show in section 6.7 have not made use of optimal saturation handling procedures. Because the limiting values, rather than the calculated control actions, were used in all subsequent calculations, wind-up did not occur. In this section an optimal means of handling saturation is presented.

The input saturation problem is easily handled for linear multivariable controllers (Segall et al., 1991), and can be broken into the following two steps. First, the bounded variables are set at their limits and the implemented control actions, rather than the calculated values, are used in future control calculations. The second step involves solving for a simultaneous adjustment used to correct the remaining unsaturated inputs. For linear controllers, this simultaneous correction step involves a simple closed form calculation.

A similar approach can be adopted for handling input saturation with multivariable nonlinear controllers. The first step of identifying saturated inputs and setting them to their limitting values is analogous to the linear control problem. However, no general analytical solution is available for the simultaneous correction of unbounded variables. Spong et al. (1986) suggest determining the positions of the unconstrained manipulated variables by solving a quadratic program on-line. However, for the 2X2

system considered in this thesis, when one of the manipulated variables saturates, only one other free variable must be determined. Thus, an analytical solution to the optimization problem can be found.

Without manipulated variable saturation, the control law is given by:

$$\dot{Y}_{1sp} - \dot{Y}_1 - \kappa_1(Y_{1sp} - Y_1) = 0 \tag{6.52}$$

$$\dot{Y}_{2sp} - \dot{Y}_2 - \kappa_2(Y_{2sp} - Y_2) = 0 \tag{6.53}$$

When one manipulated variable saturates, both of these equations cannot be solved simultaneously. The best that can be achieved is to minimize the weighted sum of squares:

$$J = w\{\dot{Y}_{1sp} - \dot{Y}_1 - \kappa_1(Y_{1sp} - Y_1)\}^2 + \{\dot{Y}_{2sp} - \dot{Y}_2 - \kappa_2(Y_{2sp} - Y_2)\}^2 \tag{6.54}$$

If u_1 is saturated, then one must determine u_2 so that:

$$\frac{\partial J}{\partial u_2} = 0 \tag{6.55}$$

This condition is satisfied at only one value of u_2, which can be determined by substituting equations 6.17, 6.18, and 6.25 to 6.32 into equation 6.54 and then differentiating with respect to u_2. A similar expression can be derived for u_1 when u_2 saturates.

In Figure 6.19, the system response to hydrogen feed saturation is tested during a Policy V $B \rightarrow C$ transition, for several values of w. In these simulations, when the hydrogen feed valve is fully open, the hydrogen feed flow is only 90% of the maximum flow in Figure 6.10. As a result, the setpoint trajectory cannot be followed exactly, and the hydrogen feed rate, shown in Figure 6.19 c) remains saturated at its upper limit for a protracted period of time. In Figure 6.19a), the instantaneous melt index is shown with the optimal saturation protection off, with $w = 25$, and with $w = 2500$. The choice of $w = 25$ corresponds to the same relative weighting between MI and ρ as that used to

develop the optimal policies in Chapter 5. $w = 2500$ places more emphasis on following the MI_i trajectory, at the expense of larger density deviations. As shown in Figures 6.18 a) and b), the output response with $w = 25$ is nearly identical to that without the simultaneous correction to u_2. However, when $w = 2500$, the controller responds to the hydrogen feed saturation by increasing the butene feed rate. Thus, MI_i is much closer to its setpoint than with the saturation handling turned off. However, this improvement in MI_i is achieved at the expense of a large deviation between ρ_i and its setpoint trajectory.

The discussion of manipulated variable saturation in this section has assumed a square controller structure, with hydrogen and butene feed rates as the manipulated variables. If the performance of this controller proves unsatisfactory, then an additional manipulated variable could be incorporated into the feedback control scheme. Since saturation of the hydrogen feed is common, perhaps the best choice of an additional variable is the bleed valve position. Opening or closing the bleed valve when the hydrogen saturates could be used to hasten the return of MI_i and ρ_i onto the nonimal trajectories. When hydrogen is not saturated, the controller can revert back to its original structure. Such a control scheme would involve the separate design of two 2X2 nonlinear controllers. The first controller would be that designed in section 6.7, and the alternative controller would use the bleed valve position and the butene feed rate to achieve the nominal trajectories. If calculation of u_1 and u_2 from the first controller results in a saturated hydrogen feed rate, then the second controller would be used to determine both the butene feed rate and the bleed valve position, to follow the desired trajectory. At each successive control interval, first the manipulations from the primary controller would be calculated with the bleed valve at its nominal feedforward position, and then then manipulations from the secondary controller with the hydrogen feed at its limit. As soon as the hydrogen feed calculated from the primary controller is no longer beyond

its limit, then the original controller would be used. The bleed valve position provides a natural choice for the alternative manipulated variable because it can be included explicitly in the gas mass balance model, and the relative order between this manipulated variable and MI_i and ρ_i is unity. Thus, the design of the secondary controller would be analogous to that of the primary controller in Section 6.7.

Figure 6.19 Optimal Saturation Handling for BC Transition with Maximum Hydrogen feed of 0.9

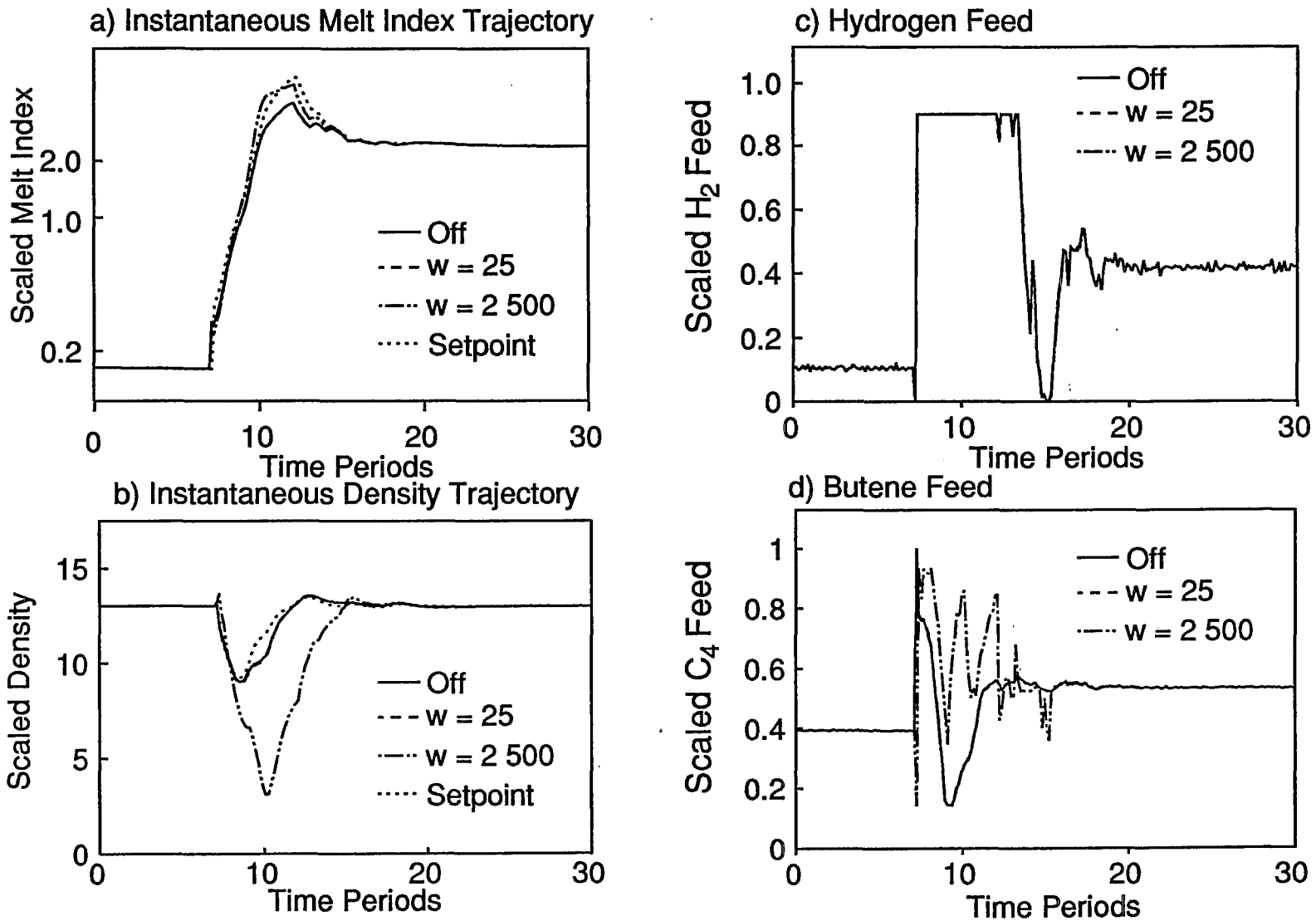

6.10 EFFECT OF THE PRODUCT PROPERTY INFERENCE SCHEME ON THE *EKF* AND THE NONLINEAR CONTROLLER

The combined response of the on-line property prediction scheme, the EKF, and the nonlinear controller has been tested for a step impurity disturbance in the reactor feed. Impurities are fed to the full reactor model at time period 25 (Figure 6.20a)). As the concentration of impurities builds, so does the rate of deactivation of catalyst sites. Each time a catalyst site is deactivated, a dead polymer chain is formed. Therefore, impurities are a major source of disturbances for molecular weight or melt index control. The concentration of impurities affects the value of $k_5[I]/[M_1]$ in equation 4.23, which influences the true value of k_0 in equation 4.65. Shown in Figure 6.20b) are the true value of k_0, and that estimated by the on-line property inference scheme. A new value of k_0 is estimated each time a laboratory result becomes available, and this estimate is used in the controller calculations until the next measurement is obtained. The true value of k_0 begins to rise at time 25 as the concentration of impurities begins to build. This rise in k_0 causes both the instantaneous and cumulative melt index to increase, as shown in Figure 6.20. The on-line property inference scheme detects the change in k_0 from the prediction error in $\ln(MI_c)$. As shown in Figure 6.20 c), between periods 30 and 50, the measured values of MI_c are consistently higher than the predicted values. The *RPE* algorithm responds by increasing the estimate of k_0, which is used by the on-line controller.

In Figure 6.20c), the predictions for MI_c with the old values of k_0 continue for four sampling intervals after the time corresponding to the measurement. These four time intervals correspond to the laboratory measurement delay used in the simulation.

Once the measurement delay has passed, then the new value of k_0 is used in the nonlinear controller, and the model predictions for these four gas sampling intervals are recalculated.

As active sites are poisoned by impurities, the production rate drops (Figure 6.20). The *EKF* accounts for the drop in production rate by increasing the catalyst deactivation rate constant, k_d, (Figure 6.20g)), which allows Y, the estimated number of active sites in the reactor (Figure 6.20 f)), to decrease. The nonlinear controller responds to both the impurity effect on melt index, and the lower production rate through a modest decrease in the hydrogen feed rate, and a larger decrease in the butene feed rate. These actions by the feedback controlled bring the true value of MI_i back to its setpoint, as shown in Figure 6.20c).

At time period 55, an $A \rightarrow B$ grade transition is implemented, followed by a $B \rightarrow C$ transition. Both changeovers use optimal policy V. The bleed valve is closed for a portion of the $B \rightarrow C$ transition, causing the level of impurities in the reactor to rise. This rise in the impurity concentration causes the true value of k_0 to increase (Figure 6.20b)). Fortunately, the production rate is very low during this period, so that the impurities have very little effect on MI_c. For this reason, the on-line inference scheme is unable to detect the rise in k_0. Even with the impurities in the reactor, the controller is able to track the instantaneous melt index trajectory in Figure 6.20e) very closely. This instantaneous melt index trajectory corresponds to the cumulative melt index trajectory in Figure 6.20c). The impurity simulated had no effect on ρ_0, the density update parameter, which is not shown in Figure 6.20. The instantaneous density setpoint trajectory was followed closely during the $A \rightarrow B$ and $B \rightarrow C$ changeovers.

Figure 6.20 Operation of the On-line Property Inference Scheme and the Nonlinear Controller in Response to Impurities

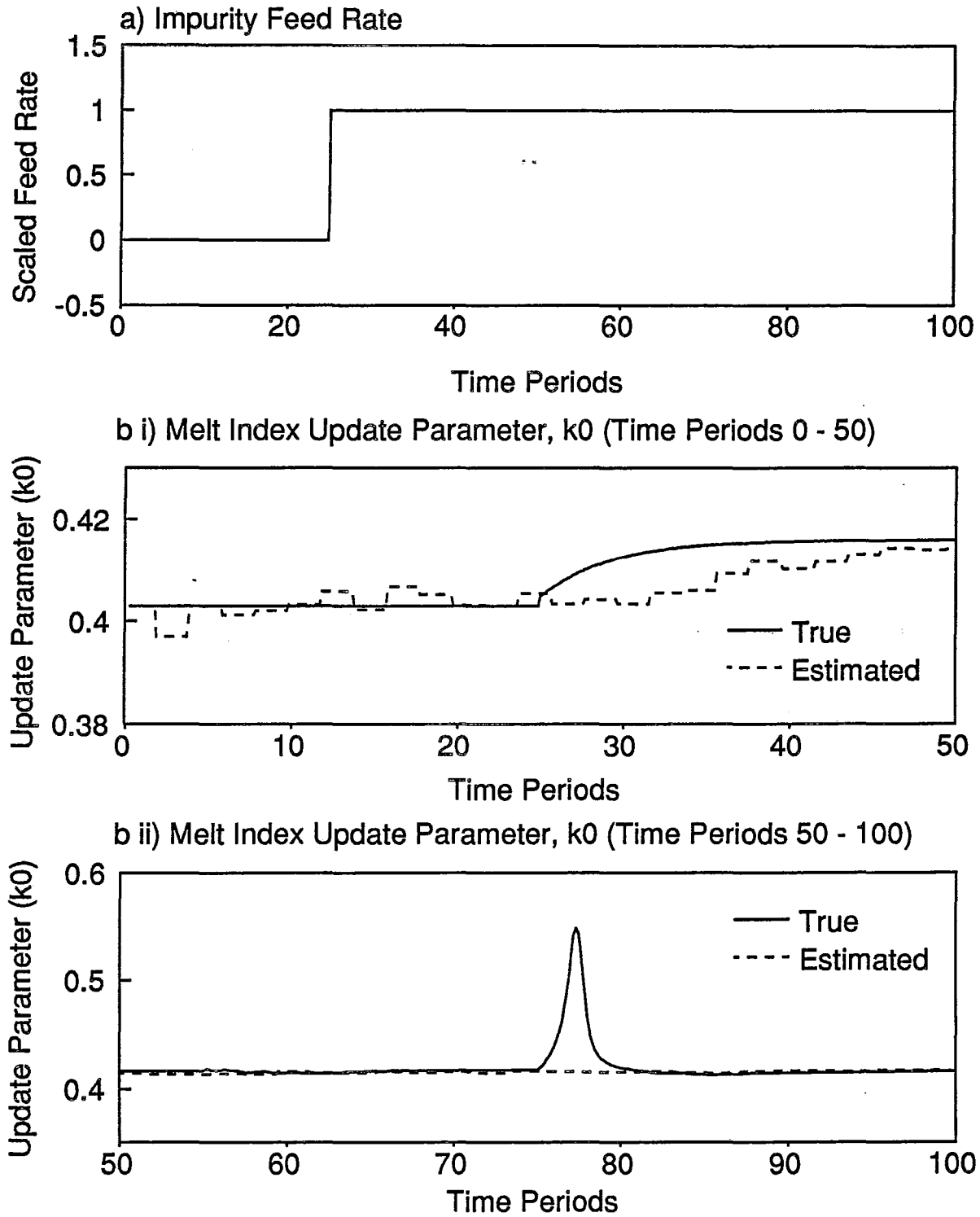

Figure 6.20 Operation of the On-line Property Inference Scheme and the Nonlinear Controller in Response to Impurities

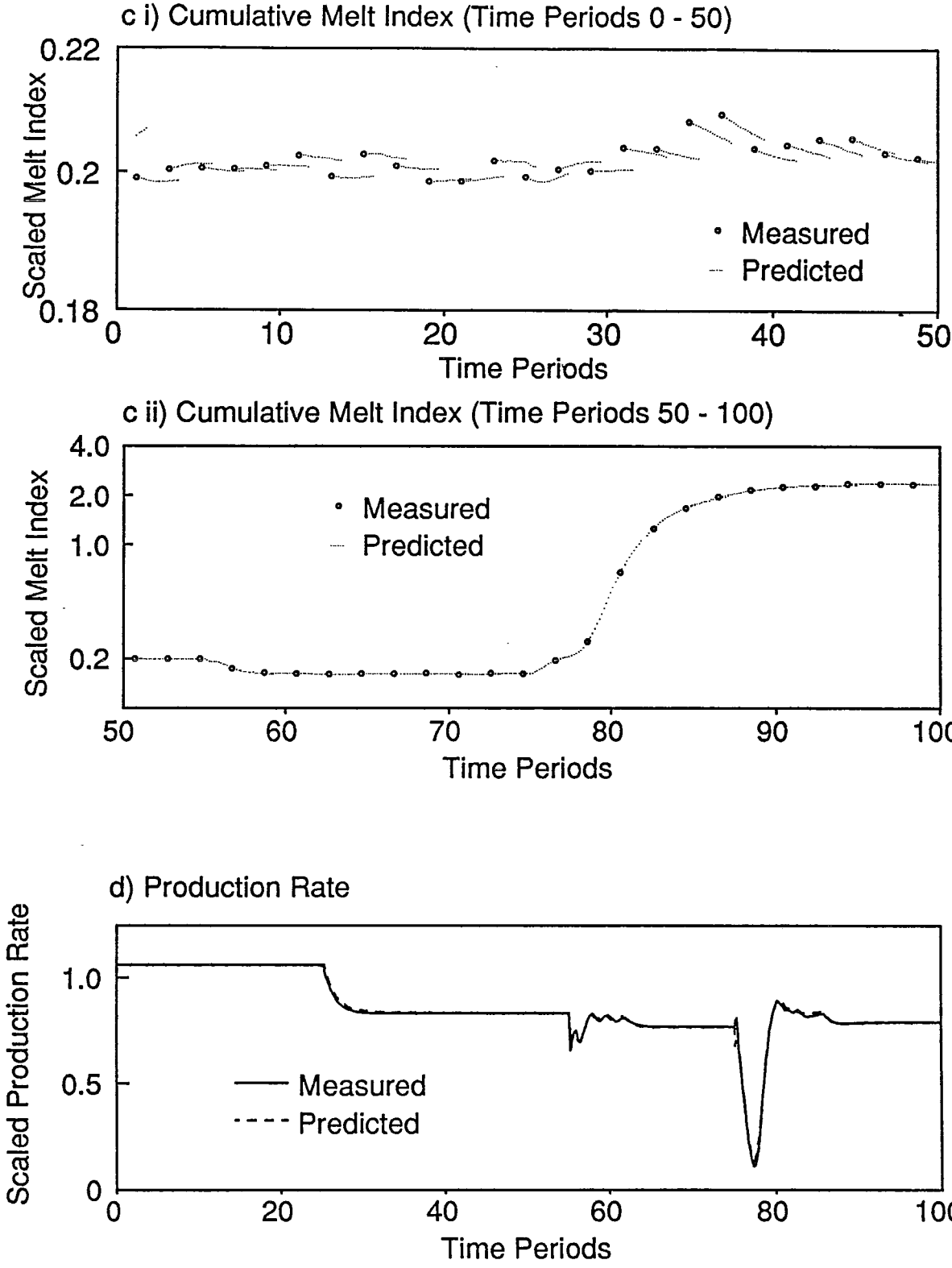

Figure 6.20 Operation of the On-line Property Inference Scheme and the Nonlinear Controller in Response to Impurities

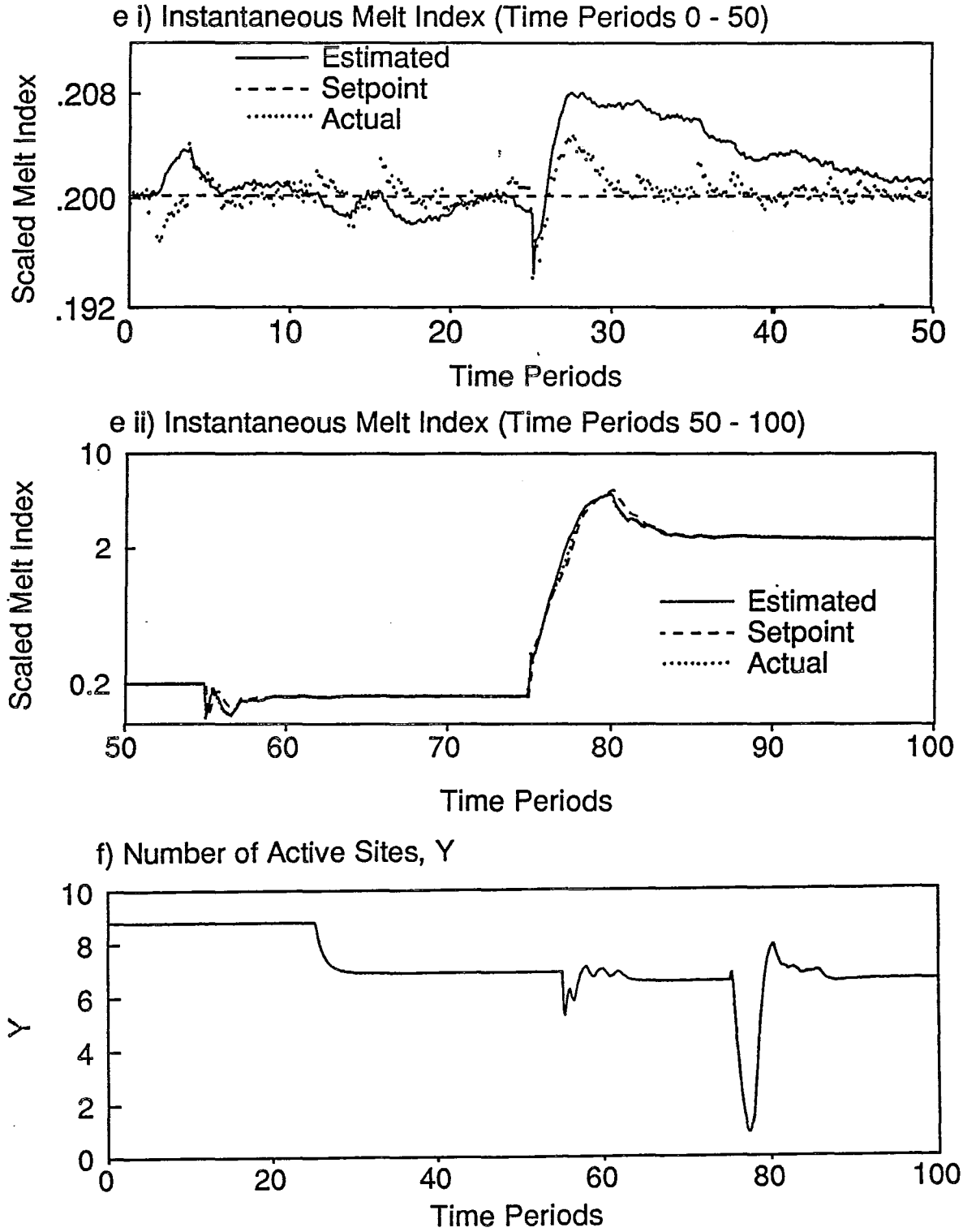

Figure 6.20 Operation of the On-line Property Inference Scheme and the Nonlinear Controller in Response to Impurities

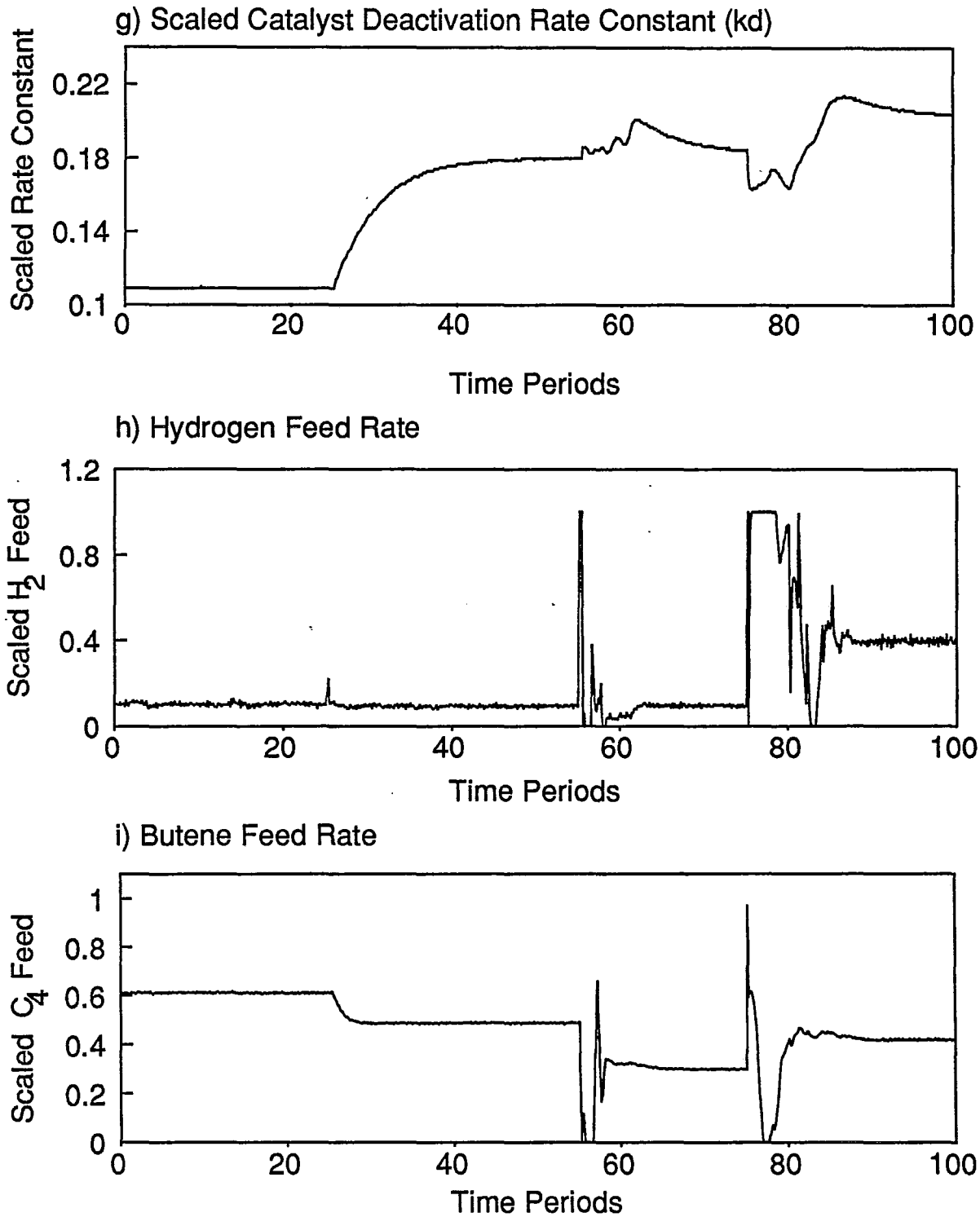

6.11 CONCLUSIONS

The nonlinear feedforward/feedback controller is able to regulate product quality and to follow optimal grade transition trajectories with feedback. The controller design is based on a decoupled first order error trajectory specification, and uses a simple nonlinear dynamics mass balance model to predict the effects of manipulated variables on product properties. Key parameters in the mass balance model are updated by an extended Kalman filter.

The performance of the nonlinear controller is far superior to that of an analogous linear *IMC* controller, indicating that proper accounting for nonlinearities is essential to good product property control.

A policy is derived for optimal saturation handling by the 2X2 feedback controller. An alternative variable structure controller, with the bleed flow as an additional manipulated variable is suggested for situations in which hydrogen saturation poses a severe problem.

The simultaneous operation of the nonlinear controller, *EKF* and product property updating scheme is tested for an impurity disturbance and grade changeovers. The control scheme reacts quickly to compensate for the impurity disturbance, and it performs very well during the grade changeovers. The control system developed in Chapter 6 shows great promise for industrial implementation.

6.12 NOTATION

$\underline{A}(\underline{x},t)$	Jacobian matrix for nonlinear model
a_{cat}	Number of catalyst sites per unit mass of catalyst
$\underline{B}(\underline{x},t)$	Coefficient matrix for control actions in equation 6.4
b_T	Total bleed stream flow rate
B_w	Mass of polymer in the reactor
$[C_T]$	Combined concentration of gas phase components
$\underline{d}$	Disturbance faced by linear controller
$\underline{D}$	Linear Feedforward transfer function model
$\tilde{\underline{D}}$	Linear Feedforward transfer function model with dead time removed
$e(t)$	Error trajectory
EKF	Extended Kalman Filter
$\underline{f}$	expression for time derivatives of model states
$\underline{F}$	*IMC* feedback filter
F_H, F_{M2}, F_{cat}	Feed rates of hydrogen, butene and catalyst
gl	Hydrogen gas loss parameter
$\underline{G}_p$	Linear process transfer function model
$\tilde{\underline{G}}_p$	Linear process transfer function model with dead time removed
h	Gas sampling and controller discretization interval
h_1, h_2	Output equations for $\ln(MI_i)$ and ρ_i
$[H_2]$	Hydrogen concentration in the gas phase
$[I]$	Impurity concentration in gas phase
$\underline{I}$	Identity matrix

IMC	Internal model control
κ_1, κ_2	Nonlinear controller tuning factors
$\underline{K}, \underline{K}_1, \underline{K}_2$	Diagonal matrices for tuning nonlinear controllers
k_0, k_1, k_3, k_5	Parameters in instantaneous melt index model
kd	Catalyst deactivation rate constant
kh	Rate constant for hydrogen consumption
$kp1, kp2$	Rate constants for ethylene and butene consumption
L	Expression defined in equation 6.39
$\underline{m}$	Diagonal matrix for linear controller tuning
M	Expression defined in equation 6.35
$[M_1], [M_2]$	Ethylene and butene concentrations in the gas phase
MI_c, ρ_c	Cumulative melt index and density
MI_i, ρ_i	Instantaneous melt index and density
MI_{sp}, ρ_{sp}	Setpoints for instantaneous melt index and density
$mw(i)$	Molecular weight of component i
N	Expression defined in equation 6.36
NLP	Nonlinear Program
O_p	Polymer outflow rate
p_0, p_1, p_2, p_4	Parameters in the instantaneous density model
P_R	Polymer production rate
P_T	Total pressure in reactor
$QDMC$	Quadratic Dynamic Matrix Control
R	Ideal gas constant
R_v	Covariance matrix for measured variables

R_w	Covariance matrix for model predictions
$S(M_2)$	Butene solubility coefficient
T	Reactor temperature
t	Time
t_d	Dead time
τ	First-order closed loop time constant
$\underline{u}$	Vector of manipulated variables
u_1, u_2	Manipulated variables (hydrogen and butene feed rates)
$\underline{v}$	Vector of feedforward variables
V_g	Volume of the gas phase
V_s	Equivalent volume of butene dissolved in the polymer
V_T	Total volume of reactor and recycle line
W	Expression defined in equation 6.40
$\underline{x}$	State vector for the mass balance model
$\underline{x}_m$	State vector for the mass balance model
$\underline{x}_p$	Vector of parameters to update using the *EKF*
Y	Moles of active sites in the reactor
$\underline{Y}$	Vector of output variables
$\underline{Y}_{sp}$	Setpoint trajectory
Y_1	Output variable 1, $\ln(MI_i)$
Y_2	Output variable 2, ρ_i
z^{-1}	Backward shift operator
α_v	Amorphous volume fraction in the polymer particles

THESIS SUMMARY

7 THESIS SUMMARY AND CONCLUSIONS

This section provides a summary of the major results and conclusions of this thesis. The summary is divided into four topic areas: modelling, property estimation, grade changeovers, and control.

7.1 MODELLING OF GAS PHASE POLYETHYLENE REACTORS

In Chapters 2 and 3, a dynamic mechanistic model for a gas phase polyethylene reactor is developed. The purpose of this model is to describe how gas feed rates, reactor temperature, and other reactor operating conditions influence product properties. This model is required for simulating reactor operation during grade changeovers, and for testing product quality control schemes. The modelling effort is divided into two stages. In Chapter 2, a kinetic model is developed to predict the product properties from the gas composition, catalyst properties, and the reactor temperature. In Chapter 3, the model is extended to include mass balances on the reactants, and a reactor energy balance, so that the gas composition and reactor temperature can be predicted.

In Chapter 2, a kinetic model is developed which predicts the weight and number average molecular weights of the copolymer, its average compostion, and the polymer production rate. Estimates of melt index and density are then calculated from empirical correlations, using the average molecular weight and composition predictions. The inputs to this model are the reactor temperature, the gas phase composition, the catalyst feed

rate, and the bed level. The model includes mechanisms for chain transfer and propagation reactions at different types of active sites on the Ziegler-Natta catalyst. Catalyst deactivation reactions and poisoning by impurities are also considered. It is assumed that the gas and polymer phases are in thermodynamic equilibrium, so that reactant concentrations at the catalyst sites can be determined from measured gas phase concentrations and solubility relationships. The influence of temperature on product quality is included in the model through both kinetic rate parameters and solubility effects.

Using industrial operating data, it is shown that a two-site model is capable of predicting the changes in production rate, average molecular weight, and copolymer composition in an industrial reactor. At the same time, the bimodal instantantaneous joint molecular weight and composition distributions generated from the model are consistent with the type of distribution observed experimentally by Wild et al. (1982) for commercial linear low density polyethylene products. This model is the first in the literature to successfully predict the dynamic behaviour of product properties in an industrial gas phase polyethylene reactor.

The reactor model is extended in Chapter 3, so that product properties can be predicted, given gas feed rates and heat exchanger operating conditions. To permit the prediction of gas phase composition, mass balances are performed on monomers, hydrogen, cocatalyst, impurities, and inerts. In addition dynamic, energy balances are performed on the reactor, and on the recycle gas cooler, to determine the reactor temperature. Low level controllers for regulation of the quantity of polymer in the fluidized bed, the ethylene inventory in the reactor, and the reactor temperature, are also added to the model. Using dynamic simulations, it is shown that the steady state operating point is open-loop unstable. If the temperature controller is turned off, then a small disturbance leads to oscillations in temperature, production rate, and product quality. In

an industrial reactor, such oscillations would be catastrophic, leading to particle agglomeration and loss of fluidization. Fortunately, the reactor simulation was easily stabilized using a simple *PID* temperature controller. For all of the cases simulated, the *PID* temperature controller led to stable reactor operation. While Choi and Ray (1985) have done some initial work on stability and temperature control in gas phase polyolefin reactors, this remains an interesting research topic for the future. The model extensions in Chapter 3 are essential for studying grade changeover and for testing product property control schemes.

7.2 ON-LINE ESTIMATION OF PRODUCT PROPERTIES IN GAS PHASE POLYETHYLENE REACTORS

On-line estimates of *MI* and ρ are required for both product property monitoring and control. Since melt index and density are not measured on-line, their values must be inferred from available on-line measurements. In Chapter 4, simple theoretically based models are developed to predict instantaneous *MI* and ρ from the gas composition and reactor temperature. One parameter in each of these models is chosen for on-line updating. Solid phase mixing models are then developed to predict cumulative *MI* and ρ from the instantaneous properties, the bed level, and the polymer production rate. When laboratory measurements become available, adjustable paramters in the instantaneous models are updated using a recursive prediction error method (*RPEM*). In Chapter 4, the *RPEM* is compared with an extended Kalman filter (*EKF*). The *RPEM* is chosen for this simple estimation problem, because it is more easily implemented. Using industrial data, it is demonstrated that this novel inference technique provides a simple and effective method for inferring both *MI* and ρ.

7.3 GRADE CHANGEOVERS

A major benefit of gas phase polyethylene technology over traditional slurry reactors is that a broad range of polymer grades can be produced in a single continuous reactor. Nevertheless, if grade changeovers are poorly executed, then large quantities of off-specification polymer can be produced. In Chapter 5, optimal transition policies are studied for a series of three grades. The goals of the study are to determine suitable transition policies for on-line implementation, and to investigate the effects of problem formulation on the optimal solution. The dynamic reactor model in Chapters 2 and 3 is integrated, along with a set of adjoint equations, to calculate both the performance index and gradients required by the optimizer. The optimizer uses this information to find optimal manipulated variable profiles. The manipulated variables considered in the study are the hydrogen and butene feed rates, the reactor temperature setpoint, the gas bleed flow, the catalyst feed rate, and the bed level setpoint.

The importance of including specific manipulated variables and objective function penalties in the problem formulation is studied by beginning with a simple problem, and then adding complexity. It is shown that if hard constraints on state variables are not required, then an embedded model approach provides a simple, effective method for solving dynamic optimization problems. Quadratic penalty terms in the objective function are used to prevent large overshoots in instantaneous properties, which lead to broad molecular weight and composition distributions. Penalty terms are also used to ensure that the bed level, production rate, bleed flow, and temperature setpoint settle at economically desirable positions. It is assumumed that desired steady state conditions for the next grade have been determined by the solution to a steady state optimization problem. This approach is much simpler that finding the optimal dynamic trajectory and the steady state conditions from a single optimization problem.

It is shown that large transitions in *MI* are hampered by slow hydrogen dynamics, and that the time required for such a transition can be greatly reduced by manipulation of the temperature setpoint and the bleed stream flow. Reduction of the bed level setpoint and catalyst feed rates during transitions can significantly reduce the quantity of off-specification polymer produced. The optimal policies determined in Chapter 5 are suitable for on-line implementation. However, the should not be implemented without feedback. Disturbances and model mismatch can result in product property trajectories which differ significantly from the nominal optimal trajectory.

7.4 ON-LINE PRODUCT PROPERTY CONTROL

In Chapter 6, a novel nonlinear model-based strategy is developed for on-line product property control. This feedforward/feedback control scheme is capable of both regulating product quality about a given target and implementing optimal transition policies with feedback. In the feedback portion of the controller, the hydrogen and butene feed rates are manipulated to keep the product properties at their required setpoints. During grade transitions, the controller implements open-loop optimal policies for the reactor temperature setpoint, the bleed valve position, the catalyst feed rate, and the bed level setpoint. The hydrogen and butene feed rates are adjusted to compensate for disturbances, and to force the instantaneous *MI* and ρ to follow the nominal optimal trajectories. The feedback controller design is based on a decoupled first-order error trajectory specification.

The simplified mass balance model used in the controller design contains four adjustable parameters which are updated using an extended Kalman filter. The controller and *EKF* provide excellent regulatory and grade transition control for the range of polyethylene products simulated. To demonstrate the importance of nonlinearities in

the product property control problem, the performance of the nonlinear controller is compared with that of an analogous linear time-invariant *IMC* design. It is shown that the performance of the linear controller is inferior to that of the proposed nonlinear controller. An optimal strategy for handling manipulated variable saturation in the 2X2 feedback controller is designed and tested, and an alternative variable structure nonlinear controller to improve performance during hydrogen saturation is discussed. Finally, the simultaneous operation of the product property inference scheme, the model-based controller, and the *EKF* is simulated. It is shown that this control scheme reacts quickly to compensate for variations in reactive impurity levels, which provide a major source of product quality disturbances in industrial gas phase polyethylene reactors. The control system proposed has great potential for improving product quality in the polyethylene industry.

REFERENCES

8 REFERENCES

Adebekun, A.K. and F.J. Schork, "Continuous Solution Polymerization Reactor Control 1. Nonliner Reference Control of Methyl Methacrylate Polymerization", *Ind. Eng. Chem. Res.*, **28**, 1308, (1989a).

Adebekun, D.K. and F.J. Schork, "Continuous Solution Polymerization Reactor Control 2. Estimation and Nonlinear Reference Control during Methyl Methacrylate Polymerization", *Ind. Eng. Chem. Res.*, **28**, 1846 (1989a).

Adebekun, A.K., K.M. Kwalik and F.J. Schork, "Steady-State Mulitiplicity during Solution Polymerization of Methyl Methacrylate in a CSTR", *Chem. Engng. Sci.*, **44(10)**, 2269 (1989).

Ahlberg, D.T. and I. Cheyne, "Adaptive Control of a Polymerization Reactor", *AIChE Symposium Series*, **No. 159, Vol. 72**, 221 (1976).

Ardell, G. and B. Gumowski, "Model Prediction for Reactor Control", *Chem. Eng. Prog.*, p. 77, June (1983).

ASTM, "1990 Annual Book of ASTM Standards", American Society for Testing Materials, Philadelphia, U.S.A., **Volume 8.01 Plastics(1)**, ASTMD 1238 and ASTMD 1505 (1990).

Balchen, J.G., B. Lie and I. Solberg, "Internal decoupling in nonlinear process control", *Modeling, Identification and Control*, **9(3)**, 137 (1988).

Bequette, B.W., "Process Control using Nonlinear Programming Techniques" in A. Bensoussan and J.L. Lions, eds., *Analysis and Optimization of Systems, Lecture Notes in Control and Information Sciences*, Springer Verlag, **144**, 57 (1990).

Bequette, B.W., "Nonlinear Control of Chemical Processes - A Review", submitted to Industrial and Engineering Chemistry Research", (1990).

Bequette, B.W., "Nonlinear Predictive Control using Multi-rate Sampling", *Can. Journal of Chem. Eng.*, **69(1)**, 136 (1991).

Biegler, L.T., J.J. Damiano and G.E. Blau, "Nonlinear Parameter Estimation: A Case Study Comparison", *AIChE J.*, **32(1)**, 29, (1986).

Biegler, L.T., "Optimization Strategies for Complex Process Models", unpublished work, Carnegie Mellon University, Pittsburgh, PA, (1990).

Boehm L.L., J. Berthold, R. Franke, W. Strobel and U. Wolfmeier, "Ziegler Polymerization of Ethylene: Catalyst Design and Molecular Weight Distribution", *Stud. Surf. Sci. Catal.*, **25**, 29 (1986).

Bremner, T., D.G. Cook and A. Rudin, "Melt Flow Index Values and Molecular Weight Distributions of Commercial Thermoplastics, *J. Appl. Polym. Sci.*, **41**, 1617 (1990).

Brengel, D.D. and W.D. Seider, "Multistep Nonlinear Predictive Controller", *Ind. Eng. Chem. Res.*, **28**, 1812 (1989).

Bryson, A.E. and Y.C. Ho, "Applied Optimal Control: Optimization, Estimation and Control", Hemisphere, Washington D.C., (1975).

Burdett, I.D., "The Union Carbide UNIPOL Process: Polymerization of Olefins in a Gas-Phase Fluidized Bed", presented at the AIChE Annual Meeting, Washington, D.C. Nov. 27- Dec. 2, (1988).

Chen, C.T., and C. Hwang, "Optimal Control Computation for Differential-Algebraic Process Systems with General Constraints", *Chem. Eng. Comm.*, **97**, 9 (1990)

Chien, D.C.H. and A. Penlidis, "On-line Sensors for Polymerization Reactors", *JMS-Rev. Macromol. Chem. Phys.*, **C30(1)**, 1 (1990).

Choi, K.Y. and W.H. Ray, "Recent Developments in Transition Metal Catalyzed Olefin Polymerization - A Survey 1. Ethylene Polymerization, *JMS-Rev. Macromol. Chem. Phys.*, **C25(1)**, 1 (1985).

Choi, K.Y. and W.H. Ray, "The Dynamic Behavior of a Fluidized Bed Reactor for Solid Catalyzed Gas Phase Olefin Polymerization", *Chem. Eng. Sci.*, **40(12)**, 2261-2279 (1985).

Dahlin, E.B., "Designing and Choosing Digital Controllers", *Instrum. Control Syst.*, **4**, 77 (1968).

Daoutidis, P., M. Soroush and C. Kravaris, "Feedforward/Feedback Control of Multivariable Nonlinear Processes", *AIChE Journal*, **36(10)**, 1471 (1990).

deCarvalho, A.B., P.E. Gloor and A.E. Hamielec, "A Kinetic Mathematical Model for Heterogeneous Ziegler-Natta Copolymerization", *Polymer*, **30**, 280 (1989).

Eaton, J.W. and J.B. Rawlings, "Feedback Control of Chemical Processes using On-Line Optimization Techniques", *Computers Chem. Engng.*, **14(4/5)**, 469 (1990).

Economu, C.G., M. Morari and B.O. Palsson, "Internal Model Control 5. Extension to Nonlinear Systems", *Ind. Eng. Chem. Proc. Des. Dev.*, **25(2)**, 403 (1986).

Elicabe, G.E. and G.R. Meira, "Estimation and Control in Polymerization Reactors - A Review", *Polym. Eng. Sci.*, **28(3)**, 121 (1988).

Ellis, M.F., T.W. Taylor, V. Gonzalez and K.F. Jensen, "Estimation of the Molecular Weight Distribution in Batch Polymerization", *AIChE Journal*, **34(8)**, 1341 (1988).

Farber, J.N. and R.L. Laurence, "Optimization of Continuous Polymerization Reactors: Start-up and Change of Specification", *Macromol. Chem., Macromol. Symp.*, **2**, 193 (1986).

Daoutidis, P., M. Soroush and C. Kravaris, " Feedforward/Feedback Control of Multivariable Nonlinear Processes", *AIChE Journal*, **36(10)**, 1471 (1990).

Floyd, S., K.Y. Choi, T.W. Taylor and W.H. Ray, "Polymerization of Olefins through Heterogeneous Catalysis III. Polymer Particle Modelling with an Analysis of Intraparticle Heat and Mass Transfer Effects, *J. Appl. Polym. Sci.*, **32**, 2935 (1986).

Floyd S., T. Heiskanen and W.H. Ray, "Solid Catalyzed Olefin Polymerization", *Chem. Eng. Prog.*, **84(11)**, 56 (1988).

Fortescue, T.R., L.S. Kershenbaum and B.E. Ydstie, "Implementation of Self-Tuning Regulators with Variable Forgetting Factors", *Automatica*, **17**(6), 831, (1981).

Foster, G.N., Union Carbide Corporation, "Production Performance Control - Polyolefins", Chapter 8 in "Polymer Reaction Engineering, an Intensive Short Course on Prodution Technology of PolyOlefins", McMaster University, Hamilton, Ontario, Canada (1990).

Frensdorff, H.K., "Diffusion and Sorption of Vapors in Ethylene-Propylene Copolymers" , *J. Polym. Sci. A-2*, **2**, 333 (1964).

Freund, E., "Decoupling and Pole Assignment in Nonlinear Systems", *Electronics Letters, 9(16)*, 373 (1973).

Freund, E., "The Structure of Decoupled Nonlinear Systems", *Int. J. Control*, **21(3)**, 443 (1975).

Freund, E., "Fast Nonlinear Control with Arbitrary Pole-Placement for Industrial Robots and Manipulators", *International Journal of Robotics Research*, **1(1)**, 65 (1982).

Frontini, G.L., G.E. Elicabe and G.R. Meira, "Optimal periodic control of a continuous living anionic polymerization II. New theoretical results", *J. Appl. Polym. Sci.*, **33(6)**, 2165 (1987).

Gagnon, L., "State Estimation and Sensor Selection for a Continuous Emulsion Polymerisation Reactor", Masters Thesis, McMaster University, Canada (1990).

Galvan, R., "Modelling of Heterogeneous Ziegler-Natta Copolymerization of α-olefins", Ph.D. Thesis, University of Minnesota, (1986).

Galvan, R. and M. Tirrell, "Molecular Weight Distribution Predictions for Heterogeneous Ziegler-Natta Polymerization Using a Two-Site Model", *Chem. Eng. Sci.*, **41**, 2385 (1986).

Garcia, C.E. and A.M. Morshedi, "Quadratic Programming Solution of Dynamic Matrix Control (QDMC)", *Chem. Eng. Commun.*, **46**, 73 (1986).

Garcia, C.E., D.M. Prett and M. Morari, "Model Predictive Control: Theory and Practice - a Survey", *Automatica, 25(3)*, 335 (1989).

Gilles, E.D., "Model-Based Techniques for Controlling Processes in Chemical Engineering", *Proc. 10th World Congress on Automatic Control*, Munich, Germany, 256 (1987).

Goodwin, C.G. and K.S. Sin, "Adaptive Filtering Prediction and Control", Prentice-Hall, (1984).

Gossen, P.D., Ph.D. Thesis, Department of Chemical Engineering, McMaster University, Hamilton, Ontario, Canada (1991).

Guyot, A., J Guillot, C. Pichot and L.R. Guerroro, "New Design for Producing Constant Composition Copolymers in Emulsion Polymerization", *ACS Symp. Series*, **165**, 415 (1981).

Hamielec A.E., J.F. MacGregor and A. Penlidis, "Multicomponent Free-Radical Polymerization in Batch, Semi-Batch and Continuous Reactors", *Macromol. Chem., Macromol. Symp.*, **10/11**, pp. 521-570 (1987).

Henson, M.A. and D.E. Seborg, "Input-Output Linearization of General Nonlinear Processes", *AIChE Journal*, **36(11)**, 1753 (1990).

Hindmarsh A.C., "LSODE and LSODI, Two New Initial Value Ordinary Differential Equation Solvers", *ACM-Signum Newsletter,* **15(4)**,10 (1980).

Hutchinson R.A. and W.H. Ray, "Polymerization of Olefins through Heterogeneous Catalysis VII. Particle Ignition and Extinction Phenomena", *J. Appl. Polym. Sci.*, **34**(2), 657 (1987).

Hutchinson R.A. and W.H. Ray, "Polymerization of Olefins through Heterogeneous Catalysis. VIII. Monomer Sorption Effects", *J. Appl. Polym. Sci.*, **41**, 51 (1990).

Jaisinghani, R. and W.H. Ray, "On the Dynamic Behavior of a Class of Homogeneous Continuous Stirred Tank Polymerization Reactors", *Chem. Engng. Sci.*, **32**, 811 (1977).

James, D.E., "Linear Low Density Polyethylene", *Encyclopedia of Polymer Science and Technology*, 2nd ed., **Vol. 6**, eds. J.I. Kroschwitz et al., pp. 429-454 (1985).

Jang, S.S., B. Joseph and H. Mukai, "On-line Optimization of Constrained Multivariable Chemical Processes", *AIChE Journal*, **33(1)**, 26, (1987).

Jayadeva, B., Y.S.N.M. Rao, M. Chidambaram and K.P Madhavan, "Nonlinear Controller for a pH Process", *Computers chem. Engng.*, **14(8)**, 917 (1990).

Jo, J.H. and S.G. Bankhoff, "Digital Monitoring and Estimation of Polymerization Reactors", *AIChE Journal*, **22**, 361 (1976).

Johnson, A.F., B. Khaligh and R. Ramsay, "Copolymerization Reaction Engineering: Controlled and Semibatch Solution Copolymerization of Styrene with Methyl Methacrylate", *ACS Symp. Series*, **197**, 117 (1982).

Kantor, J.C., An Overview of Nonlinear Geometrical Methods for Process Control", in D.M. Prett and M. Morari, eds., *The Shell Process Control Workshop*, Butterworths, Boston, 225 (1987).

Karol, F.J. and F.I. Jacobson, "Catalysis and the UNIPOL Process", *Stud. Surf. Sci. Catal.*, **25**, 323 (1986).

Kelly, S.J., J.F. MacGregor and T.W. Hoffman, "Control of a Continuous Polybutadiene Reactor Train", *Can. Journal of Chem. Eng.*, **65**, 852 (1987)

Kiparissides, C. and S.R. Shaw, "Self-tuning and Stable Adaptive Control of a Batch Polymerization Reactor", *Automatica*, **19**, 225 (1983).

Kissin Y.V., "Isospecific Polymerization of Olefins with Heterogeneous Ziegler-Natta Catalysts", Springer-Verlag, New York, (1987).

Kozub, D.J., "Multivariable Control: Design, Robustness, and Nonlinear Inferential Control for Semi-Batch Polymerization Reactors", Ph.D. Thesis, McMaster University, Hamilton, (1989).

Kravaris, C. and J.C. Kantor, "Geometric Methods for Nonlinear Process Control. 1. Background", *Ind. Eng. Chem. Res.*, **29(12)**, 2295 (1990).

Kravaris, C. and J.C. Kantor, "Geometric Methods for Nonlinear Process Control. 2. Controller Synthesis", *Ind. Eng. Chem. Res.*, **29(12)**, 2310 (1990).

Kravaris, C. and M. Soroush, "Synthesis of Multivariable Nonlinear Controllers by Input/Output Linearization", *AIChE Journal*, **36(2)**, 249 (1990).

Kozub, D.J. and J.F. MacGregor, "State Estimation and Control for Semi-Batch Polymerization Reactors", presented at the AIChE Annual Meeting, San Francisco, (1989).

Kunii, D. and O. Levenspiel, "Bubbling Bed Model for Kinetic Processes in Fluidized Beds. Gas - Solid Mass and Heat Transfer and Catalytic Reactions, *I&EC Process Design and Development*, **7(4)**, 481 (1968).

Lee, P.L. and G.R. Sullivan, "Generic Model Control", *Comput. chem. Engng.*, **12(6)**, 573 (1988).

Lee, P.L., G.R. Sullivan and W. Zhou, "Process/Model Mismatch Compensation for Model-Based Controllers", *Chem. Eng. Comm.*, **80**, 33 (1989).

Leis, J.R. and M.A. Kramer, "The Simultaneous Solution and Sensitivity Analysis of Systems Described by Ordinary Differential Equations", *ACM TOMS*, **14(1)**, 45 (1988).

Leis, J.R. and M.A. Kramer, "Algorithm 658 ODESSA - An Ordinary Differential Equation Solver with Explicit Simultaneous Sensitivity Analysis", *ACM TOMS*, **14(1)**, 61 (1988).

Lennartson, B.E.V., "Combining Infrequent and Indirect Measurements by Estimation and Control", *Ind. Eng. Chem. Res.*, **28**, 1653 (1989).

Levenspiel O., "Chemical Reaction Engineering", 2nd ed., John Wiley and Sons, Toronto, p. 144, (1972).

Li, W.C. and L.T. Biegler, "Process Control Strategies for Constrained Nonlinear Systems", *Ind. Eng. Chem. Res.*, **27**, 1421 (1988)

Liptak, B.G., "Control of Heat Exchangers", *Brit. Chem. Eng. & Proc. Tech.*, **17(7/8)**, 637 (1972).

Ljung, L., "System Identification - Theory for the User", Prentice-Hall Information and System Sciences Series, (1987).

MacGregor, J.F., "Control of Polymerization Reactors", *Proc. IFAC Symp.*, **DYCORD-86**, Bournemouth, U.K., p.31, (1986).

MacGregor, J.F., D.J. Kozub, A. Penlidis and A.E. Hamielec, "State Estimation for Polymerization Reactors", *Proc. IFAC Symp.*, **DYCORD-86**, Bournemouth, U.K. (1986).

MacGregor, J.F., A. Penlidis and A.E. Hamielec, "Control of Polymerization Reactors - A Review", *Polym. Proc. Eng.*, **2**, 179, (1984).

MacGregor, J.F. and P.W. Tidwell, "Modelling and Control of Continuous Industrial Polymerization Reactors", Computer Appl. to Chem. Eng., *ACS Symp. Ser.* **124**, 251 (1980).

Meira, G.R., "Forced Oscillations in Continuous Polymerization Reactors and Molecular Weight Distribution Control - A Survey", *J. Macromol. Sci. Rev., Macromol. Chem.*, **C20(2)**, 207 (1981).

McLellan, P.J., T.J. Harris and D.W. Bacon, "Error Trajectory Descriptions of Nonlinear Controller Designs", *Chem. Eng. Sci.*, **45(10)**, 3017 (1990).

Meira, G.R. and A.F. Johnson, "Molecular Weight Distribution Control in Continuous Living Polymerizations through Periodic Operation of the Monomer Feed", *Poly. Eng. Sci.*, **2(7)**, 415 (1981).

Morbidelli, M.A., A. Varma and R. Aris, "Reactor Steady-State Multiplicity and Stability", Chapter 14 in *Chemical and Reaction Engineering*, eds. J.J. Carberry and A. Varma, Marcel Dekker (1987).

Motkei, Y. and Y. Arai, "Operation Planning and Quality Design of a Polymer Process", *Proc. IFAC Symp.*, **DYCORD-86**, p. 159, Bournemouth, U.K., (1986).

Mujitaba, I.M. and S. Macchietto, "Optimal Control of Batch Distillation", presented at 12th IMACS World Congress, Paris, July (1988).

Murtagh, B.A. and M.A. Saunders, "Minos 5.1 User's Guide", Stanford University, Stanford, California, (1987).

Nagel E.J., V.A. Kirrillov and W.H. Ray, "Prediction of Molecular Weight Distributions for High Density Polyolefins", *Ind. Eng. Chem. Prod. Res. Dev.*, **19**, 372 (1980).

Nicoli, D.F., T. Kourti, P.D. Gossen, J.S. Wu and J.F. MacGregor, "On-line Latex Particle Size Determination by Dynamic Light Scattering, Designed for an Industrial Environment", in T. Provder (Ed.) Particle Size Characterization, *ACS Symposium Series*, ACS, Washington DC. (1992).

Parrish, J.R. and C.B. Brosilow, "Nonlinear Inferential Control", *AIChE Journal*, **34(4)**, 633 (1988).

Patino Leal H. and P.M. Reilly, "A Bayesian Study of the Error-in-Variables Model", *Technometrics*, **23**, 221 (1981).

Penlidis, A., J.F. MacGregor and A.E. Hamielec, "Dynamic Modeling of Emulsion Polymerization Reactors", *AIChE Journal*, **31**, 6 (1985).

Pollock, M.J., "Modelling and Control of Sustained Oscillations in the Continuous Emulsion Polymerization of Vinyl Acetate", Ph.D. Thesis, McMaster University, Hamilton, Ontario, Canada (1983).

Razon, L.F. and R.A. Schmitz, "Multiplicities and Instablilities in Chemically Reacting Systems - A Review", *Chem. Eng. Sci.*, **42**(5), 1005 (1987).

Ray, W.H., "Bifurcation Phenomena in Chemically Reacting Systems", in *Applications of Bifurcation Theory*, ed. P.H. Rabinowitz, Academic Press, p. 285 (1977).

Ray, W.H., "Advanced Process Control", McGraw-Hill, New York (1981).

Ray, W.H., "Modelling of Polymerization Systems", *Ber. Bunsenges. Phys. Chem.*, **90**, 947 (1986a).

Ray, W.H., "Polymerization Reactor Control", *IEEE Control Systems Magazine*, p. 3, Aug. (1986b).

Reid, R.C., J.M. Prausnitz and T.K. Sherwood, "The Properties of Gases and Liquids", 3rd ed., McGraw-Hill (1977).

Reklaitis, G.V., A. Ravindran, and K.M. Ragsdell, "Engineering Optimization", Wiley, (1983).

Richards, J.R. and P.D. Schnelle, "Perspectives on Industrial Reactor Control", *Chem. Eng. Prog.*, **84**(10), 32, (1986).

Rincon-Rubio, L.M., C.E. Wilen and L.E. Lindfors, "A Kinetic model for the polymerization of propylene over a Ziegler-Natta Catalyst", *Eur. Polym. J.*, **26(2)**, 171 (1990).

Robeson, L.M. and T.G. Smith, "Permeation of Ethane-Butane Mixtures through Polyethylene", *J. Appl. Polym. Sci.*, **12**, 2083 (1968).

Rudin, A., "Molecular Weight Distributions", Chapter 18 in "Comprehensive Polymer Science", G. Allen and J.C. Bevington, editors, Pergammon Press, Volume III, (1989).

Rushing, E.V., "Control of Solvent Extraction from Acrylic Fibers", *Proc. IFAC PRP-6 Automation*, Akron, Ohio (1986)

Sargent, R.W.H. and G.R. Sullivan, "Development of Feed Changeover Policies for Refinery Distillation Units", *I&EC Proc. Des. Dev.*, **18(1)**, 113 (1979).

Schmidt, A.D. and W.H Ray, "The Dynamic Behavior of Continuous Polymerization Reactors - I Isothermal solution polymerization in a CSTR", *Chem. Engng. Sci.*, **36**, 1401 (1981).

Schmidt, A.D., A.B. Clinch and W.H. Ray, " The Dynamic Behavior of Continuous Polymerization Reactors - III An experimental study of multiple steady states in solution polymerization", *Chem. Engng. Sci.*, **39(3)**, 419 (1984).

Schuler, H and Z. Suzhen, "Real-Time Estimation of the Chain Length Distribution in a Polymerization Reactor", *Chem. Engng. Sci.*, **40(10)**, 1891 (1985).

Secchi, A.F., E.L. Lima and J.C. Pinto, "Constrained Optimal Batch Polymerization Control", *Poly. Eng. Sci.*, **30(19)**, 1209 (1990).

Segall, N.L., J.F. MacGregor and J.D. Wright, "One-step Optimal Saturation Correction", *Automatica*, **27(1)**, 135 (1991).

Spong, M.W., J.S. Thorpe and J.M. Kleinwaks, "The Control of Robot Manipulators with Bounded Input", *IEEE Transactions on Automatic Control*, **AC-31(6)**, 483 (1986).

Stern, S.A., J.T. Mullhaupt and P.J. Gareis, *AIChE J.*, **15**, 64 (1969).

Sinclair K.B., "Characteristics of Linear LPPE and Description of UCC Gas Phase Process", Process Economics Report, SRI International, Menlo Park, California, 1983.

Slotine, J.J.E. and B.E. Ydstie, "Nonlinear Process Control: An Adaptive Approach which uses Physical Models", *Proc. IFAC Symp. on Nonlinear Control Systems Design*, Capri, Italy (1989).

Stockmayer, W.H., "Distribution of Chain Lengths and Composition in Copolymers", *J. Chem. Phys.*, **13**, 199 (1945).

Tacx, J.C.J.F, H.N. Linssen and A.L. German, "Effect of the Molar Mass Ratio of Monomers on the Mass Distribution of Chain Lengths and Compositions in Copolymers: Extension of the Stockmayer Theory", *J. Polym. Sci., Polym. Chem.*, **26**, 61 (1988).

Tait, P.J., "Monoalkene Polymerization: Ziegler-Natta and Transition Metal Catalysts", Chapter 1 in Comprehensive Polymer Science, eds. G. Allen and J.C. Bevington, Pergammon Press (1989).

Takamatsu, T., S. Shioya and Y. Okada, "Design of Adaptive/Inferential Control System and Its Application to Polymerization Reactors", *Ind. Eng. Chem. Proc. Des. Dev.*, **25**, 821 (1986).

Talbot, J.P., "The Dynamic Modelling and Particle Effects of a Fluidised Bed Polyethylene Reactor", Ph.D. Thesis, Queen's University, Kingston, Ontario, Canada (1990)

Tanner, B.M., A.K. Adebekun, and F.J. Schork, "Feedback Control of Molecular Weight Distribution during Continuous Polymerization", *Polym. Proc. Eng.*, **5(1)**, 75, (1987).

Temeng, K.T. and F.J. Schork, "Closed-Loop Control of a Seeded Continuous Emulsion Polymerization Reactor System", *Chem. Eng. Comm.*, **85**, 193 (1989).

Teymour, F. and W.H. Ray, "The Dynamic Behavior of Continuous Solution Polymerization Reactors - IV Dynamic Stability and Bifurcation Analysis of an Experimental Reactor", *Chem. Engng. Sci.*, **44(9)**, 1967 (1989).

Tirrell, M. and K. Gromley, "Composition Control of Batch Copolymerization Reactor", *Chem. Eng. Sci.*, **36**, 367, (1981).

Tjoa, I.B. and L.T. Biegler, "Simultaneous Solution and Optimization Strategies for Parameter Estimation of Differential-Algebraic Equation Systems", *Ind. Eng. Chem. Res.*, **30(2)**, 376 (1991).

Uppal, A., W.H. Ray and A.B. Poore, "On the Dynamic Behavior of Continuous Stirred Tank Reactors", *Chem. Eng. Sci.*, **29**, 967 (1974).

Usami T., Y. Gotoh and S. Takayama, "Generation Mechanism of Short-Chain Branching Distribution in Linear Low-Density Polyethylenes", *Makromolecules*, **19**(11), 2722 (1986).

Van Heerden, "Autothermic Processes - Properties and Reactor Design", *Ind. Eng. Chem.*, **45**(6),1242, (1953)

Vinogradov G.V. and A.Ya. Malkin, "Rheology of Polymers - Viscoelasticity and Flow of Polymers", Mir Publishers, Moscow, Chapter 2, pp. 153-178 (1980).

Wild L., T.R. Ryle, D.C. Knobeloch, "Branching Distributions in Linear Low-Density Polyethylenes", *Polym. Prepr. (Am. Chem.Soc., Div. Polym. Chem.)*, **23**(2), 133 (1982).

Williamson, D.A., "Rheology of Polyolefins: Film Grades", presented at the Conference on Practical Rheology in Polymer Processing, London (1969) and published in Plastics and Polymerization, p.169 (1970)

Wu, G.Z.A., L.A. Denton and R.L. Laurence, "Batch Polymerization of Styrene - Optimal Temperature Histories", *Poly. Eng. Sci.*, **22**, 1 (1982).

Zucchini U. and G. Cecchin, "Control of Molecular Weight Distributions in Polyolefins Synthesized with Ziegler-Natta Catalytic Systems", *Advances in Polymer Science, Industrial Developments*, **51**, 101 (1983).

028120001